FRACTURE TOUGHNESS

Proceedings of the
1971 National Symposium
on Fracture Mechanics
PART II

STP 514

AMERICAN SOCIETY FOR TESTING AND MATERIALS

FRACTURE TOUGHNESS

Proceedings of the 1971 National Symposium on Fracture Mechanics

PART II

Proceedings of the 1971
National Symposium on
Fracture Mechanics
University of Illinois
Urbana-Champaign, Ill., 31 Aug.-2 Sept. 1971

ASTM SPECIAL TECHNICAL PUBLICATION 514
H. T. Corten, general chairman
J. P. Gallagher, arrangements chairman

List price $18.25
04-514000-30

75TH ANNIVERSARY ASTM
AMERICAN SOCIETY FOR TESTING AND MATERIALS
1916 Race Street, Philadelphia, Pa. 19103

Library of Congress Catalog Card Number: 72-78745

NOTE

The Society is not responsible, as a body,
for the statements and opinions
advanced in this publication.

Printed in Philadelphia, Pa.
September 1972

FOREWORD

The 1971 National Symposium on Fracture Mechanics was held at the University of Illinois, Urbana-Champaign, Ill., 31 August through 2 September 1971. H. T. Corten, Department of Theoretical and Applied Mechanics, University of Illinois, presided as general chairman. J. P. Gallagher, Experimental Mechanics Branch, Air Force Flight Dynamics Laboratory, Wright-Patterson AFB, served as arrangements chairman.

The proceedings have been subjectively divided into complementary volumes: Part I – *Stress Analysis and Growth of Cracks* and Part II – *Fracture Toughness*. Part II is contained herein.

Related ASTM Publications

Current Status of Plane Strain Crack Toughness Testing of High Strength Metallic Materials, STP 410, (1967), $5.50, 04-410000-30

Electron Fractography, STP 436, (1968), $11.00, 04-436000-30

Fracture Toughness Testing at Cryogenic Temperatures, STP 496, (1971), $5.00, 04-496000-30

CONTENTS

INTRODUCTION

The papers in this volume were presented at the Fifth National Symposium on Fracture Mechanics held at the University of Illinois, Urbana, Illinois, 31 August through 2 September 1971. Beginning in 1972, The National Symposium on Fracture Mechanics will be sponsored by ASTM through Committee E-24 on Fracture Testing of Metals.

In this volume, methods of measurement of toughness of high-toughness metals are reported. Attention is focused on a variety of tests including a new fracture criteria for the elastic-plastic and fully plastic realm, the critical value of the *J* integral, and the relationship between the various toughness measurements.

In the companion volume, *STP 513,* the papers treat crack tip stress analysis and subcritical crack extension caused by repeated loads, environments, and their combination. The threshold level for fatigue crack extension is given particular attention.

H. T. Corten
Department of Theoretical
and Applied Mechanics
College of Engineering
University of Illinois
Urbana, Illinois
general chairman

J. A. Begley[1] *and J. D. Landes*[1]

The *J* Integral as a Fracture Criterion

REFERENCE: Begley, J. A. and Landes, J. D., "The J Integral as a Fracture Criterion," *Fracture Toughness, Proceedings of the 1971 National Symposium on Fracture Mechanics, Part II, ASTM STP 514,* American Society for Testing and Materials, 1972, pp. 1-20.

ABSTRACT: The path independent J integral, as formulated by Rice, can be viewed as a parameter which is an average measure of the crack tip elastic-plastic field. This together with the fact that J can be evaluated experimentally, makes a critical J value an attractive elastic-plastic fracture criterion. The J_{Ic} fracture criterion refers to crack initiation under plane strain conditions from essentially elastic to fully plastic behavior.

Experiments supporting the validity of a J_{Ic} fracture criterion are presented in this paper. Values of the J integral were determined experimentally for two steel alloys, one of low and the other of intermediate strength. A review is given of the analytic support for the J_{Ic} fracture criterion. The range of applicability of the J_{Ic} concept, its limitations, and its advantages are also discussed.

KEY WORDS: fracture (materials), failure, cracking (fracturing), crack initiation, elastic theory, plastic theory, tensile properties, stress strain diagrams, bend tests, analyzing, steels, rotor steels, pressure vessel steels

A failure criterion which could accurately predict failure of cracked bodies would be a useful engineering tool both for the evaluation of structural integrity and the selection of materials. Linear-elastic fracture mechanics provides a one parameter failure criterion for a limited class of problems; those of cracked bodies with small scale yielding where the crack tip plastic region is at least an order of magnitude smaller than the physical dimensions of the component [*1*]. It is desirable to have a failure criterion which could predict fracture in structures in cases of both small and large scale plasticity. To do this it is hoped that the concepts of fracture mechanics could be extended to include cases of large scale plastic yielding. The basis of fracture mechanics is the elastic analysis of the crack tip region which shows a unique stress-strain field with a singularity at the crack tip. The strength of the crack tip singularity is the stress intensity

[1] Mechanics Dept., Westinghouse Research Laboratories, Pittsburgh, Pa.

factor, K. The crack tip region then can be characterized by the one parameter K. Fracture must occur then for a critical value of K. A direct extension of fracture mechanics concepts to cases of large scale yielding would assume again the existence of a crack tip singularity. Work by Hutchinson [2] and Rice and Rosengren [3] shows that a singularity does exist which is uniquely dependent upon the material flow properties. An analysis of the crack tip stress field for large scale yielding gives a parameter which can only characterize the crack tip singularity to within some scaling constant. An attempt to uniquely characterize the crack tip singularity has required numerical techniques [4]. These techniques have focused attention to the region immediately surrounding the crack tip where the accuracy of the analysis becomes uncertain. An attempt to characterize the crack tip region by a crack tip radius [5] again relies on numerical techniques applied close to the crack tip. Likewise calculations of crack opening dislocation (COD) centers attention on a region which must be considered uncertain.

A characterization of the crack tip area by a parameter calculated without focusing attention directly at the crack tip would provide a more practical method for analyzing fracture. The path independent J integral proposed by Rice [6] is such a parameter. Its value depends upon the near tip stress strain field. However, the path independent nature of the integral allows an integration path, taken sufficiently far from the crack tip, to be substituted for a path close to the crack tip region. The J integral is truly path independent for linear and nonlinear elastic stress-strain laws; this includes then, the Hencky laws of plasticity. For the physically more appropriate Prandtl-Reuss representation, Hayes [7] has shown that the J integral is also nearly path independent under situations of monotonic loading. Since J can be calculated analytically by using a stress-strain analysis of regions somewhat removed from the crack tip, numerical techniques can be used to calculate J quite accurately. Also, an experimental evaluation of J can be accomplished quite easily by considering the load deflection curves of identical specimens with varying crack lengths.

The ease with which the J integral can be determined and its general applicability to both elastic and plastic behavior makes it an attractive candidate for a failure criterion. For linear elastic behavior the J integral is identical to G, the energy release rate per unit crack extension. Therefore, a J failure criterion for the linear elastic case is identical to the K_{Ic} failure criterion. The use of J provides a means of directly extending fracture mechanics concepts from linear elastic behavior to fully plastic behavior.

This paper discusses the use of the J integral as a failure criterion. The basic concept of the integral is presented along with its advantages and limitations as a failure criterion. Data is presented which experimentally substantiates use of J as a failure criterion for the case of through the thickness constraint. It is shown for one material that J at failure for fully plastic behavior is equal to the linear elastic value of G at failure for extremely large specimens.

Basis for the J_{Ic} Failure Criterion

Definition of the J *Integral*

The energy line integral, J, is applicable to elastic material or elastic-plastic material when treated by a deformation theory of plasticity. It is defined for two-dimensional problems and is given by the equation [6]

$$J = \int_{\Gamma} Wdy - \mathrm{T} \left(\frac{\partial \mathbf{u}}{\partial x}\right) ds \tag{1}$$

As illustrated in Fig. 1, Γ is any contour surrounding the crack tip. The quantity

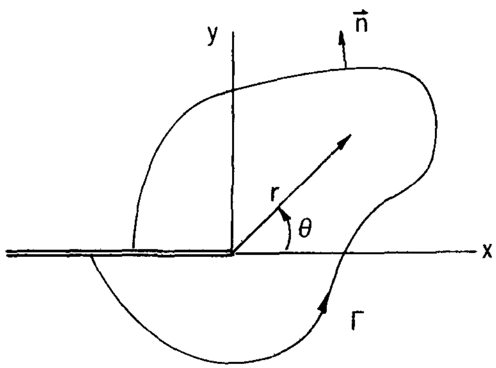

FIG. 1–*Crack tip coordinate system and arbitrary line integral contour.*

W is the strain energy density

$$W = W(\epsilon_{mn}) = \int_{0}^{\epsilon_{mn}} \sigma_{ij}\, d\epsilon_{ij} \tag{2}$$

T is the traction vector defined by the outward normal n along Γ, $\mathrm{T}_i = \sigma_{ij} n_j$, $\mathbf{u}$ is the displacement vector and s is the arc length along Γ.

Rice [6] has proven the path independence of the J integral and this together with an energy interpretation, to be discussed in a subsequent section, makes the J integral a valuable analytic tool. Since paths can be chosen close to the crack tip, the energy line integral represents some average measure of the near tip deformation field. But aside from aiding the approximate analysis of strain concentration at notches and cracks the J integral has utility as a failure criterion. The assumptions which permit this interpretation are presented below.

The J *Integral and the Near Tip Field*

For the J integral to have validity as a failure criterion it must be assumed that there is a crack tip stress-strain singularity for large scale yielding. The work of Hutchinson [*2,8*] and Rice and Rosengren [*3*] supports this assumption. They indicate that the product of stress and strain approaches a $1/r$ singularity as r tends to zero.

$$\sigma_{ij}\ \epsilon_{ij} \rightarrow \frac{\text{a function of } \theta}{r} \quad \text{as } r \rightarrow 0 \tag{3}$$

While a complete solution is lacking, the general structure of the crack tip singularity has been indicated. In fact, McClintock [*7*] has shown that by combining the work of Hutchinson [*2*] and Rice [*6*] the crack tip plastic stress and strain singularities can be expressed as a function of J.

$$\sigma_{ij}\,(r,\theta) = \bar{\sigma}_1 \left(\frac{J}{\bar{\sigma}_1\, I_n}\right)^{n/(n+1)} \frac{1}{r^{n/(n+1)}}\ \tilde{\sigma}_{ij}\,(\theta) \tag{4}$$

$$\epsilon_{ij}\,(r,\theta) = \left(\frac{J}{\bar{\sigma}_1\, I_n}\right)^{1/(n+1)} \frac{1}{r^{1/(n+1)}}\ \tilde{\epsilon}_{ij}\,(\theta) \tag{5}$$

Here, n is the strain hardening exponent in the Ramberg-Osgood relation between equivalent stress, $\bar{\sigma}$, and equivalent plastic strain $\bar{\epsilon}_p$.

$$\bar{\sigma} = \bar{\sigma}_1\,(\bar{\epsilon}_p)^n \tag{6}$$

The term I_n is a function of n and the mode of crack opening. For a plane strain tensile crack I_n has a value close to 5.0 over a wide range of n [*2*]. It is important to note that the plastic crack tip field, Eqs 4 and 5 can be more simply and appropriately written in terms of the plastic stress and strain intensity factors of Hutchinson [*2*] rather than J. However, these factors are simply related to J. J was chosen as the parameter to characterize the crack tip environment because it can be evaluated experimentally and calculated with less difficulty than the plastic stress and strain intensity factors.

From the above, it is not unreasonable to assume that near tip deformation fields and, therefore fracture, will be governed by a characteristic crack tip singularity in the plastic range. Hence, the J integral, being a field parameter whose magnitude depends on the near tip deformation field, is an attractive failure criterion. In terms of the HRR crack tip model stating that fracture initiates at a critical value of J is equivalent to saying the same event will occur in the two bodies when their crack tip environment is identical or nearly so. Since the experiments described in this paper deal only with plane strain the critical value of J is termed J_{Ic}.

The fact that the J integral and the HRR crack tip model are based upon a deformation theory of plasticity rather than the more appropriate incremental theory may lead to some reservations. However, the nature of the crack tip singularity seems to be consistent with the restrictions of the deformation theory, such as proportional loading. In addition, Hayes [*8*] has indicated that the J integral was path independent when evaluated from a finite element solution employing an incremental plasticity type formulation. He indicated that the deformation and incremental theories should yield essentially equivalent results if the loading is monotonic throughout the body.

Energy Rate Interpretation

Energy balance calculations by Irwin [*10*] and Saunders [*11*] show that Griffith type fracture criteria for crack extension in linear elastic solids are dependent on local conditions at the crack tip. Rice [*12*] has pointed out that local conditions also govern inelastic problems. Since the energy line integral reflects the crack tip deformation field it must be related to energy balance considerations. It has been shown by Rice [*6*] that the J integral may be interpreted as the potential energy difference between two identically loaded bodies having neighboring crack sizes. This is stated mathematically as

$$J = -\frac{dU}{d\ell} \tag{7}$$

where U is the potential energy and ℓ is the crack length. In the linear elastic case and also for small scale yielding, J is therefore equal to G, the crack driving force. For any nonlinear elastic body, J may be interpreted as the energy available for crack extension.

Where deformation is not reversible, the general elastic-plastic problem, J loses its physical significance as a crack driving force. It may still be considered as an energy comparison of two similar bodies with neighboring crack sizes loaded in the same manner. However, because of irreversibility, one cannot relate the energy comparison of neighboring crack sizes to the process of crack extension. This distinction will perhaps be clarified by a simple graphical illustration presented below which follows that of Rice [13].

The potential energy per unit thickness of a two-dimensional elastic body of area, A with a boundary S is given by

$$U = \int_A W dx dy - \int_{S_T} T \, (u ds) \tag{8}$$

Here W is the strain energy density and S_T is that portion of the boundary over which the tractions T are prescribed. On a generalized load deflection diagram, as shown in Fig. 2, U is represented by an area. If the boundary conditions are given in terms of the force F° the potential energy is represented by the shaded area above the load deflection curve. In this instance the potential energy is negative and is equal to minus the complementary energy. When the displacements δ° is prescribed, the negative term in Eq 8 drops out since S_T is then

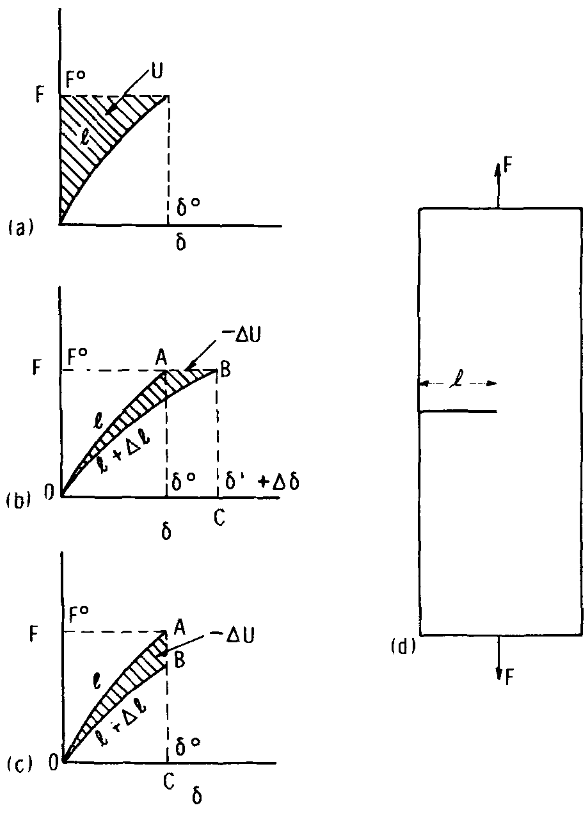

FIG. 2—*Generalized load deflection diagrams.*

nonexistent. The potential energy is then equal to the strain energy, the area under the load deflection curve.

Consider crack extension in a nonlinear elastic body having a crack length ℓ. The load deflection curve is given in Fig. 2*b*. As the crack extends from ℓ to $\ell + \Delta\ell$ under load F^o the total work done on the body is represented by the area OABCO. Because of reversibility, the unloading curve from point B is the same as the loading curve starting with a crack length of $\ell + \Delta\ell$. The strain energy of the body with crack length $\ell + \Delta\ell$ under load F^o is the area OBCO. And the shaded area, OABO, is the difference between the work done on the body to extend the crack to $\ell + \Delta\ell$ and the strain energy of the body at B. Thus it is the energy available for crack extension. But this area also represents minus the potential energy difference between cracks of length $\ell + \Delta\ell$ at load F^o. Considering that here the potential energy is equal to minus the complementary energy makes this readily apparent. Hence, because of reversibility, the J integral, being equal to $-dU/d\ell$ gives the energy available for unit crack extension in elastic materials. In linear elastic fracture mechanics, this crack driving force is termed G. The equality of J and G is evident from a simple graphic illustration. A rigorous derivation of the equality of J and G considering the definition of the J integral, Eq 1, and the linear elastic crack tip stress field equations can be found in Ref *13*. For the case of specified displacements, shown in Fig. 2*c*, the potential energy is equal to the strain energy. The equivalence of the strain energy release rate per unit crack extension and $-dU/d\ell$ is then obvious. It should also be pointed out that the shaded areas in Figs. 2*b* and 2*c*, representing $-\Delta U$ for a constant load and constant displacement are equal. The small additional area in Fig. 2*b*, due to the incremental displacement $\Delta\delta$, is a second order infinitesimal and can be neglected.

Although a deformation type theory of plasticity is essentially a nonlinear elastic theory, one of the restrictions involved in its use is that unloading is not permitted. Plastic deformation is not reversible. As a consequence, the energy interpretation of the J integral cannot be applied to the process of crack extension. It has not been shown that loading a cracked body and then extending the crack under load will give the same result as initially extending the crack and then loading. Therefore, J cannot be identified with the energy available for crack extension in elastic-plastic materials. However, the value of J is still equal to $-dU/d\ell$ and this permits J to be determined experimentally. The physical significance of J for elastic-plastic materials is that it is a measure of the characteristic crack tip elastic-plastic field.

Limitations of the J_{Ic} Approach

Since the Rice energy line integral is expressed only in two dimensions, the J approach is, therefore, limited to problems of plane strain or generalized plane stress. Another limitation is that unloading is not permitted if the deformation theory of plasticity is to be a realistic approximation of elastic-plastic behavior.

This rules out materials which exhibit significant subcritical crack growth prior to fracture. Any crack extension necessarily implies unloading near the crack tip. In general, structures failing in plane stress exhibit some subcritical crack growth. Often this is visible as a flat triangular area ahead of the crack tip denoting the region of shear lip formation. Hence, the J integral failure criterion may be limited to the case of plane strain, which is implied by the subscript I in J_{Ic}. Again as a consequence of the inadmissibility of unloading and subcritical crack growth the J_{Ic} fracture criterion refers to crack initiation rather than propagation. While for a complete treatment of fracture consideration of crack stability is essential, use of the J_{Ic} criterion in an engineering sense is no more restrictive than the use of the K_{Ic} criterion in linear elastic fracture mechanics. It too only refers to crack initiation.

In limiting ourselves to problems of plane strain the question arises, What is meant by this term? A strict analytic interpretation requires that displacements through the thickness parallel to the crack tip leading edge be zero. This is never achieved in an absolute sense. For the fracture problem, observed experimental behavior sets the limits for permissible deviation from ideally plane straining. In linear elastic fracture mechanics a thickness criterion was established based on experimental data. From a large number of tests it was found that when

$$B \geqslant 2.5 \frac{K^2}{{\sigma_{yp}}^2} \tag{9}$$

K_{Ic} was constant and independent of thickness [*1*]. Here B is the thickness, K is the applied stress intensity, and σ_{yp} is the yield strength. Stress intensity loses its normal significance in the presence of large scale yielding. Equation 9 is of no help in setting limits for the J_{Ic} approach. Such limits must be defined on the basis of experiments analogous to the case of K_{Ic} measurements. A simple rule in terms of average thickness direction strain may prove satisfactory.

It is important to note that in terms of the J integral failure criterion plane strain refers to large scale or general yielding behavior. Relatively small specimens may fail in plane strain depending on the in-plane geometry and the thickness compared to the in-plane dimensions. Linear elastic fracture mechanics requires that in-plane dimensions be large compared to the crack tip plastic zone size. This need not be true for the J_{Ic} approach. For example, a precracked Charpy bar undergoing limit load failure at a moderate deflection may fail in plane strain. Constraint is supplied by the essentially elastic material above the crack tip and a compression zone of approximately half the ligament depth. Guides to permissible dimensions may be found in the extensive literature on plane strain limit load problems. However, the real limits should be established experimentally.

The most severe criticism of a one parameter fracture criterion in the general plane strain elastic-plastic regime arises from the fact that radically different limit load slip line fields may develop. On the one hand there is the contained centered fan slip line field typified by the externally deep notched bar. The region ahead of the crack tip in Fig. 3*b* is one of high hydrostatic stress. On the other hand the slip line field for an internally notched bar does not result in hydrostatic stress elevation. McClintock [*14*] has noted that crack tip separation mechanisms should be affected by the two types of macroscopic slip line fields. Hydrostatic stresses will strongly encourage void formation and growth in the first case. In contrast, the slip line field in Fig. 3*a* may promote crack advancement by alternate slip as shown in Fig. 3*c*. These considerations are equivalent to saying remote deformation patterns will destroy any characteristic crack tip singular behavior for limit load failures. This would limit the J_{Ic} approach to contained plasticity.

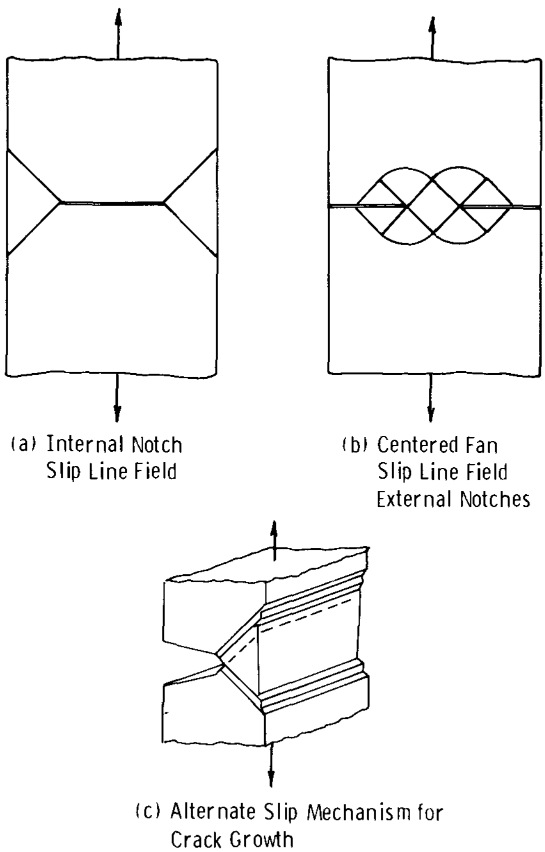

FIG. 3—*Macroscopic slip line fields and alternate slip crack growth pattern.*

Tests are in progress to examine the effect of different slip line fields on the J_{Ic} criteria. It is our speculation that crack tip "blunting" effects will override differences in macroscopic slip line fields. Just as the very presence of a sharp crack is the overwhelming consideration in determining the near tip elastic stress field, the presence of a plastic crack tip singularity and the manner in which the crack physically "blunts" may be the overwhelming considerations in the fracture of elastic-plastic solids. Rice [*13*] has pointed out that the crack tip centered fan slip line field does not result in concentrated strains ahead of the crack tip. Only by considering crack blunting is this physically realistic result obtained. Rice found the region of concentrated strain to be approximately twice the crack opening displacement (COD). Typically this is nearly two orders of magnitude smaller than other component dimensions. From a macroscopic slip line point of view crack tip blunting is negligible, whereas it may actually dominate fracture behavior.

Advantages of the J_{Ic} *Approach*

Since the path independent J integral is a field parameter, the J_{Ic} fracture criterion is compatible with any criterion based on features specific to the crack tip region. There is no discrepancy between the J_{Ic} approach and fracture criteria based on a COD, a critical strain over some characteristic microstructural distance or other like parameters. The advantage of the J integral over such parameters is that accurate analysis is not needed in the region where such calculations are most difficult. The crack tip area is precisely where analysis is most subject to error. The J integral should be accurately evaluated if the gross features of elastic-plastic behavior away from the crack tip are suitably determined. One would thus expect evaluation of the J integral to be faster and easier than calculation of crack tip features, especially for finite element techniques.

Simple compliance type experiments can be used to determine the value of the J integral. This is a distinct advantage over those parameters which depend only on analysis. Even the COD approach has its experimental pitfalls. With the British method of measurement [*15*] the assumed center of rotation of the bend bar changes with increasing amounts of plasticity. It is only after the full development of plasticity that this center of rotation remains relatively constant.

As with the COD value, J_{Ic} is simply related to the parameters of linear elastic fracture mechanics.

$$J_{Ic} = G_{Ic} = \frac{1-\nu^2}{E} \; K_{Ic}{}^2 \tag{10}$$

This relation is unambiguous. In relating COD to G_{Ic}, there is some question as to whether or not the value of the yield strength should be elevated due to constraint. Equation 10 in a sense allows a direct extension of linear elastic fracture mechanics into the elastic-plastic and general yielding range.

Experimental Procedure

Materials and Test Specimens

In order to evaluate the J integral as a failure criterion, a series of tests were performed using a pressure vessel steel, A533B Class 2, and an intermediate strength rotor steel, Ni-Cr-Mo-V alloy heat 1196. The A533B specimens were machined from part of a large test specimen used to evaluate the 02 baseplate in the Heavy Section Steel Technology program. Complete documentation of the mechanical properties of this material can be found in the work of Wessel et al [*16*] and others [*17*]. The properties of the Ni-Cr-Mo-V alloy can be found in a paper by Begley and Toolin [*18*]. For the present, it is sufficient to note that the room temperature 0.2 percent offset yield strengths of A533B, and Ni-Cr-Mo-V steels were 70 and 135 ksi, respectively.

One-inch (1TCT) and two-inch (2TCT) thick compact tension specimens of A533B were tested along with 0.788-in.^{2} bend bars. The test temperature was nominally room temperature. Loading of the compact tension specimens followed ASTM recommendations [*19*]. Three point loading was used for the bend specimens, with a nominal span of four times the depth.

Only bend bars were tested of the Ni-Cr-Mo-V alloy. The larger size was 0.948 by 0.788 by 4.3 inches. The smaller size was exactly one-half of the larger. Again three point loading was used. The test temperature was 200 F which is the start of upper shelf K_{Ic} behavior. Fully ductile fracture surfaces were observed for the rotor steel. Time to failure for all specimens was in the range of 1 to 2 min.

Evaluation of the J *Integral*

Values of the J integral were calculated from load-displacement curves following the interpretation outlined earlier. At a given total deflection the area under the load-displacement curve was found using a polar planimeter. This energy at constant displacement was plotted as a function of crack length. The slope of this curve is equal to $\Delta U/\Delta \ell$, the change in potential energy per unit change in crack length. J is merely $-\Delta U/\Delta \ell$, normalized to unit thickness.

Since J is experimentally evaluated in terms of an energy input to a system, the location of the displacement gage points must be such that the load displacement curve represents a well defined energy input. In general load versus crack opening curves cannot be used. The product of load and crack opening does not give a physically interpretable energy input to system with well defined boundaries.

For the bend bar tests, load versus ram travel curves were recorded. The area under these curves represents the energy absorbed between the gage points. Therefore, these curves are suitable for the experimental evaluation of the J integral. For tests of compact tension specimens, displacements at the face of the specimens were measured with a clip gage. These values were empirically adjusted to obtain displacements at the location of the loading pins. Hence, curves of load versus pin displacement reflecting the total work done on the test specimen, were used to experimentally determine J.

One very important characteristic of the steels tested was that prior experience showed crack initiation to be generally coincident with rapid propagation for small specimens. Instances of stable crack extension under rising load has not been observed either by ultrasonic techniques or metallographic sectioning for the relative small specimens tested. Crack initiation was unambiguously defined by a drop in load. In the pressure vessel steel the load drops were generally abrupt. For limit load ductile rupture of the rotor steel, the load drops were more gradual, probably due to rigidity of the bend specimens and fixture and the ductile mode of tearing.

Results

A summary of test data is listed in Tables 1 and 2. Values of J_{Ic} and illustrations of the method of experimentally determining J are presented in the following paragraphs.

TABLE 1–*Summary of test data of a Ni-Cr-Mo-V steel (FD1196).*

Specimen Bend Bars	Maximum Load, lb	Crack Size a, in.	a/W[a]	Total Deflection δ_{max}, in.	Plastic Deflection δ_p, in.	COD,[b] in.
0.474 by 0.394 by 2.16 in.	Span = 1.58					
1196 FC1	5700	0.123	0.259	0.0235	0.0105	0.0047
1196 FC2	5920	0.119	0.251	0.024	0.0110	0.0050
1196 FC3	4470	0.168	0.354	0.0245	0.0130	0.0051
1196 FC4	4320	0.173	0.365	0.0245	0.0112	0.0042
1196 FC5	3360	0.214	0.452	0.0245	0.0120	0.0040
1196 FC6	3270	0.218	0.460	0.0222	0.0112	0.0036
1196 FC7	2275	0.265	0.559	0.0232	0.0132	0.0035
1196 FC8	2410	0.261	0.551	0.022	0.0120	0.0032
1196 FC9	860	0.349	0.736	0.0245	0.0160	0.0025
1196 FC10	1225	0.324	0.683	0.023	0.0150	0.0029
1196 FC12	725	0.356	0.751	0.028	0.0200	0.0030
0.948 by 0.788 by 4.3 in.						
Series 1	Span = 3.90					
1196 DFC3	11900	0.362	0.382	0.062	0.015	0.0045
1196 DFC6	8100	0.452	0.488	0.059	0.012	0.0033
1196 DFC8	3100	0.643	0.679	0.064	0.022	0.0034
Series 2	Span = 3.70					
1196 DFC1	8520	0.470	0.496	0.045	0.008	0.0021
1196 DFC2	4340	0.608	0.642	0.048	0.012	0.0022

[a] W = depth of bend bar

[b] Rigid body rotation assumed about mid ligament point. Only plastic deflection was considered in COD calculation.

TABLE 2—*Summary of test data of A533B steel.*

Specimen	Maximum Load, lb	Crack Size a, in.	a/W^a	Total Deflection δ_{max}, in.	Plastic Deflection δ_p, in.	COD,[b] in.
ZTCT						
HS2-17-5	57 000	2.002	0.500	0.075	0.020	0.0048
HS2-17-6	52 000	2.095	0.526	0.080	0.025	0.0057
HS2-17-7	46 200	2.210	0.552	0.080	0.024	0.0053
HS2-17-8	41 500	2.295	0.576	0.080	0.025	0.0048
ITCT						
8-4-1	15 740	1.005	0.502	...	...	...
8-4-2	13 850	1.058	0.529	...	...	...
18-4-2	12 000	1.094	0.547	0.070	0.038	0.0079
18-4-3	10 800	1.146	0.573	0.073	0.038	0.0074
18-4-4	9 200	1.207	0.604	0.068	0.032	0.0056
Bend Bars 0.788 square by 4.3	Span = 3.15					
DCF 12	11 750	0.173	0.220	0.114	0.092	0.036
DCF 13	8 770	0.255	0.324	0.097	0.077	0.026
DCF 14	7 050	0.318	0.404	0.106	0.077	0.023
DCF 15	4 350	0.415	0.526	0.112	0.092	0.022
DCF 16	2 800	0.493	0.627	0.097	0.077	0.015

[a] W = width of CT specimens or depth of bend bar.

[b] Rigid body rotation assumed about mid ligament point.
Only plastic deflection was considered in COD calculation.

Ni-Cr-Mo-V Rotor Steel

Figure 4 shows a plot of the work done to a given deflection versus crack length for the small Ni-Cr-Mo-V bend bars. This work is simply the area under the load deflection curve at the given deflection. The slopes of the curves in Fig. 4 are the changes in potential energy per unit thickness per unit change in crack length. As stated earlier $-\Delta U/\Delta \ell$ is equal to J. Hence the slopes of the curves in Fig. 4 enable the determination of J as a function of deflection for any crack length. Values of J were calculated for straight lines fitted to the data by the method of least squares. Except for the longest and shortest crack slopes obtained from best fit second order polynominals differed by no more than a few percent. Figure 5 shows J as a function of deflection. To a good approximation J at a given deflection does not vary over the range of crack sizes studied. From Fig. 6 it is seen that the average deflection at failure was near 0.024. This results in a critical J, that is, J_{Ic}, or 950 in./lb/in.^{2} Neglecting the

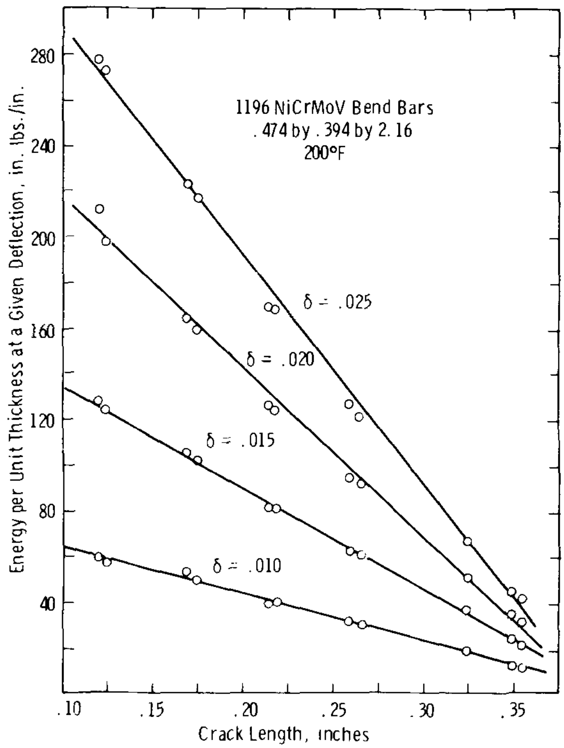

FIG. 4—*Energy absorbed at a given deflection versus crack length, NiCrMoV steel bend bars.*

extremes of crack length it is seen using Figs. 5 and 6 that J_{Ic} has a range of 850 to 1000 in./lb/in.[2] This variation of ±15 percent in J_{Ic} corresponds to a variation of nearly ±8 percent in K_{Ic}. For rotor steels K_{Ic} can easily vary as much as ±15 percent. Hence, the experimental variation in J_{Ic} is actually better than what might be expected. Values of J_{Ic} obtained from the very limited number of tests of double size bend bars are in good agreement being 1020 in./lb/in.[2] The next section discusses the relationship and significance of J_{Ic} values from these fully plastic bend bars and G_{Ic} values for the same material obtained from essential elastic failure of 8-in. thick compact tension (8TCT) specimens. For interest sake typical fracture surfaces are shown in Fig. 7.

A533B Pressure Vessel Steel

The work done on 2TCT specimens of A533B steel is plotted in Fig. 8 as a function of crack length. Each curve refers to the energy absorbed at a given deflection. Again taking the slopes of the curves for various values of deflection J values were calculated. From Fig. 8 it is seen that the deflection at failure was 0.080 in. except for the specimen with the shortest crack. In this case the deflection at failure was 0.075 in. This is consistent with the indication that the

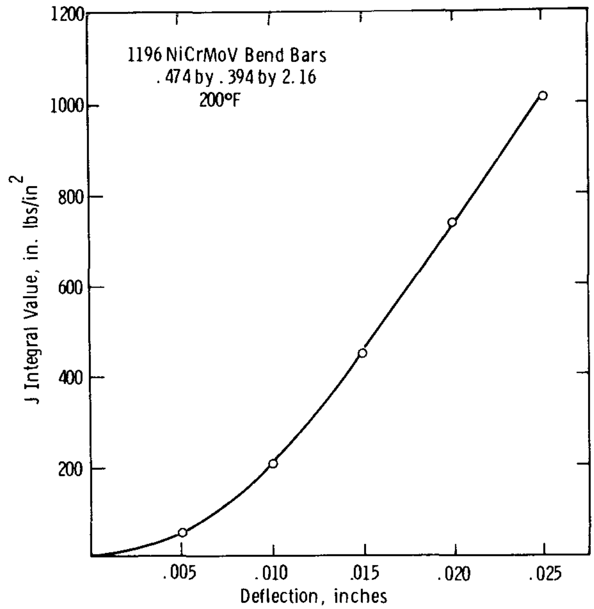

FIG. 5—J *value as a function of deflection, NiCrMoV bend bars.*

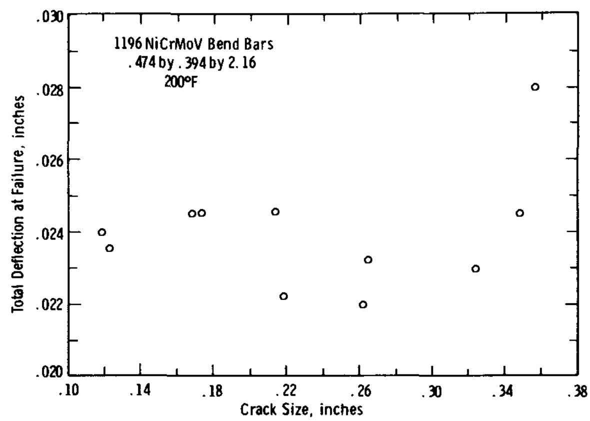

FIG. 6—*Total deflection at failure versus crack size, NiCrMoV bend bars.*

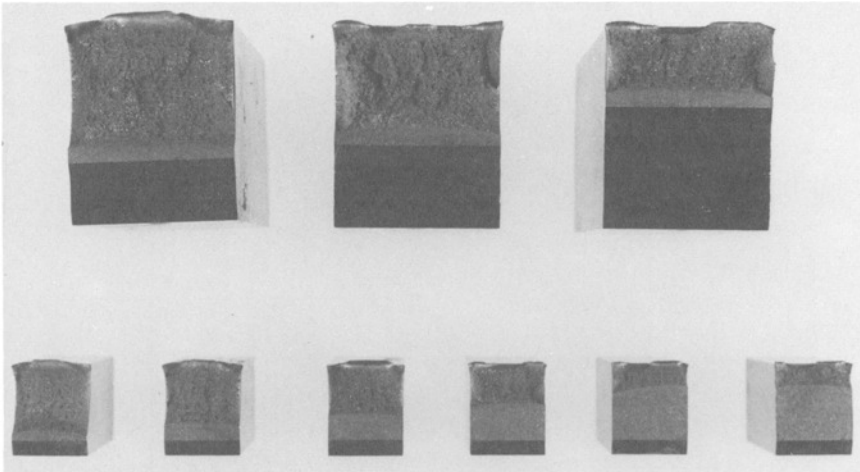

FIG. 7—*Fracture appearance of NiCrMoV steel bend bars.*

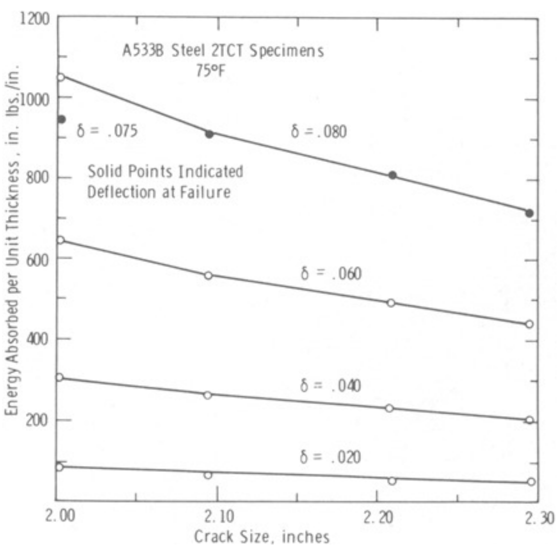

FIG. 8—*Energy absorbed at a given deflection versus crack size A533B 2TCT specimens.*

slope of the $\delta = 0.080$ curve in Fig. 8 begins to increase at the smallest crack length. Consistency of J_{Ic} then requires failure to occur at a smaller deflection. The actual value of J_{Ic} was calculated to be 945 in./lb/in.^{2} Following a similar procedure for 1TCT specimens, the experimental J_{Ic} was 1030 in./lb/in.^{2} Both of these numbers are in good agreement with results of a test on a 12-in. thick compact tension specimen of the same material and extrapolated value of the K_{Ic} versus temperature curve [*16*]. Converting expected values of K_{Ic} at 75 F to G_{Ic} yields a result of about 1100 in./lb/in.^{2} which should be equal to J_{Ic}. Considering the extreme temperature variation of the toughness of A533B near 75 F, the consistency of G_{Ic} and J_{Ic} is very good.

Bend bars of A533B steel were also tested. The test temperature was nominally 75 F, or room temperature. However, the initiation of fracture in the bend bars was ductile compared to the fully cleavage fracture of the compact tension specimens. The question of whether specimen geometry or test temperature was responsible for the difference in fracture appearance was settled by tests of identical bend bars in carefully controlled isothermal baths. Comparison of the fracture appearance of these bars with the original bend bars indicated an original test temperature of 85 to 90 F. From the work of Wessel et al [*16*], on the toughness of A533B it is evident that a change in test temperature from 75 to 85 F or higher should caused a substantial increase in toughness. The measured J_{Ic} values for the bend bars were in the range of 2000 in./lb/in.^{2} In terms of K_{Ic} this would be about 250 ksi $\sqrt{\text{in}}$. This is a reasonable estimate of the start of upper shelf toughness of the HSST 02 baseplate.

Discussion

The objective of the experiments previously described was to demonstrate the potential of the J integral as a failure criterion. If J_{Ic} is a valid failure criterion, it must be independent of geometry. Also, because the J concept applied equally well to structures failing in the essentially elastic or fully plastic range, J_{Ic} must be related to K_{Ic}. As shown earlier, this relationship can be stated in terms of

$$J_{Ic} = G_{Ic} = \frac{(1-\nu^2)}{E} \; K_{Ic}{}^2$$

This latter requirement can be tested by comparing J_{Ic} for the fully plastic Ni-Cr-Mo-V bend bars with the valid upper shelf G_{Ic} toughness established by Begley and Toolin [*18*] for the same materials. A good average J_{Ic} value is 1000 in./lb/in.^{2} The plane strain fracture toughness at the same temperature is 200 ksi $\sqrt{\text{in}}$., giving a G_{Ic} value of 1200 in./lb/in.^{2} But the agreement of J_{Ic} and G_{Ic} is even better than this indicates. The K_{Ic} value was based on 2 percent crack growth. In the 8TCT tests up to 0.160 in. of crack growth, evidenced by audible popin and load perturbations, occurred prior to the K_{Ic} load. Initiation of growth started closer to a G_I value of 1000 in./lb/in.^{2}

Additional data supporting the equivalence of experimental J_{Ic} and G_{Ic} values have been presented in the results. Measured J_{Ic} values for A533B steels at 75 and 85 F agree well with extrapolated G_{Ic} values.

The geometry independence of J_{Ic} is supported by the fact that a reasonable ±15 percent variation at most in J_{Ic} is exhibited when all the test data is compared. This includes comparison of the fully plastic single and double size bend bars of Ni-Cr-Mo-V over a range of crack lengths and the 8-in. thick essentially elastic compact tension specimens. Likewise the A533B 1 and 2-in. thick compact tension specimens have essentially the same J_{Ic} over a range of crack sizes.

Our view on the effect of radically different fully plastic slip line fields has been expressed. Preliminary results on center cracked panels bear out the original conclusion. These results will be reported shortly.

A final point which needs to be emphasized is that the J_{Ic} failure criterion has its limitations. These limitations are similar to those restricting the applicability of the linear elastic K_{Ic} criterion. As presently stated, the concept of J refers to two-dimensional problems, J_{Ic} refers to crack initiation and for the present only plane strain conditions; that is, plane strain even in the fully plastic region. The validity of the J_{Ic} failure criteria rests on the dominance of the Hutchinson-Rice-Rosengren crack tip singularity. When combinations of specimen geometry, flow properties, and other relevant factors destroy this dominance, the applicability of J_{Ic} will be limited.

Summary and Conclusions

(1) The J integral is an average measure of the near tip stress strain environment of cracked elastic plastic bodies, as such it is an attractive failure criterion.

(2) Being a field parameter J is compatible with COD and other approaches concerned with specific crack tip features.

(3) The J integral should be relatively easy to calculate compared to parameters of the near tip environment.

(4) J values were determined experimentally for a Ni-Cr-Mo-V rotor steel and a A533B pressure vessel steel. Failure occurred at a critical J, termed J_{Ic} to denote a critical plane strain value. A number of specimen types and crack lengths were included.

(5) For the J_{Ic} criterion to be truly valid J_{Ic} must equal G_{Ic}. This was shown to be true for the Ni-Cr-Mo-V steel, J_{Ic} from limit load failures of small bend bars were in excellent agreement with G_{Ic} values from essentially elastic failures of 8-in. thick compact tension specimens.

(6) The potential of the J integral as a failure criterion has been demonstrated by experiment.

(7) Limitations of the J_{Ic} concept have been reviewed in a general manner and are analogous to those involved in the use of K_{Ic}.

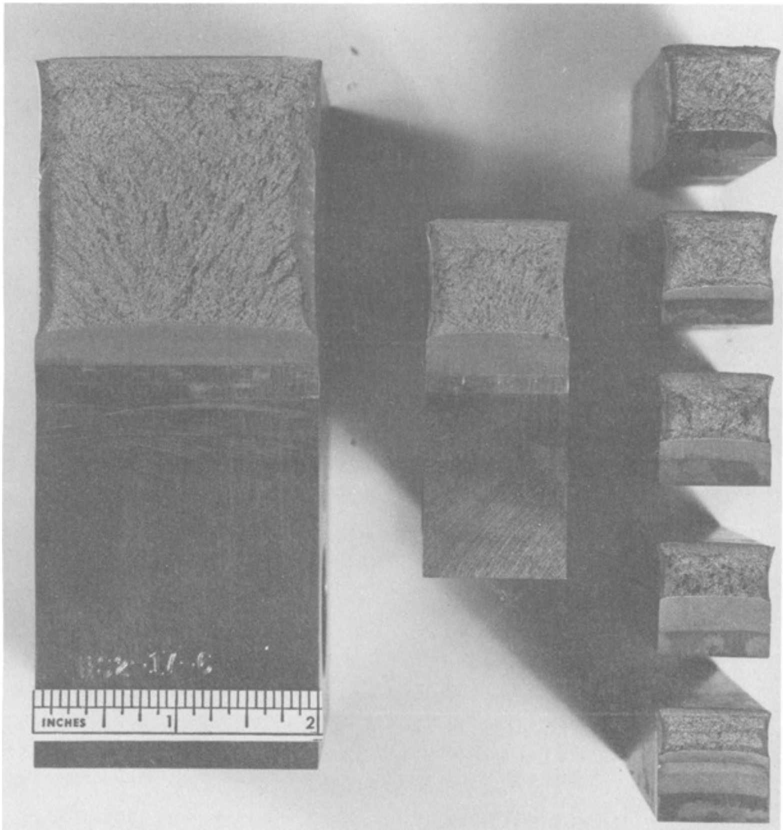

FIG. 9–*Fracture appearance of A533B steel specimens.*

(8) Radically different slip line fields may limit the applicability of J_{Ic}. But this effect will be out-weighed by the dominance of the HRR crack tip singularity.

Acknowledgments

We wish to express our appreciation to our colleagues at the Westinghouse Research Laboratories; to A.R. Petrush and F.X. Gradich who performed much of the experimental work, and especially to Dr. W.K. Wilson for many valuable discussions on the J integral and elastic-plastic analysis.

References

[1] Brown, W.F., Jr., and Srawley, J.E., *Plane Strain Crack Toughness Testing of High Strength Metallic Materials, ASTM STP 410,* American Society for Testing Materials, 1966.
[2] Hutchinson, J.W., *Journal of the Mechanics and Physics of Solids,* Vol. 16, 1968, pp. 13-31.
[3] Rice, J.R. and Rosengren, G.F., *Journal of the Mechanics and Physics of Solids,* Vol. 16, 1968, pp. 1-12.
[4] Hilton, P.D. and Hutchinson, J.W., *Plastic Stress Intensity Factors for Cracked Plates,* presented at the Third National Symposium on Fracture Mechanics, Lehigh University, Report SM-34, Aug. 1969.
[5] Srawley, J.E., Swedlow, J.L., and Roberts, E., Jr., *On the Sharpness of Cracks Compared with Wells COD,* NASA Technical Memorandum, NASA TMX-52904, Lewis Research Center, Cleveland, Ohio, Sept. 1970.
[6] Rice, J.R., *Journal of Applied Mechanics, Transactions of the American Society of Mechanical Engineers,* June 1968, pp. 379-386.
[7] McClintock, F.A. in *Fracture,* H. Liebowitz, Ed., Vol. 3, Academic Press, New York, 1971, pp. 47-225.
[8] Hayes, D.J., *Some Applications of Elastic-Plastic Analysis of Fracture Mechanics,* Ph.D. dissertation, Imperial College, University of London, Oct. 1970.
[9] Hutchinson, J.W., *Journal of the Mechanics and Physics of Solids,* Vol. 16, 1968, pp. 337-347.
[10] Irwin, G.R. in *Structural Mechanics,* Proceedings of the First Naval Symposium on Structural Mechanics, J.N. Goodier and N.J. Hoff, Eds., Pergamon, 1960, p. 557.
[11] Saunders, J.L., *Journal of Applied Mechanics,* Vol. 27, 1960, pp. 352-362.
[12] Rice, J.R. in *Fracture,* H. Liebowitz, Ed., Vol. 2, Academic Press, New York, 1968, pp. 191-311.
[14] McClintock, F.A. in *Development in Mechanics,* Vol. 5, Proceedings of the 11th Midwestern Applied Mechanics Conference, Iowa State University, University Press, Ames, Iowa, 1969, pp. 971-976.
[15] Nichols, R.W., Burdekin, F.M., Cowan, A., Elliott, D., and Inghan, T., *The Use of Critical Crack Opening Displacement Techniques for the Selection of Fracture Resistant Materials,* Proceedings of the Symposium on Fracture Toughness Concepts for Weldable Structural Steel, Culceth, England, April 1969.
[16] Wessel, E.T., Clark, W.G., Jr., and Pryle, W.H., *Fracture Mechanics Technology Applied to Heavy Section Steel Structures,* Proceedings of the Second International Conference on Fracture, Brighton, England, April 1969.
[17] Witt, F.J., *Nuclear Engineering and Design,* Vol. 8, No. 1, July 1969, pp. 22-34.
[18] Begley, J.A. and Toolin, P.R., *Fracture Toughness and Fatigue Crack Growth Rate Properties of a Ni-Cr-Mo-V Steel Sensitive to Temper Embrittlement,* Presented at the Fourth National Symposium on Fracture Mechanics, Carnegie Mellon University, Pittsburgh, Pa., Aug. 1970.
[19] "Method of Test for Plane-Strain Fracture Toughness of Metallic Materials," ASTM E 399-70T, *Annual Book of ASTM Standards,* 1970.

DISCUSSION

P.C. Paris[1] *(written discussion)*—In applying J as a failure criterion to large scale yielding problems, including fracture under limit load conditions, the ASTM plane strain thickness index, namely,

$$B \geqslant 2.5\left(\frac{K_{\mathrm{Ic}}}{\sigma_{yp}}\right)^2$$

must be replaced by a new criterion to define local plane strain. The region to which plane strain must be appropriate now seems only to be required to encompass the region at the crack tip where the critical separation processes are taking place.

It is noted that J/σ_{yp} is linearly related to COD where the constant of proportionality of nearly one mildly depends upon specimen configuration. Thus J/σ_{yp} is a size parameter which should represent the order of the process zone size. Consequently, it seems reasonable to examine replacing the ASTM criteria for plane strain by

$$B \geqslant \alpha \frac{J_{\mathrm{Ic}}}{\sigma_{yp}}$$

for use of J as a plane strain fracture criterion.

An initial suggestion or guess of an appropriate α of approximately 50 to Drs. Begley and Landes has been borne out by their data. Further exploration of this thickness requirement is desirable.

I feel that this paper finally explains the reasonableness of the Rolfe-Novak-Barsom correlation of upper shelf Charpy values, CVN, with K_{Ic} numbers, that is,

$$\left(\frac{K_{\mathrm{Ic}}}{\sigma_{yp}}\right)^2 = \frac{5}{\sigma_{yp}}\left[\mathrm{CVN} - \frac{\sigma_{yp}}{20}\right]$$

This equation relating, CVN, a limit load related energy parameter, to K_{Ic} is not only now acceptable but is, for us, in agreement with the J failure criteria.

[1] Del Research Corp., Hellertown, Pa.

Moreover, the loss of correlation by this equation at σ_{yp} less than 120 ksi (or better CVN greater than one hundred ft·lb) may be due to the violation of

$$B \geqslant 50 \frac{J_{Ic}}{\sigma_{yp}}$$

Again, all these thoughts are speculative, but so promising as to warrant requesting further comments on them by Drs. Begley and Landes.

G.R. Irwin[2] *(written discussion)*—When a critical load for crack extension is measured using a compact tension or notched-bend specimen, the only characterization parameter which is determined without ambiguity is the thickness-average value of G. Careful measurements of the change of compliance with crack size, dC/da, have agreed within a few percent with two-dimensional numerical computations. At NRL, compliance observations using notched-bend specimens showed no influence of the depth to thickness ratio across the range $W/B = 8$ to $W/B = 4/3$. From this one would expect the relationship of K^2 to the thickness-average G is given by

$$E\bar{G} = \bar{K}^2$$

From this viewpoint, the K calculations of the ASTM K_{Ic} testing method correspond nearly to assuming $K_{Ic} = \sqrt{E\bar{G}}$

Begley and Landes compare values termed J_{Ic} from specimens which undergo general yielding prior to crack extension to values of G_{Ic} from the equation

$$E\,G_{Ic} = (1 - \nu^2)\,K_{Ic}{}^2$$

where K_{Ic} is provided by ASTM K_{Ic} tests using specimens of adequate size. However, in the case of the ASTM K_{Ic} test as well as in the case of the present J_{Ic} tests, values of the characterization factor for mid-thickness regions of the initial crack are not directly determined. In both cases it is the thickness-average values of G and J which are measured.

Some readers may feel that the value of the thickness-average G (from $EG = K_{Ic}{}^2$) should have been compared to the thickness average value of J (for initiation of crack extension). The G/J ratio found by the authors was well above unity and the alternative comparison method suggested above would increase this ratio by about 9 percent. This does not lessen interest in the findings. Clarification of the situation will, in fact, be assisted if we keep in mind that the comparison which is of primary theoretical interest concerns the G and J values locally applicable to central regions of the leading edge of the initial crack rather than the thickness averages which are directly observed. For example, the plastic thickness contraction in tensile regions of the J determina-

[2] Lehigh University, Bethlehem, Pa.

tion specimen may elevate the tensile stress parallel to the leading edge of the crack, σ_z, in mid-thickness regions to a greater extent than would occur in the larger specimens used for K_{Ic} testing. Elevation of σ_z would elevate the resistance to plastic yielding and thus might elevate the J value local to central regions of the leading edge of the initial crack. The explanation by the authors of the G to J discrepancy in terms of the larger initial crack extension which accompanies a K_{Ic} observation remains applicable, but need not be regarded as the only contributing factor. This paper, along with the companion paper by the same authors, provides a new viewpoint on fracture measurements of unusual novelty and importance.

J.A. Begley and J.D. Landes (authors' closure)—We thank Dr. Paris and Dr. Irwin for their comments.

Dr. Paris' suggestion of developing limits to the applicability of J based on the thickness relative to J_{Ic}/σ_{yp} is certainly attractive. It is consistent with our premise that the logic of J as a fracture criterion rests on a crack tip plastic singularity of the HRR type. It is reasonable that this dominance should break down when the thickness and other pertinent dimensions, such as crack length and remaining ligament, become comparable with a crack tip uncertainty region characterized by J_{Ic}/σ_{yp}. Thanks to Dr. Paris our current experimental work is proceeding on this tack.

In reply to Dr. Irwin, we agree there are contributions to the difference between G_{Ic}, obtained from K_{Ic} tests, and J_{Ic} other than a large difference in the extent of crack growth at the measurement points. There are a number of viewpoints on the relationship of K_{Ic} to the thickness averaged, measured values of G_{Ic} and J_{Ic}. Our present thinking is to retain the $1-\nu^2$ term. Relating G to K in the linear elastic case by means of the stress field equations and a virtual crack advance would seem to require the $1-\nu^2$ term for plane strain. On a macroscopic basis, the problem is one of generalized plane stress, hence elastic compliance measurements might not reveal a significant thickness dependence.

J. D. Landes[1] *and J. A. Begley*[1]

The Effect of Specimen Geometry on J_{Ic}

REFERENCE: Landes, J.D. and Begley, J.A., "**The Effect of Specimen Geometry on J_{Ic}**," *Fracture Toughness, Proceedings of the 1971 National Symposium on Fracture Mechanics, Part II, ASTM STP 514,* American Society for Testing and Materials, 1972, pp. 24-39.

ABSTRACT: Rigid-plastic slip line field analysis shows that fully plastic flow fields and hydrostatic stress elevation are greatly influenced by geometry. This argues against a one parameter fracture criterion, such as J_{Ic}, which purports to work in the plastic range. Two specimen geometries, a center cracked panel and a bend bar were tested to provide a critical evaluation of the J_{Ic} concept. An intermediate strength Ni-Cr-Mo-V rotor steel was used in the investigation. Results show that J_{Ic} is a consistent fracture criterion for plane strain behavior for essentially elastic to fully plastic conditions. This work supports the contention that a plastic crack tip singularity is a dominant consideration for crack initiation even in fully plastic bodies.

Bend bars of two thicknesses were tested to show that nearly plane strain behavior can be achieved with conventional geometries as much as an order of magnitude smaller than sizes required for linear elastic plane strain fracture toughness tests. The method used for calculating the J integral for experimental load versus deflection curves is explained in detail.

KEY WORDS: fracture (materials), failure, crack initiation, cracking (fracturing), geometries, plastic theory, stresses, bend tests, rotor steels

The fracture mechanics approach of using K_{Ic} to predict unstable crack extension in a crack notched body has proved successful for the limited case of linear elastic plane strain fracture [*1*]. Complex structures may have stresses in some regions which exceed the elastic limit. This has created need for a fracture criterion which would also include elastic-plastic to fully plastic behavior. Begley and Landes [*2*] have demonstrated experimentally that the path independent J integral proposed by Rice [*3*] apparently can be used to predict fracture in low to intermediate strength steels for plane strain conditions ranging from linear elastic to fully plastic. The value of J at the onset of initial crack growth, J_{Ic}, was a constant over the entire range and was equal to G_{Ic}, the energy release rate per unit crack extension in the linear elastic range.

[1] Mechanics Dept., Westinghouse Research Laboratories, Pittsburgh, Pa. 15235.

For fully plastic behavior the stress state in the ligament ahead of the crack is greatly influenced by geometry. Rigid-plastic slip line theory shows changes in constraint or loading configuration cause radical changes in macroscopic flow fields with resultant changes in hydrostatic stress ahead of the crack. These changes might influence the fracture mode and the value of J_{Ic}. If the J integral is a valid one-parameter fracture criterion, then it cannot be influenced by these differences in specimen geometry. However, the experimental verification of J_{Ic} was conducted on only two specimen types, 3 point bend bars and compact tension specimens [*2*]. In both cases the loading is predominantly bending and the slip line fields are similar to those proposed by Green and Hundy [*4*]. To provide a critical evaluation of the J_{Ic} concept, specimens with radically different slip line fields must be tested.

In this work a first step was taken to determine what effect specimen geometry might have on J_{Ic}. Center cracked panels of an intermediate strength Ni-Cr-Mo-V rotor were tested and results were compared with previously tested bend bars of the same material. There is little if any hydrostatic stress elevation in the internally cracked geometry whereas the bend bars have a moderate stress elevation [*4*]. In addition tests were made on bend bars of double thickness to determine whether conventional thickness provides proper constraint to insure a predominantly plane strain deformation mode. The method for calculating J from load deflection curves is demonstrated in detail using these tests as examples and the determination of J_{Ic} is discussed.

Effect of Geometry

For fully plastic behavior rigid-plastic slip line theory shows the magnitude of stresses may change radically with changes in geometry. An internally notched specimen in tension has slip lines emanating from the notch tip at 45 deg to the applied load, Fig. 1*a*. There is no stress elevation ahead of the crack and the limit load, P_L, is

$$P_L = 2\tau_0 B(w - 2a) \tag{1}$$

where τ_0 is the shear flow stress, B is the thickness, w is the width, and $2a$ is the notch length.

In contrast the deep double edge notched specimen has a Prandtl slip line field, Fig. 1*b*, with a significant stress elevation ahead of the notch. For the fully plane strain case with a sharp crack the stress normal to the crack is $(2 + \pi)\,\tau_0$ and the limit load

$$P_L = (2 + \pi)\, B\,(w - 2a)\tau_0 \tag{2}$$

This gives a limit load which is $(1 + \frac{\pi}{2})$ times that of an internally notched specimen when the two have equal net sectional areas.

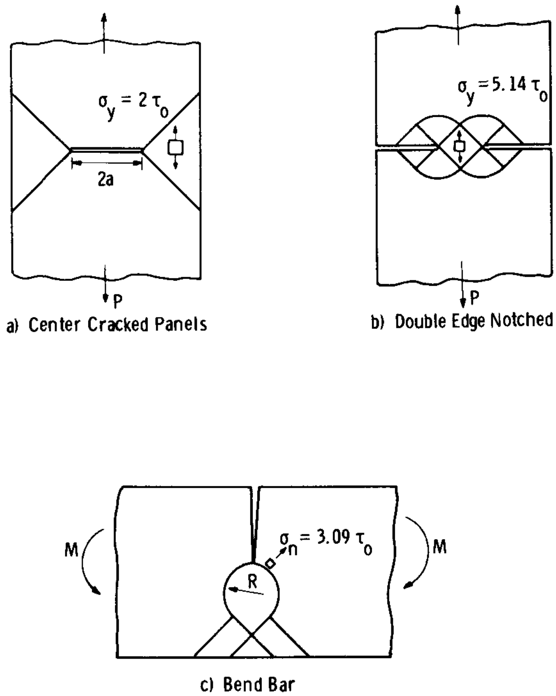

FIG. 1—*Slip line fields for three specimens.*

McClintock [5] has suggested that the mode of crack extension should be different in the two cases. Crack extension under high hydrostatic stress should be predominantly by initiation and growth of internal voids. Under low hydrostatic stress crack extension would be more likely to occur by slipping off on the shear planes. Consequently, no single parameter should apply as a fracture criterion for both cases. However the crack tip plastic singularity with subsequent crack tip "blunting" during loading may override the effect of different macroscopic slip line fields and make J a valid one-parameter fracture criterion.

For a single edge notched bar under bending the slip line field has been described by Green and Hundy [4], Fig. 1*c*. For a sharp crack the stress normal to the flow lines is $(1.543)(2\tau_0)$ [6]. The limit moment, M_L is

$$M_L = (1.261)(2\tau_0)(B)(w-a)^2/4 \tag{3}$$

This gives an elevation in limit moment which is 1.261 times that of an unnotched bar. The constraint of this geometry is intermediate to that of the center notched specimen and the deep edge notched specimen. Comparing J_{Ic} for center cracked panels to that of single edge cracked bend bars gives a first step in the evaluation of J as a valid one-parameter fracture criterion.

Experimental Procedure

Tests were conducted on an intermediate strength rotor steel, Ni-Cr-Mo-V alloy heat 1196. The chemistry and mechanical properties are shown in Table 1.

TABLE 1–*Properties of the Ni-Cr-Mo-V steel, heat 1196.*

Chemical Properties

C	Mn	P	S	Si	Ni	Cr	Mo	V	Sn	Sb
0.28	0.29	0.010	0.008	0.02	3.80	1.76	0.40	0.14	0.019	0.001

Mechanical Properties

	0.2% Offset Yield Strength	Ultimate Tensile Strength	Percent Elongation	K_{Ic}
Room temperature	916 MN/m^2	1020 MN/m^2	16	132 MN/m$^{3/2}$
394 K	855	957	16	220

The center cracked panels, Fig. 2, were loaded in tension at a constant rate of displacement. The displacement was measured over a gage length of 57 mm where stresses are essentially uniform and entirely elastic. Crack lengths ranged from 6.8 to 15.3 mm.

The double thickness bend bars, Fig. 3, were tested in three-point loading. Crack lengths ranged from 3.5 to 9.8 mm. Displacement was measured at the center load point. In both cases the test temperature was 394 K which is in the range of upper shelf K_{Ic} behavior. Specimens were initially notched and then precracked in fatigue prior to testing.

Calculating *J* Experimentally

J can be measured experimentally by a specimen compliance method which is equally applicable from linear elastic to fully plastic behavior. The general approach is evident from the graphical presentation of Rice in Ref *7*. The specific approach of the authors was outlined earlier [*2*] and is recounted here in detail.

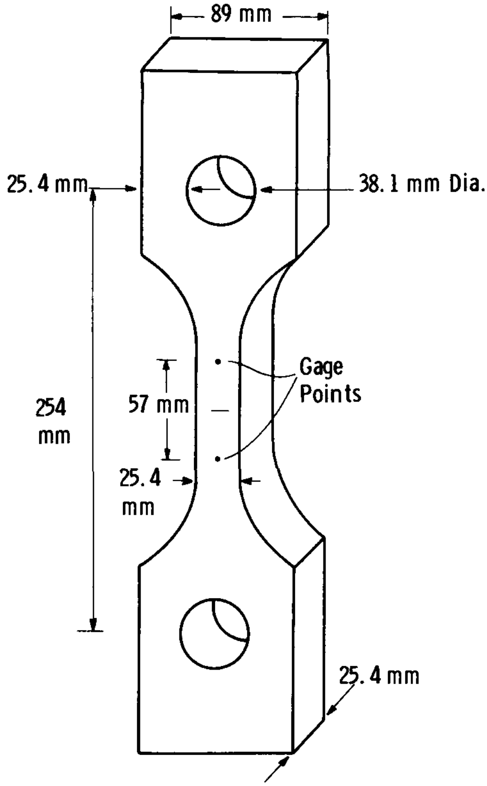

FIG. 2–*Center cracked panel.*

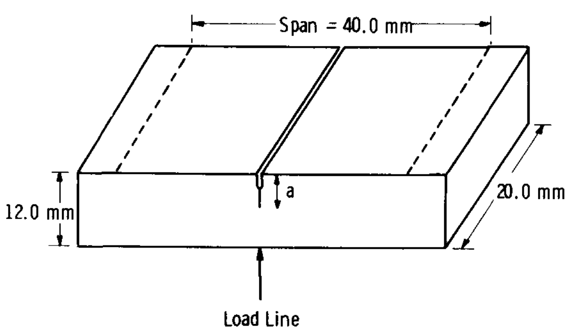

FIG. 3–*Double thickness bend bar.*

As discussed by Rice [7], the J integral can be interpreted as the potential energy difference between two identically loaded specimens of unit thickness having neighboring crack sizes. That is

$$J = -\frac{dU}{da} \tag{4}$$

where U is the potential energy and a is the crack length. The potential energy of a body of area A with a boundary S is given by

$$U = \int_A W dx dy - \int_{S_T} \overline{\mathbf{T}}\,\overline{\mathbf{u}}\, ds \tag{5}$$

The first term is the integrated strain energy density or simply the work done on the body in loading to a given condition. In the second term, $\overline{\mathbf{T}}$ is the traction vector, which specifies the stresses on the boundary S, $\overline{\mathbf{u}}$ is the displacement vector of points on S, and S_T refers to that portion of the boundary over which stresses are prescribed as boundary conditions.

On a plot of load versus load point displacement constructed for two specimens with crack lengths a and $a + \Delta a$, the area between the curves is $J\Delta a$. This is illustrated in Fig. 4. In the case of constant load the additional triangular

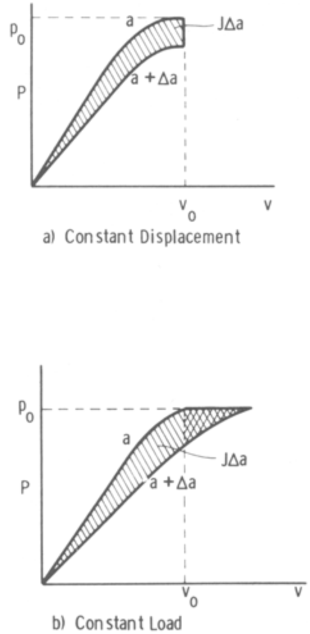

FIG. 4—*Graphical measurement of* J.

area is a second order differential and may therefore be neglected. Hence, J is the same whether determined at constant load or constant deflection.

It is ridiculous, of course, to attempt to measure J by testing two specimens with slightly different crack lengths. By testing specimens of a range of crack length the potential energy U at a given load or displacement can be plotted as a function of crack length. The slope of this curve is dU/da which is $-J$. In essence, this is the procedure which was followed. It is important to note that when displacements are the prescribed boundary condition, that is, when J is evaluated as a function of displacement, the potential energy, U, reduces to the area under the load deflection record. If J is evaluated in terms of load, U is the negative of the area above the load deflection record. Because of the leveling off of load deflection records and the eventual attainment of a limit load, it is more definitive to evaluate J in terms of displacement when there is large scale plasticity. In the latter case, the second term of Eq 5 drops out and the potential energy U is the work done on the body (boundary S) that is, the area under the load deflection curve. In the following sections the thickness, B, appears in some equations since the actual load deflection curves were not normalized to unit thickness.

Bend Bars

To calculate J experimentally load displacement curves are generated for specimens with different crack lengths. For the bend bars some examples are shown in Fig. 5. The curve is integrated graphically to determine the work done in loading to a given displacement. (Areas were measured with a compensating polar planimeter.) Figure 6 shows an example of this; the work done in loading

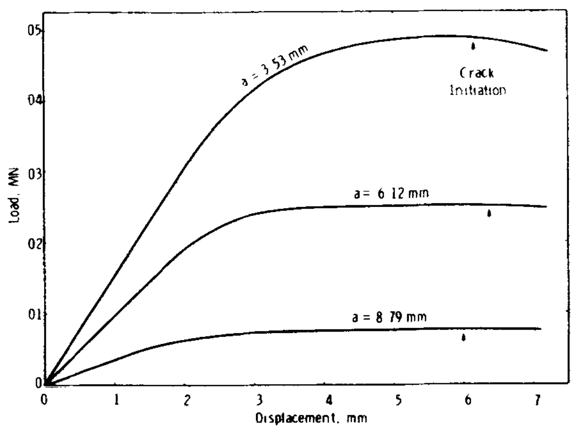

FIG. 5—*Load-displacement curves for double thickness bend bars.*

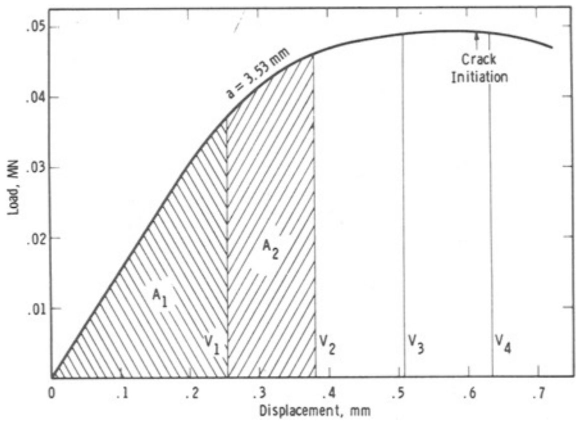

FIG. 6—*Illustration of work to a given displacement.*

to v_1 is A_1, the work done in loading to v_2 is A_1 plus A_2. For each specimen the work was determined at four different displacements. Work was measured to the same four displacement values for each specimen so that a plot of work versus crack length could be made for each of the displacements, Fig. 7. J at constant displacement for a specimen of thickness B,

$$J = -\frac{1}{B} \left. \frac{\partial U}{\partial a} \right|_{v\ =\ \text{constant}} \tag{6}$$

is measured by taking the negative of the slopes of the curves in Fig. 7 and dividing by B. J is then a function of crack length and displacement. The curves in Fig. 7 can be fitted numerically to a polynomial so that J can be determined by differentiating the polynominal. A plot of J versus displacement can then be made, Fig. 8. To determine the critical value of J for crack initiation, J_{Ic}, a critical value of displacement must be determined. From previous work [*2*] it was determined that crack initiation corresponds to the point where the maximum load first begins to drop off, Fig. 5. Therefore, from each load-displacement curve a critical value of displacement is determined and plotted as a function of crack length, Fig. 9. J_{Ic} can then be determined by taking the critical displacement from Fig. 9 and determining its corresponding value of J in Fig. 8.

We do not mean to imply that crack initiation in general, occurs at point of drop off of maximum load. This was found to be true for the particular material tested and only with the relatively small fully plastic test specimens employed. Defining crack initiation and determining its onset is perhaps the most difficult part of measuring J_{Ic}.

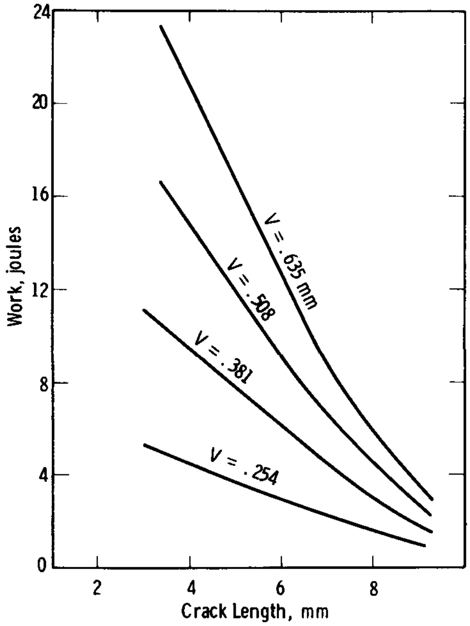

FIG. 7–*Work to a fixed displacement versus crack length for double thickness bend bars.*

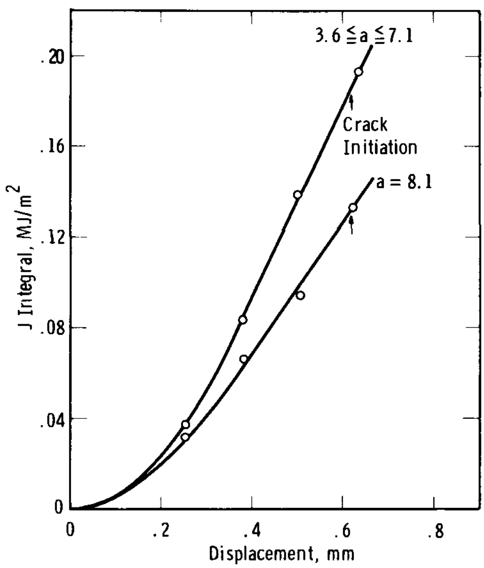

FIG. 8–J *versus crack length for double thickness bend bars.*

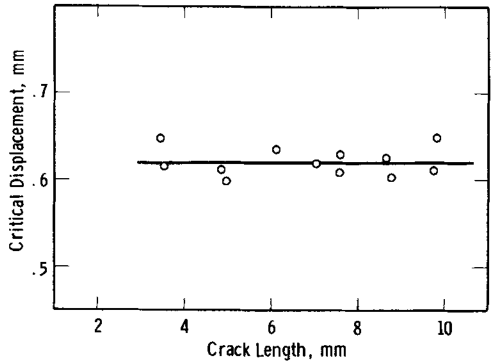

FIG. 9—*Critical displacement for crack initiation versus crack length double thickness bend bars.*

A check can be made on the constraint caused by the specimen geometry, that is, the degree of plane strain, by plotting limit moment versus crack length, Fig. 10. Using the limit solution from Green and Hundy [*4*] and the tensile properties, an estimation of the limit moment for a properly constrained plane strain specimen can be made, Fig. 10. This is done for the specimens used in this experiment as well as conventional thickness bend bars reported in a previous

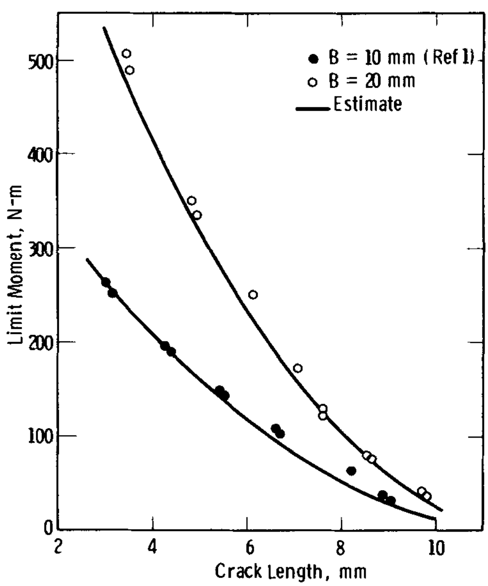

FIG. 10—*Limit moment versus crack length for single and double thickness bend bars.*

work [2]. The value used for shear flow stress, τ_0, was determined from the uniaxial ultimate stress to account for strain hardening, the constant, $\sqrt{3}$, is a consequence of using the von Mises yield criterion.

$$\tau_0 = \sigma_{uts}/\sqrt{3} \tag{7}$$

Center Cracked Panels

J is calculated for the center cracked panels by using the same technique. The load displacement curves, Fig. 11, are integrated graphically and the work to a given displacement is plotted as a function of crack length for several displacements, Fig. 12. J is the negative of these slopes, that is the slope/2 because of the presence of two crack tips. J is plotted as a function of displacement for several crack lengths, Fig. 13. The critical displacement for crack initiation is determined as a function of crack length, Fig. 14. In contrast to the bend bars, this is not a constant. To find J_{Ic} the critical displacement must be taken for a specific crack length, Fig. 14. When J_{Ic} is determined for several crack lengths the results show a nearly constant value.

The limit load was plotted as a function of the crack length and compared with an estimate using $\tau_0 = \sigma_{uts}/\sqrt{3}$, Fig. 15.

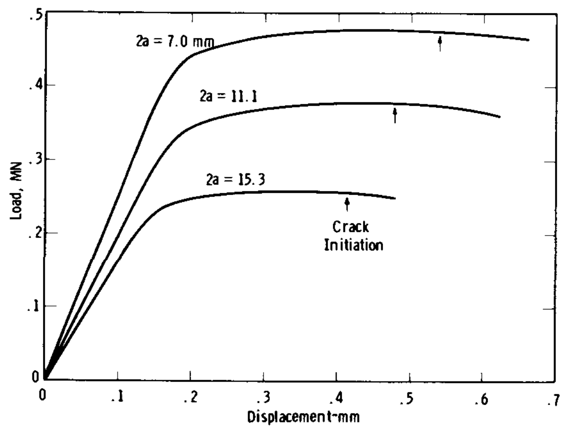

FIG. 11—*Load-displacement curves for center cracked panels.*

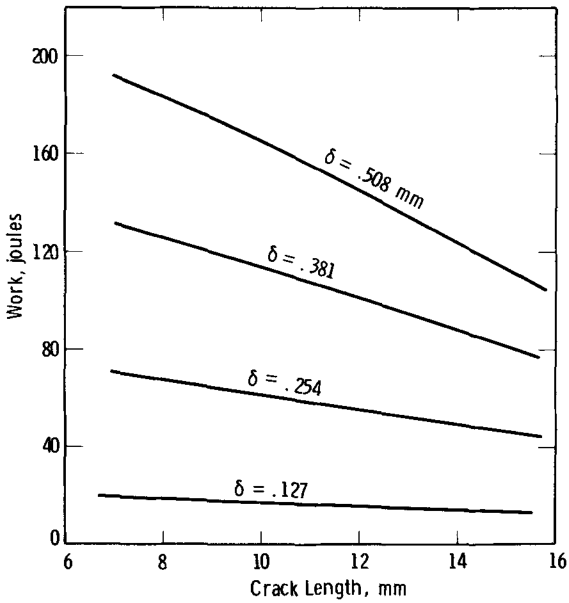

FIG. 12—*Work to a fixed displacement versus crack length for center cracked panels.*

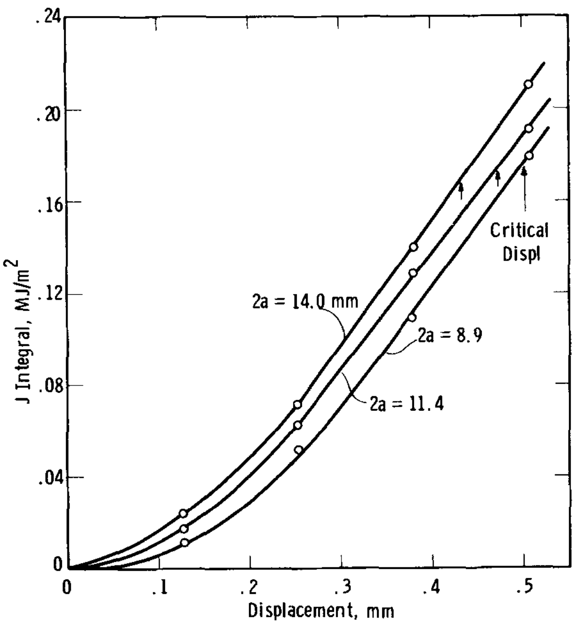

FIG. 13—J *integral versus displacement for center cracked panels showing* J_{Ic}.

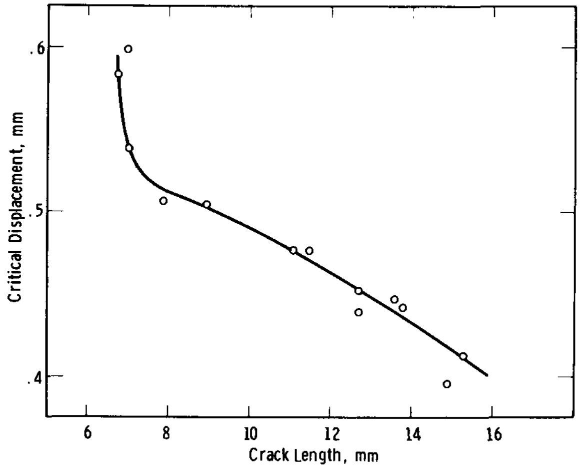

FIG. 14–*Critical displacement for crack initiation versus crack length, center cracked panels.*

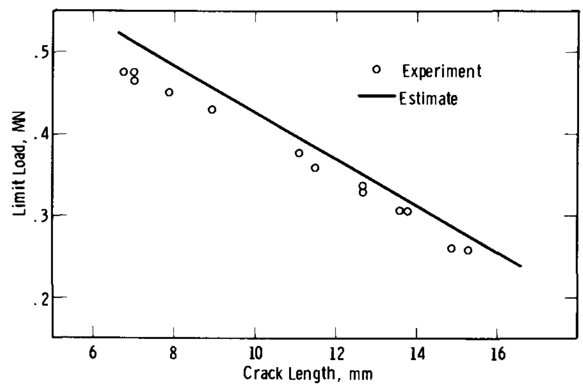

FIG. 15–*Limit load versus crack length for center cracked panels.*

Results

J_{Ic} for the center cracked panels averaged 0.172 MJ/m^2 for crack lengths varying from 8.9 to 14.0 mm, Fig. 13. Considering the variation in critical displacement from Fig. 14 the values of J_{Ic} could vary from 0.158 to 0.184 MJ/m^2. This is a scatter of less than ± 8 percent. This variation is insignificant considering that the variation in G_{Ic} from K_{Ic} testing is typically ± 30 percent for rotor steels. Comparing the actual limit loads with the estimated ones shows that there is no stress elevation in the net section due to the presence of a crack, Fig. 15.

The double thickness bend bars show an average J_{Ic} of 0.187 MJ/m^2 for cracks ranging from 3.6 to 7.1 mm, Fig. 8. The variation in J_{Ic} was from 0.175 to 0.200 MJ/m^2, about ± 7 percent. From previous tests on standard thickness bend bars the values of J_{Ic} ranged from 0.15 to 0.19 MJ/m^2 [*2*].

For longer cracks J_{Ic} begins to deviate significantly. For example at a crack length of 8.1, where the remaining ligament is only 3.9 mm, J_{Ic} is about 0.13 MJ/m^2. This value is below the scatter band of previous results. As the crack length increases farther, the value of J_{Ic} appears to become even lower. It appears that J_{Ic} is not valid for these longer cracks due probably to a minimum size limitation being reached in the uncracked ligament of the specimen.

The limit moments for the bend bars agree very well with the estimate from Green and Hundy [*4*], Fig. 10, for both thicknesses. This indicates that a sufficient degree of constraint is achieved in both thicknesses.

Discussion

The values of J_{Ic} for the two geometries, center cracked panels and bend bars, show no effect of the radically different slip line fields. This gives support to the argument that the local plastic crack tip singularity and subsequent crack tip "blunting" overrides the effect of slip line fields in determining J_{Ic}. Hence the J integral is a valid fracture criterion for elastic-plastic behavior. A more severe test of the applicability of J to cracked bodies would be the testing of a highly constrained specimen such as the deep double edge notched specimen. These tests are being conducted presently.

Comparison of the results from standard thickness bend bars with those of the double thickness specimens shows good agreement in the value of J_{Ic}. This indicates that nearly plane strain results can be obtained from the standard thickness bend bars, that is, ones with a nearly square cross section.

The results of most of the J_{Ic} tests to date are shown in Table 2. These results show that the J integral fracture criterion has worked successfully for two materials, an A533B pressure vessel steel and a Ni-Cr-Mo-V rotor steel for several different specimen geometries.

Some limitations on the application of J as a fracture criterion must be explored before it can be used as an engineering tool. The effect of stress state, that is, plane strain versus plane stress, is not known. All test results to date have been for plane strain behavior. Also, there should be a size limitation for the use of the J fracture criterion. When the thickness or uncracked ligament is small compared with some theoretical fracture zone the results for J_{Ic} would not be valid. It has been proposed [*8*] that this fracture zone should be a function of J_{Ic} divided by the yield stress of the material. The results from the bend bars show that J_{Ic} begins to deviate when the uncracked ligament is less than 5 mm. This gives a ratio of size limitation to J_{Ic}/σ_{yp} of about 25 for this material. The possible size limitation is very important to the development of J as a fracture criterion and should be explored fully.

TABLE 2–*Results of* J_{Ic} *tests to date.*

Specimen Type	Dimensions, mm	Temperature, deg K	J_{Ic} MJ/m^2
	Ni-Cr-Mo-V		
Center cracked panels	25.4 x 25.4 x 57	394	0.172
Double thickness bend bars	12 x 20 x 40	394	0.187
Single thickness bend bars [2]	12 x 10 x 40	366	0.167
Compact tension (8TCT) [2]	406 x 203 x 488	394	0.175
Bend bars double size [2]	24 x 20 x 96	366	0.179
	A533B Class II		
2TCT [2]	102 x 51 x 122	298	0.165
1TCT [2]	51 x 25.4 x 61	298	0.180

Until these limitations can be understood and regions of validity established for J_{Ic} its status should be that of an experimental quantity rather than a usable engineering tool.

Conclusions

(1) The J integral has proved to be a successful fracture criterion for behavior ranging from linear elastic to fully plastic in low to intermediate strength steels.

(2) J_{Ic} is not influenced by radical differences in fully plastic slip line fields for the two geometries center notched panels and single edge notched bend bars.

(3) Bend bars of conventional thickness, namely, a square cross section, provide sufficient constraint to achieve nearly plane strain results with respect to fracture properties, in the fully plastic state.

Acknowledgments

We would like to express our appreciation to our colleagues at the Westinghouse Research Laboratories who contributed to various phases of this investigation; to Dr. W.K. Wilson who contributed valuable discussions on the J integral and to R.B. Stouffer, A.R. Petrush, and F.X. Gradich who assisted with the experimental work.

References

[1] Brown, W.F., Jr., and Srawley, J.E., *Plane Strain Crack Toughness Testing of High Strength Metallic Materials, ASTM STP 410,* American Society for Testing and Materials, 1966.

[2] Begley, J.A. and Landes, J.D. in *Fracture Toughness, Proceedings of the 1971 National Symposium on Fracture Mechanics, ASTM STP 514,* American Society for

[3] Testing and Materials, 1972, pp. 1-20.
Applied Mechanics, Vol. 35, 1968, pp. 379-386.

[4] Green, A.P. and Hundy, B.B., *Journal of the Mechanics and Physics of Solids,* Vol. 4, 1956, pp. 128-144.

[5] McClintock, F.A. in *Development in Mechanics,* Vol. 5, Proceedings of the 11th Midwestern Applied Mechanics Conference, Iowa State University Press, Ames, Iowa, 1969, pp. 971-976.

[6] McClintock, F.A. in *Fracture,* H. Liebowitz, Ed., Vol. 3, Academic Press, New York, 1971, pp. 47-225.

[7] Rice, J.R. in *Fracture,* H. Liebowitz, Ed., Vol. 2, Academic Press, New York, 1968, pp. 191-311.

[8] P.C. Paris, private communication, April 1971.

R. J. Bucci,[1] *P. C. Paris,*[1] *J. D. Landes,*[2] *and J. R. Rice*[3]

J Integral Estimation Procedures

REFERENCE: Bucci, R.J., Paris, P.C., Landes, J.D., and Rice, J.R., "*J* **Integral Estimation Procedures,**" *Fracture Toughness, Proceedings of the 1971 National Symposium on Fracture Mechanics, Part II, ASTM STP 514,* American Society for Testing and Materials, 1972, pp. 40-69.

ABSTRACT: By making use of plastically adjusted linear elastic fracture mechanics analysis and plastic limit load solutions, a method is developed for reasonable approximation of Rice's path independent *J* integral which is applicable for test specimens or other configurations which exhibit considerable plasticity prior to fracture. Employing this, *J* is expressed as a function of load point displacement. Estimations of the *J* versus displacement relationships developed compared quite well to those previously established experimentally at Westinghouse Research Laboratories for Ni-Cr-Mo-V and A533B steels. For these comparisons, the test specimen configurations considered were three point bend, center notch, and compact tension test specimen configurations, all of which exhibit significantly different plastic limit load slip line flow fields. Thus, the method developed for approximating *J* is thought to be widely applicable.

KEY WORDS: fracture (materials), fracture strength, toughness, loads (forces), tensile properties, plastic analysis, stressing, cracking (fracturing), elastic limit, plastic limit, tension tests, fracture tests, alloy steels

Recent experiments by Begley and Landes [*1*] have demonstrated the potential of Rice's path independent integral, *J* [*2*], as an effective criterion for the initiation of crack extension. The critical *J* fracture criterion was found to be applicable for situations which sustain either small or large scale plasticity prior to fracture. Therefore, if such results continue to prevail, a significant extension of fracture toughness concepts into the plastic range has been discovered.

The *J* integral is defined for two dimensional problems and is given by [*2*]

$$J = \int_R Wdy - \mathbf{T} \cdot \frac{\partial \mathbf{u}}{\partial x} ds \tag{1}$$

[1] Del Research Corporation, Hellertown, Pa. 18055.

[2] Research and Development Center, Westinghouse Electric Corporation, Pittsburgh, Pa. 15235.

[3] Brown University, Providence, R.I. 02912.

where W is the strain energy density as defined by

$$W = W(\epsilon_{ij}) = \int_0^{\epsilon_{ij}} \sigma_{pq}\, d\epsilon_{pq} \tag{2}$$

and as shown in Fig. 1, R is any contour surrounding the crack tip, $\mathbf{T}$ is a traction vector defined by outward normal m along R, $\mathbf{T}_i = \sigma_{ij}m_j$, $\mathbf{u}$ is the displacement vector, and s is arc length along R. For any elastic or elastic-plastic material treated by deformation theory of plasticity, Rice [*2*] has proven path independence of the J integral. Other recent studies [*3*, *4*] using incremental theory for finite element analysis also demonstrate an approximate path independence within the plastic region, although it is not clear that this prevails for contours immediately adjacent to the crack tip [*5*].

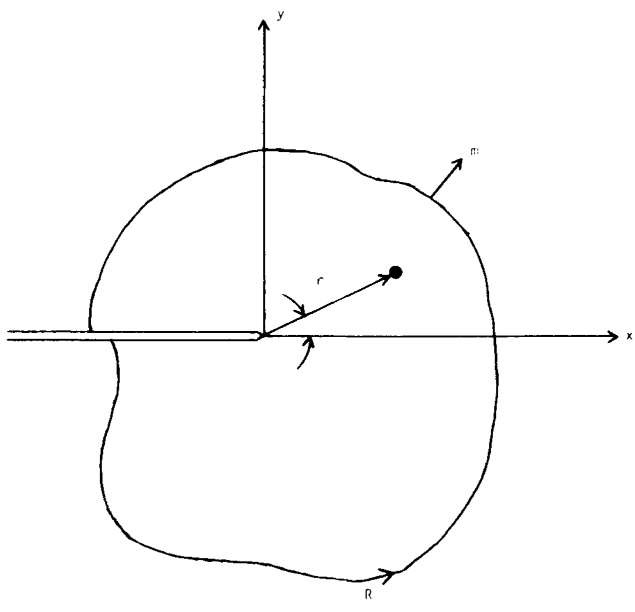

FIG. 1–*Crack tip coordinate orientation and arbitrary line integral contour.*

An alternate and equivalent interpretation [*6*] of J for elastic (linear or non-linear) materials is that of a potential energy difference for identically loaded configurations having neighboring crack sizes a and $a + da$. In particular

$$J = -\frac{\partial (U/B)}{\partial a} \tag{3}$$

where U/B is the potential energy normalized per unit thickness B. This is defined by

$$U/B = \iint_A W dx dy - \int_{c_t} \mathbf{T} \cdot \mathbf{u} \; ds \tag{4}$$

where W is the strain energy density and c_t that portion of boundary contour on which tractions $\mathbf{T}$ are prescribed. For elastic-plastic materials, we shall take Eq 3 as defining J, where it is to be understood that the *pseudo-potential energy* U/B corresponding to any given crack length is defined by Eq 4 with W then being the work of stress deformation as experienced during monotonic increase of the boundary loads on a body which has that same crack length in an unloaded reference state. This precision of definition is necessary in view of the dependence of plastic response on prior deformation history. Within the context of deformation plasticity theory, the above definition of J is equivalent to that as given by the line integral Eq 1 although a similar equivalence cannot be proven for actual incremental plastic materials. In analogy with the linear elastic fracture mechanics interpretation of the energy release rate [*7*, *8*], the area between two monotonic load deflection curves for neighboring crack sizes a and $a + \Delta a$ is, from the adopted definition of J, $BJ\Delta a$ to first order. This interpretation is illustrated in Fig. 2; moreover, it allows rather simple calculations of J as will be developed herein.

Noting the above interpretations, Begley and Landes [*1*] previously developed a procedure which permits J evaluation from a family of load-displacement records experimentally determined from test specimens of varying initial crack length. Their suggested procedure for this calculation is outlined in Appendix 1 and amplified in Ref *1*.

Equations 1 and 3 may be physically regarded as characterizing the Applied J and as providing methods of evaluating the J imposed by external sources. On the other hand the J, so imposed, causes processes to occur in the vicinity of the crack tip in such a way that J may be regarded as a measure of the resulting crack tip field of deformation. Thus, the J integral characterizes the near tip stress-strain environment of cracked elastic-plastic bodies, which offers the distinct advantage that it is possible to characterize the local crack tip phenomena by a single field parameter which does not focus attention directly to specific crack tip features. This is again analogous to the linear elastic fracture mechanics interpretation that the extent of the near tip process may be evaluated in terms of the imposed crack tip stress field intensity, K, or its equivalent elastic strain energy release rate, G. It is noted that in fact J approaches G in the limit of the purely elastic case. It remains, however, an open question as to the suitability of a one-parameter characterization in the large scale yielding range.

Hopefully, the J integral representation of fracture can be successful so long as the stress strain environment within some "fracture process zone" is

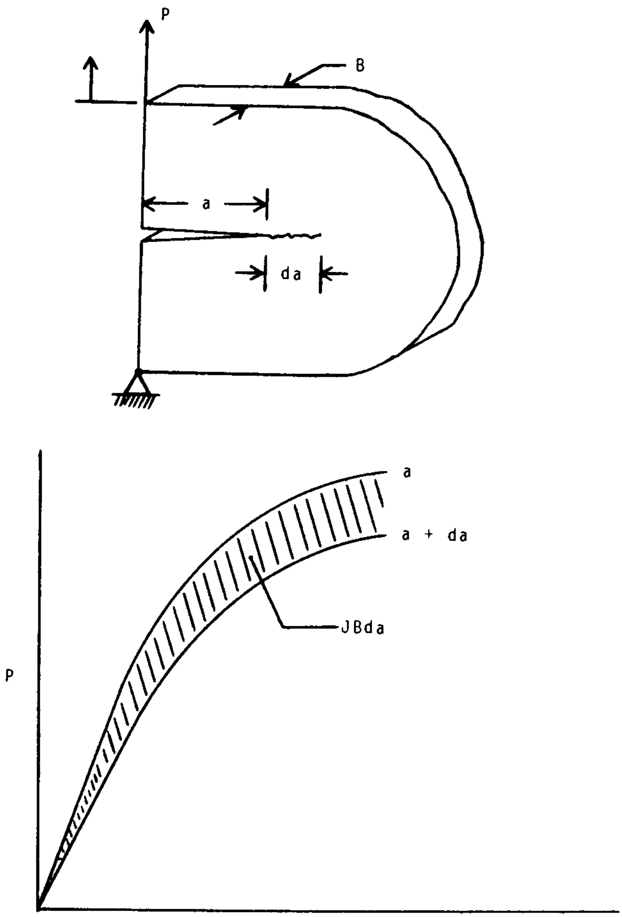

FIG. 2–*Interpretation of* J *integral.*

dominated by conditions local to the crack tip leading edge and is also insensitive to length factors such as crack size, net ligament, and thickness [*9, 10*]. Moreover, deformation theory of plasticity is meaningless when unloading occurs and this implies that substantial subcritical crack extension (beyond that associated with plastic blunting of the tip) is not permitted.. Therefore, the J fracture criterion must presently be restricted to crack initiation rather than propagation, as indicated by Begley and Landes [*1*]. However, these restrictions might not turn out to be any more restrictive than those caused by analogous plasticity effects in linear elastic fracture mechanics, and local unloading would then be admissable within some size of region which might be analogously described as proportional to J/σ_{ys}, where σ_{ys} is the tensile yield stress. In spite of these apparent "size" limitations [*9, 10*], the determination of which must be left largely to experiment, Begley and Landes have demonstrated with success [1] that relatively small specimens which exhibit fracture at full limit load conditions satisfy these dimensional requirements and provide valid interpretation of the J criterion. For both a low and intermediate strength steel, Begley and Landes [1] were able to determine experimentally a critical plane strain J value (J_{Ic}, which satisfied "degree of plastic restraint" requirements) at which elastic-plastic and fully plastic fracture occurred for a variety of crack lengths and specimen types. Their critical J_{Ic} determination was consistent with the linear elastic fracture mechanics interpretation of G_{Ic}. That is, their critical plane strain J_{Ic} obtained from smaller fully plastic specimens agreed favorably with critical G_{Ic} obtained from fracture of large specimen configurations which satisfied ASTM plane strain criterion [11].[4]

Objectives

Encouraged by the experimental success of Begley and Landes and their development of a fracture criterion based on the J integral, an attempt is made here to provide simple but effective approximate methods of calculating the "applied" J utilizing a minimum amount of concomitant supporting experimental effort.

The Begley and Landes procedure [1] (outlined in Appendix 1) used for the establishment of a relationship between J and the load point displacement, δ, required both procurement and analysis of a large number of experimental load-displacement records, which is both time consuming and costly. It would be a great advantage and is an objective herein to be able to estimate the J versus δ relationship for a given test specimen configuration and from this, supplemented by *one* experimental load-displacement record (which determines a displacement at fracture), establish a critical value of J.

For practical structural applications where more complex flaw and loading geometries are apparent, a purely experimental evaluation of the J versus δ relationship may not always be conveniently possible. If, for these practical component-flaw geometries, one could make meaningful J versus δ approximations, derived using no more than linear elastic fracture mechanics and plastic limit analysis, then along with critical J (or G) values established from simpler test configurations, one might effect reasonable predictions for loads and load point displacements at fracture, and hence, for practical applications, establish critical flaw sizes or design stress levels or both.

Towards the achievement of the above goals, the primary purpose of this work is to provide simple but effective methods for approximating the J versus δ relationship based on no more than linear elastic fracture mechanics and plastic

[4] For a valid fracture criterion, J_{Ic} should equal G_{Ic}. Since for small scale yielding J is identical to G, this implies that J_{Ic} may be related to plane strain fracture toughness, K_{Ic}, as $J_{Ic} = (1-\nu^2)\, K_{Ic}^2/E$.

limit analysis. The effectiveness of the approximating techniques will be evaluated for three common test specimen configurations, the three point bend bar, the center notch, and compact tension specimen, all of which exhibit grossly different limit load slip line fields [12]. In order to judge the analytically developed expressions for the J versus δ relationship, they will be compared to those experimentally established by Begley and Landes [1] for Ni-Cr-Mo-V and A533B steels.

Some Useful Observations

Following the J interpretation outlined earlier, and also discussed in Appendix 1, that J, as given by Eq 3, may simply be evaluated from the area between load-deflection curves of slightly different crack lengths, it becomes relevant to examine one's ability to generate reasonable estimates of load-displacement behavior for cracked configurations and especially their variation with crack size. The limiting cases of load-displacement character are those exhibited by either purely elastic or rigid plastic behavior, Fig. 3*a*. For the pure elastic case, J is identical to G, the energy release rate [1], and may be expressed as [13]

$$J = G = \frac{P^2}{2} \frac{\partial \lambda}{B \partial a} \tag{5}$$

where P is the applied load, ∂a represents an increment of crack extension, B is the material thickness, and where load and displacement are related by

$$\delta = \lambda P \tag{6}$$

λ is an inverse spring constant, or compliance which is a function of flaw size, specimen geometry, and elastic material constants, namely, E, Young's modulus, and sometimes ν, Poisson's ratio. Since Eq 6 J is proportional to δ^2, J as a function of δ, for pure elastic behavior, assumes the form of a parabola for a given constant crack size, Fig. 3*b*.

For the rigid plastic load-displacement relationship, deformation or δ extension is unlimited at the limit load, $P = P_L$, while for $P < P_L$, $\delta = 0$, Fig. 3*a*. Interpreting Eq 3 for J in terms of the area between two successive load displacement records, J as a function of δ for the rigid plastic material is given as

$$J = -\frac{\delta}{B} \frac{\partial P_L}{\partial a} \tag{7}$$

where the derivative $\partial P_L/\partial a$ is evaluated for the crack length of interest. The resulting rigid plastic expression for J is simply a linear function of δ, and thus

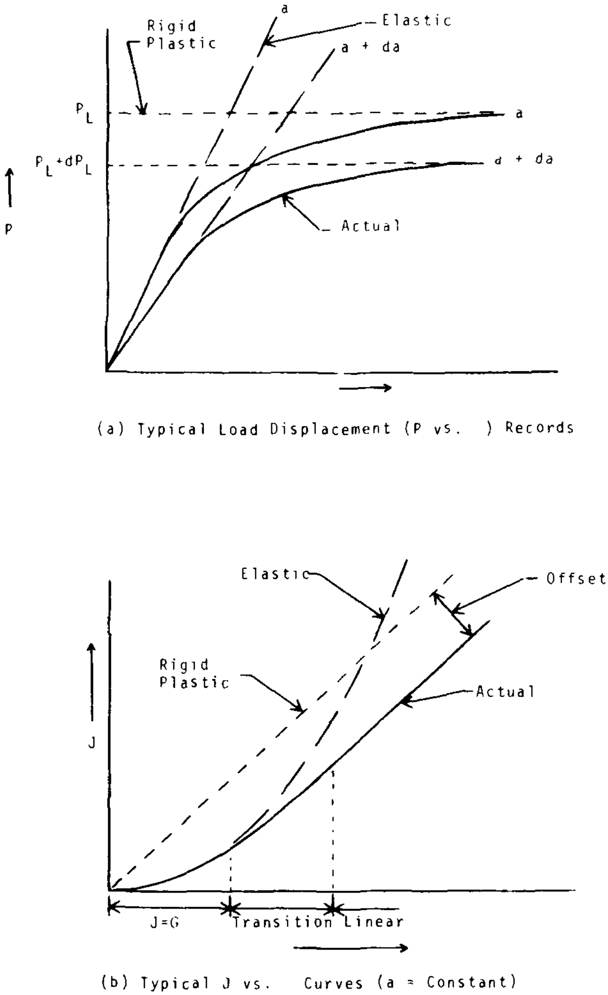

FIG. 3—*Idealized versus actual behavior for load versus displacement and J versus displacement.*

the J versus δ relationship for constant crack size is a straight line emanating from the origin, Fig. 3*b*.

In reality actual load versus displacement characteristics border the two extremes exhibited by purely elastic and rigid plastic behavior, Fig. 3*a*. For low loads and associated small scale plasticity, a load-displacement behavior can always be approximated by linear elastic analysis giving a slope (or compliance) which is a function of crack size, specimen geometry, and elastic material constants. As loading progresses, increased plasticity introduces nonlinearity, and if fracture has not yet ensued prior to the attainment of limit load, a marked increase in deflection, which ultimately leads to separation will occur without any substantial increase in load, Fig. 3*a*.

For a flawed configuration which sustains large scale yielding prior to fracture, it seems logical to expect similarly that the J versus δ relationship also resembles the two extremes at low and high δ (or J). For small δ, and consequently small scale plasticity, J can be represented simply by the linear elastic solution, $J = G$, which is parabolic in δ for constant crack length. For large δ where limit load is attained prior to fracture, J as a function of δ becomes a linear relationship with a slope parallel to the idealized rigid plastic relationship, Fig. 3*b*. The offset between parallel segments of the rigid plastic and actual J versus δ curves of Fig. 3*b* is governed in part by the nonlinearities in the P versus δ records which occur in the transition region. Hence, estimation of the actual J versus δ relationship rests on the ability to effectively approximate the elastic to plastic transition, or more specifically, the variation with crack length of the curved portion of the load displacement relationship up to limit load, as well as the limit load itself.

Estimation Techniques

A logical first attempt at providing estimated load-displacement records for successive crack sizes and hence, J versus δ approximations would be to consider a family of purely elastic and perfectly plastic load-displacement records. For each particular crack size development of perfectly plastic behavior from the original elastic slope would occur at limit load, ignoring the nonlinear portion of the load-displacement relationships. Further, for fractures commencing after large deformations at limit load even the elastic portion might be ignored, proceeding in a manner consistant with Eq 7. However, it becomes evident that these first approximations are not adequate except for special situations and a more general approximation procedure would be advantageous.

A slightly more refined approximation can be made by amending the linear elastic portion of the load-displacement relationship analysis by use of an r_y plasticity adjustment factor [*14*] which considers the leading edge of the crack to be given a central location within the plastic zone [*15*]. The plasticity adjustment results in an equivalent elastic or effective crack size, a_{eff}, given by

$$a_{\text{eff}} = a + r_y \tag{8}$$

where

$$r_y = \frac{1}{2\pi}\left(\frac{K}{\sigma_{ys}}\right)^2 \tag{8a}$$

for plane stress and

$$r_y = \frac{1}{6\pi}\left(\frac{K}{\sigma_{ys}}\right)^2 \tag{8b}$$

for plane strain. a is the actual crack size, K the stress intensity factor (based on actual crack size), and σ_{ys} the yield point (or small strain plastic flow stress) for the material in simple uniaxial tension. Utilization of the r_y plasticity adjustment appropriately introduces nonlinearity which is thought to be rather accurate for small scale yielding and which is at least more realistic than pure linear elastic analysis as yielding progresses. Employing the plasticity adjustment, a family of load-displacement records can be provided by using the plastically (r_y) adjusted elastic analysis up to limit load and limit load analysis thereupon. A simple procedure used to apply the r_y plasticity adjustment to linear elastic load-displacement relations is discussed in Appendix 2.

Estimating schemes based on the observations cited above were tried and compared to existing Westinghouse experimental data on Ni-Cr-Mo-V (200-250 F) and A533 B(75 F) steels [*1*]. The three specimen configurations considered were the center notch, the three point bend bar (single and double thickness) for Ni-Cr-Mo-V steel, and the compact tension (H/W = 0.6) for A533 B steel. The test configurations are sketched in Figs. 4 through 6.

J versus δ Computation and Analyses

Families of load displacement records developed by analytical estimation and by Westinghouse experiments, [*1, 2*], were curve fit by computer using an orthogonal polynomial relationship. The computational process was carried out in the manner prescribed in Appendix 1. That is, load displacement records were used to obtain apparent or "pseudo-potential energy" for constant displacement as a function of crack length (that is, U/B versus a curves). The U/B versus a

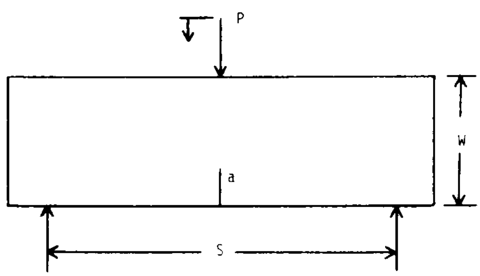

B = Thickness = 0.394" and 0.788"
W = 0.474"
S = 1.57"
· = Load Point Displacement

FIG. 4—*Westinghouse Ni-Cr-Mo-V three point bend bar test configuration.*

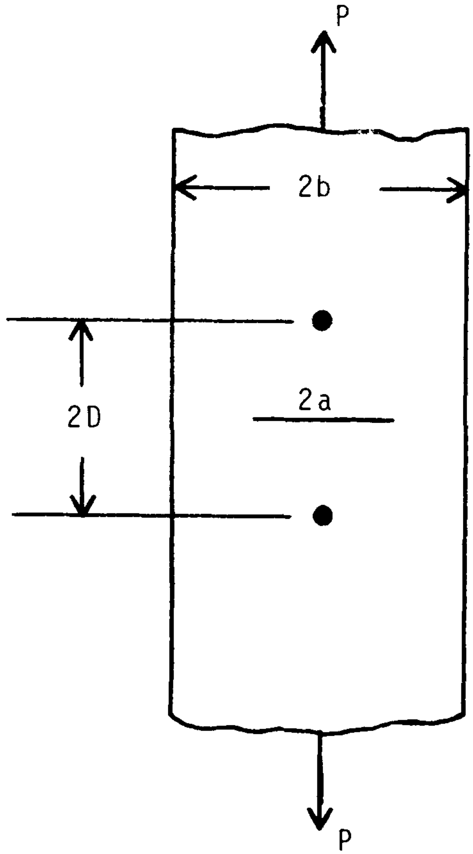

B = Thickness = 1.00"

2b = 1.00"

2D = Gage Length = 2.25"

FIG. 5–*Westinghouse Ni-Cr-Mo-V center notch specimen configuration.*

curves were best fit by a low order orthogonal polynomial and their slopes evaluated to yield J as a function of displacement, δ, and crack size, consistent with Eq 3.[5]

Analytically estimated J versus δ relationships for Ni-Cr-Mo-V steel specimens were compared to those obtained using actual Westinghouse load-displacement

[5] Since for the center notch specimen, the area between load-displacement records of neighboring crack sizes is representative of the total change in "pseudo-potential energy" for two cracks, an appropriate adjustment by a factor of 1/2 was necessary to evaluate J for each crack tip.

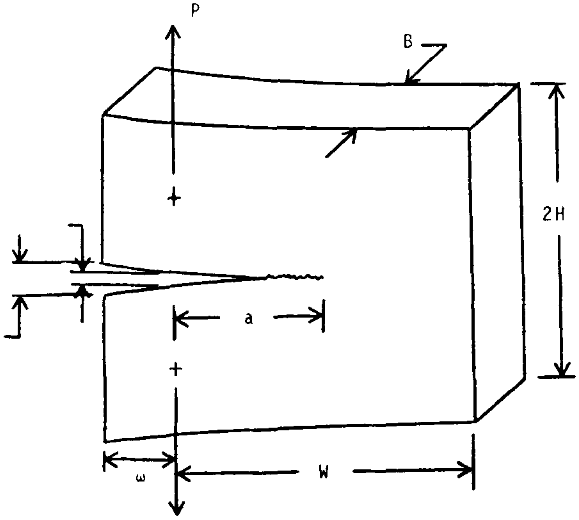

B = 1.00"
W = 2.00"
H = 1.20"
ω = Location of Gage from Load Line = 5/8"
δ = Displacement at Load Line
δ' = Displacement at Gage Location

FIG. 6—*Westinghouse A533B compact tension test specimen configuration.*

records [1]. For the A533 subsized compact tension test configuration, analytical estimates of the J versus δ relationship were compared to the critical plane strain J (J_{Ic}) and fracture displacement previously established by Westinghouse experiment on identical test configurations.

Development of Load Displacement Records for Each Specimen Configuration

Pure Elastic

Load-displacement relationships for the three point bend bar and center notch test configurations of Figs. 4 and 5 were analytically developed for pure elastic loading and are given below for the three point bend bar of Fig. 4 where δ is measured at the point of load application.

$$\delta = \frac{0.24\,PS^3}{BEW^3}\,[1.04 + 3.28\,(W/S)^2\,(1 + \nu)]$$

$$+ \frac{2PS^2}{BE'W^2}\left(\frac{a}{W}\right)\left[4.21\left(\frac{a}{W}\right) - 8.89\left(\frac{a}{W}\right)^2 + 36.9\left(\frac{a}{W}\right)^3 - 83.6\left(\frac{a}{W}\right)^4 + 174.3\left(\frac{a}{W}\right)^5 - 284.8\left(\frac{a}{W}\right)^6 + 387.6\left(\frac{a}{W}\right)^7 - 322.8\left(\frac{a}{W}\right)^8 + 149.8\left(\frac{a}{W}\right)^9\right] \quad (9)$$

where

B, S, W, a are defined in Fig. 4, and E = Young's modulus,
ν = Poisson's ratio, and
E' = E for plane stress
= $E/(1-\nu^2)$ for plane strain.

For the center notch specimen of Fig. 5 where the gage is located a distance D above and below the center line of the crack

$$\delta = \frac{P}{B}\left[\frac{D}{bE} + \frac{4}{\pi E'}\left\{\left(\frac{\pi a}{2b}\right)^2 + \frac{1}{4}\left(\frac{\pi a}{2b}\right)^4 + \frac{5}{72}\left(\frac{\pi a}{2b}\right)^6 + \cdots\right\}\right] \quad (10)$$

where B, D, b, a are defined in Fig. 5 and where E and E' have the same interpretation as above, and where it is assumed that $D/a \gg 1$. The derivation of Eqs 9 and 10 are outlined in Appendix 2.

Earlier established boundary collocation results [*16, 17*] were used to obtain load-displacement (at the load line and gage location) relationships for the compact tension specimen. A dimensionless plot of these results is given in Fig. 7.

For pure elastic loading, the J calculation could be simplified by acknowledging that $J = G$. Consequently, for a single crack tip, J can be calculated from

$$J = \frac{K^2}{E'} \quad (11)$$

where

E' = E for plane stress
= $E/(1-\nu^2)$ for plane strain

and K is simply the appropriate test configuration stress intensity factor.

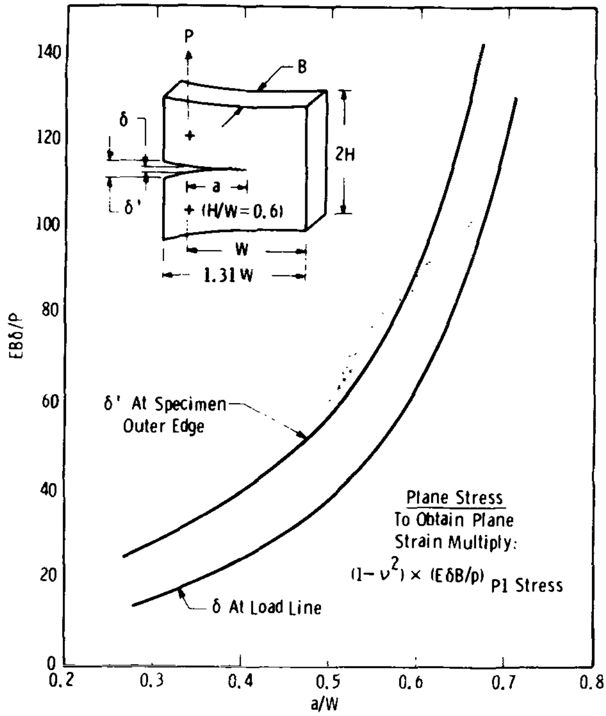

FIG. 7—*Boundary collocation results for elastic loading of compact tension specimen* [16, 17].

A tabulation of K calibrations used for the test configurations considered are given below for three point bend bar as shown in Fig. 4 [*10*][6]

$$K = \frac{PS}{B(W)^{3/2}} \left[2.9 \left(\frac{a}{W}\right)^{1/2} - 4.6 \left(\frac{a}{W}\right)^{3/2} + 21.8 \left(\frac{a}{W}\right)^{5/2} - 37.6 \left(\frac{a}{W}\right)^{7/2} + 38.7 \left(\frac{a}{W}\right)^{9/2} \right] \tag{12}$$

For the center notch specimen, Fig. 5 [*18*]

$$K = \frac{P}{2Bb} \sqrt{\pi a \sec \frac{\pi a}{2b}} \tag{13}$$

[6]Equation 12 was obtained for a bend beam with S/W = 4 [*10*, *20*]. However, by extrapolation of results given in Ref *20*, Eq 12 was found not to differ significantly from the expression obtained for a bend bar of S/W = 3.31 (the actual S/W ratio for bend bar of Fig. 4).

For the compact tension specimen $H/W = 0.6$, Fig. 6 [*10, 19*]

$$K = \frac{P}{B\sqrt{W}} \left[29.6 \left(\frac{a}{W}\right)^{1/2} - 185.5 \left(\frac{a}{W}\right)^{3/2} + 655.7 \left(\frac{a}{W}\right)^{5/2} - 1017.0 \left(\frac{a}{W}\right)^{7/2} + 638.9 \left(\frac{a}{W}\right)^{9/2} \right] \tag{14}$$

For the linear elastic case, since K is usually expressed as a function of applied load or nominal stress, then J (or G) as a function of δ may be expressed simply by inversion of the configuration compliance relationship, for example, inversion of Eq 6 as:

$$P = \delta/\lambda \tag{15}$$

and substituting for the appropriate K expression of Eq 11.

Rigid Plastic

Limit load solutions were developed by Green and Hundy [*21*] for bars subject to pure bending.

$$P_L = 1.456\ \sigma_{ts} \frac{B}{S} (W - a)^2 \tag{16}$$

and for the center notch specimen by McClintock [*22*]

$$P_L = \frac{2\sigma_{ts}}{\sqrt{3}} (2b - 2a) B \tag{17}$$

Where σ_{ts} is the material uniaxial tensile strength. These limit load results were employed as analytical expressions for the prediction of limit load and limit load variation with crack size, for the above two test configurations. The agreement between limit load predictions of Eqs 16 and 17 and Westinghouse experimentally established limit loads for Ni-Cr-Mo-V steel ($\sigma_{ts} \simeq 135$ ksi) [*1*] is shown to be quite good on Figs. 8 and 9.

Assuming that uniaxial tensile yield stress, σ_{ys}, equals twice the flow stress in shear, τ_{ys}, an upper bound limit analysis provided by Rice [*23*], for which he considered an edge crack specimen subjected to combinations of tension and bending, was used to predict limit loads for the compact tension specimen. For a limited range of crack lengths ($a/W = 0.5$ to 0.6), the agreement of the Rice

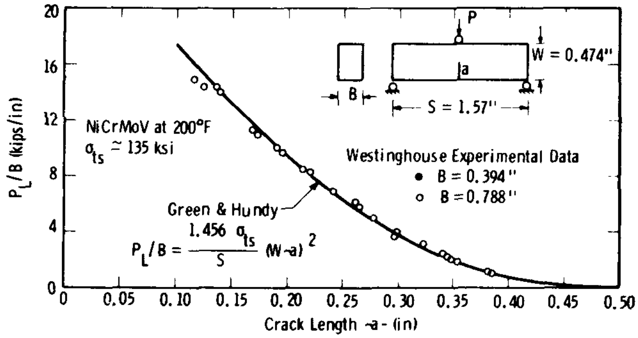

FIG. 8—*Limit load per unit thickness as a function of crack length for Westinghouse Ni-Cr-Mo-V three point bend test configuration.*

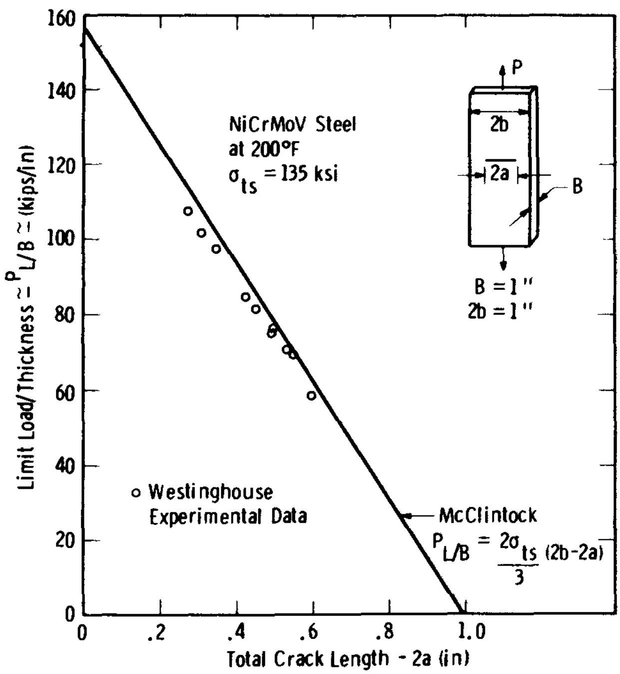

FIG. 9—*Limit load per unit thickness as a function of total crack length for Westinghouse Ni-Cr-Mo-V center notch test specimen configuration.*

solution was found to be quite sufficient when compared to actual Westinghouse limit load data on A533 B steel ($\sigma_{ys} \simeq 70$ ksi) 1TCT and 2TCT compact tension specimens [1], Fig. 10.[7]

To compute the J versus δ relationship for rigid plastic material behavior, one could use the procedure outlined in Appendix 1 or more simply employ Eq 7. Rewriting Eq 7 to consider the possibility of more than one crack tip:

$$J = -\frac{\delta}{B}\frac{\partial P_L}{\partial(\alpha a)} \tag{18}$$

where $\alpha = 1$ for configurations with one crack tip
$\alpha = 2$ for configurations with two crack tips

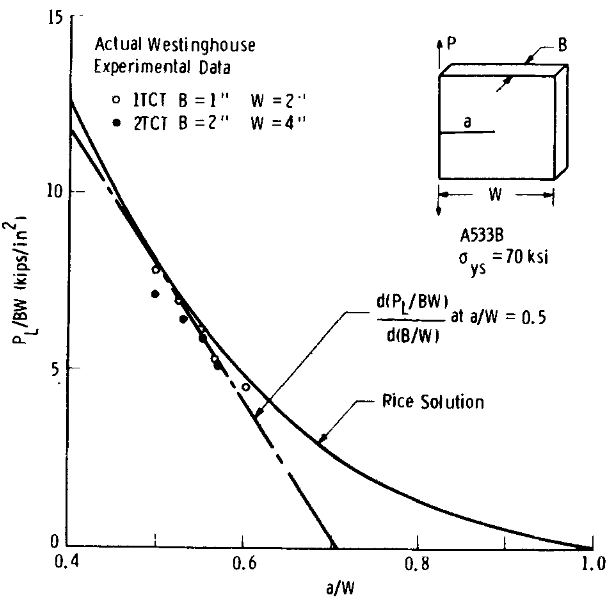

FIG. 10—*Limit load divided by* B W *as a function of dimensionless crack size,* a/W *for Westinghouse A533B compact tension specimen.*

[7]In order to calculate limit load for the three configurations, uniaxial tensile strength was employed in Eqs 16 and 17 for the bend bar and center notch configuration, whereas the Rice approximation for the compact tension configuration contains yield strength. The above selection was based upon success demonstrated by Eqs 16 and 17 and the Rice procedure in predicting actual limit load, refer to Figs. 8 through 10. For a mild steel alloy, subsequent unpublished results have shown when final fracture occurs prior to the attainment of full limit load conditions, the critical J estimation is rather insensitive to precise definition of a suitable plastic flow parameter for example, σ_{ys}, σ_{ts}, 1/2 ($\sigma_{ys} + \sigma_{ts}$), etc.). For the mild steel investigated ($\sigma_{ys\,min}$ = 50 ksi $\sigma_{ts\,min}$ = 80 ksi) a ±10 percent variation in averaged flow stress resulted in critical J estimates within ±15 percent.

Thus for the bend bar

$$J = 2.912\,\sigma_{ts}\,\frac{\delta}{S}\,(W-a) \tag{19}$$

and for the center notch specimen

$$J = \frac{2\sigma_{ts}}{\sqrt{3}}\,\delta \tag{20}$$

For the compact tension specimen $\partial P_L/\partial a$ could be determined graphically, Fig. 10, and substituted into Eq 18.

For the three chosen specimen configurations, Figs. 11 through 13 show typical analytically generated load displacement records for three different crack sizes for both the elastic (plane stress), perfectly plastic, and the elastic (plane

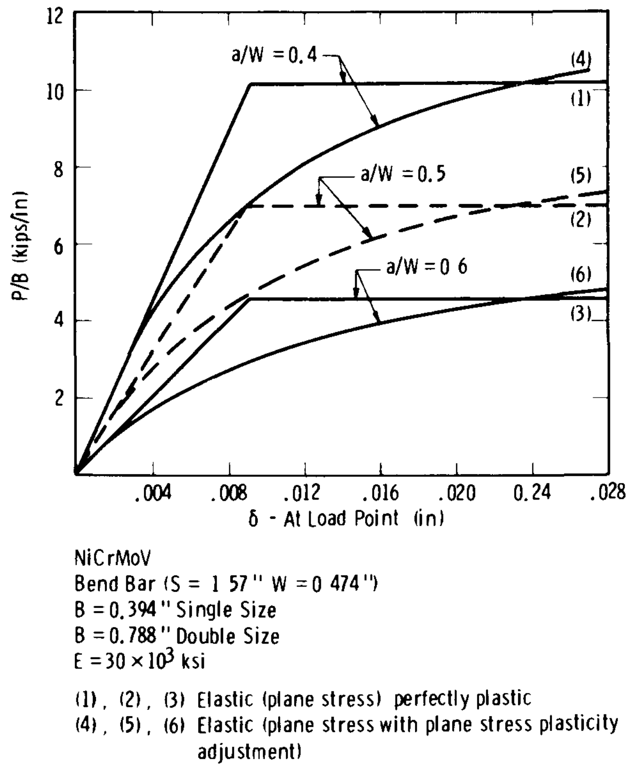

FIG. 11—*Typical estimated load displacement relationships for Westinghouse Ni-Cr-Mo-V single and double thickness three point bend bars.*

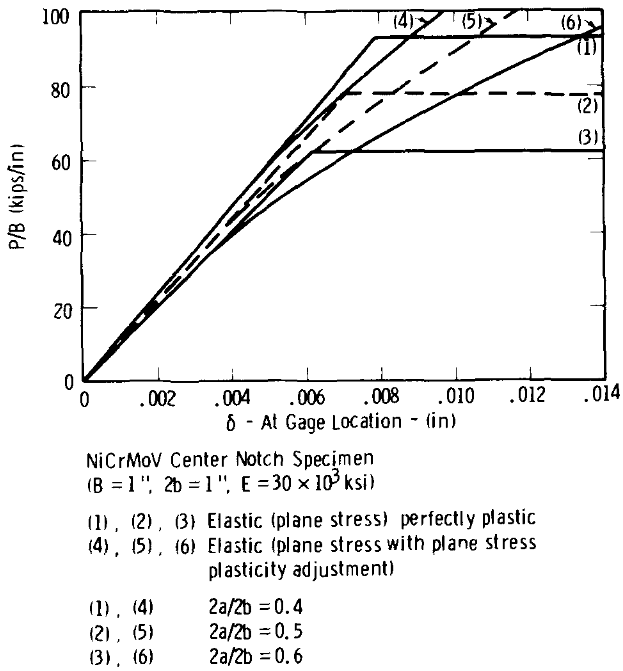

FIG. 12—*Typical estimated load displacement relationships for Westinghouse Ni-Cr-Mo-V center notch specimen.*

stress) with plane stress plasticity adjustment assumptions. An even better approximation of actual load-displacement records may be obtained by taking the plastically adjusted elastic behavior for loads less than limit load with a switch to perfectly plastic behavior at limit load.

Elastic load displacement relationships were chosen to be those for plane stress which differs from that of plane strain *at most* by a factor of $(1 - \nu^2) \simeq 0.90$. (This can be verified upon examination of Fig. 7 and Eqs 9 and 10). Use of the plane stress plasticity adjustment, Eq 8a, is justified by having a specimen *thickness* which gives plane stress conditions for most of the plastic zone (during the time the correction is used). Even so, it is the difference between load-displacement curves for changes in crack length which seems best approximated here by plane stress. However, thicker specimens (all other dimensions remaining equal) might require use of a plane strain adjustment factor, for example, Eq 8b.

Figure 14 presents a typical comparison between plane stress and plane strain estimations of load displacement behavior for the A533 B compact tension specimen considered. The area beneath both pure elastic (plane stress and plane strain) and plane strain plastically adjusted curves are essentially similar. Thus, it appears that pragmatic selection of a plane stress plasticity adjustment is justified for the specimen configuration and size considered.

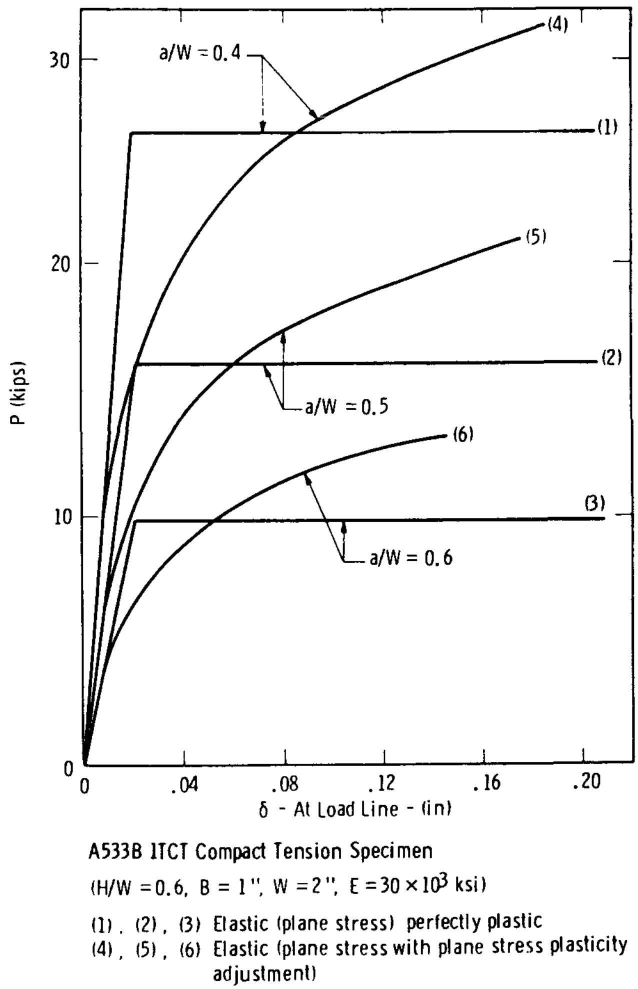

FIG. 13—*Typical estimated load displacement relationships for Westinghouse A533B 1TCT compact tension specimen.*

It is perhaps worthy of note that the bend specimen and compact tension specimen estimated deflection at limit load (both for perfectly elastic and plastically adjusted loading) is rather insensitive to crack length for the range of a/W ratios plotted on Figs. 11 and 13. On the other hand, from Fig. 12, estimated center notch specimen limit load deflection appears to be somewhat sensitive to crack length. This sensitivity might suggest that the center notch configuration is more difficult to develop approximations for J integral calculation than either of the other two configurations.

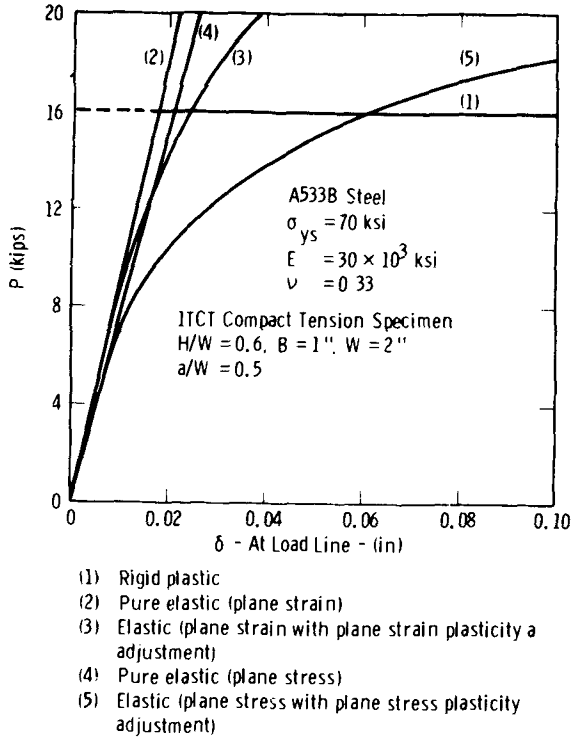

FIG. 14—*Typical estimated load displacement relationships for Westinghouse A533B 1TCT compact tension specimen,* a/W = *0.5.*

Results

For the Ni-Cr-Mo-V single and double thickness, three point bend bars of geometry prescribed in Fig. 4, Fig. 15 presents J as a function of δ determined from both analytically approximated and Westinghouse experimentally established load displacement records. Results for a crack length to width ratio, a/W, equal to 0.50 are shown; however, a/W ratios of 0.40 and 0.60 were also tried and found to give essentially similar comparisons. The analytical model does not involve thickness except for the "either-or" choice of plane stress or plane strain. Hence, for in-plane specimen geometry of Fig. 4, analytically estimated results (Fig. 15) were independent of thickness, while those results based on experiment exhibited a slight change with thickness. However, it should be noted that the specimen of smallest thickness (B = 0.394 in.) did not quite meet a "degree of plane strain" requirement based on experimental observations of Begley and Landes [*1, 9*]. Based on their observations for the specimen geometry considered, an approximate thickness B = 0.42 in. would be required to satisfy the "degree of plane strain" requirements. Greater than this thickness (namely, $B > 0.42$ in.) experimental results should be essentially thickness insensitive.

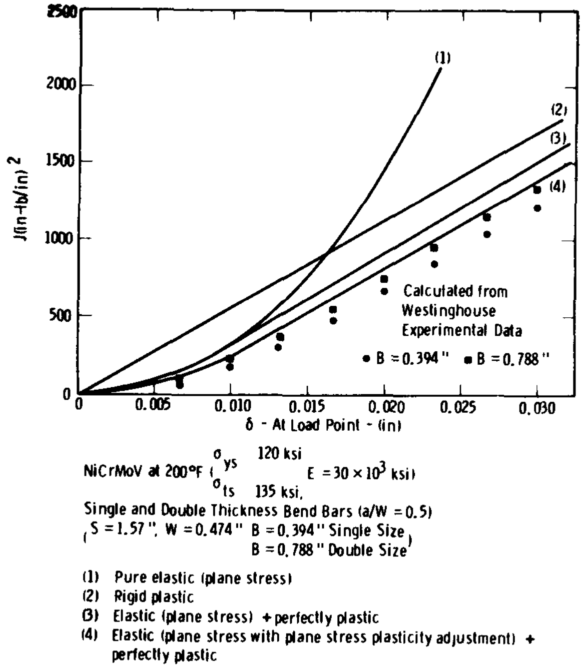

FIG. 15—*J as a function of load point displacement, δ, for Westinghouse Ni-Cr-Mo-V single and double thickness bend bars.*

Experimental results of the thicker specimen (B = 0.788 in.) shown in Fig. 15 satisfy such a requirement.

Of the various analytical schemes tried, those results derived from load-displacement behavior considered to be elastic plane stress, r_y plasticity adjusted, plus perfectly plastic (curve 4) agreed best with those results computed from the Westinghouse experimental data. Analytical agreement with experimental data was best for the thick specimen.

For both the single and double thickness bend bars, Westinghouse experimentally determined displacement, δ, at fracture ranged between 0.22 and 0.24 in. for a/W ratios of magnitude comparable to 0.5. Employing these experimentally determined fracture displacements and the a/W = 0.5 J versus δ relationship approximated by plastically adjusted elastic plane stress plus perfectly plastic loading (curve 4, Fig. 15), an estimated range of critical J would be 900-1100 in. • lb/in.² This agrees very well with an average critical plane strain $J(J_{Ic})$ of 1000 in. • lb/in.² experimentally established by Begley and Landes [1] and is also within good agreement[8] with upper shelf

[8]Since J_{Ic} is determined for the beginning of crack extension and G_{Ic} for a 2 percent crack extension, it follows that G_{Ic} should be larger than J_{Ic}.

(200 F) G_{Ic} = 1200 in.• lb/in.^{2} established from Westinghouse K_{Ic} fracture toughness tests on thicker test specimens [*1, 24*].

For the Ni-Cr-Mo-V center notch specimen, a comparison of J versus δ relationships based upon analytical and experimental load displacement records are presented, Fig. 16, for, $2a/2b$ = 0.5. Crack length to width ratios $2a/2b$ = 0.4 and 0.6 were also tried and found to yield similar comparisons. Again, J versus δ agreement of actual experiment and assumed elastic-plastic adjusted (plane stress) perfectly plastic loading (curve 4) are quite good. For comparable crack lengths, a Westinghouse experimentally determined δ at fracture was generally found to be in the range of 0.016 and 0.018 in. which corresponds to an estimated central J range, 800-900 in.·lb/in.^{2} This is in excellent agreement with previous Ni-Cr-Mo-V results and is well within the experimental bounds of fracture toughness determination of rotor steels for which K_{Ic} may vary as much as 15 percent, and which corresponds to a J critical variation of as much as ±30 percent [*1*].

Analytical J versus δ estimations for an A533 compact tension (CT) specimen, a/W = 0.5, are presented in Fig. 17. For the 1-in.-thick CT specimen, W equaled 2.00 in., and gage location was at the specimen outer edge, 5/8 in. from the load line (corresponding to a total specimen width of 1.31 W). For the 1-in. CT specimen, a/W = 0.5, gage location deflection at fracture was

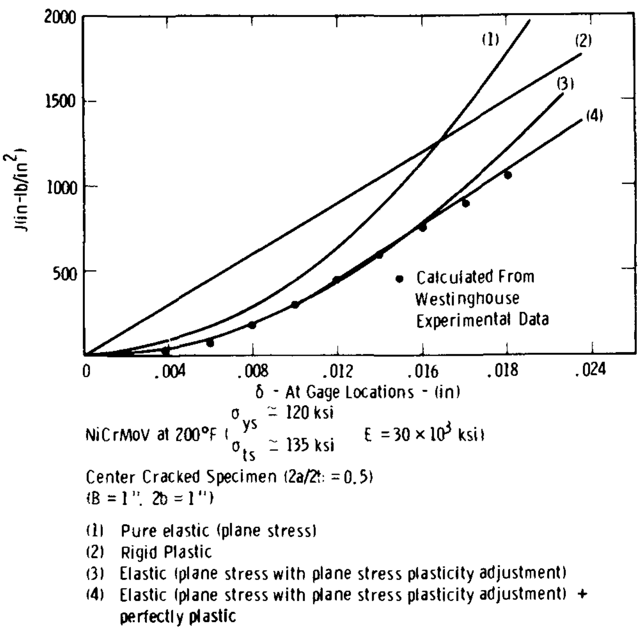

FIG. 16 – *J as a function of gage point displacement, δ, for Westinghouse Ni-Cr-Mo-V center notch test specimen.*

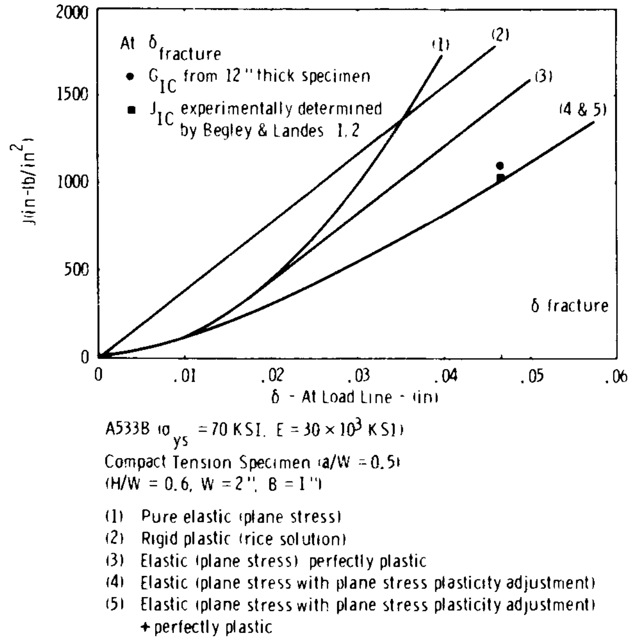

FIG.17 – *J as a function of load line displacement, δ, for Westinghouse A533B compact tension test specimen.*

experimentally determined to be 0.07 in. [*1*]. Boundary collocation results on the CT specimen in Fig. 7 indicate that a/W = 0.5 load line deflection is approximately two-thirds of that deflection at the outer specimen edge. This implies that a gage deflection of 0.07 in. corresponds to a load line deflection of 0.0467 in. For a load line fracture deflection of 0.0467 in. a critical value of J estimated for elastic (plastically adjusted) plus perfectly plastic loading is found to be 1025 in.·lb/in.^{2}, Fig. 17. This is in extraordinary agreement with the Westinghouse experimentally determined plane strain critical J value (J_{Ic} = 1030 in.·lb/in.^{2}) for the same material test configuration [*1*]. The estimated critical J is also in very good agreement with plane strain (G_{Ic} = 1100 in.·lb/in.^{2}) results converted from fracture toughness measurements on specimens 12 inches thick [*1*].

Consequently, upon examination of Figs. 15 through 17, it appears that very simple estimation of elastic perfectly plastic J versus δ may be provided from extension of a line parallel to the rigid plastic solution at its point of tangency with the plasticity adjusted elastic solution.

Summary

For the materials and test configurations considered, reasonable estimations of the J versus δ relationship were made utilizing generated load displacement records assumed to be plane stress, plastically adjusted linear elastic, plus perfectly plastic.

Provided that suitable approximations of the J versus δ relationship exist, it appears that critical J estimations, for a particular material test configuration, could be obtained given the additional experimental knowledge of the load point deflection δ at the inception of fracture. For a given flaw size, a minimum of one (or possibly two) experimental load displacement record(s) would be sufficient to establish this information, along with the analytical procedures demonstrated herein.

Employing these procedures, and utilizing Westinghouse data [1], analytical predictions of critical plane strain J (J_{Ic}) were found to agree quite well with Westinghouse J_{Ic} results [1]. Moreover, the estimated critical J was also found to agree quite well with G_{Ic} as determined from state-of-the-art valid plane strain (K_{Ic}) fracture toughness tests.

It also becomes apparent that the ability to effect reasonable approximations of the J versus δ relationship does not rest entirely on an ability to estimate load displacement behavior with great precision. Instead, J versus δ approximation appears to be appropriately related to estimating characteristic changes in load displacement behavior with changing flaw size.

The J versus δ estimation technique considered herein, which utilizes no more than elements of linear elastic fracture mechanics and plastic limit analysis, appears to offer considerable promise in application related to elastic-plastic failure analysis of complex engineering structures for which it might be difficult to obtain exact solutions for the relationship.

Acknowledgments

We fully acknowledge sponsorship of this work by Westinghouse Research Laboratories' Fracture Mechanics Group. Special acknowledgment is due to E.T. Wessel, manager of the Westinghouse Fracture Mechanics Group, for his leadership, cooperation, and interest which helped greatly to stimulate the progress of this work, and, similarly, acknowledgment is due to his co-worker, J.A. Begley with whom we worked very closely.

We are extremely grateful to S. Shadle and R. Lane of Del Research for their development of suitable computer programs and for their effective assistance through all the numerical work. In addition, acknowledgment is made to J.A. McCall for her secretarial assistance.

APPENDIX 1

Computation of J as a Function of δ from a Family of Load-Displacement Records [1]

Given a typical test specimen configuration, Fig. 18*a*, load-displacement (P-δ) records are obtained for a number of constant crack lengths, Fig. 18*b*. For given

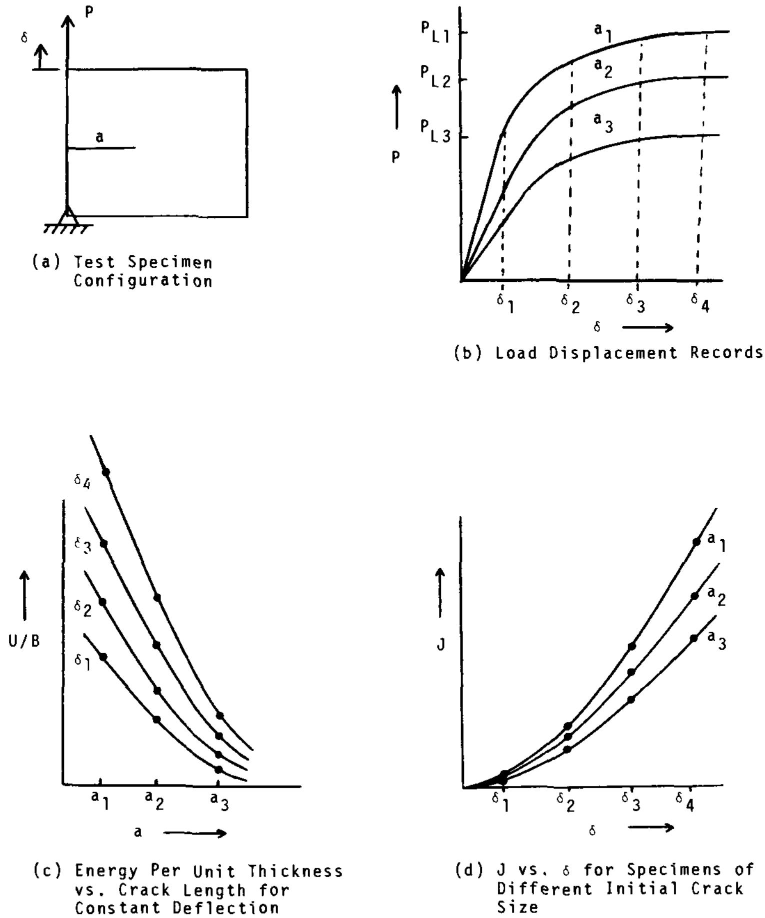

FIG. 18—*Schematic diagram of* J *versus* δ *evaluation employing a family of load displacement records.*

values of deflection, δ, the area under each load-displacement record may be interpreted as "pseudo-potential energy" of the body at that displacement. This can then be plotted, Fig. 18*c*, as pseudo-potential energy normalized per unit thickness, U/B, versus crack length, a, for constant δ. Following Eq 3, J may be interpreted as the area between load-displacement curves of neighboring crack size, or more simply as the negative slope of the U/B versus a curves, for given constant δ. This permits evaluation of a J versus δ relationship which is also a function of crack size, Fig. 18*d*. Given the J versus δ relationship for a given crack size, an experimentally determined fracture displacement which characterizes onset of unstable fracture may be used to determine a critical J.

APPENDIX 2

Calculation of Elastic and Plastically Adjusted Load-Displacement Relationships

Three Point Bend Bar

For the three point bend bar of Fig. 4 where δ is the deflection of the load point, an elastic compliance calibration may be derived as follows [*14*].

Define U_{tot} as the total amount of strain energy stored in a cracked bend bar. The total strain energy may be divided into that which would exist if no crack were present, plus that which is due to the introduction of a crack. That is,

$$U_{tot} = U_{no\ crack} + U_{due\ to\ crack} \tag{21}$$

The no crack contribution may simply be divided into bending and shear contributions which can be calculated from well known strength of material results [*25*]. That is,

$$U_{no\ crack} = U_{bending} + U_{shear}$$

where

$$U_{bending} = \int_0^s \frac{M^2\,dx}{2EI}$$

$$M = 1/2\,Px$$

and

$$U_{shear} = \int_{-W/2}^{W/2} \int_0^s \frac{\tau^2}{2G}\,Bdxdy$$

where

$$\tau = \frac{V}{IB} \int_y^{W/2} ydA$$

I = moment of inertia, E = elastic modulus, G = shear modulus, τ = shear stress, M = cross sectional bending moment, V is average shear force across a cross sectional area, all other symbols are defined in Fig. 4.

To determine the strain energy contribution due to the crack, one may recall from the Griffith approach [*7, 8, 13, 26*] that G, the energy available for crack extension, is defined as

$$G = \frac{\partial U_{due\ to\ crack}}{B\partial a} \tag{22}$$

from which

$$U_{\text{due to crack}} = B \int_0^a G da$$

Converting G to K, the stress intensity factor

$$U_{\text{due to crack}} = \frac{B}{E'} \int_0^a K^2 da$$

where

$E' = E$ for plane stress
$\quad = E/(1 - \nu^2)$ for plane strain

and

$$K = \frac{PS}{BW^{3/2}} \quad F\left(\frac{a}{W}\right)$$

is the form of the stress intensity expression for the three point bend bar, Eq 12. The total deflection δ_{tot} may be summed as a contribution without the crack plus a contribution due to the crack. That is,

$$\delta_{tot} = \delta_{\text{no crack}} + \delta_{\text{due to crack}} \tag{23}$$

Employing Castigliano's theorem and Eqs 21-23

$$\delta_{tot} = \frac{\partial U_{tot}}{\partial P} = \frac{\partial U_{\text{no crack}}}{\partial P} + \frac{\partial U_{\text{due to crack}}}{\partial P}$$

which gives δ as a linear function P

$$\delta = P \times F' \quad (a/W, S, B, W, E, \nu)$$

For the configuration of Fig. 4, this relationship is given by Eq 9.

Center Notch Specimen

For the center notch specimen of Fig. 5, one may compute the compliance relationship as follows. Two components of deflection may be considered as that due to the crack and that which would exist if no crack were present. From which,

$$\delta_{tot} = \delta_{\text{no crack}} + \delta_{\text{due to crack}} \tag{24}$$

$\delta_{\text{no crack}}$ is simply,

$$\delta_{\text{no crack}} = \frac{P(2D)}{(2bB)E} \tag{25}$$

where all specimen dimensional symbols are given in Fig. 5. To find the contribution of the crack, the total energy release rate for the two crack tips may be written as

$$G = \frac{P^2 \partial\lambda}{2(2B\partial a)}$$

but $G = K^2/E' + K^2/E'$ (since there are two cracks) and,

$$\lambda = \frac{\delta_{\text{due to crack}}}{P} = \frac{4B}{P^2 E'} \int_0^a K^2 da \tag{26}$$

employing the appropriate stress intensity factor, Eq 13, a δ contribution due to the crack may be computed. Summing the deflection contributions given by Eqs 25 and 26 results in a final compliance relationship given by Eq 10 where higher order terms are neglected.

r_y *Plasticity Adjustment*

A simple technique for applying an r_y plasticity adjustment to a linear elastic load displacement relationship can be illustrated as follows.

Consider that by linear elastic fracture mechanics techniques a purely elastic compliance relationship has been developed. A typical relationship for a compact tension specimen is graphically represented in Fig. 19*a* where compliance is dimensionlessly plotted as a function of dimensionless crack size. Employing the plasticity adjustment suggested by Eqs 8 and 8a

$$\frac{a_{\text{eff}}}{W} = \frac{1}{W}\left[a_0 + r_y\right] = \frac{1}{W}\left[a_0 + \frac{1}{2\pi}\left(\frac{K}{\sigma_{ys}}\right)^2\right] \tag{27}$$

where a_0, is the actual original crack size. Typically, substituting the stress intensity expression for a compact tension specimen, Eq 27 becomes

$$\frac{a_{\text{eff}}}{W} = \frac{a_0}{W} + \frac{P^2 F^2 (\frac{a_0}{W})}{2\pi B^2 W^2 \sigma_{ys}{}^2} \tag{28}$$

for a given load P_1, an $\left(\frac{a_{\text{eff}}}{W}\right)_1$ may be computed from Eq 28 as

$$\left(\frac{a_{\text{eff}}}{W}\right)_1 = \frac{a_0}{W} + \frac{P_1{}^2 F^2 (\frac{a_0}{W})}{2\pi B^2 W^2 \sigma_{ys}{}^2}$$

from which an adjusted $(E\delta B/P)_1$ may be determined from Fig. 19*a*. Having P_1 and $(E\delta B/P)_1$ known, as adjusted deflection, δ_1, can be computed as

$$\delta_1 = \left(\frac{E\,\delta\,B}{P}\right)_1 \frac{P_1}{Eb}$$

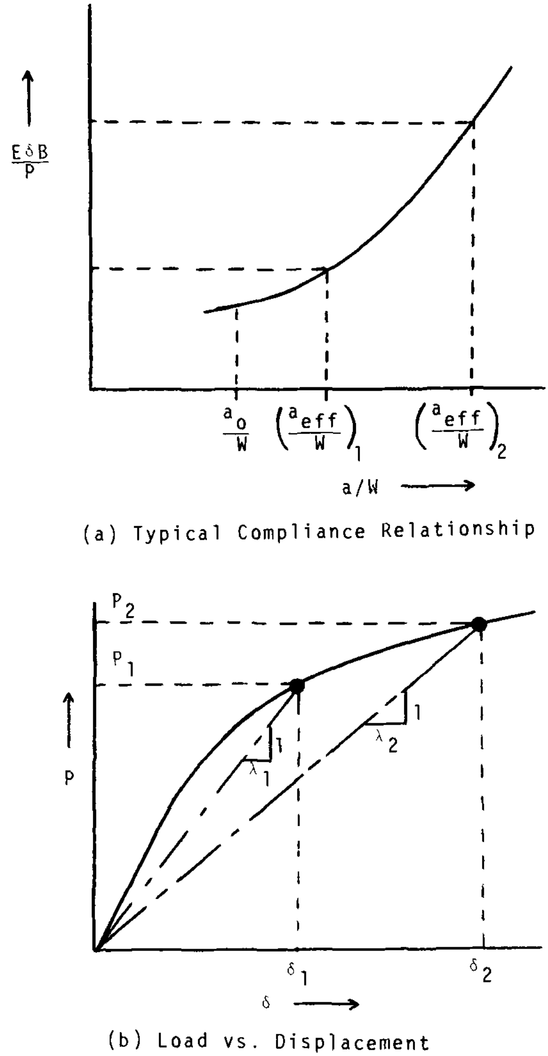

FIG. 19—*Sample calculation of* r_y *plasticity adjusted load displacement records.*

Hence, P_1 and δ_1 are known and can be plotted as a point on a load displacement record, Fig. 19*b*. The same procedure may be followed to generate a series of points (P_2, δ_2) . . . (P_n, δ_n) which will produce a plastically adjusted elastic load displacement record for a given initial crack size.

References

[*1*] Begley, J.A. and Landes, J.D., "The *J* Integral as a Fracture Criterion," and "The Effect of Specimen Geometry on J_{Ic}," *Fracture Toughness, Proceedings of the 1971 National Symposium on Fracture Mechanics, ASTM STP 514*, American Society for Testing and Materials, 1972, pp. 1-20 and 24-39.

[*2*] Rice, J.R., *Journal of Applied Mechanics, Transactions of the American Society of Mechanical Engineers*, June 1968, pp. 379-386.

[*3*] Hayes, D.J., "Some Applications of Elastic-Plastic Analysis of Fracture Mechanics," Ph.D. dissertation, Department of Mechanical Engineering, Imperial College, University of London, Oct. 1970.

[*4*] W.K. Wilson and S.K. Chan, private communication, Westinghouse Research Laboratories, Pittsburgh, Pa., 1971.

[*5*] Levy, N., Ostergren, W.J., Marcal, P.V., and Rice, J.R., *International Journal of Fracture Mechanics*, Vol. 7, No. 2, 1971, pp. 143-156.

[*6*] Rice, J.R. in *Fracture*, Vol. II, Academic Press, New York, 1968.

[*7*] Irwin, G.R., *Welding Journal Research Supplement*, 1954.

[*8*] Irwin, G.R., *Journal of Applied Mechanics, Transactions of the American Society of Mechanical Engineers*, 1957.

[*9*] Paris, P.C., Dicussion in *Fracture Toughness, Proceedings of the 1971 National Symposium on Fracture Mechanics, ASTM STP 514*, American Society for Testing and Materials, 1972, pp. 21-23.

[*10*] Irwin, G.R., "Plasticity Characterizations of Progressive Crack Extension," comments made at ASTM E 24 Task Group meeting, ASTM Headquarters, Philadelphia, 8 Sept. 1971.

[*11*] "Tentative Method of Test for Plane Strain Fracture Toughness of Metallic Materials," ASTM E 399-70T; also, *Review of Developments in Plane Strain Fracture Toughness Testing, ASTM STP 463,* American Society for Testing and Materials, 1970.

[*12*] McClintock, F.A., in *Fracture*, Vol. III, Academic Press, New York, 1971.

[*13*] Paris, P.C. and Sih, G.C. in *Fracture Toughness Testing and Its Applications, ASTM STP 381*, American Society for Testing and Materials, 1965.

[*14*] Paris, P.C., "The Mechanics of Fracture Propagation and Solutions to Fracture Arrestor Problems," Document D2-2195, Boeing Company, 1957.

[*15*] Irwin, G.R. and Paris, P.C. in *Fracture*, Vol. III, Academic Press, New York, 1971.

[*16*] Gross, B., Roberts, E., and Srawley, J.E., *International Journal of Fracture Mechanics*, Vol. 4, No. 3, Sept. 1968.

[*17*] Roberts, E., *Materials Research and Standards*, MTRSA, Vol. 9, No. 2, Feb. 1969.

[*18*] Fedderson, C., Discussion to *Plane Strain Crack Toughness Testing of High Strength Metallic Materials, ASTM STP 410*, American Society for Testing and Materials, 1967, p. 77.

[*19*] Wessel, E.T., *Journal of Engineering Fracture Mechanics*, Vol. 1, No. 1, 1968, p. 77f.

[*20*] Brown, W.F., Jr., and Srawley, J.E., *Plane Strain Crack Toughness Testing of High Strength Metallic Materials, ASTM STP 410,* American Society for Testing and Materials, 1966, p. 13.

[*21*] Green, A.P. and Hundy, B.B., *Journal of the Mechanics and Physics of Solids*, Vol. 4, 1956, pp. 128-144.

[*22*] McClintock, F.A., *Welding Journal Research Supplement*, Vol. 26, 1961, pp. 202-208.

[*23*] Rice, J.R., *"The Line Spring Model for Surface Flaws"* to be published in Proceedings of the Surface Flaw Symposium, ASME Winter Annual Meeting, Nov. 1972.

[*24*] Begley, J.A. and Toolin, P.R., "Fracture Toughness and Fatigue Crack Growth Rate Properties of a NI-Cr-Mo-V Steel Sensitive to Temper Embrittlement," presented at the Fourth National Symposium on Fracture Mechanics, Carnegie-Mellon University, Pittsburgh, Pa., Aug. 1970.

[*25*] Den Hartog, J.P., *Strength of Materials*, McGraw Hill, New York, 1949.

[*26*] Griffith, A.A., *Philosophical Transactions of the Royal Society,* Vol. A-221, 1920.

W. A. Maxey,[1] *J. F. Kiefner,*[1] *R. J. Eiber,*[1] *and A. R. Duffy*[1]

Ductile Fracture Initiation, Propagation, and Arrest in Cylindrical Vessels

REFERENCE: Maxey, W.A., Kiefner, J.F., Eiber, R.J., and Duffy, A.R., "**Ductile Fracture Initiation, Propagation, and Arrest in Cylindrical Vessels,**" *Fracture Toughness, Proceedings of the 1971 National Symposium on Fracture Mechanics, Part II, ASTM STP 514,* American Society for Testing and Materials, 1972, pp. 70-81.

ABSTRACT: Presented is a discussion of an hypothesized analytical explanation of ductile fracture initiation, propagation, and arrest in cylindrical pressure vessels and piping. The hypothesized analytical treatment is an attempt to predict initiation and arrest conditions for ductile fractures using Charpy V-notch plateau energy as a means of determining the toughness of the material. Data from a number of full-scale experiments on gas transmission pipe, nuclear reactor piping, and other cylindrical vessels are presented and are shown to be in agreement with the hypothesis.

KEY WORDS: fracture (materials), fracturing (cracking), crack propagation, crack initiation, failure, fracture strength, toughness, ductility, yield strength, geometries, pressure vessels, stainless steels, steels

Research concerning the initiation of flaws and the propagation of fractures in cylindrical vessels has been conducted at Battelle Memorial Institute, Columbus Laboratories for a number of years. This research has been conducted for the American Gas Association to investigate the behavior of large-diameter, high-pressure gas transmission pipes and for the U.S. Atomic Energy Commission to investigate large-diameter, primary coolant piping at elevated temperatures for nuclear reactors. Numerous failure investigations have also been conducted to keep abreast of current problem areas. The details of the experimental procedures, have been reported previously [*1-4*] and will not be discussed here.

Most of the research that has been conducted at Battelle has been on low-to-medium strength steels which are strain rate sensitive and which exhibit ductile to brittle transitions; however, there are a few experiments on 9-Ni, 316-stainless, and 304-stainless steels included. The discussions presented herein are applicable to these classes of material but will be limited to their ductile

[1] Battelle Memorial Institute, Columbus Laboratories, Columbus, Ohio 43201.

behavior. The discussion is broken down into the initiation behavior of flaws, the effect of vessel geometry, critical flaw size relationships, the effect of yield strength, and the effect of Charpy V upper plateau energy, and the propagational behavior of fractures, unloading of force, effect of fracture speed on unloading, and fracture arrest. Also a section is included describing problem areas requiring further research.

The cylindrical vessels that have been examined have ranged from 6.62 to 48 in. in diameter, from 0.190 to 1.730 in. in wall thickness, and have yield strengths in the range of 22 to 111 ksi.

Fracture Initiation Behavior

The initiation of fracture requires the presence of a defect in a structure. In the cylindrical vessel, subjected only to internal pressure loading, the most critical defect orientation is axially as this is normal to the maximum stress field.

The through-wall axial defect has been examined experimentally and has led to the development of semi-empirical formulae to predict the critical defect size. The vessel's geometry and the material's yield strength and ductile toughness are the important factors and these factors are examined below.

Geometry and K_c *Equation*

The product of cylinder radius, R, and thickness, t, as a normalizing parameter for axial perturbations of cylindrical shells has been in use for some time. Folias [*5*] has used $c/\sqrt{Rt}$ for normalizing the effect of through-wall cracks of total length $2c$ in cylindrical pressure vessels. The experiments at Battelle have shown this parameter to be very useful in comparing critical crack lengths in vessels of different geometry [*4, 6*].

The other factor relating to geometry is the stress concentration factor, M, a function of $c/\sqrt{Rt}$ which accounts for the outward bulging associated with a through-wall axial crack in a pressure vessel loaded only by internal pressure. Fig. 1 shows the relationship between M and $c/\sqrt{Rt}$. The product of the M factor and the nominal hoop stress, σ_H (calculated by the Barlow formula $\sigma_H = PR/t$ where P is internal pressure) in Folias' analysis is equivalent to the stress normal to a crack of the same length in an infinite plate. Although the analysis is strictly elastic, it has been found to be very useful in predicting the gross hoop stress for ductile initiation of pressure vessels containing through-wall cracks.

The equation defining plane stress fracture toughness, K_c, that has consistently agreed with the experimental data, was proposed by Hahn et al [*7*]. This equation is the plate equation derived by Goodier and Field [*8*] and modified by Hahn et al [*7*] to include the geometry terms and the materials apparent flow stress, $\bar{\sigma}$:

$$K_c^2 = \frac{8c\,(\bar{\sigma})^2}{\pi}\ \ell n \sec \frac{\pi M\,\sigma_H}{2\bar{\sigma}} \qquad (1)$$

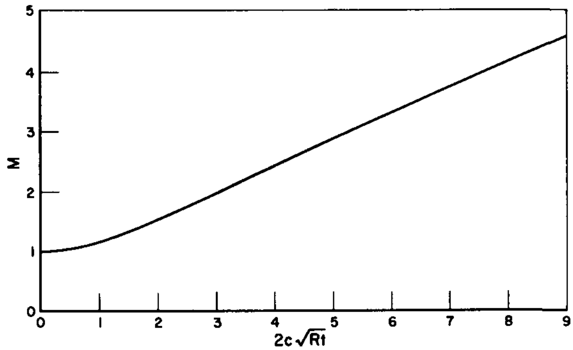

FIG. 1 - *Exact Folias* M *for steel as a function of* $2c/\sqrt{Rt}$.

Flow stress has been used here to describe the properties of a strain-hardening material in terms of an equivalent elastic-plastic material having a yield strength, $\bar{\sigma}$ somewhat larger than the material's yield strength, Y.

Examination of Eq 1 shows that for high toughness materials $M\ \sigma_H$ approaches an equality with $\bar{\sigma}$ and this phenomenon has been described by Hahn et al [7] as failure by large-scale yielding or plastic instability. In this region of toughness, the failure stress is governed by the material flow stress and the vessel geometry only and is described by the equation

$$\sigma_H = \frac{\bar{\sigma}}{M} \tag{2}$$

By using the experimental data $M\ \sigma_H > Y$, where Y is measured transverse to the pipe axis, we can empirically arrive at a value for $\bar{\sigma}$ and in so doing we have found the best value to be

$$\bar{\sigma} = (Y + 10) \text{ ksi} \tag{3}$$

with the quantity $(M\sigma_H - Y)$ ranging from 0 to 18.7 ksi and one standard deviation being 4 ksi. The following table lists ranges and averages of the quantity $(M\ \sigma_H - Y)$ for various mean yield strength levels.

Y mean, ksi	Number of Data Points	Average $(M\ \sigma_H - Y)$, ksi	Range $(M\ \sigma_H - Y)$, ksi
35	26	10.8	0 to +18.7
45	10	10.1	0 to +17.6
52	15	9.1	0 to +18.1
60	37	8.9	0 to +16.8

Fig. 2 describes much of what has been discussed up to this point. The data selected for this figure represent data where $M\sigma_H > Y$ and the yield strength variation has been eliminated in that all the data used have a measured Y of 60 ksi within 2 ksi. The average Y of all the materials is 60.4 ksi. The lower part of Fig. 2 shows the raw data plotted as hoop stress, σ_H, at failure versus half crack length, c, and it is seen that much scatter exists in this plot. The upper part of Fig. 2 shows the plot of σ_H versus $c/\sqrt{Rt}$ and the scatter is reduced essentially to that normally experienced for experimental data. The solid line through the data in the upper plot of Fig. 2 is the plot of Eq 2 combined with Eq 3 and the average yield strength, 60.4 ksi, of this material, which is seen to be very representative of the data. Thus, $c/\sqrt{Rt}$ is a normalizing parameter for various radius and thickness vessels.

Charpy V Correlation

The data above have covered the high toughness region of Eq 1. At this point materials of lower toughness will be examined. If the data are restricted to those whose experimental $M\sigma_H$ is less than 80 percent of $\bar{\sigma}$ we can calculate a valid K_c using Eq 1 and a corresponding G_c where

$$G_c = \frac{K_c^{\ 2}}{E} \tag{4}$$

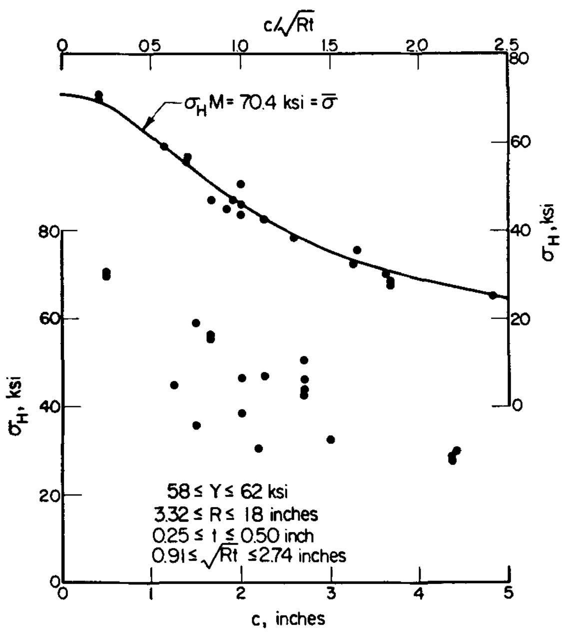

FIG. 2—*Through-wall failure data for 60,000 psi yield strength pipe.*

as is normally defined in fracture mechanics. The one material property that appears to correlate with G_c is the Charpy-V upper plateau energy. Fig. 3 shows the correlation between G_c and Charpy-V upper plateau energy converted to inch pounds, and divided by the net cross-sectional area, A, of the Charpy bar in order to get consistent units with G_c. It can be seen in Fig. 3 that a fairly good correlation exists on a one-to-one basis. Irwin et al [9] calculated a relationship relating G_c with the unit area work requirements for fracture of a sharply notched bar in bending and concluded G_c was equal to 90 percent of the unit area work requirement.

Evaluation of the Initiation Formula Over Total Range of Data

The effects of geometry and material yield strength for high toughness materials have been considered. For low-toughness materials Charpy-V plateau energy, geometry, and material yield strength are the important parameters. If Eqs 1 and 4 are combined and the unity correlation of G_c with Charpy-V plateau energy is used, the terms in Eq 1 can be transposed to obtain

$$\left[\frac{K_c{}^2\pi}{8c(\bar{\sigma})^2}\right] = \left[\frac{C_v \max \frac{12}{A} E\pi}{8c(\bar{\sigma})^2}\right] = \ell n \sec \frac{\pi}{2} \left[\frac{M\sigma_H}{\bar{\sigma}}\right] \qquad (5)$$

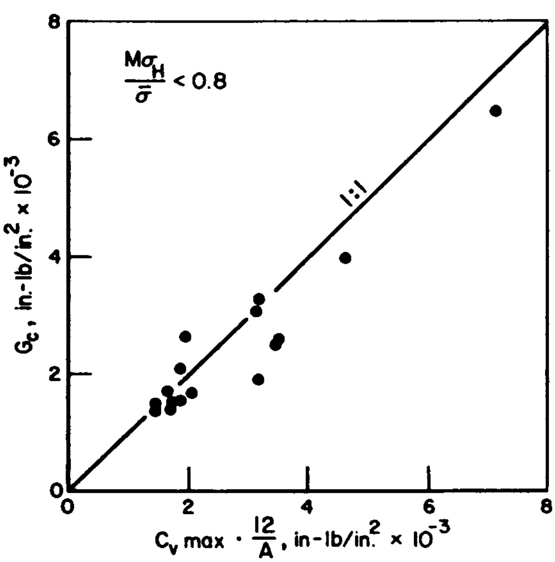

FIG. 3—*Charpy-V upper plateau energy correlation with* G_c.

which can be considered a two-parameter equation with $[M\sigma_H/\bar{\sigma}]$ as one parameter and the two equal parameters on the left as the second parameter. Fig. 4 is a log-log plot of Eq 5 where the parameter containing K_c in the abscissa is used for plotting the solid curve and the parameter containing C_v max on the abscissa is used to plot the experimental data. The dashed lines represent ±10 percent variation in $M\sigma_H/\bar{\sigma}$ against the solid line. Statistics on the ratio $[M\sigma_H/\bar{\sigma}]_{\text{experimental}}$ to $[M\sigma_H/\bar{\sigma}]_{\text{calculated}}$ show this ratio to be 0.997 with one standard deviation of 8.0 percent. These data show that we can closely predict the ductile failure stress of a through-cracked pressure vessel in regions of relatively low, intermediate, and high toughness using Eq 5 and the easily obtainable material properties of yield strength and Charpy-V plateau energy. The study of the through-wall crack in itself is not of practical importance in pressure vessels, but the understanding of the through-wall crack is necessary to the understanding of the propagation and arrest of ductile fracture in pressure vessels.

Fracture Propagation and Arrest

Contrary to some beliefs, the long-running ductile fracture does exist. So far the long-running ductile fractures experienced have been of the Mode I (tensile strains) type of fracture traveling in the axial direction having 100 percent shear lips, but being a tensile failure. Also short fracture lengths with the nominal appearance of antiplane shear fracture have occurred at the arrest of the Mode I fracture and this type always extends in a helical direction on the pipe. The need to be able to predict and control the unstable Mode I fracture led to the analysis of this section. Knowledge of the unloading of internal pressure and the

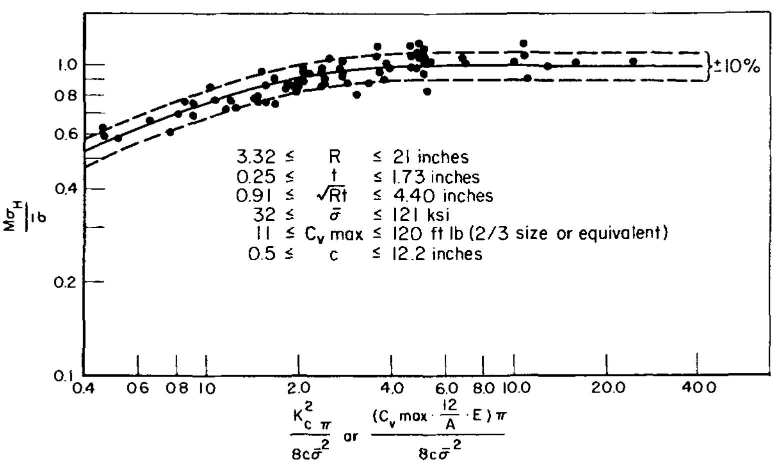

FIG. 4—*Correlation between data and* K_c *equation.*

structure arrest stress level are the important parameters in the propagation of ductile fracture and these will be discussed separately below.

Unloading of Internal Pressure

The experiments described are of three different types:

Subcooled Water—These are pressure vessel tests where the water is heated and the pressure allowed to rise from the expansion of the heated water until failure occurs. Unloading occurs rapidly through the water phase to the saturation pressure corresponding to the temperature of the heated water and depending on the saturation and corresponding hoop stress ($\sigma_H = P_{sat}R/t$) the fracture either continues or arrests.

Water-Air—These are pressure vessel tests where the vessel is filled to approximately 90 percent with water and pressured to failure with air. Unloading is not accurately known for these experiments but the arrest stress level is assumed to be the highest level at which the crack (with an internal patch) can be forced to grow at relatively slow velocities and then arrest as the crack grows beyond the patch and leakage occurs.

All Gas—These are buried pipe tests designed in all aspects to simulate the long buried pipeline. The internal pressure in the region at the crack tip will drop, in a nonlinear fashion, according to the ratio of the speed of the fracture [*1*, *2*] to the acoustic velocity of the gas. Fig. 5 shows the relationship between nominal hoop stress at the fracture front and fracture speed. The minimum value is at zero fracture speed where the pressure is maintained at 29 percent of the initial pressure until the arrival of the reflected decompression wave.

The latter type experiments are most important to the study, but types 1 and 2 will be used to help define the boundary between arrest and propagation.

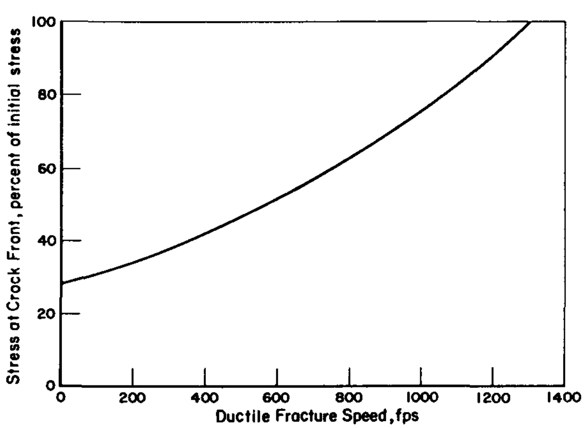

FIG. 5—*Decompression at different fracture speeds.*

Arrest Stress of the Structure

Structure is emphasized here because the section on initiation of through-wall defects described the importance the geometry of the structure plays and it is believed that it plays the same role toward the arrest of the crack. An arrested crack has zero fracture velocity and is only believed to be different from initiation in that it is a longer crack at a lower stress level. Fig. 6 is a simplified schematic based upon the curve from Fig. 4 and describing the stages a crack in a pipe goes through between initiation and arrest. These stages, assuming gas is the pressurizing medium, are:

(1) Initiation

(2) The crack lengthens and correspondingly M increases and the fracture velocity increases through some supercritical zone of acceleration. The internal gas pressure will momentarily remain the same, as the full opening necessary for nonsteady outflow of the gas has not yet been established.

(3) It is assumed that some maximum effective crack length $(c/\sqrt{Rt})_{max}$ and the corresponding M value is achieved.

(4) At this point, a full opening develops and decompression starts so that the internal pressure and corresponding σ_H drops. The level to which the pressure drops will depend upon the fracture speed.

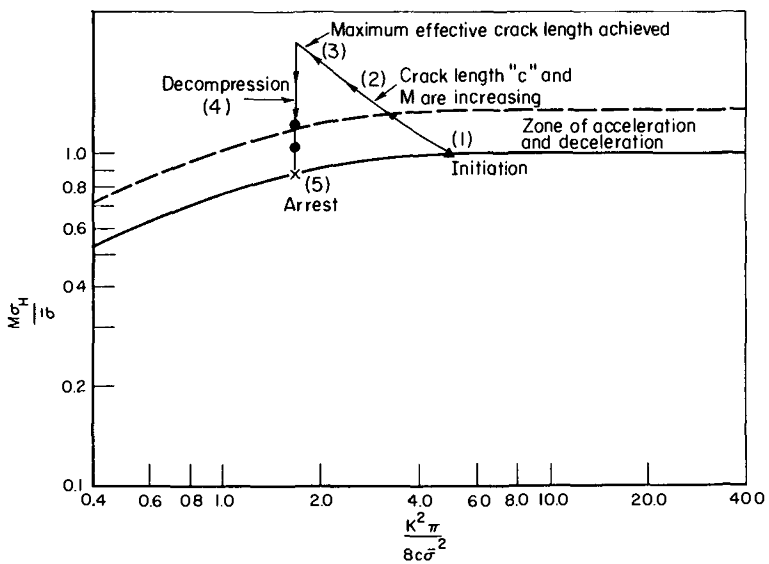

FIG. 6—*Schematic describing initiation, propagation, and arrest.*

(5) Arrest will occur if the decompressed level is within the decelerate zone and if the zero speed stress level (0.29 of the initial stress level) is beneath the initiation curve.

Although gas pressure loading has been assumed, the other types of loading described would be expected to behave similarly except decompression might occur faster and points 1 and 5 in Fig. 6 would be expected to lie closer together on the abscissa.

The one parameter that has an unknown value, but which is believed to be constant, is the maximum effective crack length. Eq 1 can be written in another form by transposing $\bar{\sigma}^2$ and dividing both sides by $\sqrt{Rt}$ so that we obtain Eq 6.

$$\frac{K^2}{\bar{\sigma}^2 \sqrt{Rt}} = \frac{8}{\pi} \frac{c}{\sqrt{Rt}} \ln \sec \frac{\pi M \sigma_H}{2\bar{\sigma}} \tag{6}$$

The bracketed quantity on the left side of the equation can be considered to be a normalized toughness parameter. The arrest data can be plotted as $\sigma_H'/\bar{\sigma}$ (where σ_H' is now at the decompressed level) versus the normalized toughness by making the $C_{v\,max}$ substitution for K^2/E. Since M is determined by the quantity $c/\sqrt{Rt}$, lines of constant $c/\sqrt{Rt}$ can be used as the third parameter on the plot and, if there is a maximum effective crack length, one of these lines should divide the data between arrest and propagate. Fig. 7 is such a plot where the three types of experiments described above are coded and in all three types the solid data points are arrests and the open data points represent propagation. The data points labeled decelerate represent data where sufficient fracture velocity measurements were made to know that the fracture was slowing down and could be expected to arrest if that pipe were long enough. The solid line represents $c/\sqrt{Rt} = 3$ and the corresponding $M = 3.33$. The dashed lines represent ±10 percent of $\sigma_H'/\bar{\sigma}$ error band like that observed on the initiation data of Fig. 4. The materials and range of parameters is the same for both Figs. 4 and 7.

It is observed in Fig. 7 that the line of $c/\sqrt{Rt} = 3$ closely defines an arrest stress level that is dependent only on normalized toughness. A reason for this particular value being the maximum effective crack length may be apparent from the work of Copley and Sanders [*10*]. They have described two modes of bending behavior for a cracked cylindrical shell under internal pressure: one corresponds to singular bending tension on the outside surface of the shell for $c/\sqrt{Rt} < 3$ and the other to tension on the inside surface for $c/\sqrt{Rt} > 3$ with uniform tension through the wall thickness at $c/\sqrt{Rt} = 3$. The Folias analysis has been found to predict the same phenomenon. Fig. 8 shows the derived circumferential strain (ϵ_c) magnification factors for the inside and outside diameters. It is seen in Fig. 8 that at $c/\sqrt{Rt} = 3$ ($2c/\sqrt{Rt} = 6$) the circumferential strain is uniform through the wall thickness and that in going from low to high

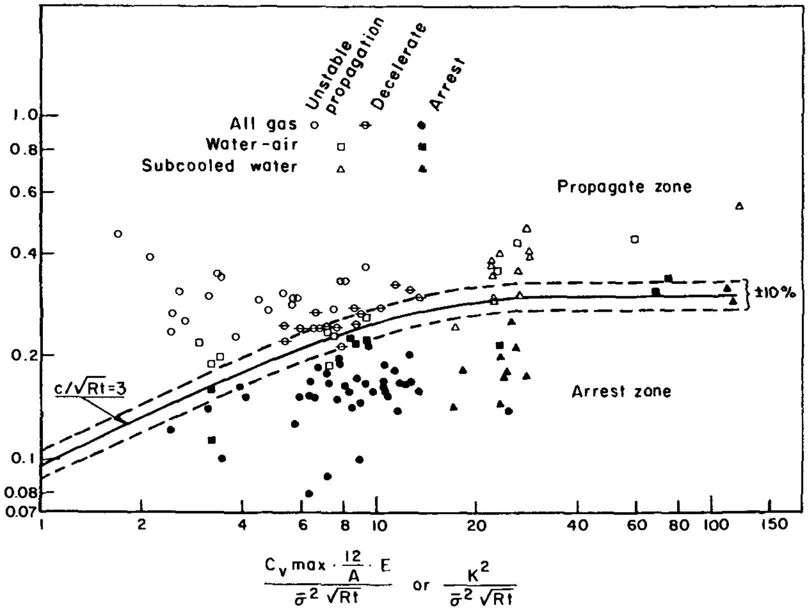

FIG. 7—*Ductile propagation and arrest at decompressed stress levels.*

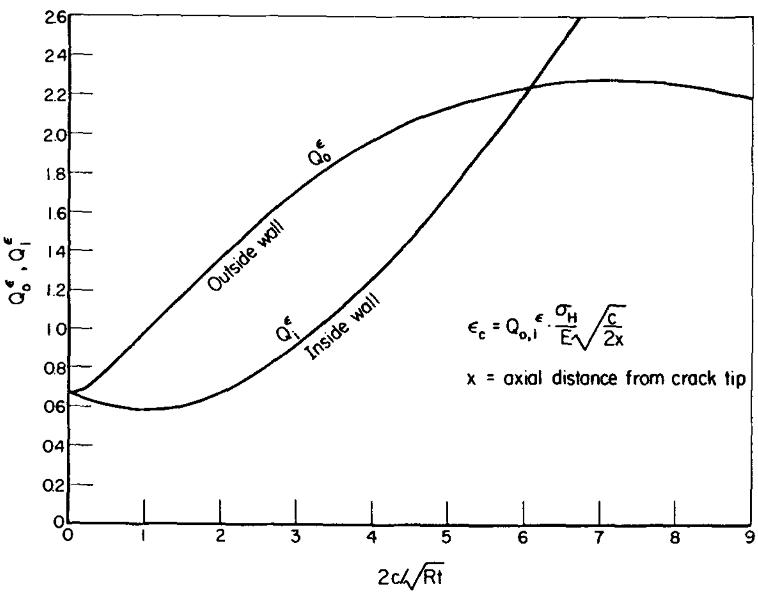

FIG. 8—*Circumferential strain magnification factors.*

$c/\sqrt{Rt}$ the maximum strain changes from the outside diameter to the inside diameter with $c/\sqrt{Rt} = 3$ being the changeover point. These observations, combined with the dividing line between the propagation and arrest data shown in Fig. 7, seem to indicate, at least when plasticity is involved, that $c/\sqrt{Rt}$ does not exceed 3 and correspondingly M does not exceed 3.33.

The all-gas data in Fig. 7 indicate two types of propagation behavior: one is a relatively higher and constant fracture speed that is completely unstable and the other is a slower, decelerating fracture speed that would be expected to arrest provided it can decelerate to a decompressed stress level that causes arrest. Fig. 9 is a plot similar to Fig. 7 except that only the all-gas data points have been used. The dividing line between propagation and arrest has been carried to Fig. 9 and a new line is included that separates the constant speed data within a ±10 percent error band from the decelerating speed. This new line has a constant $c/\sqrt{Rt}$ equal to 2.25 and corresponding M equal to 2.67 and, although it gives a good fit with the data, it is also the line defined in taking Eq 6 to the limit of low K^2 and halving K^2 for arrest while holding σ'_H constant. These constants are being successfully used to set up new experiments designed to obtain additional data on the value of the constant shear fracture speed and hopefully determine those parameters that this speed is dependent upon.

Conclusions

The results of the research to date indicate that the hypothesis described in this progress report provides a method of predicting initiation, propagation, and arrest of ductile fracture. This research is continuing and additional results that are obtained will be used to provide additional confirmation of the hypothesis. If pipe size and strength level are known, then the two parameters that are necessary to use this hypothesis are the Charpy upper plateau energy level and knowledge that the material is used above its ductile to brittle transition temperature as defined in the drop weight tear test (ASTM E 436).

Areas Requiring Further Research

As pointed out above, this hypothesis has been successful in designing recent experiments. The important quantity necessary in designing an experiment is the constant fracture speed, which at present can only be estimated based on accumulated experience and past water-air pressure vessel experiments. Recently two observations have been made. One, that the fracture velocity near the origin (where the pressure is still high) in an all-gas test is higher than the constant speeds observed 20 to 30 feet from the origin and, two, that in special instrumentation areas where there was no backfill covering the pipe an increased fracture velocity was observed. Both of these observations cast doubts on the pertinence of fracture velocities measured in short water-air pressure vessel experiments conducted previously. All-gas experiments are currently being designed to look at the effect of gas pressure and the effect of backfill on ductile fracture speed. These experiments will be in the constant speed region, that is, above the line representing $c/\sqrt{Rt} = 2.25$ in Fig. 9.

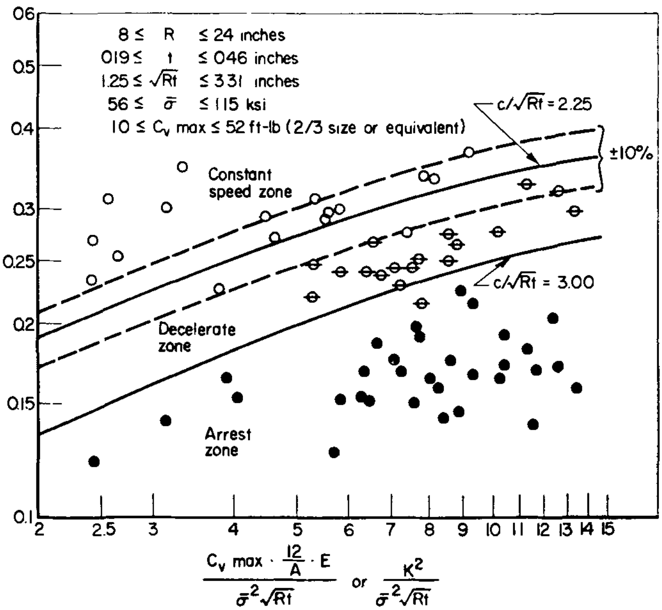

FIG. 9—*Ductile propagation and arrest of the all-gas experiments.*

References

[1] *Symposium on Line Pipe Research*, American Gas Association, Catalogue No. L30000, March 1966.

[2] *Fourth Symposium on Line Pipe Research*, American Gas Association, Catalogue No. L30075, Nov. 1969.

[3] Eiber, R.J., Maxey, W.A., Duffy, A.R., and Atterbury, T.J., "Investigation of the Initiation and Extent of Ductile Pipe Rupture", Final Report, Phase I, USAEC Contract W-7405-eng-92, Task 17, BMI-1866, July 1969

[4] Eiber, R.J., Maxey, W.A., Duffy, A.R., and Atterbury, T.J., "Investigation of the Initiation and Extent of Ductile Pipe Rupture", Final Report, USAEC Contract W-7405-eng-92, Task 17, BMI-1908, June 1971.

[5] Folias, E.S., *Engineering Fracture Mechanics*, Vol. 2, 1970, pp. 151-164.

[6] Eiber, R.J., Maxey, W.A., Duffy, A.R., and McClure, G.M., "Further Work on Flaw Behavior in Pressure Vessels", Conference on Practical Applications of Fracture Mechanics to Pressure-Vessel Technology, The Institution of Mechanical Engineers, London, 1971.

[7] Hahn, G.T., Sarrate, M., and Rosenfield, A.R., *International Journal of Fracture Mechanics*, Vol. 5, 1969, pp. 187-210.

[8] Goodier, T.N. and Field, F.A., *Fracture of Solids*, Interscience Publishers, Inc., New York, 1963, p. 103.

[9] Irwin, G.R., Krafft, J.M., Paris, P.C., and Wells, A.A., "Basic Aspects of Crack Growth and Fracture", NRL Report 6598, Nov. 1967, p. 72.

[10] Copley, L.G. and Sanders, J.L., *International Journal of Fracture Mechanics*, Vol. 5, 1969, pp. 117-131.

J. G. Kaufman [1]

Sharp-Notch Tension Testing of Thick Aluminum Alloy Plate with Cylindrical Specimens

REFERENCE: Kaufman, J.G., "**Sharp-Notch Tension Testing of Thick Aluminum Alloy Plate with Cylindrical Specimens,**" *Fracture Toughness, Proceedings of the 1971 National Symposium on Fracture Mechanics, Part II, ASTM STP 514,* American Society for Testing and Materials, 1972, pp.82-97.

ABSTRACT: Tension tests of notched cylindrical specimens can be used for screening thick aluminum alloy plate, extruded shapes, and forgings for fracture toughness. The influence of certain testing variables, such as method of gripping, specimen diameter and length, notch tip radius, eccentricity, and rate of loading have been studied.

KEY WORDS: fracture (materials), fracture strength, toughness, stresses, loads (forces), yield strength, plasticity, eccentricity, fracture tests, tension tests, impact tests, aluminum alloys

Thick (2 to 8 in.) plate of several high strength aluminum alloys is being marketed on the basis of higher toughness than is achieved with conventional products. A typical example is 2124-T851 plate, marketed by all major aluminum producers, which has appreciably higher toughness by any index than does conventional 2024-T851 plate, particularly in the short-transverse direction. There are other high toughness products available, and new products of this type are likely to be forthcoming. The higher toughness of these products is amply demonstrated by their plane-strain fracture toughness, K_{Ic}, determined in accordance with ASTM E 399 [*1*].

There is a need for a test to determine by relatively economical means a comparative measure of resistance to unstable fracture of relatively thick aluminum alloy plate, extruded shapes and forgings, similar to that available in ASTM E 338 [*2*] for sheet and, possibly in the future, for plate up to 1 in. in thickness. This would not replace the need for direct measurement of K_{Ic}, but would

[1] Aluminum Company of America, Alcoa Research Laboratories, Mechanical Testing Division, New Kensington, Pa.

provide means of screening large numbers of samples in alloy development programs, quality control testing, and checking temperature sensitivity. Notch tension tests of cylindrical specimens have been shown to provide data which correlate well with plane-strain fracture toughness [*3*], and so are being considered for this purpose. In order to aid in the development of standardized procedures for performing this type of test, the influence of a number of variables in specimen design, grips, and testing technique have been evaluated.

Object

The object of this investigation was to establish the effect of certain variables, including specimen diameter, type of grip, length of reduced section, notch tip radius, and rate of loading, on the results of notch tension tests of cylindrical specimens for fracture toughness screening testing of thick aluminum alloy products.

Background

The notch tension test has been used for many years to evaluate relative notch toughness [*3-6*]. The tensile strength of the notched specimen is the primary data obtained from the test, but this strength by itself does not always provide much information about the inherent toughness of a material. More useful information is obtained by comparison of the notch tensile strength with the tensile properties of the material. For example, the ratio of the notch tensile strength to the tensile strength of the material (notch-strength ratio) is a measure of tensile efficiency. For many years, it also was considered a measure of notch toughness. More recently, the ratio of notch tensile strength to the tensile yield strength of the material (notch-yield ratio) has been recognized [*2, 7*] as providing more meaningful information about the inherent notch toughness of the material, that is, its ability to deform plastically in the presence of a severe stress raiser and thus avoid the development of a free-running crack leading to catastrophic failure of the component. The tensile yield strength of the material, though arbitrarily defined, is a measure of the stress at which appreciable plastic deformation first takes place. Thus, it is a reasonable basis for comparison to determine whether the notch tensile strength was developed with or without appreciable plastic deformation. It is this characteristic that has been shown to be related to other measures of fracture toughness [*5, 8*], and it is upon this basis that the notch tension test could be useful as a quality control test for fracture toughness.

Given a useful relationship between notch tension test data and K_{Ic}, there are several practical reasons why the notch tension test is preferred over other types of screening tests for which some relationship to K_{Ic} has been shown. First, the notched round specimen is the most economical to machine from thick products, requiring only one lathe setup. Second, it is tested in the same basic equipment already present in most industry laboratories, and thus would require no major new capital investments. Third, the data are readily recorded and analyzed by personnel experienced in standard tension testing. These advantages have led to a focus on notch tension testing of cylindrical specimens in the non-ferrous metals industry.

It is recognized that data from notched cylindrical specimens can be expressed in terms of stress intensity factor [9], but that capability is not utilized herein to minimize confusion concerning direct measurements of plane-strain fracture toughness, K_{Ic}, from notched cylindrical specimens. The test procedures described below are intended solely for developing screening data, and therefore the use of the notch tensile strengths and ratios seem appropriate.

Experimental Work

The designs of notched tension specimens upon which most work on aluminum alloys, including that described in this paper, are consistent with the recommendations in the Fourth Report of ASTM Committee E 24 [6]. The notch is a sharp (notch-tip radii $\lesssim$ 0.0005 in.) 60 deg V notch, with a depth of 30 percent (d/D = 0.707, a/A = 0.5); that should provide about the maximum sensitivity [6]. Two general sizes of specimen have been utilized, with major diameters of 1/2 and 1 1/16 in. The 1/2-in. diameter specimen has been widely used by many investigators in the past, and the 1 1/16-in. diameter specimen has been used for about four years in the aluminum industry [8].

To learn more about the influence of variables in specimen configuration and test procedure, the following program was carried out:

(1) To establish the relative suitabilities of threaded-end and tapered-seat specimens, tests were made of eight lots of material, in one case in two directions, with the full-length 1/2-in. diameter specimens of the design in Figs. 1 and 2, with both threaded and tapered seat grips, respectively.

(2) To establish the relative suitabilities of 1/2-in. and 1 1/16-in. diameter specimens, tests were made of the same eight lots with threaded-end specimens of the design in Fig. 3.

(3) To establish the importance of specimen length (which might be short in short-transverse tests), tests were made of the same samples with specimens of the various lengths in Figs. 1, 2, and 3 with reduced sections as short as 1/2 in. for the 1/2-in. diameter specimen and 1 1/2 in. for the 1 1/16-in. diameter specimen. The reduced length was achieved by shortening the grip ends as well as the reduced section.

(4) To establish the influence of notch-tip radius on notch tensile strength, and hence, the tolerable limits for notch sharpness, tests were made of transverse specimens of the types in Figs. 2 and 3, with notch-tip radii ranging from 0.0002 in. to as much as 0.031 in.

(5) To establish an indication of the acceptable tolerance on eccentricity during the test, and the degree to which threaded and tapered seat specimens

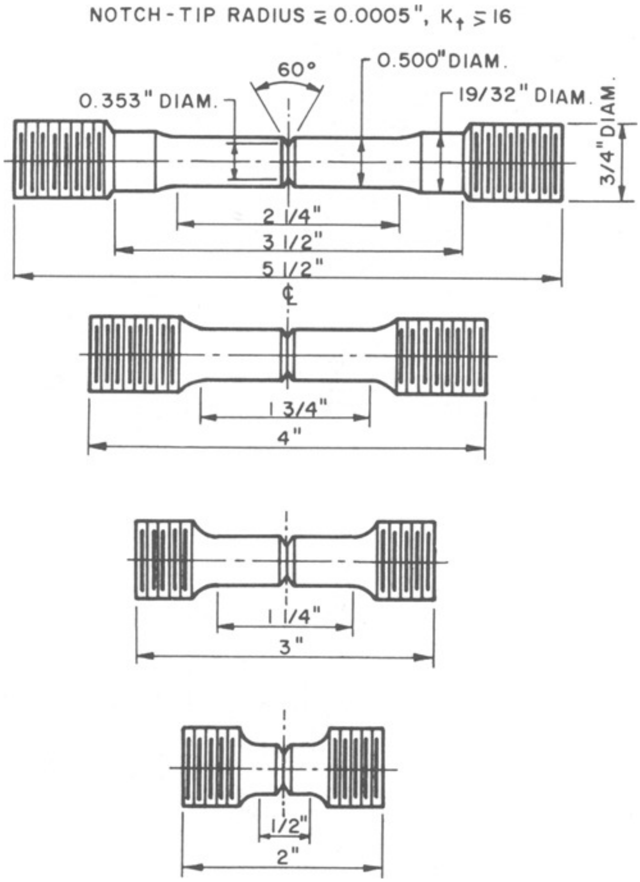

FIG. 1—*Threaded end notched 1/2-in. diameter tension specimen.*

"adjust" to eccentricity, tests were made of the sample of 3-in. diameter 7075-T6 rod with specimens of the designs in Figs. 1 and 2, where the eccentricity *e* (measured from the axis of the reduced section to the axis of the grip ends) was varied from 0 to 0.063 in.

(6) To establish the usefulness of tension-bolt aligners of the type in Fig. 4 to align specimens and tension bolts after a small load has been applied at the start of a test, tests were made of each of eight lots of material in some cases with specimens of all three types (Figs. 1, 2, and 3) and two different lengths, with and without the aid of a pair of aligners.

(7) To establish the effectiveness of the crossed knife edge device in Fig. 5, tests were made of 2024-T851 and 7079-T651 plate with 1/2-in. diameter tapered seat specimens (Fig. 2) using that device and the results were compared to those from tests of the same materials with the tension bolts and aligners used in most other tests.

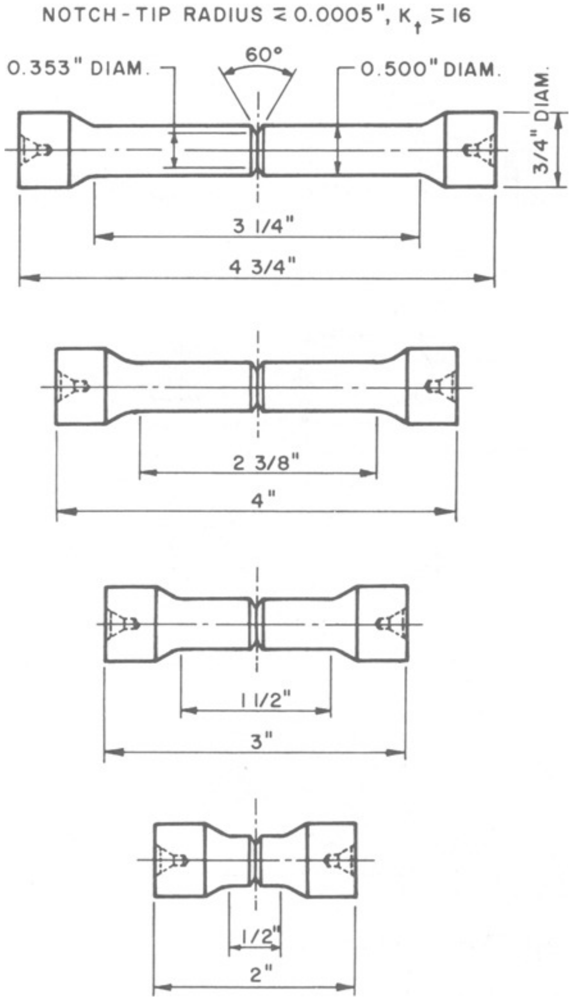

FIG. 2—*Tapered seat notched 1/2-in. diameter tension specimen.*

(8) To establish tolerances on rate of loading, tests were made of longitudinal and long-transverse specimens from the 1 3/8-in. 2024-T851 plate (two designs of transverse specimens, Figs. 2 and 3), at loading speeds from the lowest to highest practical rates in a typical universal testing machine (approximately 800 to 100,000 lb/min).

With a few exceptions, the procedures used in the tests of the notched specimens were consistent with the general provisions of ASTM E 338 [*2*]. Special precision spherical seats and long tension bolts designed to provide good alignment were used in all tests, except those in which the crossed knife-edge device

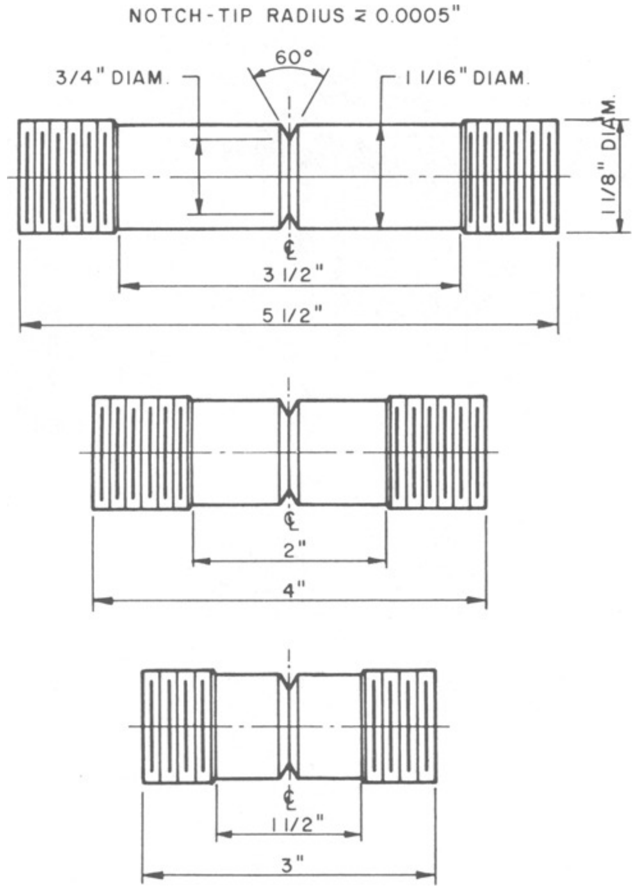

FIG. 3–*Threaded end notched 1-1/16-in. diameter tension specimen.*

(Fig. 5) was used. The dimensions of the notched specimens were measured with a microprojector (100X). Notch tensile strengths were calculated by dividing the maximum load by the original net section area at the root of the notch.

Generally tests were made in triplicate, unless noted otherwise. All longitudinal and long-transverse specimens from samples thicker than 1 1/2 in. were taken midway from surface to center in the thickness; all other specimens were taken from the center of the thickness of the material.

In interpreting the results, the effectiveness of alignment and gripping methods is judged in part by the uniformity and level of test data. It is recognized that this type of judgment is clouded by the inherent material variability. Nevertheless, these are indicators of the relative efficiencies of the various techniques and devices in reducing the effects of any eccentricities which are present.

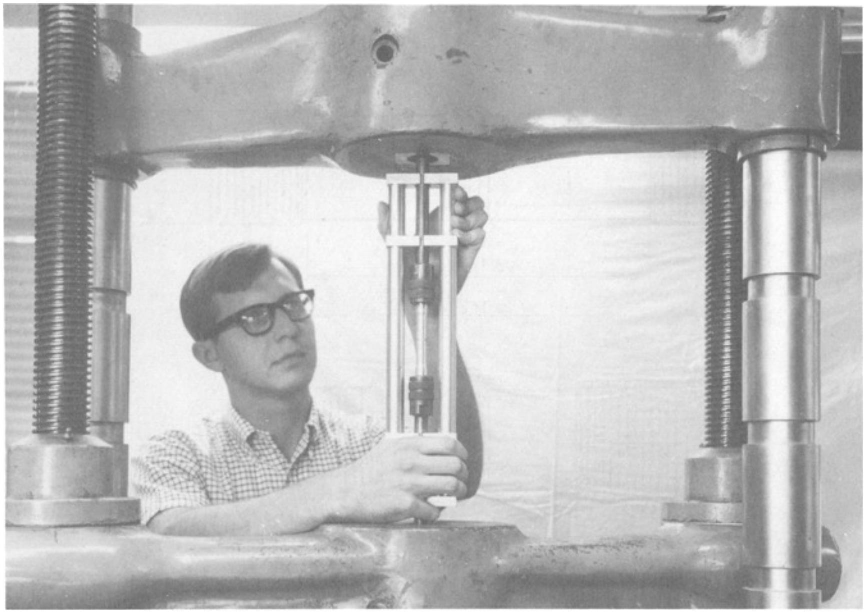

FIG. 4—*Use of aligners to control alignment of tension bolts during notch tension tests.*

Results

The tensile properties of the lots of aluminum alloy plate and rod used in these tests are shown in Table 1.

Representative results of the tests of notched specimens showing the influence of variables in specimen design and test procedure are presented as follows:[2]

Variables	Figure
Method of Gripping (threaded end versus tapered seat)	6, 7
Diameter of Specimen (1/2 or 1 1/16 in.)	6, 7
Length of Specimen (2 to 5 1/2 in.)	6, 7
Notch-Tip Radius (0.0002 to 0.031 in.)	8
Amount of Eccentricity (0 to 0.063 in.)	9
Effectiveness of Aligners	10
Rate of Loading (800 to 100,000 lb/min)	11

[2]Because of the vast quantity of data, it is impossible to present the individual test results. The author will, upon request, provide a detailed report providing all the test data.

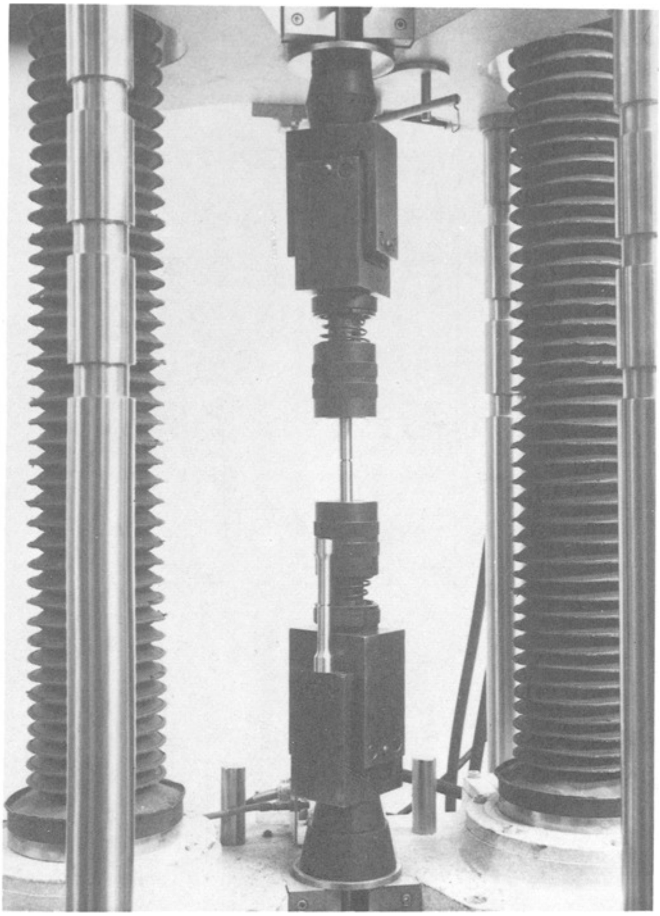

FIG. 5—*Crossed-knife edge alignment fixture.*

Discussion of Results

Method of Gripping

The results in Figs. 6 and 7 (which were obtained without the use of aligners) show that, for specimen lengths from 3 to 5½ in. (reduced sections greater than 1 in.), there were no consistent differences in the values obtained with 1/2-in. diameter threaded-end and tapered-seat specimens. However, for the 2-in. long 1/2-in. diameter (reduced section = 1/2 in.) specimens, higher notch tensile strengths and less divergence from the general trend of results were obtained with short tapered-seat specimens than with short threaded-end specimens, possibly because of the greater capability for alignment adjustment in the grips.

TABLE 1 – *Tensile properties of test materials.*

Alloy and Temper	Product	Thickness or Diameter, in.	Sample Number	Direction[a]	Tensile Strength, ksi	Yield Strength, ksi	Elongation in 4D, %
2024-T851	Plate	1 3/8	301999	LT	71.2	64.8	6.0
		5	301771	LT	66.2	58.8	5.0
		6	317200-2A	ST	60.8	56.0	1.0
			317201-2A	ST	62.8	55.6	2.5
			317232-B	LT	67.2	59.2	7.2
			317235-B	LT	68.1	60.6	7.0
2219-T851	Plate	4	317276	LT	66.6	48.3	9.5
7075-T6	Rod	3	. . .	L	83.0	73.0	11.0
7079-T651	Plate	6	301852-A	LT	74.9	64.0	6.8

[a]L – Longitudinal; parallel to direction of rolling.
LT – Long-transverse; normal to direction of rolling, in plane of plate.
ST – Short-transverse; normal to direction of rolling, and plane of plate.

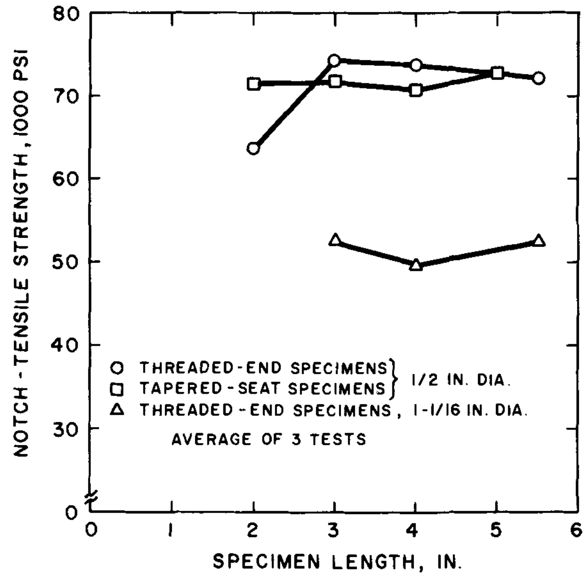

FIG. 6—*Long transverse notch tensile strengths of 1 3/8-in. 2024-T851 plate.*

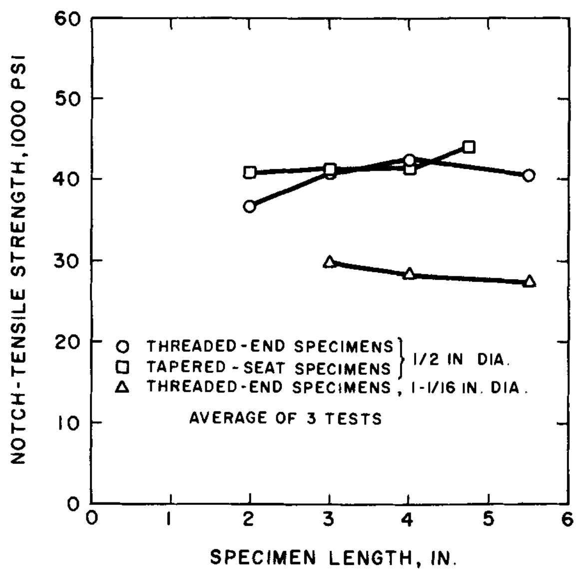

FIG. 7—*Short transverse notch tensile strengths of 6-in. 2024-T851 plate.*

Further evidence of an advantage for the tapered-seat specimens is provided by the data in Fig. 9, which show that the results of tests of tapered-seat specimens were less influenced by intentionally introduced eeccentricity than those of threaded-end specimens. These differences were not entirely consistent or large, but the implication is that, while threaded-end and tapered-seat specimens develop approximately the same strengths if alignment is carefully controlled, the tapered-seat specimen has an advantage in minimizing the effect of extreme eccentricities if they develop through machining errors, for example. Jones and Brown [10] have previouslyshown that button-head specimens also provide good axial alignment provided the associated gripping devices are carefully machined.

Diameter of Specimen

As expected, the 1 1/16-in. diameter specimens develop appreciably lower notch tensile strengths than the 1/2-in. diameter specimens. This is a geometry (size) effect related to the greater theoretical stress concentration factor for the larger specimen. The data can be normalized on the basis of stress intensity factor [*9*], but as indicated previously, this is not done to avoid confusion concerning appropriate ways to measure the plane-strain fracture toughness [*1*]. An implication of the difference in notch tensile strength level is an advantage for the larger specimen in indicating the toughness level of relatively tough materials, as the most explicit correlations would be expected when the notch tensile strength is less than the yield strength.

Length of Specimen

Data for specimens of various lengths in Figs. 6 and 7 illustrate that specimens shortened to as little as 3 in. (reduced sections shortened to as little as 1-1/4 in.) provide essentially the same results as the longer specimens. There was considerable evidence from the tests of 1/2-in. diameter threaded-end specimens that reducing the length to 2 in. (reduced section $\lesssim$ 1/2 in.) can result in greater scatter and lower strengths, probably because of the smaller amount of reduced section available to help minimize slight misalignments. However, the values for 2-in. long tapered-seat specimens were satisfactory and, as data in Fig. 10 indicate, careful control of alignment results in higher values or less scatter or both for 2-in. long threaded-end specimens as well.

Notch-Tip Radius

As indicated in Fig. 8, notch tensile strength decreased with decrease in notch-tip radius for both 1/2 and 1 1/16-in. diameter specimens. For radii from 0.0002 to 0.0007 in., there was little difference in strengths, however, and the values of the notch tensile strength appeared at a minimum. The use of a tolerance range of 0.0002 to 0.0007 in. (or $\lesssim$ 0.0007 in.) should be satisfactory for

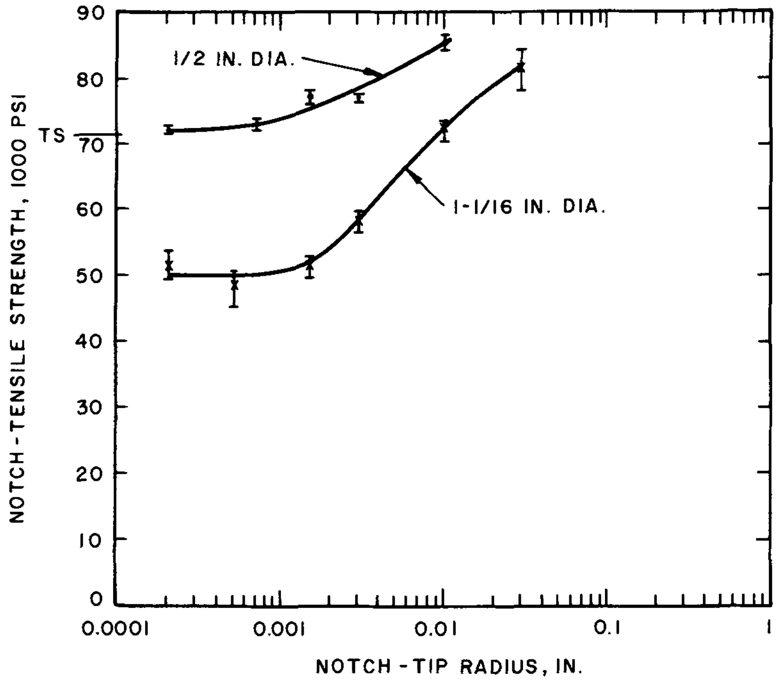

FIG. 8—*Effect of notch tip radius on long transverse notch tensile strength of 1 3/8-in. 2024-T851 plate.*

screening or quality control testing. Because of the potential variation in notch tensile strength with increase in radius above 0.0007 in., it will be necessary to measure not only the root diameter but also the notch-tip radius of every specimen used in such tests.

Amount of Eccentricity

Measurements were made of the total eccentricity from the top of the exposed upper tension bolt to the bottom of the exposed lower tension bolt during notch tension tests in which there was no positive control of alignment. Surprisingly, the eccentricity was as much as 0.050 in., and averaged 0.010 to 0.020 in., over the 18-in. span of the measurement gage. This is much larger than one would usually expect and, presumably because of the inefficiencies of spherical seats, it decreases only slightly as the test progresses. It is important to recognize that the specimen itself may not "feel" the entire eccentricity because of the nullifying influence of (a) the long tension bolts, (b) in some cases, the long reduced section, and (c) the adjustments in threads or tapered-seat holders. Nevertheless, the effect may be serious.

The results of tests of longitudinal specimens from 7075-T6 rod with various amounts of eccentricity ranging from 0.005 to 0.063 in. to obtain an indication of the effect of eccentricity on the notch tensile strength are shown in Fig. 9. The notch tensile strength decreased with increase in eccentricity, even for small amounts, although the most serious differences are apparent for eccentricities greater than 0.010 in. As indicated previously, the effect was consistently slightly less for tapered-seat specimens than for threaded-end specimens. These data illustrate that positive control is needed to assure that the eccentricity is kept to a minimum, and surely less than 0.010 in.

Effectiveness of Aligners

Aligners of the type shown in Fig. 4 were developed to provide a very fast, simple means of aligning the tension bolts, so that the only potential misalignment would be in the grips and specimens themselves, which can and should be carefully controlled by the precision to which the grips and specimens are machined. As illustrated in Fig. 10, tests made with and without the aligners showed that the aligners were usually effective in increasing the reproducibility (decreasing the scatter) or increasing the average notch tensile strength, or both for the larger diameter specimens and for the relatively short specimens. For the longer 1/2-in. diameter specimens, the differences were inconsistent and sometimes insignificant; in these cases, the inherent variability in the material may have been the governing factor. The potential usefulness of the aligners in reducing excessive misalignment is indicated.

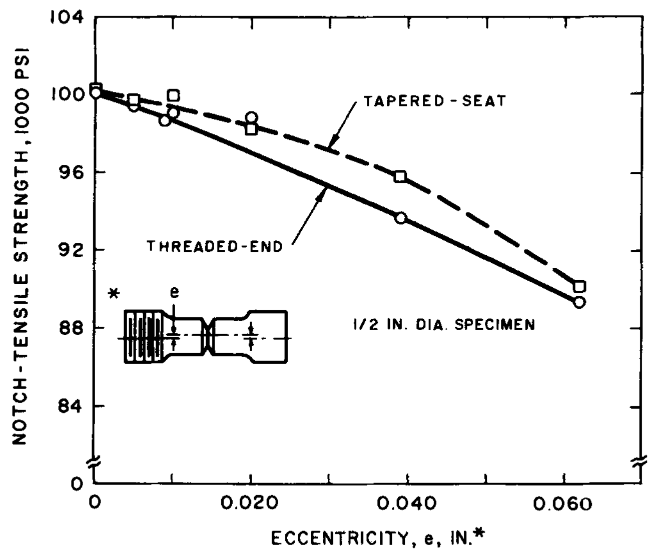

FIG. 9—*Effect of eccentricity on longitudinal notch tensile strength of 3-in. 7075-T6 rolled rod.*

Crossed-Knife Edge Device

Data for 2024-T851 and 7079-T651 plate obtained with the tapered-seat 1/2-in. diameter specimen with the crossed-knife edge device (Fig. 5) are compared with those obtained with the aligners below:

Alloy and Temper	Notch Tensile Strength, ksi	Aligners	Crossed-Knife Edges
2024-T851	avg	73.5	74.2
	min	69.2	70.8
	max	76.6	76.7
	range	7.4	5.9
7079-T651	avg	48.9	49.8
	min	45.9	47.2
	max	50.2	51.8
	range	4.3	4.6

The crossed-knife edge device resulted in about the same average values and range in values as the best of the other aligning procedures investigated, and so seems reasonably well suited for this purpose.

Rate of Loading

Over most of the range of loading rates studied (the whole range conveniently attainable with the usual universal testing machine), there was little variation in

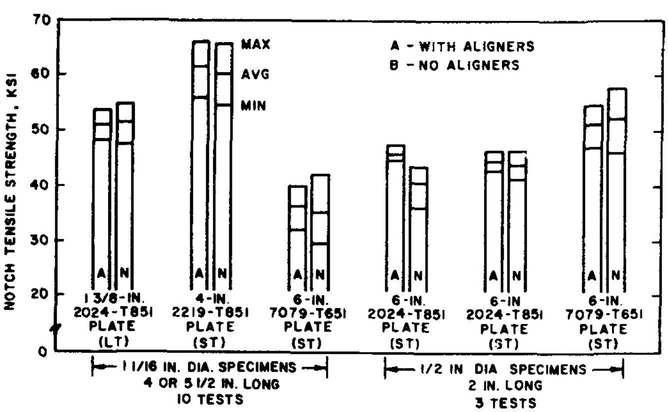

FIG. 10—*Effectiveness of aligners in tension tests of notched specimens.*

notch tensile strength (Fig. 11). Lower values were obtained at the highest rate in two out of the three cases studied. Consistent with these data and practical testing limitations, the rates should be controlled between the 5000 and 10,000 lb/min, which would result in tests taking from about 1 to 2 min to complete.

Summary

The influences of certain specimen and procedural variables on the results of notch tension tests of cylindrical specimens have been evaluated, and the results may be summarized as follows:

(1) Threaded-end and tapered-seat specimens provide comparable values of notch tensile strength when axiality of loading is maintained, but tapered-seat specimens minimize the effects of any eccentricity which is inadvertently introduced.

(2) The 1/2 and 1 1/16-in. diameter notched specimens of the designs evaluated provide approximately equal reproducibility of results.

(3) Threaded-end or tapered-seat specimens may be shortened to about 2 in. (reduced sections to 1/2 in.) for short-transverse tests, without influencing the numerical results or introducing undue scatter into the data, provided positive control of tension-bolt alignment is maintained.

(4) Notch tensile strength decreases with decrease in notch-tip radius, reaching a nearly uniform "minimum" value for radii in the range of 0.0002 to 0.0007 in.

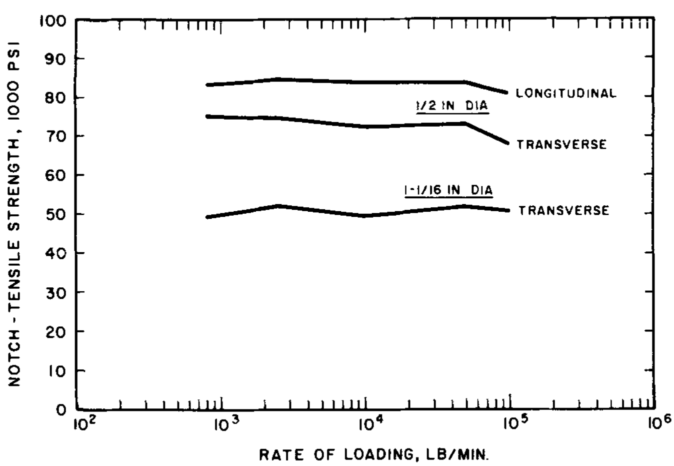

FIG. 11—*Effect of rate of loading on notch tensile strength of 1 3/8-in. 2024-T851 plate.*

(5) Even small amounts of eccentricity reduce the notch tensile strength, and the effect becomes very large if the eccentricity exceeds 0.010 in.

(6) Four-point aligners provide positive alignment of precision-machined tension bolts and grips and are particularly helpful in tests of short specimens. A crossed-knife edge loading device also is effective in reducing scatter in data due to eccentricity in the testing machine.

(7) Notch tensile strength is not sensitive to loading rate in the range from 2000 to 50,000 lb/min, but tends to decrease at higher rates.

References

[*1*] "Tentative Method of Test for Plane-Strain Fracture Toughness of Metallic Materials," ASTM E 399-70T, *1971 Annual Book of ASTM Standards,* Part 31, American Society for Testing and Materials, Philadelphia, 1971, pp.919-935.

[*2*] "Standard Method of Sharp-Notch Tension Testing of High Strength Sheet Materials," ASTM E 338-68, *1971 Annual Book of ASTM Standards,* Part 31, American Society for Testing and Materials, 1971, Philadelphia, pp. 855-862.

[*3*] Kaufman, J.G. and Holt, Marshall, "Fracture Characteristics of Aluminum Alloys," Technical Paper 18, Alcoa Research Laboratories, 1965.

[*4*] Sachs, G., Ebert, L.J., and Brown, W.F., Jr., *Transactions of the A.I.M.E.,* American Institute of Mining, Metallurgical and Petroleum Engineers, Iron and Steel Division, 1948, p. 424.

[*5*] Baker, J.F. and Tipper, C.F., *Welding Research Council Bulletin,* No. 37, June 1957.

[*6*] "Screening Tests for High-Strength Alloys Using Cylindrical Specimens," Fourth Report of ASTM Special Committee on Fracture Testing of High Strength Materials, *Materials Research and Standards,* MTRSA, Vol. 2, No. 3, March 1962, pp. 196-203.

[*7*] Kaufman, J.G. and Johnson, E.W., *Proceedings,* American Society for Testing and Materials, ASTEA, Vol. 62, 1962, pp. 778-793.

[*8*] Kaufman, J.G., *Journal of Materials,* JMLSA, Vol. 2, No. 4, 1967, pp. 889-914.

[*9*] Brown, W.F., Jr., and Srawley, J.E., *Plane Strain Crack Toughness Testing of High Strength Metallic Materials, ASTM STP 410,* American Society for Testing and Materials, 1967.

[*10*] Jones, M.H. and Brown, W.F., Jr., *ASTM Bulletin,* American Society for Testing and Materials, ASTBA, No. 211, Jan. 1956, pp. 53–60.

C. N. Freed,[1] *A. M. Sullivan,*[1] *and J. Stoop*[1]

Influence of Dimensions of the Center-Cracked Tension Specimen on K_c

REFERENCE: Freed, C.N., Sullivan, A.M., and Stoop, J., "Influence of Dimensions of the Center-Cracked Tension Specimen on K_c," *Fracture Toughness, Proceedings of the 1971 National Symposium on Fracture Mechanics, Part II, ASTM STP 514,* American Society for Testing and Materials, 1972, pp. 98-113.

ABSTRACT: The fracture resistance of three high strength aluminum alloys, two titanium, and one steel alloy has been investigated with a center-cracked tension specimen. Specimen geometric dimensions such as width, thickness, and crack length, together with yield strength were studied to ascertain their influence on the K_c parameter. The specimen thicknesses ranged from 1/16 to 1/18 in., width from 3 to 12 in., and crack length from 0.5 to 7 in.

The K_c parameter has been found to be unaffected by specimen width and crack length provided the width dimension is sufficient and the crack length/width ratio is within the range of 0.15 to 0.5. The fracture resistance is dependent upon sheet thickness and inversely proportional to yield strength.

KEY WORDS: fracture (materials), failure (materials), stresses, fracture strength, toughness, crack initiation, yield strength, crack propagation, tension tests, alloy steels, aluminum alloys, titanium alloys

The catastrophic collapse of numerous structures over the past decade – high performance aircraft, missile casings, thin-walled pressure vessels – illustrates the reality of the notch brittle fracture problem in structures fabricated from high and ultrahigh strength sheet metal alloys.

Fracture resistance may be defined as the strength manifested by a metal in the presence of a crack. Due to the inverse relationship between strength and fracture toughness, high strength sheet alloys are susceptible to unstable fracture emanating from small flaws. The likelihood that a crack will undergo instability depends upon the critical relationship between the size of the crack and the stress acting on the segment of the structure in which the crack is embedded. The fracture mechanics relationship which predicts the size of the crack required

[1] Fracture Mechanisms Section, Metallurgy Division, Naval Research Laboratory, Washington, D.C. 20390.

for the onset of rapid fracture at a particular applied stress for an infinitely wide panel is given below:

$$K_c = \sigma_f \sqrt{\pi a_c} \qquad (1)$$

σ_f = failure stress
a_c = one-half of the critical crack
K_c = plane stress fracture toughness parameter

The K_c parameter defines in a single term the resistance of a metal sheet to crack instability.

The designer can employ the K_c value of the particular alloy in two ways: (a) the toughness of candidate alloys may be compared to allow a more rational selection in the choice of a fracture resistant alloy for a particular application, and (b) the fracture stress and critical crack length relationship can be calculated for the selected metal to permit prediction of the conditions at which crack instability will initiate.

Experimental Procedure

Test Method

At the present time, there is no standard fracture toughness test for determination of the stress and critical crack length relationships in these low-toughness sheet metals. In order to evolve standard test procedures, a renewed effort to explore the influence of specimen dimensional variables has been initiated. Because the stress analysis of the center-cracked sheet panel is well documented and the testing procedure adaptable for laboratory use [*1,2*], the center-cracked specimen was selected for these studies.

The center-cracked tension (CCT) specimen is presented in Fig. 1. In the center of the sheet specimen a crack-like slit has been introduced by electric discharge and within the slit a beam displacement gage instrumented with a four strain-gage circuit has been placed. Upon loading, the borders of the slit are displaced and cracks will initiate from the slit tips along a plane perpendicular to the applied stress. The displacement gage will monitor the crack-opening displacement (COD) via an electrical readout to an X-Y recorder; a previous calibration between COD and crack length enables calculation of crack length at any point during the test [3]. Stable crack growth occurs from each slit tip until the total crack reaches a critical length for the applied stress, whereupon unstable crack propagation ensues and the specimen fractures.

The behavior of a CCT specimen in a rising load test can take one of three forms. For the highly frangible metals, fracture can occur without precedent crack growth; the crack length used in the K_c calculation is the original slit

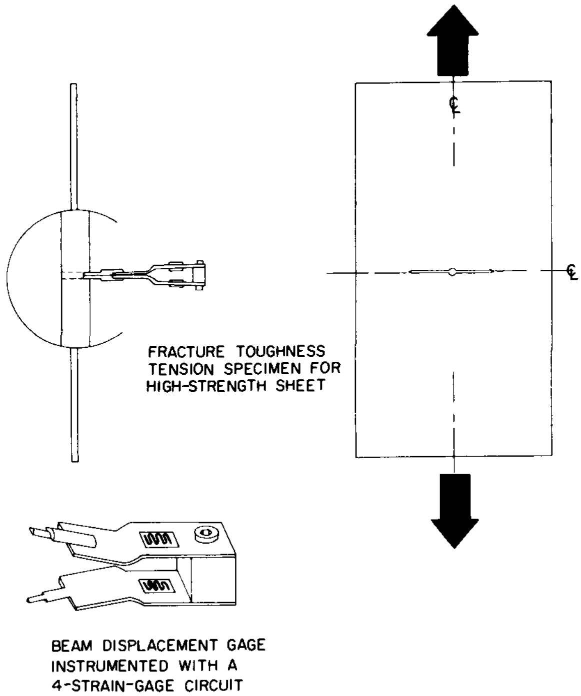

FIG. 1—*Center cracked tension (CCT) specimen and beam displacement gage used to monitor crack opening displacement.*

length. Materials which are less frangible evidence slow stable crack growth as the load increases; if the load is held constant the crack will arrest. The slit length plus the crack length at fracture (as determined by the COD crack length calibration) is used to determine K_c. Some alloys which are relatively tough do not fracture under a rising load. Instead, after the crack has slowly grown some distance the crack velocity markedly increases while the load on the specimen remains constant. The crack will extend at an increasing velocity until instability results in fracture of the specimen. For practical purposes, the point at which the crack begins to grow under constant load marks the limit of structural integrity and the crack length at that point is used to calculate K_c.

Materials

The fracture resistance of three high-strength aluminum alloys, two titanium, and one steel alloy was investigated. The influence of sheet width and thickness, initial crack length, and yield strength on K_c was studied and is reported in this paper. All tests were conducted with cracks parallel to the sheet rolling direction.

The three aluminum alloys investigated were 7178-T6, 7075-T6, and a recently developed alloy, 7475. The available quantity of the last alloy was limited to two 24 by 24-in. sheets which were 0.090 in. thick. One sheet was heat treated to a T61 temper while the other sheet received an additional aging treatment of 15 to 18 h at 325 F to provide a T761 temper.

The mechanical properties of the alloys are presented in Table 1. The yield strength values of 7075-T6 and 7178-T6 were similar, 76.5 and 78.9 ksi, respectively, while the yield strength of 7475 ranged from 58.6 to 61.5 ksi.

The steel sheet employed in the program was AISI 4130, a low alloy metal containing about 1 percent Cr, and 0.1 percent Mo. Sheet specimens, 1/16 in. thick by 12 in. square, were normalized and austenitized at temperatures indicated in Table 2. One group of specimens was tempered at 700 F for 2 h while a second group was tempered at 500 F for 30 min to achieve two yield strength levels of 169.5 and 178.4 ksi, respectively. The close proximity of the ferrite "nose" to zero time on the isothermal transformation diagram militated against the acquisition of ultrahigh strength properties by heat treatment.

The titanium alloys investigated were Ti-6Al-4V and Ti-13V-11Cr-3Al (Ti-120 VCA). The former alloy is a high alpha, lean beta composition which is responsive to thermal treatment. The metal is widely used in the aerospace industry in such applications as pressure vessels, rocket motor casings, and aircraft structural members. Ti-13V-11Cr-3Al is a metastable titanium alloy capable of heat treatment to very high strengths. Because of the high-strength-to-weight ratio which can be achieved, the alloy has found application in high-performance airborne vehicles.

Specimen Size Considerations

Earlier work has indicated that specimen dimensions must be sufficiently generous to isolate the crack tip stress distribution from the borders of the specimen [*3*]. Otherwise, the calculated K_c value would not solely be a characterization of the fracture resistance of the sheet but would also depend on the size of the panel which was employed in the test. Specimen dimensions which can influence K_c include width (W), crack length/width ($2a/W$) ratio, and thickness.

An example of the interdependence of specimen width and crack length/width ratio and the gross stress is presented in Fig. 2. In this three-dimensional drawing, width, $2a/W$, and gross stress are plotted to form a curved surface indicated by the bold lines; every point on this surface is equivalent to a K_c value of 100 ksi $\sqrt{\text{in.}}$ A requirement for a valid K_c value is that unstable fracture must commence at a stress less than the yield stress of the alloy. If it is assumed that the yield stress of this hypothetical alloy is 60 ksi, a plane can be drawn through the figure at the 60 ksi level and parallel to the base of the figure; the region lying above the plane represents an area in which yielding has occurred and the region below the plane indicates an area where valid K_c values can be obtained.

TABLE 1 – *Mechanical property data.*

Alloy	Fracture Direction	Sheet Thickness, in.	Yield Strength 0.2% offset, ksi	Tensile Strength, ksi	Elongation, %	Reduction in Area, %	Hardness
4130	WR	0.063	169.5	192.5	3.9	11.3	40.8 HRC
4130	WR	0.063	178.2	225.1	5.3	27.8	46.3
Ti-6Al-4V	WR	0.063	151.1	156.3	1.0	2.0	38.5
Ti-6Al-4V	WR	0.125	146.0	158.2	4.3	7.5	37.0
Ti-13V-11Cr-3Al	WR	0.063	207.3	220.9	2.8	6.3	44.8
Ti-13V-11Cr-3Al	WR	0.125	216.5	227.0	2.3	2.1	45.0
7178-T6	RW or WR	0.063	78.9	88.7	9.9	. . .	. . .
7075-T6	RW or WR	0.063	76.5	88.5	10.9	. . .	. . .
7475-T61	WR	0.090	59.3	70.4	12.5	32.3	83.0 HRB
	RW	0.090	61.5	69.8	11.5	39.7	82.0
7475-T761	WR	0.090	58.6	70.5	10.5	27.4	84.0
	RW	0.090	60.7	70.0	11.5	43.3	82.0

TABLE 2–*Thermal treatment data.*

Alloy	Heat Treatment	
4130 (σ_{ys} = 169.5 ksi)	Austenitize:	1575 F, 1 h, water spray
	Temper:	700 F, 30 min, air cool
4130 (σ_{ys} = 178.4 ksi)	Austenitize:	1575 F, 1/2 h, water spray
	Temper:	500 F, 30 min, air cool
Ti-6Al-4V[a]	Solution Anneal:	1700 F, 20 min, water spray
	Age:	975 F, 8 h, air cool
Ti-13V-11Cr-3Al	Received in solution annealed condition	
	Age:	900 F, 72 h, air cool

[a]Both thicknesses of each alloy received the same heat treatment.

The influence of width and $2a/W$ on K_c can now be examined. For this alloy, Fig. 2 indicates that if the test panel were 3 in. wide, any $2a/W < 0.45$ would produce invalid K_c values, that is, yielding will occur before the K_c value is attained. As panel width is increased, the region in which valid K_c values can be obtained grows larger until at a 12-in. width, any value of $2a/W$ between 0.15 and 0.50 may be employed without invalidating K_c. A similar analysis can be made holding $2a/W$ constant and determining the minimum width required to achieve a valid K_c: at small crack lengths where $2a/W$ approaches 0.10, specimen width must be large to prevent yielding.

In addition to the constraints demonstrated in Fig. 2, other restrictions on specimen dimensions exist. For instance at large crack lengths where $2a/W$ exceeds 0.50, the stress distribution at the crack tip may be affected by the edge of the specimen and excessive data scatter has been observed.

The plot in Fig. 2 was drawn from schematic K_c and yield strength data and the restrictions on valid K_c values are readily ascertainable. In practice, however, the K_c value of the alloy which is the subject of the investigation is unknown. Therefore, the investigator cannot *a priori* determine the specimen dimensions which will assure a valid K_c test. While some generalizations regarding the toughness can be made from knowledge of the yield strength, the investigator must still perform series of tests using specimens of varied width and $2a/W$ to obtain assurance that only valid K_c values will be reported. As more fracture toughness information is gained from different metal systems and strength levels, it will be possible to predict K_c approximations with greater accuracy and therefore reduce the number of tests required for each new alloy.

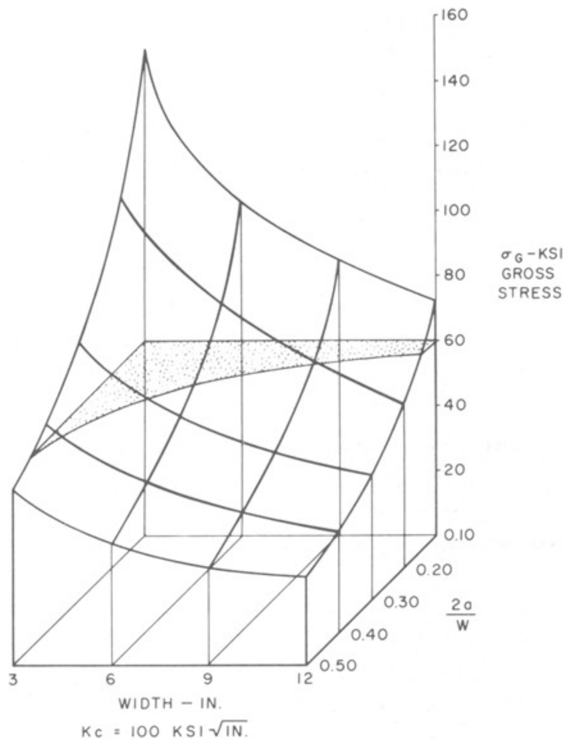

FIG. 2–*Influence of specimen width, crack length,* 2a, *(normalized by width), and failure stress on* K_c. *Every point on the surface reflects a* K_c *= 100 ksi* $\sqrt{in.}$ *For a metal sheet with this* K_c *value and* σ_{ys} *= 60 ksi, all tests in which the gross failure stress lies above the plane represent invalid data while* K_c *tests in which the fracture stress lies below the plane indicate valid* K_c *values.*

Dicussion Of Results

Effect of Width and Crack Length on K_c *for Aluminum Alloys*

The specimens for the K_c test were prepared by cutting the 7075 and 7178 sheet into panels 12 in. wide by 36 in. long. The slit opening was 1/16 in. and the slit length, $2a$, varied between $2a/W$ of 0.04 to 0.6. The slit tip radius ranged between 2 to 5 ml; the slits were not extended by fatigue cracks as the stable crack growth which preceded fracture provided sufficient crack acuity to eliminate crack sharpness as a variable [*4*].

The limited quantity of 7475 alloy required the use of foreshortened specimens 12 in. wide by 12 in. long. To achieve the desired specimen length, extension tabs were fastened to the specimen width bolts. Previous K_c tests on foreshortened aluminum specimens which were lengthened by extension tabs indicated that the K_c value was unaffected by this technique [5].

The 12-in. panel which was chosen at the commencement of the investigation as a reasonable and a conservative size that should be large enough to eliminate specimen width as a test variable. To ensure that K_c would not be affected by the width dimension, specimens were prepared from the 7075 and 7178 alloys which were 3, 6, 9, and 12 in. wide. The original slit length, $2a$, was held to approximately one-third of the width ($2a/W \approx 1/3$) for each specimen.

The results of the study on specimen geometry factors are presented in detail in Ref *3*, and the influence of width on K_c is summarized in Fig. 3. The data for 7178-T6 denote that the average K_c value of 55.4 ksi $\sqrt{\text{in.}}$ is unaffected as the specimen width is decreased from 12 in. to 3 in. Likewise, the average K_c of 65.2 ksi $\sqrt{\text{in.}}$ for 7075-T6 is independent of the width dimension over this range. Thus, the 12-in. specimen width for the 7475 sheet specimens appeared adequate for valid K_c measurements.

Another specimen variable which can influence K_c is the length of the crack at instability. On the basis of other investigations, center cracks which were too short or too long provided erroneous K_c measurements [5]. A test series was initiated to determine the range over which K_c would be unaffected by crack length for specimens of different widths. Lightweight restraint plates lined with teflon sheet were used to prevent buckling.

The original slit length ($2a_0$) was varied for 12-in.-wide specimens of three ultrahigh strength aluminum alloys. The original length of the slit ranged from 0.5 to 7 in. long ($0.04 < 2a_0/W < 0.6$). The curves of Fig. 4 indicate that data scatter is increased for both 7075 and 7178 when the final crack length/width

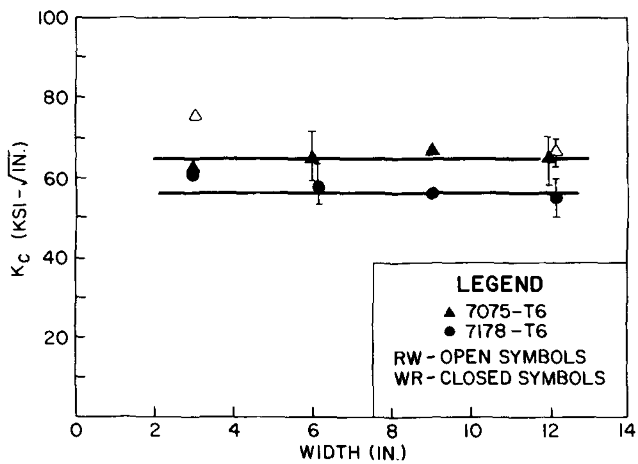

FIG. 3—*Specimens as narrow as 3-in.-wide can be used to determine* K_c *for these high-strength aluminum alloys.*

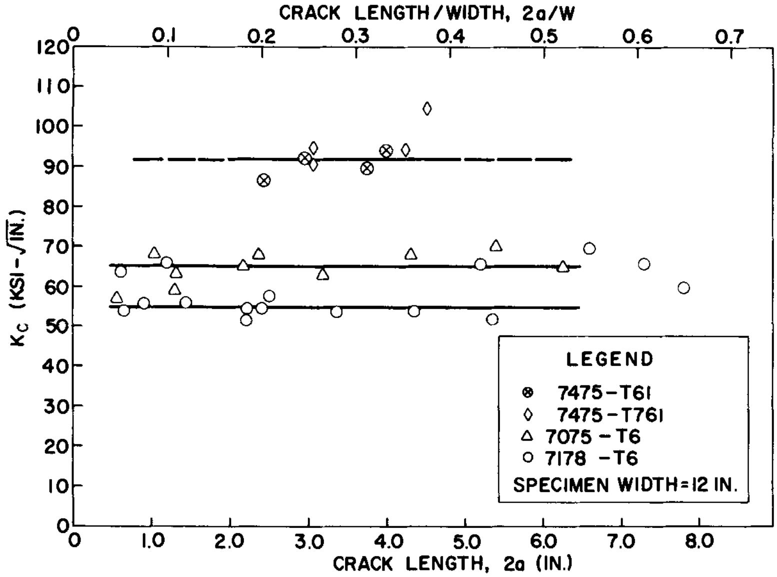

FIG. 4—K_c *is independent of crack length if* $0.50 \geq 2a/W \geq 0.15$.

ratio, $2a/W$, approaches 0.1 or less. For the very large cracks, 7075 showed no scatter at $2a/W = 0.5$ which represents a 6-in.-long crack in a 12-in.-wide specimen, but the data scatter was excessive for 7178 once the crack exceeded a $2a/W = 0.5$. While further experiments could delineate with greater accuracy the trends of the scatter for the very long and very short cracks, it can be concluded that as long as the $2a/W$ value at instability is greater than 0.15 and less than 0.50, the particular crack length will not affect K_c for these alloys.

Comparison of Fracture Resistance for the Three Aluminum Alloys

Based on the data reflecting the influence of $2a/W$ on K_c for 7075-T6 and 7178-T6, slit lengths of 2.0 and 3.0 in. ($2a_0/W = 0.18$ to 0.25) were chosen for the two tempers of 7475. The fracture toughness properties of these three alloys are presented in Table 3. Due to the limited quantity of 7475 sheet, the K_c value of each fracture direction (WR and RW) for each temper (T61 and T761) was established with two specimens for each condition, for example, two specimens were used to determine K_c of 7475-T61 in the RW direction.

For the 7475 alloy, little difference in toughness is observed between the two tempers. The T61 temper evidences slightly lower resistance to fracture in a specified fracture direction than is measured in the T761 temper. For both tempers, the WR fracture direction (short longitudinal) indicates a slightly lower K_c than does the RW direction. While all of the data points are plotted for this

TABLE 3—*Summary of fracture toughness data for aluminum alloys.*

Alloy	Fracture Direction	Yield Strength (σ_{ys}) 0.2% offset, ksi	K_c, ksi $\sqrt{\text{in.}}$	K_c/σ_{ys}, $\sqrt{\text{in.}}$	Critical Crack Length at: $\sigma_{ys}/2$	$3(\sigma_{ys})/4$	σ_{ys}
7178-T6	RW or WR	78.9	55.4	0.70	1.29 in.	0.57 in.	0.32 in.
7075-T6	RW or WR	76.5	65.2	0.85	1.87	0.83	0.47
7475-T61	WR	59.3	88.4	1.49	5.71	2.53	1.42
	RW	61.5	93.6	1.52	5.91	2.64	1.48
7475-T761	WR	58.6	91.6	1.56	6.26	2.77	1.56
	RW	60.7	98.4	1.62	6.71	2.99	1.68

alloy in Fig. 4, a single line is drawn through them to represent the average K_c of both tempers and both fracture directions.

The summary of K_c data in Table 3 signifies that the fracture resistance of 7475 is approximately 50 percent higher than that of the 7178-T6 or 7075-T6 alloys. This higher fracture resistance is reflected in the larger critical crack length which can exist in the sheet stressed to a specified fraction of its yield strength before unstable fracture commences. The right-hand columns of Table 3 indicate the critical crack length for each alloy and temper when the sheet is loaded to 1/2, 3/4, and finally to its yield stress. For instance, when 7178-T6 sheet is stressed to 3/4 yield strength a 0.57-in.-long crack will initiate catastrophic fracture of the sheet. A crack as long as 2.6 in. is required for instability in 7475-T61 (RW) under the same level of applied stress. While the 7178-T6 and 7075-T6 alloys are subject to brittle fracture from relatively small cracks, the 7475 alloy manifests much greater resistance to crack propagation under elastic stresses.

Influence of Yield Strength on K_c *for 4130 Steel*

The purpose of applying different heat treatments to each of the two series of 4130 specimens was to obtain distinguishable strength levels among sheets of similar thickness. The mechanical properties recorded in Table 1 indicate that while the yield strength differed only 9 ksi between the two series of specimens, the difference in tensile strength, reduction in area, and hardness demonstrate a more significant influence of heat treatment.

The influence of yield strength (σ_{ys}) on K_c fracture resistance is demonstrated in Fig. 5. The average K_c value of the lower yield strength sheet was 160.0 ksi $\sqrt{\text{in.}}$ while the sheet tempered to the higher strength evidenced an average K_c = 140.7 ksi $\sqrt{\text{in.}}$ The specimens at both strength levels were 0.063 in. thick and 12 in. wide.

The 4130 specimens heat treated to 178.2 ksi yield strength contained initial slit lengths, $2a_0$, of 2, 3, 4, and 5 in. long, while the lower strength specimens were slitted to lengths of 2, 3, and 4 in. Two panels were machined slightly differently than the rest; instead of a center slit, a hole was drilled in the center of each and from this hole slits were extended perpendicular to the loading direction. For both the conventional specimens and the hole-slit specimens, the K_c value was unaffected throughout the entire $2a_0/W$ range between 0.166 and 0.416.

The fracture resistance for this alloy at both strength levels was moderately high as indicated by K_c/σ_{ys} ratio of 0.95 for the lower strength specimens and 0.79 for the higher strength panels. This moderate toughness is reflected in the length to which a crack must grow before commencement of unstable crack propagation can occur; at 1/2 σ_{ys} stress level, the critical crack length for the higher strength sheet is 1.6 in. while unstable fracture would require a crack 2.3 in. long for the lower strength panels.

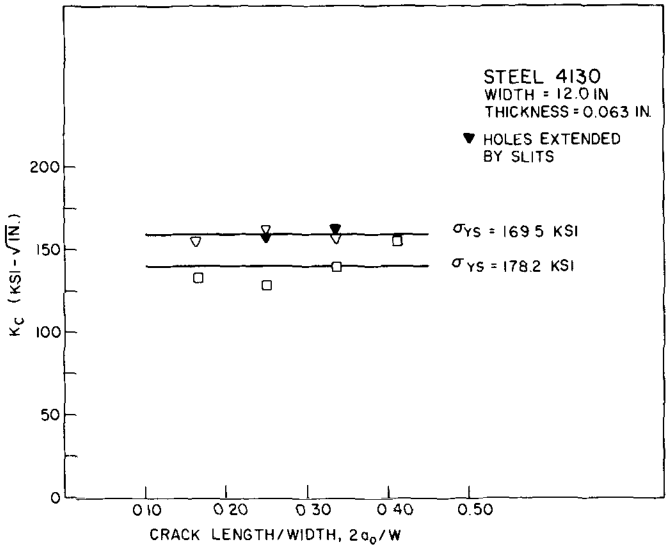

FIG. 5—*Fracture resistance is inversely proportional to yield strength.*

Effect of Sheet Thickness on K_c *for Two Titanium Alloys*

For each of the titanium alloys, both the 1/8-in. and 1/16-in.-thick specimens received the same heat treatment. The mechanical properties are presented in Table 1 and the fracture toughness data are recorded in Table 4. All data represent tests conducted in the "weak" WR fracture direction.

Titanium 13V-11Cr-3Al (Ti-120 VCA)—The influence of sheet thickness on the fracture resistance K_c parameter is shown in Fig. 6. Initial slit lengths of 2 to 4 in. were cut into each of two series of specimens. Both series received the same heat treatment to achieve similar mechanical properties. The only significant difference between the two series of specimens was thickness; one series was 1/8-in. thick while the other was 1/16-in. thick.

As Fig. 6 indicates, the fracture resistance of this alloy for either thickness is very low. The K_c value for the 1/16-in.-thick sheet was 41.5 ksi $\sqrt{\text{in.}}$ while the thicker sheet manifested a slightly lower value of 35.7 ksi $\sqrt{\text{in.}}$ The brittle character of Ti-13V-11Cr-3Al at this strength level is better exemplified by noting that if the sheet was stressed to 1/2 σ_{ys}, the critical crack lengths sufficient to initiate unstable fracture would be 0.10 and 0.07 in., respectively.

It should be noted that the 120 VCA specimens manifested no stable crack growth prior to unstable fracture but rather exhibited instantaneous fracture at maximum load. When no crack growth precedes instability, the 2 to 5-ml radius slit tip may cause K_c to be overestimated. Although any overestimation of K_c for this brittle alloy would have little engineering significance, specimens will be tested in which the slit tips are sharpened by fatigue cracks to determine the

TABLE 4–*Fracture toughness data for 4130 steel and two titanium alloys.*

Alloy	Fracture Direction	Specimen Dimensions: Thickness, in.	Width, W in.	Initial Crack Length, $2a_o$ in.	Crack Length in K_c Calculation, $2a$ $2a_o'$, in.	Failure Stress ksi	Yield Strength, ksi	K_c ksi $\sqrt{\text{in.}}$
4130	WR	0.063	12	2.00	2.76	73.3	169.5	156.8
(σ_{ys} = 169.5 ksi)				3.00	3.78	62.9		163.3
				3.00[a]	3.72	60.0		162.2
				4.00	4.80	50.9		156.3
				4.00[b]	5.04	48.0		160.6
4130	WR	0.063	12	2.00	2.40	68.0	178.4	135.0
(σ_{ys} = 178.4 ksi)				3.00	3.48	68.0		128.2
				4.00	4.60	47.3		140.9
				5.00	5.58	46.0		159.0
Ti-13V-11Cr-3Al	WR	0.063	12	2.00	2.00	25.3	207.3	45.2
				3.00	3.00	18.0		40.4
				4.00	4.00	14.4		38.8
Ti-13V-11Cr-3Al	WR	0.125	12	2.00	2.00	18.0	216.5	32.2
				3.00	3.00	18.5		41.6
				4.00	4.00	12.3		33.2
Ti-6Al-4V	WR	0.063	12	2.00	2.16	42.2	151.1	78.8
				3.00	3.12	31.7		73.0
				4.00	4.38	26.6		76.4
				5.00	5.38	21.0		69.4
Ti-6Al-4V	WR	0.125	12	2.00	2.04	53.6	146.0	97.0
				3.00	3.96	32.0		85.7
				4.00	5.16	26.0		84.4
				5.00	6.30	24.6		94.4

[a] Initial crack consisted of a 2-in. diameter hole with 1/2-in. slits extending radially perpendicular to direction of applied stress.
[b] Initial crack consisted of a 3-in. diameter hole with 1/2-in. slits extending as above.

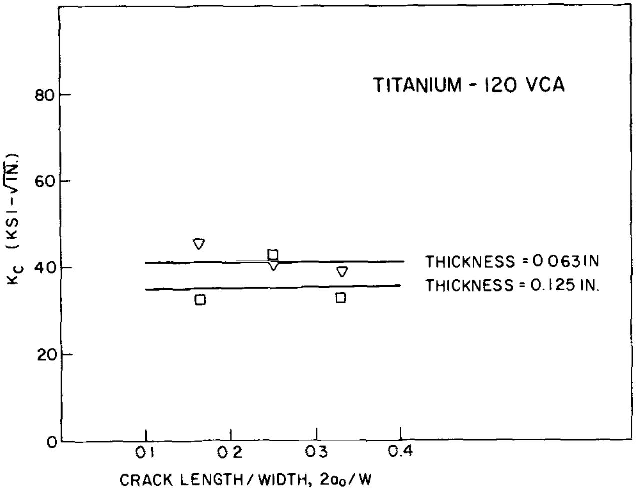

FIG. 6—*The 1/16-in.-thick Ti-120 VCA (Ti-13V-11Cr-3Al) manifests a slightly higher* K_c *value than 1/8-in.-thick panels. At this strength level specimens of both thickness series are brittle.*

effect of crack acuity. With only one exception, all of the other aluminum, steel, and titanium specimens evidenced at least 0.10-in. crack growth before fracture (Table 4).

Although definitive conclusions are not possible from the limited data, there seems to be no dependence of K_c on $2a_0/W$ within the range of crack lengths reported in Fig. 6. If the dependence of large values of $2a_0/W$ on K_c is based on interference of the crack tip stress field with the edge of the sheet, the small values of $2a_0/W$ reported herein and the localization of the stress field in brittle materials would militate against any influence of $2a_0/W$ on toughness for this alloy.

Titanium-6Al-4V—The fracture resistance of two thicknesses of this alloy was measured for different values of $2a_0/W$. The results of this study are presented in Fig. 7.

The toughness of Ti-6Al-4V specimens was about double the K_c values of the higher strength Ti-13V-11Cr-3Al. The thicker specimens evidenced a K_c value of 90.4 ksi $\sqrt{\text{in}}$. while the toughness of the 1/16-in.-thick specimens averaged 74.4 ksi $\sqrt{\text{in}}$. The critical crack lengths at the onset of instability for 1/2 σ_{ys} level are 0.98 and 0.61 in., respectively.

Unlike the data obtained from Ti-13V-11Cr-3Al, the 1/8-in.-thick Ti-6Al-4V manifested a higher fracture resistance than the 1/16-in.-thick specimens. It is possible that the thickness commensurate with maximum fracture toughness for this strength level will occur at a thickness greater than 1/8 in. A complete survey of the influence on K_c for this alloy will be conducted. Over the $2a_0/W$ range investigated for both thicknesses, there was no discernible influence of crack length on K_c.

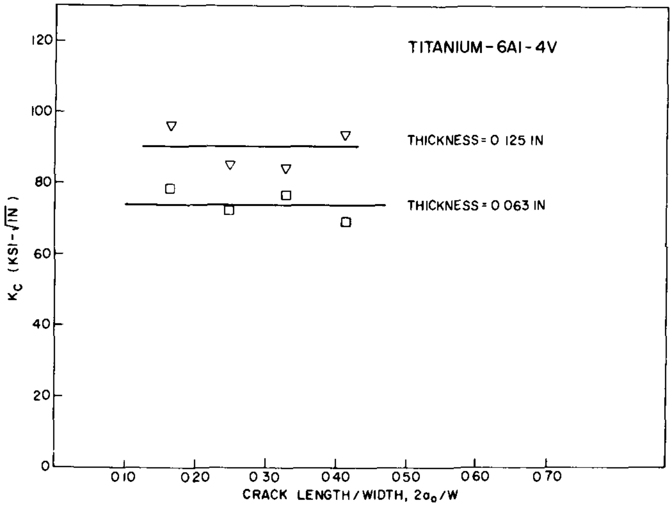

FIG. 7—*The 1/8-in.-thick specimens of Ti-6Al-4V are tougher than the thinner panels.*

Discussion

This work represents the first step in the evolution of analytical procedures to characterize fracture resistance of high-strength sheet metals. These procedures will allow engineering predictions of structural performance in relation to flaw-size and stress factors. The application of this test method to a broad spectrum of metal alloys will permit the employment of the analytical techniques to improve metal quality and to develop failure-safe design procedures.

Conclusions

(1) Plane stress fracture toughness values can be measured for 7178-T6 and 7075-T6 aluminum alloys using specimens as narrow as 3 in. Valid K_c data can be obtained over the range of $0.50 \geqslant 2a/W \geqslant 0.15$.

(2) The fracture resistance of 7475-T61 and T761 (3/32 in. thick) is about 50 percent higher than the K_c values of 1/16-in.-thick 7178-T6 and 7075-T6. The K_c of 7475 for both tempers is 88 to 98 ksi $\sqrt{\text{in.}}$ while K_c of 7178-T6 and 7075-T6 is 55 and 65 ksi $\sqrt{\text{in.}}$, respectively.

(3) The K_c values of two series of 4130 steel specimens, each series heat treated to a different strength level, indicate an inverse relationship between strength and toughness.

(4) The influence of two sheet thickness on K_c was investigated for specimens of Ti-13V-11Cr-3Al (Ti-120VCA) and Ti-6A-4V. The Ti-13V-11Cr-3Al indicated a lower K_c value for the thicker sheet while the Ti-6A-4V

evidenced a higher K_c for the 1/8-in.-thick sheet than for the thinner 1/16-in. sheet.

References

[1] Paris, P.C. and Sih, G.C., in *Fracture Toughness Testing and Its Applications, ASTM STP 381*, American Society for Testing and Materials, 1965.
[2] *Fracture Testing of High-Strength Sheet Materials,* 1st Committee Report, ASTM Bulletin, Jan. 1960.
[3] Sullivan, A.M. and Freed, C.N., "The Influence of Geometric Variables on K_c Values for Two Thin Sheet Aluminum Alloys," NRL Report 7270, 17 June 1971.
[4] Broek, D., "The Residual Strength of Aluminum Alloy Sheet Specimens Containing Fatigue Cracks or Saw Cuts," National Aerospace Laboratory (Amsterdam) Technical Report NLR-TR m. 2143, 1966.
[5] Freed, C.N., Sullivan, A.M., and Stoop, Jr., "Comparison of Plane Stress Fracture Toughness for Three Aluminum Sheet Alloys," NRL Report 7299, 11 Aug. 1971.

S. D. Antolovich,[1] P. M. Shete,[1] and G. R. Chanani[1]

Fracture Toughness of Duplex Structures: Part I - Tough Fibers in a Brittle Matrix

REFERENCE: Antolovich, S.D., Shete, P.M., and Chanani, G.R., "**Fracture Toughness of Duplex Structures: Part I – Tough Fibers in a Brittle Matrix**," *Fracture Toughness, Proceedings of the 1971 National Symposium on Fracture Mechanics, Part II, ASTM STP 514*, American Society for Testing and Materials, 1972, pp. 114-134.

ABSTRACT: Tough maraging steel fibers were embedded in a relatively brittle maraging steel matrix by a special diffusion bonding and heat treating technique. Three indices of fracture toughness were computed. K_{1c} as recommended by the ASTM, K^{o}_{max}, the fracture toughness based on the maximum load and initial crack length and K^{i}_{max}, the fracture toughness based on the maximum load and instantaneous crack length. While K_{1c} for the fibrous composite was no higher than K_{1c} for the matrix material, both K^{o}_{max} and K^{i}_{max} were significantly higher for the composite. Since fracture of the fibrous composites occurred in a stable manner (fast fracture was not observed) the load displacement records were converted into crack growth resistance curves. The R curves exhibited a serration at G_{Ic}, but continued to increase significantly above G_{1c} and multiple serrations, apparently as a result of the fibers, were present. An approximate calculation shows that the increase in crack growth resistance cannot be attributed solely to plastic deformation of the fibers. Scanning electron microscopy revealed local decohesion between the fibers and the matrix and the character of the R curve was attributed to local crack front pinning by blunting or reduction in constraint. As a model of delamination in a fibrous structure, holes were drilled perpendicular to the parting plane in 7075–T6 aluminum specimens. The load versus displacement and R curves were similar to those observed in the fibrous composites. In addition, pinning of the fatigue crack was observed in the vicinity of the holes.

KEY WORDS: fracture strength, toughness, fracture (materials), fatigue (materials), crack propagation, cracks, maraging steels, fiber composites, metals, fractography

There have been numerous studies carried out on systems in which strong but brittle fibers have been incorporated in ductile matrices. The goal is to improve the strength while taking advantage of the inherent toughness of the matrix. Another possibility which has not been studied extensively is to embed tough fibers in a brittle matrix thereby taking advantage of the inherent strength of the

[1]Department of Materials Science and Metallurgical Engineering, University of Cincinnati, Cincinnati, Ohio 45221.

matrix and obtaining a toughness improvement from the fibers. In this study the fracture characteristics of specimens containing unaged maraging wires in an aged maraging matrix have been studied.

Experimental Technique

Specimens containing 5.7 percent of tough maraging steel fibers were embedded in a relatively brittle maraging steel matrix by a hot pressing technique. Initially, the fibers were in the aged (high strength) condition while the plates were unaged (low strength). Both plates and fibers were electropolished to produce very clean surfaces. The fibers were then spot welded to the plates and the fiber-bearing plates were stacked so that the fibers would form an approximately hexagonal array. The aggregate was then cold pressed to partially embed the hard fibers in the relatively soft plates and minimize flattening of the fibers during hot pressing. The composite was then hot pressed at 1150 C and about 3000 psi pressure for two hours. Both the fibers and the plates were austenitic and relatively soft at 1150 C. After hot pressing, the composite was reaustenitized at 1150 C for one hour in a programable furnace and cooled to 200 C where the matrix was completely martensitic and the fibers were austenitic. The sample was then immediately heated to 500 C and held for 3 h to age the matrix. After cooling to room temperature the fibers transformed to unaged martensite and the sample consisted of unaged fibers (unaged maraging steel is quite tough and ductile) in an aged matrix (aged maraging steel is strong but relatively brittle). More complete details of the fabrication technique are described elsewhere [*1*]. Both steels were specially melted for this investigation and their compositions are shown in Table 1. The matrix steel falls approximately within the composition range of commercial 250 grade maraging steels while the fiber material corresponds to a 350 grade maraging steel.

The samples were then machined into compact tension toughness specimens as recommended by the ASTM [*2*]. The specimen geometry is shown schematically in Fig. 1. Fatigue starter-cracks were placed at the tip of the

TABLE 1—*Compositions of maraging steels used.*

Element	Matrix wt. %	Fiber wt. %
Ni	18.6	17.7
Co	8.5	12.7
Mo	5.1	3.7
Ti	0.73	1.76
Al	0.08	0.23
Fe	balance	balance

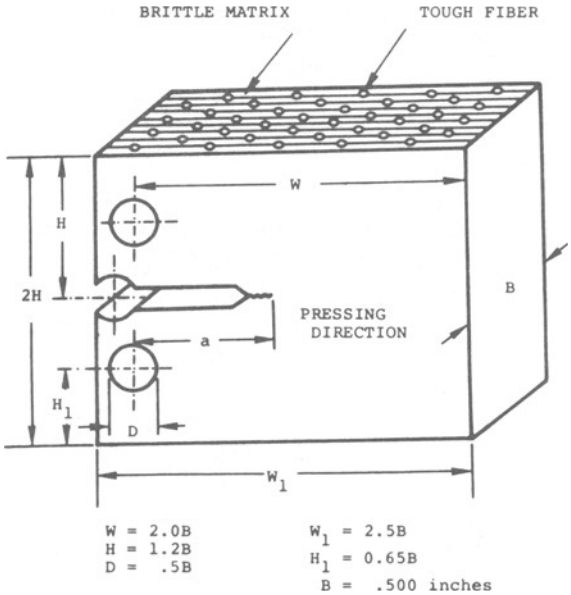

FIG. 1–Compact tension specimen containing tough fibers in a brittle matrix.

machine notch and the specimens were loaded to fracture using an Instron tester and load versus displacement records were obtained using an X-Y recorder. A typical load versus displacement record is shown in Fig. 2. All aspects of testing were done in accordance with the ASTM recommendations [2]. The load versus displacement records were used to calculate the following quantities:

(1) The plane-strain fracture toughness K_{Ic}, according to the ASTM recommendations.

(2) The fracture toughness based on the maximum load and the initial crack length, $K^o{}_{max}$.

(3) The fracture toughness based on the maximum load and instantaneous crack length, $K^i{}_{max}$.

(4) Crack growth resistance curves as discussed by Srawley and Brown [3].

The fractured specimens were then examined both metallographically and by scanning electron microscopy to further evaluate the effects of the microstructure on the crack propagation characteristics.

Since decohesion between the fibers and the matrix could play an important role in fracture some attempt was made to evaluate this effect by drilling a series of holes perpendicular to the potential crack plane. The hole sizes used were 0.063, 0.094, and 0.125 in. and approximately 15 volume percent of the base metal was removed. For this purpose 7075 aluminum alloys were used primarily because it is much easier to drill small holes in aluminum than it is in maraging

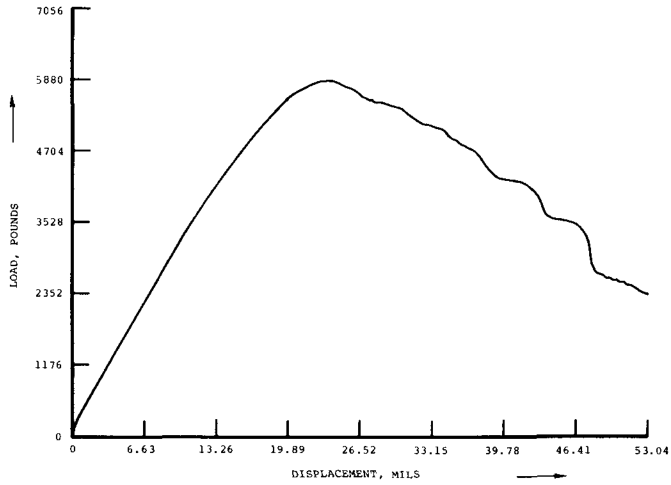

FIG. 2—*Typical load versus displacement record obtained from specimen containing approximately 6 percent tough fibers. The record qualifies as a valid plane strain test.*

steel. After the holes were drilled the 7075 specimens were heat treated to the T6 condition. In addition to strengthening, the heat treatment should also relieve residual stresses that may have been caused by drilling. The 7075-T6 specimens were then tested in the same way as were the maraging steels.

Results and Discussion

The fracture toughness values calculated by the techniques discussed above are shown in Table 2. The first point to notice is that laminating had little or no effect on the fracture toughness regardless of the way in which the toughness was calculated. This behavior was expected since, as indicated elsewhere [*1*], very high quality bonds were produced by the hot pressing technique used to make these composites.

Inclusion of the ductile fibers had little effect on improving the plane strain fracture toughness. This is understandable since the secant offset technique used to calculate K_{Ic} is adjusted so as to correspond to real or virtual crack extension of approximately one plane strain plastic zone radius [*4*]. Initial crack extension corresponding to K_{Ic} undoubtedly takes place in the more brittle matrix and the fibers can make their full contribution much later in the fracture process. Gerberich [*5*] has considered the case where high strength/high toughness stainless steel fibers were embedded in a low strength/low toughness aluminum alloy matrix. Post fracture metallographic examination revealed that the fibers suffered plastic deformation approximately one fiber diameter on either side of the fracture surface. On the basis of those observations he postulated that the

TABLE 2–*Fracture toughness and mechanical property data of composites.*

Specimen Number	Microstructure	Strength of[a] composite, ksi	Plane-strain[b] fracture toughness, K_{Ic} ksi/$\sqrt{in.}$	Fracture toughness calculated from maximum load and original crack length, K^{o}_{max} ksi/$\sqrt{in.}$	Fracture toughness calculated from maximum load and instantaneous crack length, K^{i}_{max} ksi/$\sqrt{in.}$
B_1	Aged, bulk matrix material	237	96	100	100
B_2	Diffusion bonded plates of matrix material in aged condition	246	90	107	107
A_1	5.7% of 0.030-in. diameter unaged fibers in aged matrix	240	84	120	147
A_2		240	83	133	183
A_4		217	72	138	172
A_5		226	72	135	178
A_6		213	97	143	177
A_7	15.4% of 0.030-in. diameter unaged fibers in aged matrix	207	75	122	159

[a]Calculated from the rule of mixtures. The strength of the matrix and fibers were determined by converting Knoop microhardness measurements to tensile strengths. The resultant values fall into the accepted ranges for the materials used.

[b]All specimens qualified as valid plane strain tests except A_6 which failed to meet the requirement that $B \geq 2.5\ (K_{Ic}/\sigma_{ys})^2$.

contribution to the over-all fracture toughness made by plastic deformation of the fibers be calculated from:

$$G_f = \sigma_f \epsilon_f 2d\,(V_f) \tag{1}$$

where

σ_f = fiber strength
ϵ_f = fracture strain of the fibers
d = fiber diameter
V_f = volume fraction of fibers

Post fracture metallographic examination of the specimens used in this study revealed that the zone of decohesion between the fibers and the matrix was on the order of approximately two fiber diameters on either side of the fracture surface. A typical macrograph is shown in Fig. 3. This observation implies that Eq 1 can be used provided that $2d$ is replaced by $4d$. The appropriate equation for the present study is:

$$G_f = \sigma_f \epsilon_f 4d(V_f) \tag{2}$$

The above expression assumes that the elastic strain energy is released to plastic deformation and hence that an essentially elastic parameter (namely, G_f)

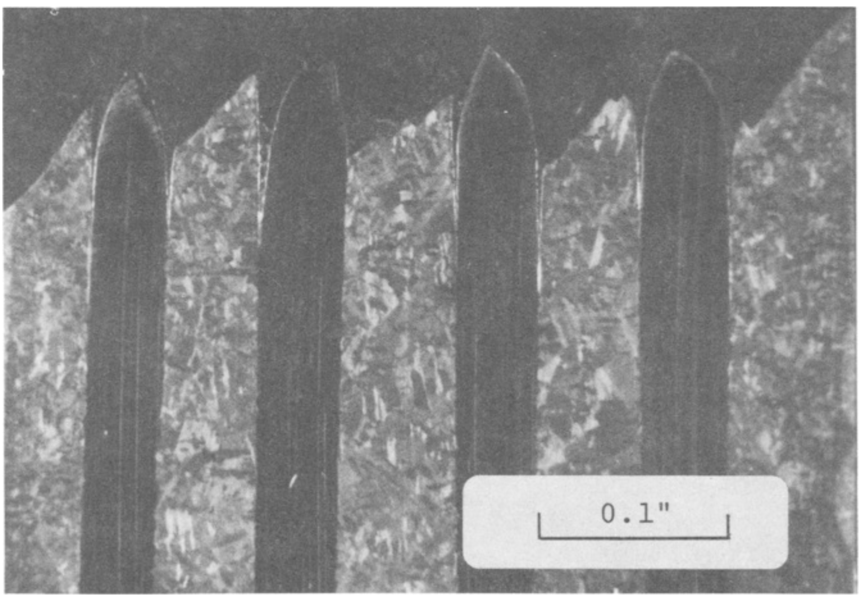

FIG. 3—*Macrograph showing decohesion between the fibers and the matrix. The zone of decohesion is approximately two fiber diameters on either side of the fracture surface.*

can be calculated from the plastic energy absorbed. This approach has been used elsewhere by Antolovich [6] and by others [7]. The calculation also assumes that there is little or no strain hardening of the fibers and that the plastic portion of the stress strain curve is much larger than the elastic portion. These assumptions are valid for maraging fibers. Appropriate values may be substituted into Eq 2 to estimate the contribution made by the fibers:

$$\begin{aligned} \sigma_f &= 150{,}000\ \text{lb/in.}^2 \qquad [8] \\ \epsilon_f &\simeq 0.18 \text{ for gage length equal to four diameters} \qquad [8] \\ V_f &\simeq 0.06 \\ d &\simeq 0.03 \end{aligned} \tag{3}$$

The result is that

$$G_f \simeq 194\ \text{in.} \cdot \text{lb/in.}^2 \tag{4}$$

It should be emphasized that the fibers make essentially no contribution at the initial point of instability (that is, at G_{Ic}) and make their full contribution very late in the fracture process.

The toughness based on the maximum load and original crack length $K^o{}_{max}$ are substantially the same for both the bulk material as well as the "matrix laminate". However, the matrix laminate exhibits a greater percentage increase over K_{Ic} than does the bulk matrix material. This is understandable since at the maximum load more delamination and hence a greater reduction in constraint will have occurred in the matrix laminate than at the loads corresponding to K_{Ic}. The striking feature, however, is that the toughness of the fibrous specimens increased quite significantly. Using $K^o{}_{max}$ the toughness increased from approximately 100 ksi $\sqrt{\text{in.}}$ for the bulk of matrix laminate to an average value of 134 ± 14 ksi $\sqrt{\text{in.}}$ In terms of the crack extension force the increase is from approximately 300 in. · lb/in.^{2} to approximately 600 in. · lb/in.^{2} The crack extension force is calculated from the well-known equation

$$G \simeq \frac{K^2}{E} \tag{5}$$

where E = Young's modulus.

The fracture toughness $K^i{}_{max}$ measured by the maximum load and instantaneous crack length[2] increases to an average value of 171 ksi $\sqrt{\text{in.}}$

[2]The instantaneous crack length was measured by a compliance technique discussed in the Appendix.

corresponding to a crack extension force of approximately 1010 in. · lb/in.^{2} This represents an increase of almost 800 in. · lb/in.^{2} beyond G_{Ic} and since the fibers account for on the order of 200 in. · lb/in.^{2} this increase cannot be attributed solely to plastic deformation of the fibers. This conclusion is further strengthened by the observation that even at $K^i{}_{max}$ fracture was not complete but continued in a stable manner at gradually decreasing loads as shown in Fig. 2. The large increases in toughness beyond G_{Ic} tend to indicate that use of a single parameter to characterize fracture masks some important features or crack extension in these composites.

Brown and Srawley [*3*] have pointed out that using a single parameter such as K_{Ic} or K_c to characterize the fracture process is like characterizing the tensile properties of a metal by its ultimate tensile strength. They discussed the concept of crack growth resistance curves, or R curves. Basically as the crack is loaded, the crack extension force G increases tending to promote crack extension. This driving force is balanced by the material's resistance to crack growth, R, and is generally manifested by plastic enclave development. Thus for all applied values of G up to catastrophic failure equilibrium is established between G and R. This is similar to the way in which the combination of increased load and decreased cross sectional area is balanced by increased strain hardening in a uniaxial tension test up to the point of necking. Crack growth resistance curves have recently been used by Heyer and McCabe [*9*] to explain crack extension in a wide range of materials.

Although the compact tension (CT) specimen geometry is not usually an ideal one for deducing the form of the R curve,[3] for the composites studied in this investigation catastrophic fracture was not observed: the crack would extend and then be arrested. It would not extend again until the faces were further displaced by the cross head of the Instron test machine. A typical load versus displacement curve is shown in Fig. 2 and the corresponding R curve is shown in Fig. 4. The R curve may be deduced from the load versus displacement record if the compliance is known as a function of crack length. The procedure used in this investigation is described below.

(1) Join any point on the load displacement curve to the origin by a straight line. The inverse slope of the straight line is the effective compliance, C_{eff}.

(2) Through knowledge of the compliance versus crack length curve, convert C_{eff} to the effective crack length a_{eff}. The effective crack corresponds to the real crack plus the plastic zone radius [*4*].

(3) Calculate the stress intensity using the appropriate sample calibration function, the load and the effective crack length. Convert stress intensity to crack extension force through use of Eq 5.

[3] A specimen for which G decreases as the crack extends under constant load is ideal for R curve determinations since catastrophic failure is not possible and the full R curve can be developed. The crack-line-loaded center cracked specimen [*10*] is ideal since $G = P^2/\pi a E$.

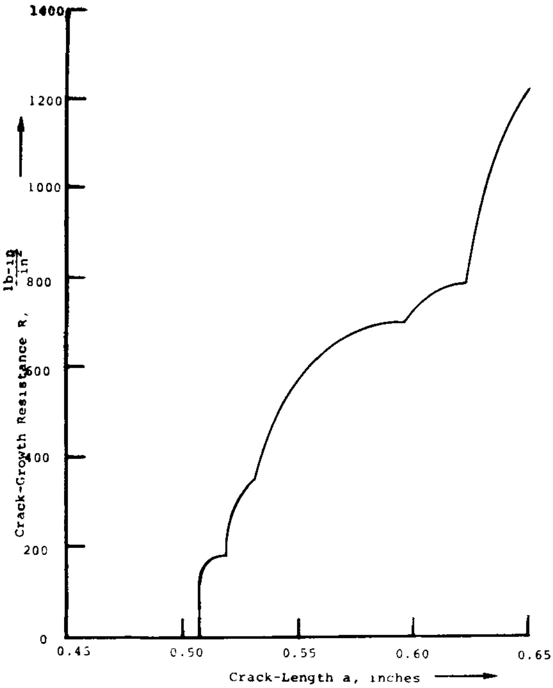

FIG. 4–*Crack growth resistance curve obtained from the curve of Fig. 2.*

(4) Noting that $G = R$ up to the point of catastrophic fracture construct a plot of R versus a.

The compliance curve for the CT specimen is not available in the literature but can be deduced if the compliance is known accurately at one crack length by appropriate integration of the calibration function. The details of the compliance determination are discussed in the Appendix.

The form of the R curves of the composites is quite different from those usually obtained from isotropic specimens. There are multiple steps which seem to be associated with the presence of the fibers. As previously mentioned, all R curves had substantially the same form as that shown in Fig. 4. A possible explanation for the observed behavior is that the fibers tend to locally restrain crack extension. The local restraint could be a result of crack front blunting due to plastic deformation or blunting due to decohesion between the fiber and the matrix as discussed by Cook and Gordon [*10*] for all-brittle systems containing internal interfaces and by McCartney et al [*11*] for metal laminates.

The crack could also be locally pinned as a result of the reduction in constraint associated with decohesion. If decohesion takes place, there would be a "hole" in the matrix surrounded by a region in which the state-of-stress is closer to plane stress than is the material remote from the hole which is closer to plane strain. The material close to the hole would be tougher and crack extension would be restrained. This concept was used by Gerberich et al [12] to explain multiple pop-in in 7075-T6 aluminum. They considered the crack to be restrained at the surface by tough plane-stress "hinges" and free to extend in the center where the material is closer to plane strain and hence more brittle.

The model is shown schematically in Fig. 5. On the basis of this model the first small increment of crack extension should take place at K_{Ic} of the matrix. As the crack extends, the crack front assumes a serrated form and the radius of curvature of each segment decreases as the crack extends. Each segment is like a penny shaped crack and following Paris and Sih [13] and as discussed elsewhere [14], the stress intensity may be estimated to be:

$$K = 2\sigma \left(\sqrt{\frac{\rho}{\pi}}\right)\alpha \qquad (6)$$

where

σ = applied stress
ρ = radius of curvature
a = factor that contains both geometric and free surface corrections

For continued crack extension in the matrix the stress intensity must be maintained at the plane strain toughness of the matrix $K_{Ic}{}^{M}$ and the following equation applies:

$$\sigma = \frac{K_{Ic}{}^{M}}{2\alpha}\sqrt{\frac{\pi}{\rho}} \qquad (7)$$

The stress required for the crack to break away from one row of fibers corresponds to the minimum radius of curvature which depends on the geometry

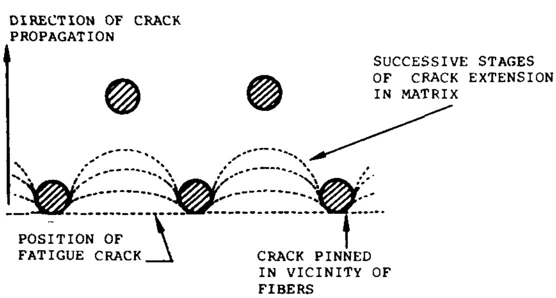

FIG. 5—*Mechanism of crack extension in fibrous composite. The crack is pinned in the vicinity of the fibers and extends in the matrix.*

of the composite. If the interfiber spacing is λ then the minimum radius of curvature is $\lambda/2$ and Eq 7 becomes

$$\sigma = \frac{K_{Ic}{}^{M}}{\alpha} \sqrt{\frac{\pi}{2\lambda}} \tag{8}$$

Equation 8 has a similar form to the expression for a dislocation passing through a dispersoid where the flow stress is proportional to the shear modulus and inversely proportional to the spacing between precipitates. This is not unexpected since just as a dislocation may be thought of as a linear defect forming a boundary between slipped and unslipped regions the crack front may be thought of as a linear defect separating parted and unparted regions of a material.

Equation 8 implies that a constant stress must be maintained for fracture to continue and that small decreases in stress should cause crack-arrest. Consequently crack extension through the composite can easily be made to occur under near-equilibrium conditions. If the crack is extending at its propagation stress defined by Eq 8, the average crack length continually increases and there should be a corresponding increase in the apparent crack growth resistance.[4]

The experimental data showed no increase in K_{Ic} above that of the matrix, the crack grew in a stable manner and the R curve increased significantly above G_{Ic}. These observations are in complete accord with the predictions of the model, which then appears to offer a partial framework for understanding fracture in composites where the fibers are tougher than the matrix.

As a partial check of the conclusion that the presence of the fibers causes the multiple serrations in the R curve, a specimen containing approximately 15 percent of tough fibers was fabricated. In this case, the crack encounters more rows of fibers and if the fibers are responsible for the serrations in the R curve, more serrations should be observed. Figure 6 shows the R curve for this specimen and there are indeed more serrations present, which lends credence to the hypothesis that the fibers are responsible for the observed R curve behavior. The test record of this specimen met all the requirements of the ASTM for a valid plane strain fracture toughness and K_{Ic} was calculated to be 75 ksi $\sqrt{\text{in.}}$ while $K^{o}{}_{max}$ was 122 ksi $\sqrt{\text{in.}}$ and $K^{i}{}_{max}$ was 159 ksi $\sqrt{\text{in.}}$ These values are somewhat lower than was observed for specimens containing 6 percent tough fibers.

Some comments are in order relative to the scale on which crack front curvature is expected to play an important role in the fracture process. Most materials contain structural and chemical heterogeneities that are very small typically on the order of 0.001 in. which would cause extremely small radii of

[4]The term "apparent crack growth resistance" is used because in constructing crack growth resistance curves, formulas are used which assume that the crack front is straight, even though as discussed in the text this may not be the case.

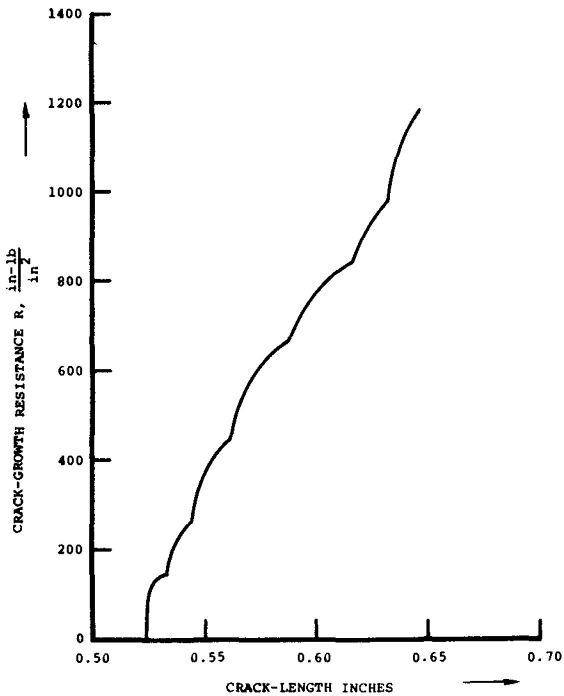

FIG. 6—*Crack growth resistance curve for specimen containing 15 percent of 0.030-in. diameter fibers.*

curvature and a fracture mechanism as discussed above. Obviously, this does not occur. It appears reasonable to assume that crack front curvature will be important only when the radius of curvature is large with respect to the plastic zone size. If the plastic zone is significantly larger than the local radius of curvature, it is evident that the curvature will be unresolvable and will have no effect on the fracture process. For the aged maraging steel matrix used in this investigation, the plane-strain plastic zone size is calculated to be about 0.017 in. Thus, the interfiber spacing must be at least 0.017 in. for crack front curvature to be important. The interfiber spacing is approximately 0.08 in. for composites containing 6 percent of 0.030-in. diameter tough fibers and 0.04 in. for composites containing 16 percent of the tough fibers. In both cases, the interfiber spacing is significantly larger than the plastic zone size and crack front curvature is expected to play an important role in the fracture process.

Scanning fractography was carried out to observe the character of the fracture surfaces. Figure 7 is a typical fractograph and shows that there is decohesion between the fibers and the matrix, that the fibers are tough as evidenced by their ductile failure mode and that the matrix is brittle, as evidenced by its flat fracture mode. Decohesion between plates constituting the matrix was considerably less pronounced than between the matrix and the

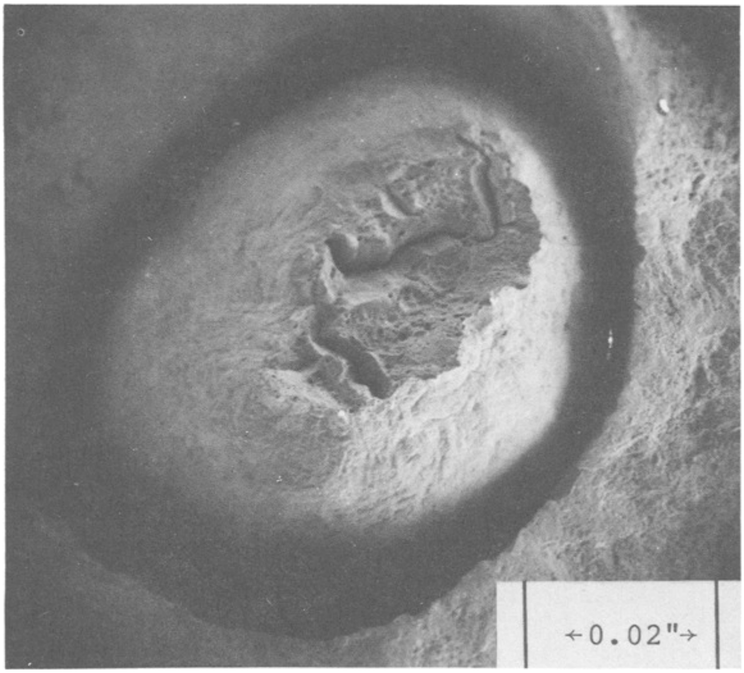

FIG. 7—*Scanning fractograph showing delamination between fibers and matrix.*

fibers. Figure 8, taken from an area in the matrix, shows a region in which partial decohesion occurred between matrix plates. In fact, while scanning the fracture surface, areas in which there was observable decohesion in the matrix were far less prevalent than those in which there was no decohesion. Since there was significant decohesion between matrix and fiber, crack pinning appears to be a consequence of decohesion.

A series of holes perpendicular to the crack plane represents a reasonable approximation to decohesion. Holes of 0.063, 0.094, and 0.125-in. diameter were drilled perpendicular to the crack plane in 7075-T6 aluminum alloys. Approximately 10 to 15 volume percent of material was removed and the specimens were 1/2 in. thick, except for those containing 0.125-in. diameter holes in which case they were 3/4 in. thick in order to appropriately accommodate the holes. The specimens were fatigue cracked and fractured according to the ASTM recommendations. Figure 9 shows the appearance of two fractured specimens. Although the fatigue crack of the specimen containing the large holes was never in physical contact with the holes the crack front is curved and apparently pinned by the holes behind it. This can be explained by assuming that a plane-stress ring exists around the holes. In fatigue, the state-of-stress thickness transition, if any, is expected to occur at thicknesses much smaller

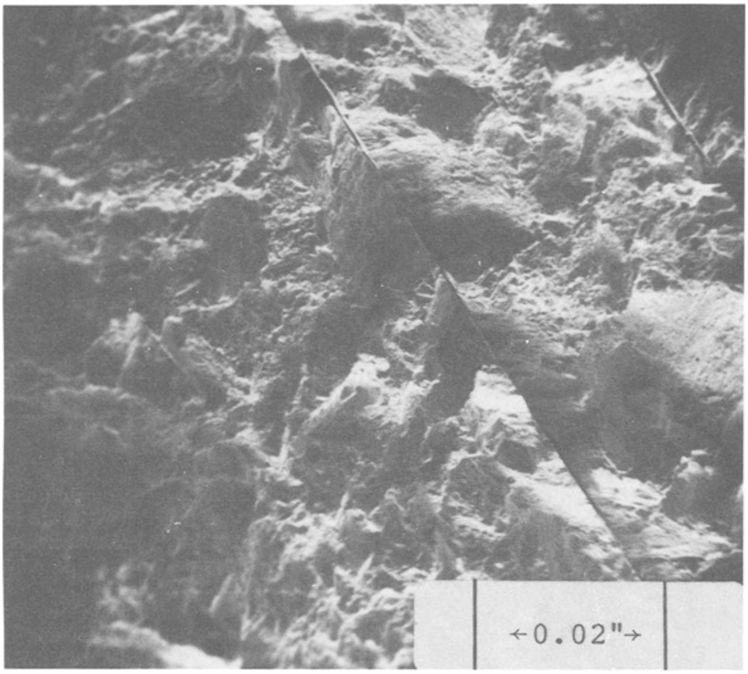

FIG. 8 –*Scanning fractograph showing partial delamination in the matrix.*

than it does for fracture under monotonic loading because the fatigue plastic zone is much smaller than the monotonic plastic zone at the same stress intensity level [*15*]. Consequently, the fatigue zone is subject to higher constraint at equivalent stress intensity levels. The implication is that the plane stress "hinges" in fatigue are much smaller and hence probably less effective in causing crack front perturbation than they would be in monotonic fracture. Nonetheless even in fatigue they do cause the crack front to be curved and the effect is probably accentuated in monotonic loading. The same effect can be seen in the specimen containing 0.094-in. diameter holes. In this case, the fatigue crack is in contact with the holes and crack front pinning occurs as a result of local blunting or plane stress hinges.

A typical load displacement curve for a specimen containing 0.125-in. diameter holes is shown in Fig. 10. The serrated horizontal portion of the curve is particularly interesting since it is reproducible in specimens containing holes of this diameter and never occurred in ordinary bulk specimens. An explanation is that as the load is increased the crack front starts to bow out between the holes. As it bows out the radius of curvature starts to bow out between the holes. As it bows out the radius of curvature decreases causing the effective stress intensity to decrease and eventually the crack stops. The process of initiation and arrest is repeated several times until finally the crack is free from the restraining effect of the holes (however that

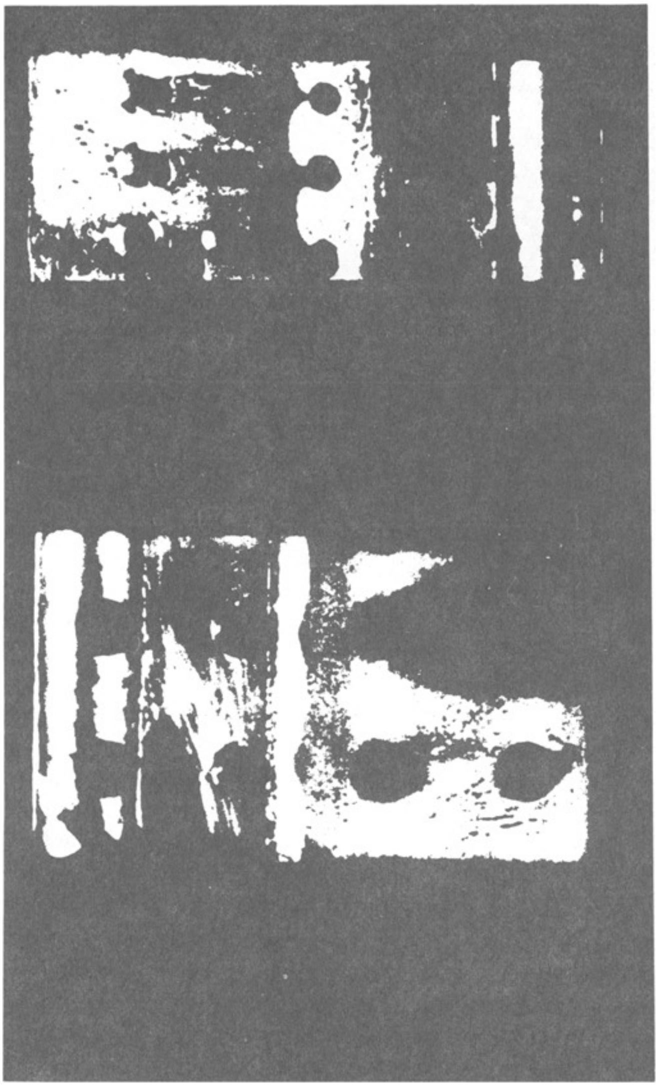

FIG. 9—*Fracture appearance of 7075-T6 aluminum specimens in which holes 0.090 and 0.125 in. were drilled. In both cases the fatigue crack was restrained by the holes. In particular even though the fatigue crack was never in physical contact with the holes it was restrained in the specimen containing the large holes.*

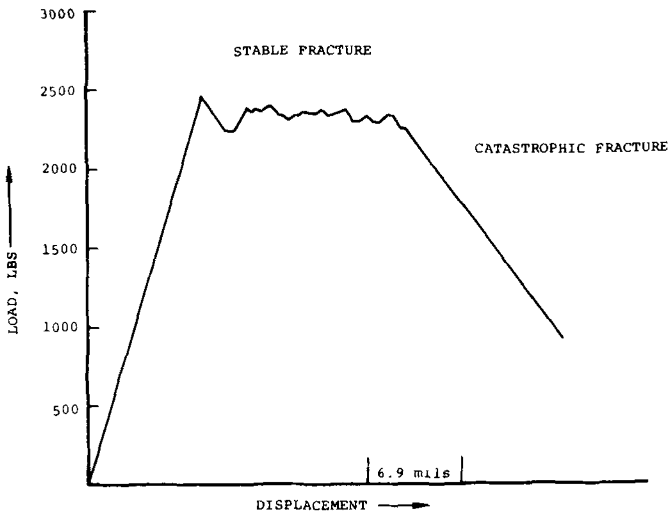

FIG. 10—Typical load versus displacement record for specimens containing 0.125-in. diameter holes. The record qualifies as a valid plane strain test.

restraint arises) and, since the distance between rows is large, catastrophic fracture takes place. The corresponding R curve is shown in Fig. 11 where it can be seen that crack growth resistances far in excess of G_{Ic} are developed. A typical R curve for a specimen containing holes 0.090 in. in diameter and from which approximately 15 percent of material was removed is shown in Fig. 12. Again there are a large number of serrations on the R curve corresponding to the large number of holes.

Conclusions

1. Specimens containing approximately 6 percent of tough unaged maraging steel fibers 0.030 in. in diameter in a relatively brittle, aged, maraging steel matrix exhibited significant increases in fracture toughness beyond K_{Ic} which could not be attributed solely to plastic deformation of the fibers.

2. The R curves (crack growth resistance curves) rose significantly beyond G_{Ic} and had multiple serrations corresponding to the rows of fibers.

3. Increasing the volume fraction of fibers to approximately 16 percent did not cause any increase in K_{Ic} but did cause more serrations in the R curve corresponding to the increased number of rows of fibers.

4. The results can be explained using a simple model that assumes the crack is pinned in the vicinity of the fibers and extends in the matrix. The model predicts that K_{Ic} for the composite should be the same as K_{Ic} for the bulk material and that the R curve should rise significantly above G_{Ic}. The experimental observations were in agreement with the predictions of the model.

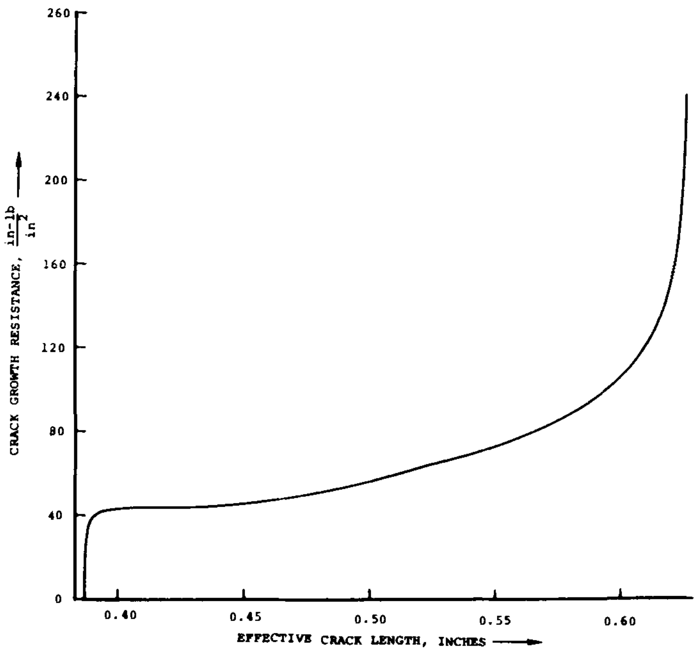

Fig. 11—*Crack growth resistance curve obtained from the curve of Fig. 10.*

5. Fractography showed that there was significant decohesion between the fibers and the matrix which implies crack front pinning was a result of decohesion.

6. To model the effects of decohesion, holes of various sizes were drilled in 7075-T6 aluminum alloys. As was the case for the maraging steel composites, K_{Ic} was unchanged from the bulk material while the R curves showed large increases beyond G_{Ic} and contained serrations corresponding to the rows of holes. The fatigue starter cracks were restrained in the area of the holes and extended in the matrix in agreement with the proposed mechanism of crack extension.

7. A single fracture mechanics parameter does not adequately describe crack extension characteristics in these highly directional structures.

Acknowledgments

We are deeply grateful to the American Iron and Steel Institute (Grant 61-247) and to NASA (Grant NGR 36 004 014) for research grants supporting this work. We also would like to acknowledge the Paul D. Merica Research Laboratory of the International Nickel Company for supplying the maraging steel wires and the Armco Research and Technology Center for use of their metal working facilities.

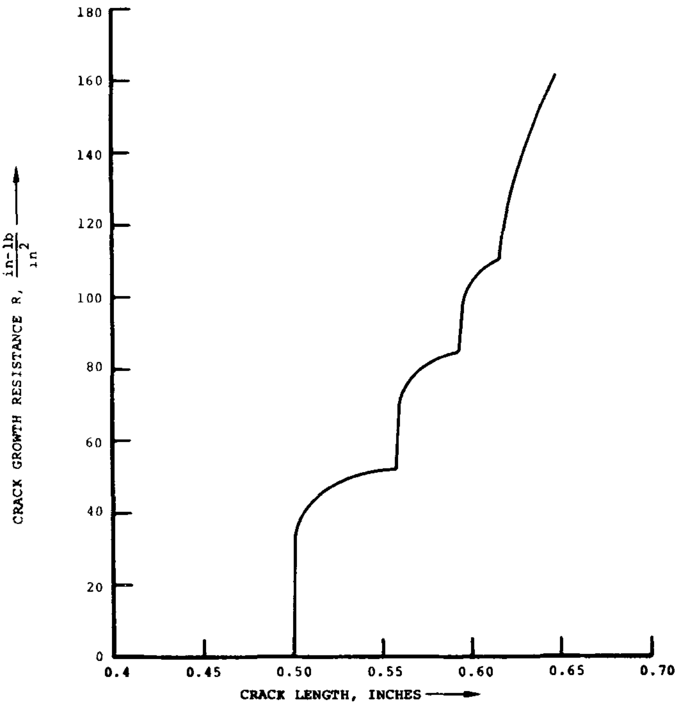

FIG. 12—*Crack growth resistance curve for specimen containing 0.090-in. diameter holes.*

APPENDIX

If the appropriate calibration function is known, it can be used, along with the Irwin-Kies [*16*] equation to determine the compliance. The Irwin-Kies relationship states that:

$$K = \frac{P\sqrt{a}}{BW}\left(\frac{BEW^2}{2a}\ \frac{dC}{da}\right)^{1/2} = \frac{P\sqrt{a}}{BW}\cdot Y\left(\frac{a}{W}\right) \qquad (9)$$

where

P = load
a = crack length
W = specimen width
E = Young's modulus
$Y(\frac{a}{W})$ = calibration function that depends on specimen geometry

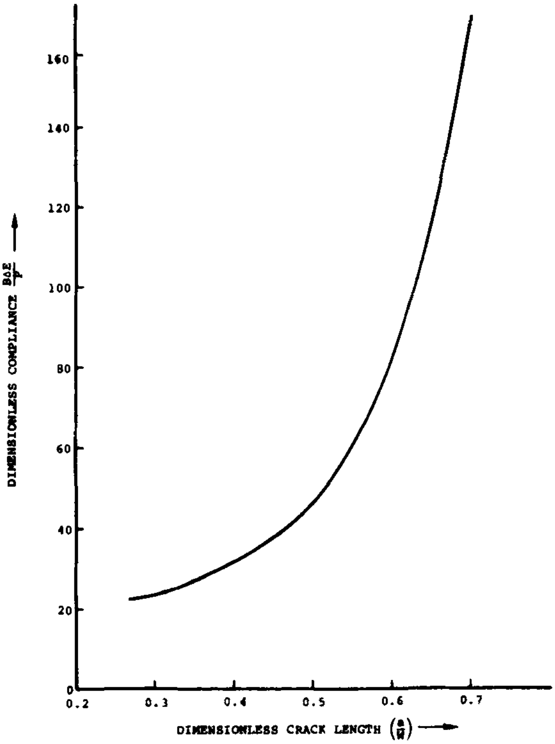

FIG. 13–*Dimensionless compliance as a function of dimensionless crack length for compact tension specimen.*

The compliance C as a function of a can be extracted from the following expression:

$$C = \int \frac{2a Y^2}{BEW^2} \, da + C_o \tag{10}$$

where C_o is a constant of integration and can be determined if C is known at one crack length. For specimens used in this investigation the following quantities apply:

$$B = 0.500 \text{ in.}$$

$$W = 1.000 \text{ in.}$$

$$E = 27 \times 10^6 \quad [8]$$

$$Y = \left[0.2960 - 1.855 \left(\frac{a}{W}\right) + 6.557 \left(\frac{a}{W}\right)^2 - 10.17 \left(\frac{a}{W}\right)^3 + 6.389 \left(\frac{a}{W}\right)^4 \right] 10^2 \quad [17] \tag{11}$$

The compliance of specimens containing machine notches 0.400, 0.501, and 0.701 in. long was measured to be 2.740×10^{-6}, 4.160×10^{-6}, and 12.80×10^{-6} in./lb respectively. The corresponding values of the integration constant were 1.028×10^{-6}, 2.284×10^{-6}, and 3.324×10^{-6} in./lb. Ideally, regardless of the crack length used to evaluate the constant, the result should be invariant. While that is not the case, the compliance calculated using a constant of 2.284×10^{-6} in./lb differs by a few percent at most from the compliance calculated at the same crack length using either of the other constants. Thus the constant was chosen to be 2.284×10^{-6} in./lb and using this value, Eq 10 becomes

$$C = \left[2.284 + 64.46\left(\frac{a}{W}\right)^2 - 540.5\left(\frac{a}{W}\right)^3 + 2707\left(\frac{a}{W}\right)^4 - 8985\left(\frac{a}{W}\right)^5 + 20860\left(\frac{a}{W}\right)^6 - 33230\left(\frac{a}{W}\right)^7 + 34690\left(\frac{a}{W}\right)^8 - 21370\left(\frac{a}{W}\right)^9 + 6046\left(\frac{a}{W}\right)^{10}\right]10^{-6} \qquad (12)$$

Multiplication of the compliance by the thickness and modulus puts the compliance on a dimensionless basis: this has been done in Fig. 13 where the dimensionless compliance has been plotted as a function of dimensionless crack length. Equation 12 was used to determine effective crack lengths from effective compliances in the R curve calculations. Values obtained using Eq 12 were checked experimentally by comparing the crack length corresponding to the initial linear portion of load displacement records with the measured fatigue crack length and the agreement was usually within 5 percent.

References

[1] Shete, P.M., Masters thesis, University of Cincinnati, June 1970.

[2] *Annual Book of ASTM Standards*, American Society for Testing and Materials, Part 31, 1970, pp. 911-927.

[3] Srawley, J.E. and Brown, W.F., Jr., in *Fracture Toughness Testing and its Applications*, *ASTM STP 381*, 1965, pp. 133-198.

[4] Brown, W.F., Jr., and Srawley, J.E., *Plane Strain Fracture Toughness Testing of High Strength Metallic Materials*, *ASTM STP 410*, 1966, pp. 56-60.

[5] Gerberich, W.W., *Journal of the Mechanics and Physics of Solids*, Vol. 1, 1971, pp. 71-87.

[6] Antolovich, S.D. and Singh, Birindar, *Metallurgical Transactions*, Vol. 2, 1971, pp. 2135-2141.

[7] Gerberich, W.W., Hemmings, P.L., Zackay, V.F., and Parker E.R., *Fracture 1969*, Chapman and Hall Ltd., London, 1969, pp. 288-305.

[8] Hall, A.M. and Slunder, C.J., "The Metallurgy, Behavior and Application of the 18 Percent Nickel Maraging Steels," NASA SP 5051, National Aeronautics and Space Administration, 1968.

[9] Heyer, R.H. and McCabe, D.E., "Plane-Stress Fracture Toughness Testing Using a Crack-Line-Loaded Specimen," presented at the Third National Fracture Mechanics Symposium, Lehigh University, 25 Aug. 1969.

[10] Cook, J. and Gordon, J.E., *Proceedings of the Royal Society*, Vol. 282, 1964, pp. 508-520.

[11] McCartney, R.F., Richard, R.C., and Trozzo, P.S., *Transactions of the American Society for Metals*, Vol. 60, 1967, pp. 384-394.

[12] Gerberich, W.W., Key, P.L., and Parker, E.R., *Engineering Fracture Mechanics,* Vol. 2, 1970, pp. 47-60.
[13] Paris, P.C. and Sih, G.C. in *Fracture Toughness Testing and its Applications, ASTM STP 381* 1965, pp. 30-83.
[14] Antolovich, S.D., *Metal Science Journal,* Vol. 3, 1969, pp. 45-47.
[15] Johnson, H.H. and Paris, P.C., *Engineering Fracture Mechanics,* Vol. 1, 1968, pp. 3-45.
[16] Irwin, G.R. and Kies, J.A., *Welding Journal,* Vol. 33, 1954, p. 1935.
[17] Wessel, E.T., *Engineering Fracture Mechanics,* Vol. 1, 1968, pp. 77-103.

S. D. Antolovich,[1] *K. Kasi,*[1] *and G. R. Chanani*[1]

Fracture Toughness of Duplex Structures: Part II - Laminates in the Divider Orientation

REFERENCE: Antolovich, S. D., Kasi, K., and Chanani, G.R., "**Fracture Toughness of Duplex Structures: Part II–Laminates in the Divider Orientation,**" *Fracture Toughness, Proceedings of the 1971 National Symposium on Fracture Mechanics, Part II, ASTM STP 514*, American Society for Testing and Materials, 1972, pp. 135-150.

ABSTRACT: Laminates containing 25 percent of tough (unaged) maraging steel plates and 75 percent of brittle (aged) maraging steel plates were prepared by a special diffusion bonding and heat treating technique so that the thickness of the tough constituent was either 0.02, 0.04, 0.06, or 0.08 in. Compact tension fracture toughness specimens were machined so that the laminates were parallel to the sides of the specimens. They were then fractured according to the recommendations of the ASTM and three indices of toughness were measured: K_{Ic}, as recommended by the ASTM, K^{o}_{max} based on the maximum load and original crack length and K^{i}_{max}, based on the maximum load and instantaneous crack length. Four tests were performed at each thickness of the tough constituent; two each at crack lengths of approximately 0.30 and 0.55 in. The plane-strain fracture toughness of the laminates was slightly higher than K_{Ic} of the monolithic brittle constituent and was independent of either crack length or the dimensions of the tough constituent. Regardless of the thickness of the tough phase the composite toughness was highest for specimens containing cracks 0.30 in. long when the toughness was measured in terms of K^{o}_{max} or K^{i}_{max}. The toughness as a function of thickness exhibited a relative maximum when the tough phase was 0.04 in. thick and a relative minimum when the tough phase was 0.06 in. thick for both the 0.30 and 0.55-in. crack lengths. The experimental results are in broad agreement with a proposed model for crack extension in the divider orientation.

KEY WORDS: fracture strength, toughness, fracture (materials), maraging steels, laminates, metals, fractography, analytic geometries

The fracture toughness of laminates has been the subject of numerous investigations [*1-8*]. Those laminates investigated included single constituents bonded together [*1-3*] as well as duplex laminates, both artificial [*4-6*] and natural [*7, 8*] formed by a variety of techniques. In a laminate there are two conceivable geometries in which the toughness can be improved: the crack arrester orientation where the crack front is perpendicular to the short transverse dimension of the laminates and the crack divider orientation where the crack

[1] Department of Materials Science and Metallurgical Engineering, University of Cincinnati, Cincinnati, Ohio 45221.

front is parallel to the short transverse dimension of the laminates. In both cases the plane of the crack is perpendicular to the plane of the plates. Both types have been shown under appropriate conditions to give rise to improvements in the fracture characteristics. While the structural parameters affecting the toughness of specimens in the arrester orientation have been considered and explained in a satisfactory manner [*3, 6*], crack extension in the divider orientation is somewhat ambiguous: in some cases there is little or no reported improvement while in others the toughness of the divider specimens is as high as the arrester [*5*]. The purpose of this investigation is to systematically study those variables that in themselves are not materials parameters but that can conceivably have significant influences on the fracture behavior of the composites. In particular the effect of crack length as well as the absolute dimensions of the constituents making up the laminate are considered in detail.

Experimental

Laminates were produced by diffusion bonding two maraging steels at 1150 C for 2 h at a sample pressure of 3000 psi. After bonding the composite was austenitized at 1150 C and cooled to a temperature where one of the constituents (denoted B) transformed to martensite, leaving the other (denoted T) still austenitic. The sample was then immediately heated to 500 C for 3 h to harden steel B. After cooling to room temperature the composite consisted of aged (B) and unaged (T) maraging steels. The aged material was relatively brittle while the unaged material was tough. The diffusion bonding and selective hardening treatments are described in more detail elsewhere [*9*]. The compositions of the two steels are given in Table 1. Steel B is a 350 commercial grade maraging steel while T was specially melted for these experiments and corresponds to the composition range of a 300 grade maraging steel with the chemistry balanced so as to allow the special heat-treating process to be carried out. Specimens in which the tough constituent was 0.02, 0.04, 0.06, and 0.08-in. thick were fabricated. In all instances the volume fraction of the tough constituent was maintained constant at 25 percent. Thus regardless of the absolute dimensions of the two constituents, the well-verified "rule of mixtures" predicts that the strength parallel to the plates should be approximately constant [*10*]. The composites were then machined into compact tension fracture toughness specimens as shown in Fig. 1 and fractured according to recommendations of the ASTM [*11*] except that the fatigue cracks were propagated so that the final crack lengths were either 0.30 or 0.55 in. long. The crack lengths were determined by applying a small load, unloading, and measuring the compliance. The compliance versus crack length has been previously determined for the compact tension geometry [*12*]. Two specimens were fractured at each crack length and at each constituent dimension.

In addition to the duplex laninates, 350 grade toughness specimens were fabricated in both the bulk and laminate form to obtain some indication of the effect of delamination on fracture toughness aside from the other factors being investigated.

The bond strength of the laminates was determined by machining tension specimens as shown in Fig. 2. They were tested in two conditions: (a) as hot pressed (both constituents unaged martensite) and (b) heat treated (tough constituent unaged martensite and the brittle constituent aged martensite). In this way the effects of heat-treating on bond properties could be evaluated.

The fracture surfaces were examined by scanning electron microscopy to investigate the mechanism of crack extension.

TABLE 1–*Compositions of maraging steels used.*

Element	Steel T (wt. %)	Steel B (wt. %)
Ni	19.0	17.41
Co	8.5	12.24
Mo	5.2	4.74
Ti	0.80	1.40
Al	0.084	0.15
B	0.003	0.0018
Ca	0.05	0.0018
Zr	0.02	0.012
C	. . .	0.01
V	. . .	0.26
Mn	. . .	0.01
Si	. . .	0.01
S	. . .	0.008
P	. . .	0.005
Fe	Bal	Bal

Results and Discussion

The results of the bond strength tests showed that the intrinsic bond quality, as measured by the strength of the laminates in the as-pressed condition was excellent. The laminates in this condition had an ultimate tensile strength of 147 ksi, exhibited necking and were, without recourse to metallographic examination, indistinguishable from an unaged monolithic maraging steel test specimen. This strength level is representative of the strength of unaged maraging steel [*13*]. The heat-treating cycle used to selectively age steel B caused the bond strength to decrease to 90 ksi and tensile failure occurred by decohesion. While the reason for this decrease is beyond the scope of this paper, a plausible explanation is that the internal interfaces were preferential sites for nucleation of intermetallic compounds during aging which during tension testing acted as internal stress raisers. High magnification scanning microscopy tends to substantiate this idea. Figure 3, taken from a toughness specimen, shows what appear to be intermetallic particles in the interface between T and B and such particles were observed frequently in delaminated regions.

Three indices of fracture toughness were measured: K_{Ic}, as recommended by the ASTM [*11*], $K^{o}{}_{max}$, based on the maximum load and initial crack length, and $K^{i}{}_{max}$, based on the maximum load and instantaneous crack length. An indication of the strength of the composites was obtained by measuring the hardness of each constituent, converting the hardness to tensile strength and using the rule of mixtures to determine the strength. On the basis of the hardness measurements, the strength of the aged phase was about 250 ksi while the unaged phase had a strength of approximately 155 ksi. The composite strength determined in this manner turns out to be about 230 ksi, which appears to be reasonable.[2] The experimental data is shown in Table 2. The laminates exhibit only a small increase in K_{Ic} (including the laminate that was fabricated using only 350 grade steel and subsequently aged to 250 ksi). This is understandable since at the load corresponding to K_{Ic}, there is only a small amount of crack extension in the brittle phase and the full effects of laminating have yet to develop. While the toughness based on the maximum load does not increase for the monolithic material there is an increase for the 350 grade laminate and even larger increases for the other laminates. The increase in toughness for the 350 grade laminate can be understood in terms of partial delamination causing a reduction in constraint, a corresponding reduction in triaxiality and hence an increase in toughness. To understand the toughness characteristics of the other laminates, $K^{o}{}_{max}$ has been plotted as a function of the thickness of the tough phase in Fig. 4.[3] The toughness based on the

[2] Because of the metallurgical transformation characteristics of the two steels, the nominally 350 grade steel could not be strengthened to more than 250 ksi without excessively strengthening the tough constituent. This accounts for the somewhat high fracture toughness exhibited by the 350 grade steel as shown in Table 2. The bulk and laminate 350 grade toughness specimens D2, D4-01, and D4-02 were strengthened to the same level of the 350 grade plates that were used in the composite.

[3] The curves in Fig. 4 would exhibit the same general trend, (with somewhat more scatter in the data) if the data were plotted as a function $K^{i}{}_{max}$.

maximum load and original crack length was used since it is only at the higher loads that the full effects of lamination can be expected to develop. Regardless of the thickness of the tough phase, (the strength is constant since all laminates contain 75 percent of the brittle constituent and 25 percent of the tough constituent) those specimens containing shorter cracks are significantly tougher than those containing longer cracks. For both the 0.30 and 0.55-in. crack lengths there is a relative maximum when T is 0.04 in. thick and a relative minimum when T is 0.06 in. thick.

These results can be understood in terms of an idealized model of crack extension that is shown schematically in Fig. 5. As the stress intensity increases beyond K^{B}_{Ic} for the brittle constituent, the crack tends to extend in B. Since T is tougher than B, the crack front will be pinned at T. As the crack extends in B its radius of curvature decreases and so the load must be increased for further propagation, since as the in-plane crack front curvature increases, the stress intensity tends to drop unless the load is increased [14]. As the load increases, the stress intensity in T increases and eventually T fractures. Finally fracture occurs simultaneously in both phases with the crack front extending further in B than in T. As the crack extends in B, the constraint on T is reduced. The T phase can then develop a higher fraction of the toughness characteristic of the particular thickness being used in the composite.

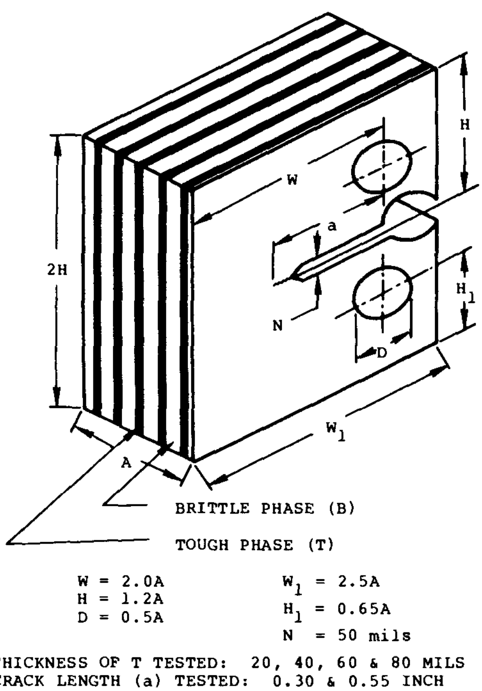

FIG. 1–*Compact tension fracture toughness specimen showing laminates in the divider orientation.*

TABLE 2–*Fracture toughness data for laminates in divider orientation.*

Specimen Number	Microstructure (All specimens except D2, D4-01 and D4-02 contain 75% brittle constituent)	Average Crack Length, in.	Plane Strain Fracture Toughness, K_{Ic}, ksi$\sqrt{\text{in.}}$	Fracture Toughness Based on Maximum Load and Original Crack Length, K^{o}_{max}, ksi$\sqrt{\text{in.}}$	Fracture Toughness Based on Maximum Load and Instantaneous Crack Length, K^{i}_{max} ksi$\sqrt{\text{in.}}$
D2	350 grade bulk specimen in aged condition.	0.507	55	55	55
D4-01	350 grade laminate with plates 0.010 in. thick.	0.497	59	72	81
D4-02	350 grade laminate with plates 0.020 in. thick	0.496	58	70	77
D5-201	Duplex laminates with tough plates 0.020 in. thick	0.298	70	84	114
D5-202	Duplex laminates with tough plates 0.020 in. thick	0.579	62	73	99
D6-201	Duplex laminates with tough plates 0.020 in. thick	0.306	69	85	98
D6-202	Duplex laminates with tough plates 0.020 in. thick	0.552	54	74	96
D7-401	Duplex laminate with tough plates 0.040 in. thick	0.312	77	93	108
D7-402	Duplex laminate with tough plates 0.040 in. thick	0.543	61	79	95

D8-401	Duplex laminate with tough plates 0.040 in. thick	0.322	59	90	112
D8-402	Duplex laminate with tough plates 0.040 in. thick	0.581	60	79	102
D11-601	Duplex laminate with tough plates 0.060 in. thick	0.292	- -	80	94
D11-602	Duplex laminate with tough plates 0.060 in. thick	0.550	57	75	90
D12-601	Duplex laminate with tough plates 0.060 in. thick	0.290	60	80	97
D12-602	Duplex laminate with tough plates 0.060 in. thick	0.549	53	69	86
D9-801	Duplex laminate with tough plates 0.080 in. thick	0.293	68	85	106
D9-802	Duplex laminate with tough plates 0.080 in. thick	0.554	57	80	98
D10-801	Duplex laminate with tough plates 0.080 in. thick	0.299	70	87	107
D10-802	Duplex laminate with tough plates 0.080 in. thick	0.548	56	71	91

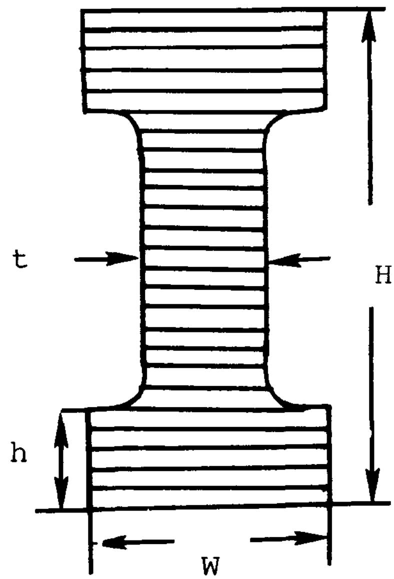

H = 1.20"
h = 0.25"
t = 0.30"
W = 0.60"
thickness = 0.125"

FIG. 2—*Tension specimen used to evaluate bond strength of the laminates.*

These ideas can be quantified. For purposes of calculation, assume that there is a central crack of length $2a$ in a wide panel fabricated from the composite in the divider orientation. Assume also that the crack tends to extend parabolically in B. Initial parabolic crack extension has been observed in both polymers [*15*] and metals [*16*] and has been used by Gerberich et al [*17*] in studies of multiple pop-in in 7075-T6 aluminum alloys. For fracture to continue in B, the following equation must be obeyed [*14*]:

$$K^{B}{}_{Ic} = 2\sigma \sqrt{\frac{\rho}{\pi}} \tag{1}$$

where

$K^{B}{}_{Ic}$ = toughness of B at the laminate thickness being used in the composite
σ = remote applied stress
ρ = in-plane radius of curvature of the crack

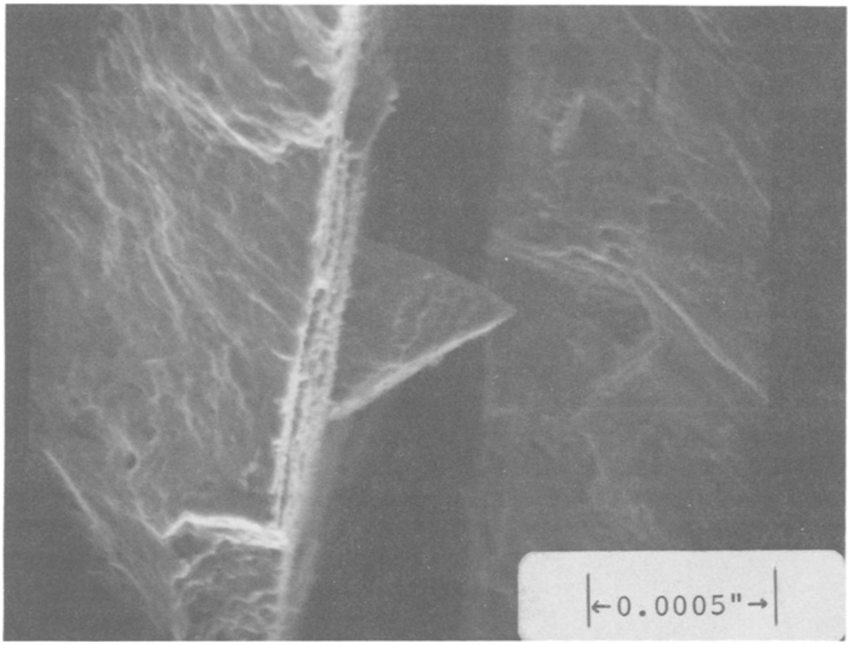

FIG. 3—*Scanning fractograph showing delamination and what appear to be intermetallic precipitates in the interface region.*

The equation of a parabolic crack having the geometry shown in Fig. 5 is:

$$y = h\left[1-4\left(\frac{X}{t_B}\right)^2\right] \quad (2)$$

where

y = variable parallel to crack propagation direction
x = variable perpendicular to crack propagation direction
t_B = thickness of the brittle phase
h = distance the crack extends in B past the fatigue crack

At the mid-thickness of B, the in-plane radius of curvature is given by:

$$\rho = \frac{1}{|y''|_o} = \frac{t_B^2}{8h} \quad (3)$$

where

$|y''|_o$ = positive value of the second derivative of Eq 2 evaluated at the mid-thickness of the brittle phase.

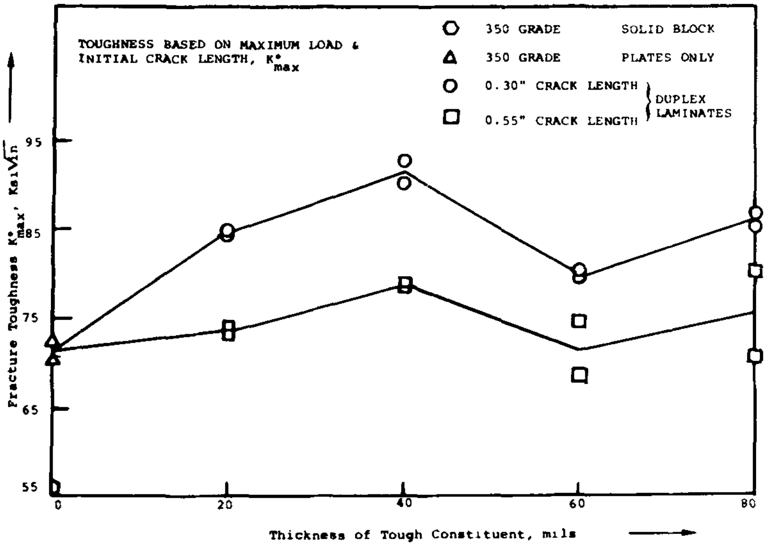

FIG. 4–*Fracture toughness* $K^o{}_{max}$ *as a function of the laminate thickness of the tough constituent for cracks 0.30 and 0.55 in. long. All specimens contain 75 percent of the brittle constituent.*

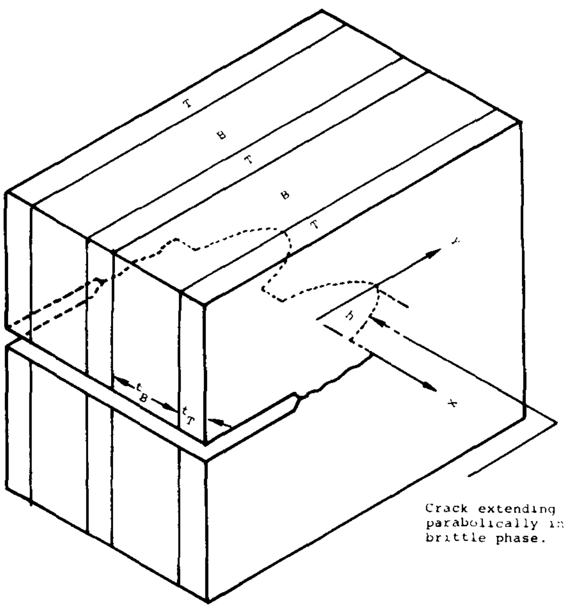

FIG. 5–*Crack extension in the divider orientation. The crack extends first in the brittle constituent reducing the constraint on the tough constituent.*

As the stress is increased, eventually T begins to fracture. At this point, since the crack front at T is assumed to be straight, the following equation applies [14]:

$$K^{T}{}_{c} = \sigma\sqrt{\pi a} \tag{4}$$

where

$K^{T}{}_{c}$ = toughness of T at the laminate thickness being used in the composite.

Substitution of Eq 3 into Eq 1 and elimination of σ between Eqs 1 and 4 yields the result:

$$h = \left(\frac{K^{T}{}_{c}t_{B}}{K^{B}{}_{Ic}\pi}\right)^{2}\frac{1}{2a} \simeq \left(\frac{K^{T}{}_{c}t_{T}}{K^{B}{}_{Ic}}\right)^{2}\frac{1}{2a} \tag{5}$$

where t_T = thickness of the tough phase and

$$t_B = 3t_T \tag{6}$$

since the composite is 75 percent B.

For a given composite t_T, t_B, $K^{T}{}_{c}$, $K^{B}{}_{c}$ are fixed. Thus, Eq 5 indicates that as the crack length decreases, h increases. Since increasing h is associated with decreasing constraint on T, T is then free to exhibit a higher fraction of its potential toughness and the overall composite toughness should increase. This is exactly what was observed for all composites tested, as can be seen from Fig. 4.

The effect of increasing the lamellae thickness is more difficult to evaluate than a cursory examination of Eq 5 would suggest. The reason for this is that $K^{T}{}_{c}$ and to a lesser degree, $K^{B}{}_{c}$ can vary with thickness. If the tough phase was not constrained by the brittle phase, some estimates made by Hahn and Rosenfield [18] could be used to inform that the maximum plane stress toughness would occur at a thickness t_o defined by the approximate equation

$$t_o \simeq \frac{1}{4\pi}\left(\frac{K_{Ic}}{\sigma_{ys}}\right)^{2} \tag{7}$$

The plane strain fracture toughness of the tough phase is not known and is difficult to determine since an excessively large specimen would be required to produce full plastic constraint at the crack tip. It can, however, be estimated to be about 270 ksi $\sqrt{\text{in.}}$ by extrapolating some data presented by Kies [19] for maraging steels at various strength levels. Using this value and noting that the strength was about 150 ksi, Eq 7 predicts that plane stress is fully developed when the thickness approaches 0.25 in. Thus, the toughness of the monolithic unaged maraging steel used in this investigation would be expected to increase up to 0.25 in. and decrease thereafter. The effect of laminating would be to greatly reduce the thickness at which this transition takes place by increasing the plastic constraint. On the other hand, the toughness of the brittle phase is essentially constant at K^{B}_{Ic}. This conclusion follows from the empirical observation that plane strain develops when the following equation is obeyed [*20*]:

$$t_1 \simeq 2.5 \left(\frac{K_{Ic}}{\sigma_{ys}}\right)^2 \tag{8}$$

Equation 8 predicts a plane strain thickness of about 0.12 in. The thickness of the aged lamellae were 0.06, 0.12, 0.18, and 0.24 in. Thus, the aged phase was essentially in plane strain except when the composite was comprised of unaged laminates 0.02 in. thick and aged laminates 0.06 in. thick. This conclusion is further supported by the observation that the fracture surfaces in the aged phase were flat while those in the unaged phase were slanted, which can be inferred from Fig. 6.

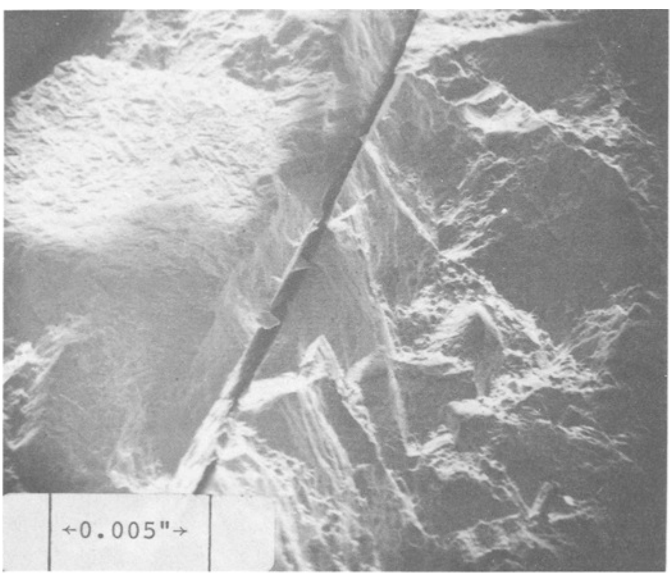

FIG. 6–*Region showing relatively brittle fracture on left side and relatively ductile fracture on the right side. Note what appear to be intermetallic particles in the delaminated interface between the tough and brittle phases.*

The variation in toughness as a function of thickness for both phases is shown schematically in Fig. 7. Substitution of values taken from the curves of Fig. 7 into Eq 5 predicts a variation in h similar to the variation in toughness that was observed experimentally in Fig. 4. Since, in light of the preceding discussion the curves shown in Fig. 7 are qualitatively reasonable, it appears that the model is also able to account for the effect of laminate thickness on the fracture toughness of the composite.

Both the experimental results as well as the preceding calculation imply that in the divider orientation, fracture toughness is not solely a materials parameter but depends strongly upon crack length, and to a lesser extent on the dimensions of the constituent phases. It thus appears that a single fracture mechanics parameter does not fully describe fracture of laminate composites in the divider orientation. In an attempt to more fully characterize the fracture process, all of the load displacement records were converted into R curves, using a technique described elsewhere [*12*]. Some typical R curves, shown in Fig. 8, were taken from specimens containing toughness laminates 0.06 and 0.08 in. thick.

The fracture surfaces were examined by scanning electron fractography. Figure 9 shows an area in which there is a transition from fatigue to fracture

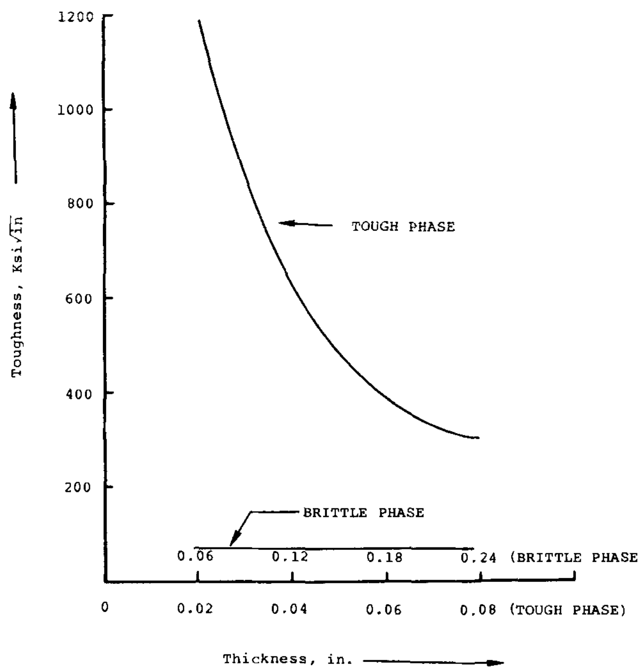

FIG. 7—*Toughness versus thickness dependence of the constituent phases that would cause a variation in composite toughness similar to that shown in Fig. 4.*

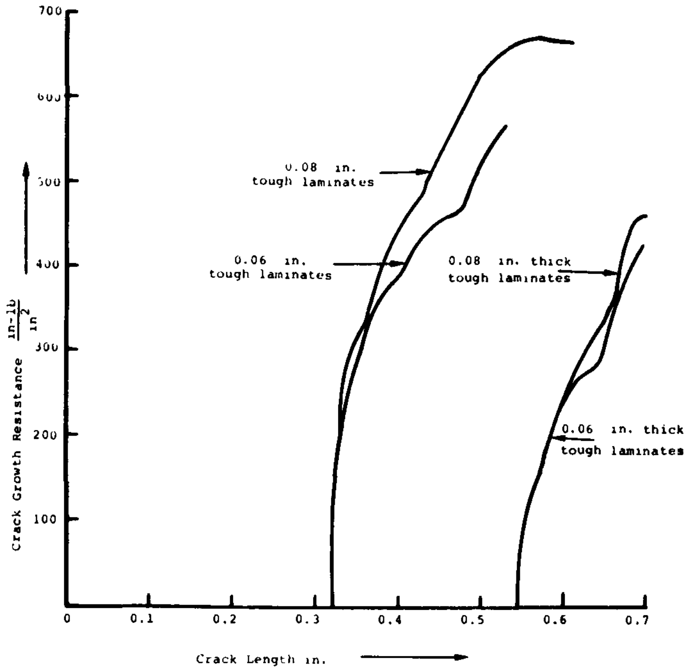

FIG. 8—*Crack growth resistance as a function of crack length for specimens containing tough laminates 0.06 and 0.08 in. thick.*

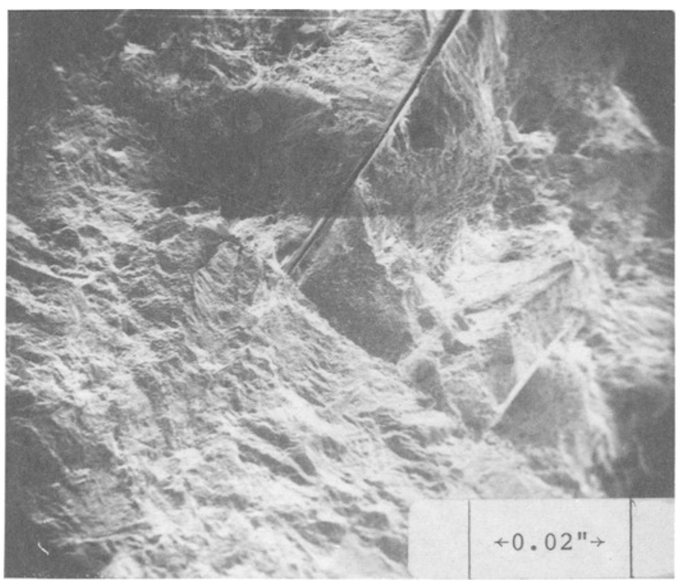

FIG. 9—*Transition region showing fatigue in lower left and fracture with delamination under monotonic loading in the upper right.*

under monotonic loading. It can be seen that there was no delamination in the fatigue region, in agreement with previous studies on metal laminates [3] while there is partial delamination in the normal fracture area. The area shown in Fig. 9 is representative of other areas scanned in the transition region. Figure 6 shows a region in which there is relatively brittle fracture in the plate on the left hand side, delamination and what appear to be intermetallic particles in the delaminated region. Relatively ductile fracture is observed in the plate on the right hand side as evidenced by the coarser features and more slanted appearance.

Conclusions

(1) The fracture toughness of laminate composites fabricated from tough and brittle maraging steels exhibits significant improvements over the brittle constituent in the bulk form and some improvement over the brittle material in the laminated form when toughness is measured in terms of $K^{o}{}_{max}$ or $K^{i}{}_{max}$. The plane strain fracture toughness is not an appropriate characterization of composite toughness since significant toughness beyond K_{Ic} can be developed.

(2) When tested at a constant volume fraction of the brittle constituent (and hence constant strength level) the toughness $K^{o}{}_{max}$ was significantly higher for cracks approximately 0.3 in. long than for cracks 0.5 in. long.

(3) The fracture process in the composite was modeled and analyzed using a fracture mechanics approach. The results indicated that the constraint on the tough constituent is reduced with decreasing crack length and also depends on laminate thickness. Since reduced constraint is associated with increasing toughness the results of the calculation are in general agreement with the experimental observations.

Acknowledgements

We are deeply grateful to the American Iron and Steel Institute (Grant 61-247) and to NASA (Grant NGR 36-004-014) for research grants supporting this work. We would also like to thank the Paul D. Merica Research Laboratory of the International Nickel Company for supplying the maraging steel wires, and the Armco Research and Technology Center for use of their metal working facilities.

References

[1] Leichter, H.L., *Journal of Spacecraft and Rockets*, Vol. 3, 1966, pp. 1113-1120.
[2] Almond, E.A., Petch, N.J., Wraith, A.E., and Wright, E.S., *Journal of the Iron and Steel Institute*, Vol. 207, 1969, pp. 1319-1323.
[3] McCartney, R.F., Richard, R.C., and Trozzo, P.S., *Transactions of the American Society for Metals*, Vol. 60, 1967, pp. 384-394.
[4] Embury, J.D., Petch, N.J., Wraith, A.E., and Wright, E.S., *Transactions of TMS-AIME*, Vol. 239, 1967, pp. 114-118.

[5] Floreen, S., Hayden, H.W., and Steigelman, J.Q., *Transactions of the American Society for Metals*, Vol. 62, 1969, pp. 812-815.
[6] Floreen, S., Hayden, H.W., and Pilliar, R.M., *Transactions of TMS-AIME*, Vol. 245, 1969, pp. 2529-2536.
[7] Hayden, H.W. and Floreen, S., *Transactions of the American Society for Metals*, Vol. 61, 1968, pp. 474-488.
[8] Pellissier, G.E., *Engineering Fracture Mechanics*, Vol. 1, 1968, pp. 55-75.
[9] Shete, P.M., M.S. thesis, University of Cincinnati, June 1970.
[10] Kelley, A. and Tyson, W.R. in *High Strength Materials*, V.F. Zackay, Ed., Wiley, New York, 1965, pp. 578-602.
[11] *Annual Book of ASTM Standards*, Part 31, 1970, pp. 911-927.
[12] Antolovich, S.D., Shete, P.M., and Chanani, G.R. in *Fracture Toughness, Proceedings of the 1971 National Symposium on Fracture Mechanics, ASTM STP 514*, American Society for Testing and Materials, 1972, pp. 114-134.
[13] Hall, A.M. and Slunder, C.J., "The Metallurgy, Behavior and Application of the 18 Percent Nickel Maraging Steels," NASA SP 5051, 1968.
[14] Paris, P.C. and Sih, G.C., *Fracture Toughness Testing and its Applications, ASTM STP 381*, American Society for Testing and Materials, 1965, pp. 30-83.
[15] Key, P.L. and Katz, Y., *International Journal of Fracture Mechanics*, Vol. 5, 1969, pp. 63-68.
[16] Hartbower, C.E., Gerberich, W.W., Reuter, W.G., and Crimmins, P.P., "Stress-Wave Characteristics of Fracture Instability in Constructional Alloys," Contract N00014-66-C0340, Office of Naval Research, 1967.
[17] Gerberich, W.W., Key, P.L., and Parker, E.R., *Engineering Fracture Mechanics*, Vol. 2, 1970, pp. 47-60.
[18] Hahn, G.T., Rosenfield, A.R. in *Applications Related Phenomena in Titanium Alloys, ASTM STP 432*, American Society for Testing and Materials, 1967, pp. 5-32.
[19] Kies, J. A., *Weld Imperfections*, Pfluger A.R. and Lewis R.E., Eds. Addison-Wesley, 1968, p. 333.
[20] Brown, W. F., Jr., and Srawley, J.E., *Plane Strain Crack Toughness Testing of High Strength Metallic Materials, ASTM STP 410*, American Society for Testing and Materials, 1966, p. 23.

J. R. Hawthorne[1] *and T. R. Mager*[2]

Relationship Between Charpy V and Fracture Mechanics K_{Ic} Assessments of A533-B Class 2 Pressure Vessel Steel

REFERENCE: Hawthorne, J.R. and Mager, T.R., "**Relationship Between Charpy V and Fracture Mechanics K_{Ic} Assessments of A533-B Class 2 Pressure Vessel Steel,**" *Fracture Toughness, Proceedings of the 1971 National Symposium on Fracture Mechanics, Part II, ASTM STP 514,* American Society for Testing and Materials, 1972, pp. 151-263.

ABSTRACT: A cooperative program between the Naval Research Laboratory and the Westinghouse Nuclear Energy Systems Division was established to explore possible relationships between postirradiation Charpy-V and fracture mechanics (K_{Ic}) data. Initial efforts centered on a 6 3/8-in. A533 grade B Class 2 steel plate for which the preirradiation condition had been well characterized by Charpy-V (C_v), tension, dynamic tear, and fracture mechanics tests. Low (<250 F, 121 C) temperature-high fluence exposure conditions were utilized to obtain large C_v, tensile and plane strain fracture toughness (K_{Ic}) property changes over the preirradiation condition.

The simultaneous exposure of C_v and 1-in.-thick compact tension (CT) specimens produced comparable increases in C_v 30 ft · lb transition temperature and K_{Ic} 65,000 psi $\sqrt{\text{in.}}$ temperature. The C_v shelf energy was reduced from 74 to 46 ft · lb. The postirradiation 75 F (24 C) yield strength was 127.3 ksi compared to a preirradiation value of 74.2 ksi; however, postirradiation yield strength decreased markedly with increasing temperature.

The test capacity of the 1-in. CT specimen was found insufficient for ASTM valid K_{Ic} determinations at the C_v shelf level temperature for pre- or postirradiation conditions. The estimate of postirradiation K_{Ic} at C_v shelf temperatures would require a CT specimen thickness of at least 5 in. The data suggest that, if power reactor surveillance programs restrict test specimen size to a maximum of 1-in. thickness, and if the measuring capacity of CT specimens is the function of thickness described by ASTM, an empirical or correlation-projection approach would be required to utilize fracture mechanics specimens in such programs.

KEY WORDS: fracture (materials), fatigue (materials), fracture strength, impact tests, tension tests, fracture tests, irradiation, yield strength, stresses, cracks, pressure vessel steels

The postirradiation notch ductility of pressure vessel steels has been assessed largely by means of the Charpy-V (C_v) test method. The method and its

[1] Reactor Materials Branch, Naval Research Laboratory, Washington, D.C.

[2] Nuclear Energy Systems, Westinghouse Electric Corp., Pittsburgh, Pa.

relatively small specimen size (2.165 by 0.394-in. square) have proven both convenient for the qualification and comparison of plate and weld metals with neutron exposure and sufficiently sensitive for comparisons of the effects of different neutron exposure environments and fluences. However, the C_v method has an inherent limitation in that critical flaw size-applied stress relationships cannot be determined directly from the data. Hence, designers must resort to other test methods to obtain the requisite information. One method, based on fracture mechanics, determines the plane strain fracture toughness, K_{Ic} (psi $\sqrt{\text{in.}}$), of the material. Critical flaw size-applied stress conditions can be calculated from K_{Ic} using established formulae. To explore possible relationships between postirradiation C_v and K_{Ic} performance, a cooperative program between the Naval Research Laboratory (NRL) and the Westinghouse Nuclear Energy Systems (WNES) was established. It was considered that the identification of such relationships would be of value to reactor component design and operation. Specifically, the large bank of C_v irradiation data generated by past research on steel alloys through correlation would become useful to flaw size-stress analyses. The present bank of K_{Ic} data is extremely limited by comparison.

For unirradiated steels of moderate to low yield strength, K_{Ic} is most readily measured in the range of frangibility at temperatures below the drop weight nil-ductility transition (NDT) temperature. This property is temperature dependent and, for A533-B steel, characteristically exhibits a transition from low to high values within a relatively narrow temperature interval.

Specimen size limitations and material yield strength, however, determine whether or not sufficient plane strain constraint can be provided for valid K_{Ic} determinations at temperatures approaching the C_v shelf temperature. Specimen size requirements have been described in detail [1] by ASTM Committee E-24 on Fracture Testing of Metals; requirements increase rapidly with increasing shelf level toughness. It is noted that graphic and formula relationships between K_{Ic} and C_v shelf energy have been established [2, 3] for unirradiated steels with higher yield strengths.

Irradiation has the propensity for both lowering the C_v shelf energy and raising the yield strength of a steel [4] thereby making the material much more amenable to fracture mechanics analysis. In this study, low temperature-high fluence exposure conditions were utilized to obtain large C_v and tensile property changes over the preirradiation condition. Initial program efforts centered on a thick A533-B Class 2 steel plate for which the preirradiation condition has been well characterized by C_v, tension, dynamic tear, and fracture mechanics tests. The Westinghouse-developed compact tension (CT) specimen, type 1T, was selected for K_{Ic} determinations; the geometry and dimensions of this specimen design are particularly well suited for reactor in-core irradiation experiments.

This report presents initial program findings of C_v versus K_{Ic} postirradiation performance, including observations on the relative effect of radiation on C_v and K_{Ic} transition behavior.

Experimental Program

Material and Specimens

The chemical composition and heat treatment history of the 6 3/8-in.-thick A533-B Class 2 test plate are given in Table 1. Specimens were taken from the plate mid-thickness region (1/2T) and represented the transverse (WR) test orientation. Preirradiation yield and tensile strengths (WR orientation) at plate mid-thickness were 74,200 psi and 94,200 psi, respectively. The nil-ductility transition (NDT) temperature was 0 F (-18 C). The Charpy-V (C_V) 30 ft · lb transition temperature was -30 F (-34 C). Through-thickness preirradiation dynamic tear test data are documented elsewhere [5].

TABLE 1 –*Chemical composition and heat treatment of 6 3/8 in. A533-B Class 2 test plate.*

Composition, wt %										
C	Mn	P	S	Si	Ni	Cr	Mo	Cu	V	Al
0.24	1.27	0.008	0.015	0.19	0.53	0.14	0.48	0.09	0.02	0.031

Heat Treatment

Austenitized at 1670-1685 F (910-918 C) for 6 1/2 h, water dip quenched

Reaustenitized at 1650-1660 F (899-904 C) for 6 1/2 h, water dip quenched

Tempered at 1115-1125 F (602-607 C) for 6 1/2 h, air cooled

Specimen types included the standard Charpy-V (C_V) specimen, 0.252-in. diameter by 1.750-in. gage length tension test specimens, and 1.0-in.-thick compact tension (IT-CT) specimens. The configuration and dimensions of the IT-CT specimen are shown in Fig. 1.

Preparation and Testing of Compact Tension Specimens

Experimental procedures for fracture mechanics K_{Ic} determinations, as recommended by ASTM Committee E-24 [1] and Wessel [6] were followed closely for all CT specimen operations. Prior to irradiation, the specimens were fatigue precracked at room temperature (75 F, 24 C). The fact that neutron irradiation increases the yield strength of a steel complicates the advance prediction of the maximum allowable K_f level for fatigue precracking. In the present study, the maximum K_f level for the tension-zero-tension fatigue cycle was 15,000 psi $\sqrt{\text{in.}}$

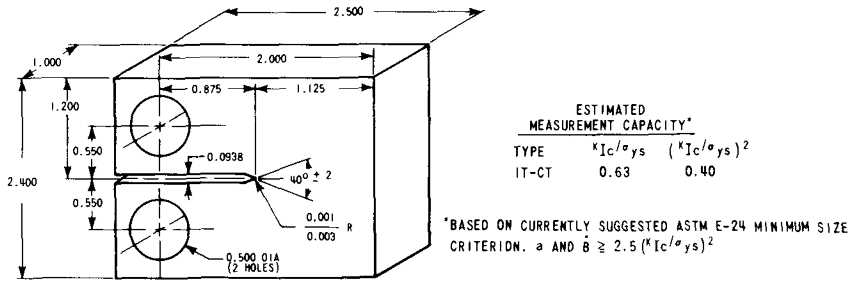

FIG. 1—*Compact tension specimen.*

The requirements of fracture toughness testing in the fracture mechanics approach are unusual in that it is necessary to compare post-test data with specimen pretest dimensions to determine if the value of fracture toughness measured (K_Q) is indeed the critical value (K_{Ic}) for the material. In other words, the validity of the test can only be determined after testing. Two criteria for validity have been proposed: (1) the ASTM criteria [*1*] proposes that

$$a \text{ and } B \geqq 2.5 \left[\frac{K_Q}{\sigma_{ys}}\right]^2$$

where σ_{ys} is the 0.2 percent offset yield strength of the material at the same temperature and loading rate as the temperature and loading rate of the fracture test; and (2) Reference *7* proposes use of the secant offset method to determine that the majority of displacement is due to crack elongation.

Fracture toughness K_Q measured for specimens meeting both these criteria is considered to be the critical value K_{Ic} for the material. If the criteria are not met, the measured fracture toughness K_Q is considered to have been biased by specimen size.

Fracture toughness K_Q was determined from the expression:

$$K_I = \frac{YP\sqrt{a}}{BW}$$

where P is the maximum load (lb) occurring before 4 percent secant offset, a is the crack length (in.) measured at the centerline of loading, B and W are respectively the specimen thickness and width (in.) and Y is a numerical correction factor dependent on the crack length and specimen geometry. Y was determined by compliance and analytical procedures.

Irradiation Experiment

Specimen irradiations were performed in the Union Carbide Research reactor (UCRR) A-4 fuel core position. Neutron spectrum calculations for this exposure facility suggest the following relationship:

$$\text{fluence, } \phi^{cs} > 1 \text{ MeV} = \text{fluence } \phi^{fs} > 1 \text{ MeV} \times \frac{98.26}{111}$$

The fission spectrum fluence ϕ^{fs}, assumes a fission spectrum average cross section, σ, of 68 mb for the ^{54}Fe (n,p) ^{54}Mn reaction and a fission averaged cross section for neutrons/cm^2 >1 MeV of 68/0.693 or 98.26 mb.

The irradiation assembly developed for this investigation is shown schematically in Fig. 2. The unit contained 16 C_v specimens, 8 IT-CT specimens, and 8 tension specimens. Low melting point alloys were placed within the specimen array to determine peak exposure temperatures. Iron and cobalt (aluminum wire 0.15 percent cobalt) neutron monitor wires were employed to aid the determination of the total exposure (fluence).

This report contains test results from two separate reactor experiments. Radiation exposures of each experiment encompassed thirteen 100-h reactor cycles. Experiments were rotated 180 deg relative to the reactor core midway through the exposure period to reduce cross section fluence gradients to a minimum. Fluence variations over the entire specimen array were less than 5 percent for unit one and less than 8 percent for unit two. Average fluence exposures, ϕ^{fs}, were, respectively, 3.3×10^{19} neutrons/cm^2 >1 MeV and 3.9×10^{19} neutrons/cm^2 >1 MeV.

Experimental Results

Postirradiation Charpy-V (C_v) and tensile properties were determined at the Naval Research Laboratory (NRL); postirradiation fracture toughness (K_{Ic}) assessments were conducted by Westinghouse NES at the Advanced Reactor Division Postirradiation Test Facility.

Charpy-V Properties

The postirradiation Charpy-V properties of the A533-B Class 2 steel are shown in Fig. 3. Also shown in Fig. 3 are the preirradiation Charpy-V properties and thus the extent of radiation-induced changes observed with experiments 1 and 2. The Charpy-V 30 ft · lb transition temperature was elevated by 330 F (167 C), and the shelf level was lowered by 28 ft · lb.

Note that the fluence difference between experiments is not discernable in the Charpy-V data either in terms of transition temperature behavior or shelf

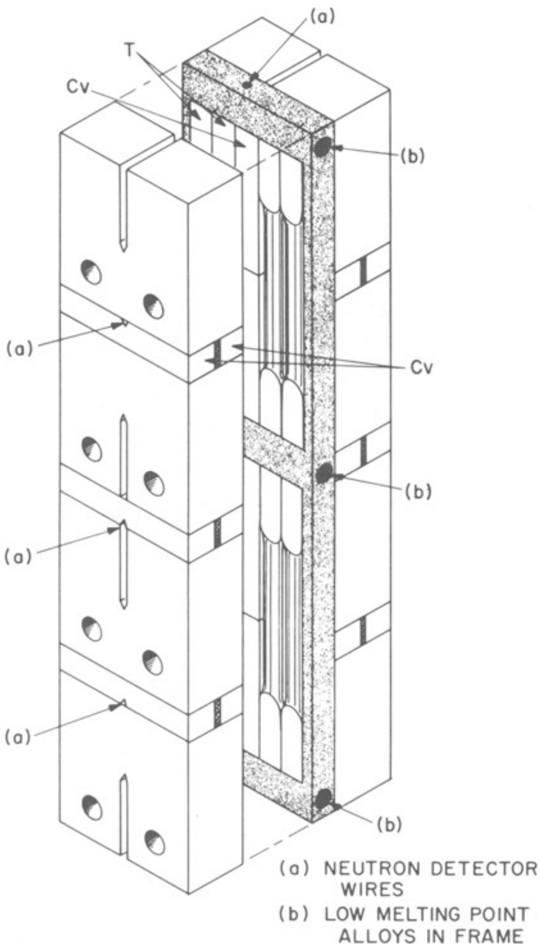

FIG. 2–*Irradiation assembly for the simultaneous exposure of Charpy V, compact tension, and tension specimens at <250 F (121 C).*

level (half filled versus filled points). The extent of data scatter indicated in Fig. 3 is not considered unusual for the steel type, plate thickness, and sampling location.

Tensile Properties

Postirradiation tensile properties are summarized in Table 2. Unlike the Charpy-V properties, the small fluence difference between experiments can be distinguished in the data. Yield strength determinations over the range, 75 to

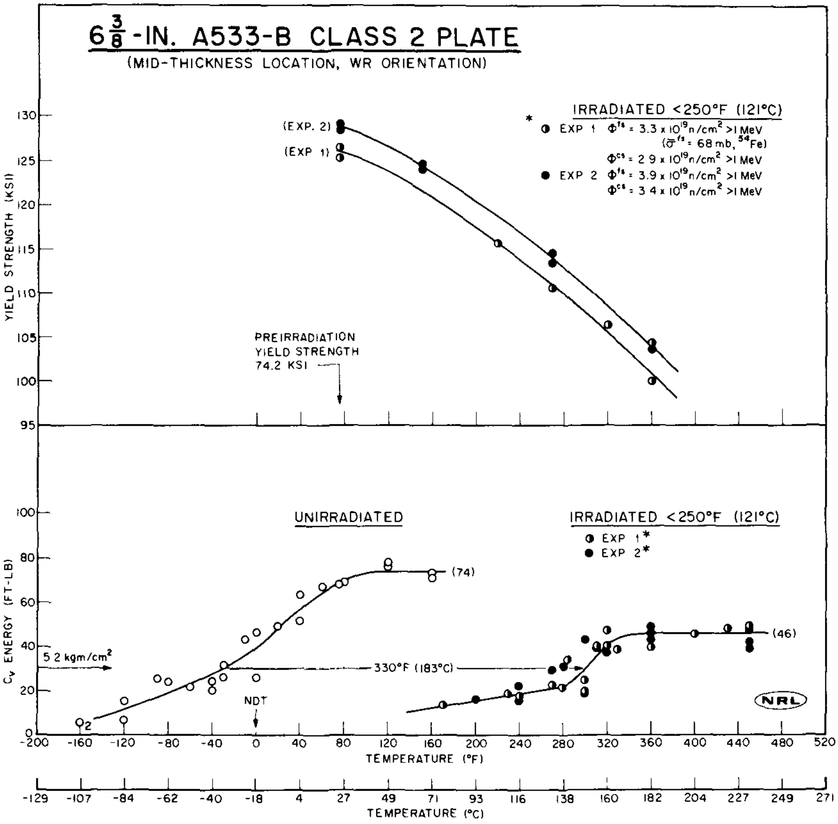

FIG. 3–*Charpy V and yield strength properties of the 6 3/8-in. A533-B Class 2 test plate before and after irradiation.*

360 F (24 to 182 C), are plotted for both experiments in Fig. 3 (upper graph). A rapid fall in yield strength with increasing test temperature is indicated for the irradiated condition. Yield strength determinations for the unirradiated state, on the other hand, do not indicate a comparable strength decrease with increasing temperature. Yield values at 75 F (24 C) and 360 F (182 C) were, respectively, 74,200 psi and 66,200 psi for the material in the unirradiated condition.

Plane Strain Fracture Toughness

Postirradiation determinations of plane strain fracture toughness (K_{Ic}) are summarized in Table 3 and Fig. 4. The two validity criteria cited earlier were applied to all the data. Preirradiation data [*8*] are also given in Fig. 4 as reference for the irradiation effect. In Fig. 5 the fracture surface of a valid postirradiation test (150 F, 66 C) is compared to the fracture surface of an

TABLE 2–*Postirradiation tensile properties of A533-B Class 2 test plate.*[a]

Material Condition	Test Temperature deg F	deg C	Yield Strength,[b] ksi	Tensile Strength,[c] ksi	Percent Reduction of Area	Percent Elongation, 1-in. gage
Preirradiation	75	24	74.2	94.2	61.7	23.4
	360	182	66.2	88.4	58.7	21.8
	75	24	75.6[a]	94.5	67.9	27.1
	360	180	66.2[a]	88.8	65.0	22.3
Postirradiation:	75	24	125.5	126.3	43.8	11.7
Experiment 1	75	24	126.3	127.5	49.0	14.3
3.3×10^{19} neutrons/cm^2	220	104	115.6	116.5	49.5	11.4
	270	132	110.5	111.7	50.1	12.8
	320	160	106.5	108.3	50.7	12.9
	360	182	100.0	105.8	. . .	. . .
	360	182	104.3	105.5	37.0	12.5
	420	216	96.8	101.1	41.3	13.3
Postirradiation:	75	24	128.3	128.7	41.3	12.7
Experiment 2	75	24	129.1	129.1	46.1	12.7
3.9×10^{19} neutrons/cm^2	150	66	123.9	124.1	49.0	11.9
	150	66	124.5	124.9	50.7	13.2
	270	132	113.5	114.1	47.8	13.1
	270	132	114.5	115.3	40.1	11.0
	360	182	103.9	105.7	49.5	14.3

[a] Mid-thickness location; WR orientation

[b] 0.2% offset

[c] Specimen gage section: 0.252-in. diameter by 1.750 in. long.

[a] RW (longitudinal) orientation.

invalid postirradiation test (250 F, 121 C). Valid tests typically produced fracture surfaces which were predominately flat with no evidence of shear lips. Invalid tests produced similar fracture surfaces but with evidence of very small shear lip formation.

Discussion

One stated objective of the experimental program was to explore possible relationships between postirradiation C_v properties and K_{Ic} fracture toughness. The material selected should have been ideal for investigating such relationships since its C_v shelf energy before irradiation was relatively low (74 ft · lb).

According to ASTM validity criteria [1], the K_{Ic} measuring capacity of a CT specimen of a given thickness is governed by the K_{Ic}/σ_{ys} ratio. The maximum allowable K_{Ic}/σ_{ys} ratio suggested by ASTM for a 1-in.-thick specimen is 0.63.

TABLE 3—*Postirradiation plane strain fracture toughness determinations for A533-B Class 2 test plate.*[a]

Specimen Number	Size, in.	Test Temperature, deg F	Yield Strength, ksi	a, in.	a/W	Plastic Zone Size, in. Precracking	Plastic Zone Size, in. Test	Stress Intensity Factor K_Q ksi $\sqrt{\text{in.}}$	Validity[b]
Y7-20	1TCT	RT	128.3	1.045	0.522	0.0025	0.0118	60.4	1
Y7-16	1TCT	RT	128.1	1.025	0.512	0.0023	0.0118	60.4	1
Y7-15	1TCT	150	123.9	1.025	0.512	0.0023	0.0157	68.1	1
Y7-11	1TCT	150	124.5	1.015	0.507	0.0022	0.0141	64.6	1
Y7-17	1TCT	200	121.0	1.015	0.507	0.0022	0.0255	84.0	2
Y7-18	1TCT	250	117.0	1.035	0.517	0.0024	0.0279	85.0	4

[a] Mid-thickness location; WR orientation.

[b] 1—Meets both criteria; a and B greater than 2.5 $(K_{Ic}/ys)^2$ and secant offset.
2—Fails; a and B greater than 2.5 $(K_{Ic}/ys)^2$, meets secant offset.
3—Meets; a and B greater than 2.5 $(K_{Ic}/ys)^2$, fails secant offset.
4—Fails both criteria.

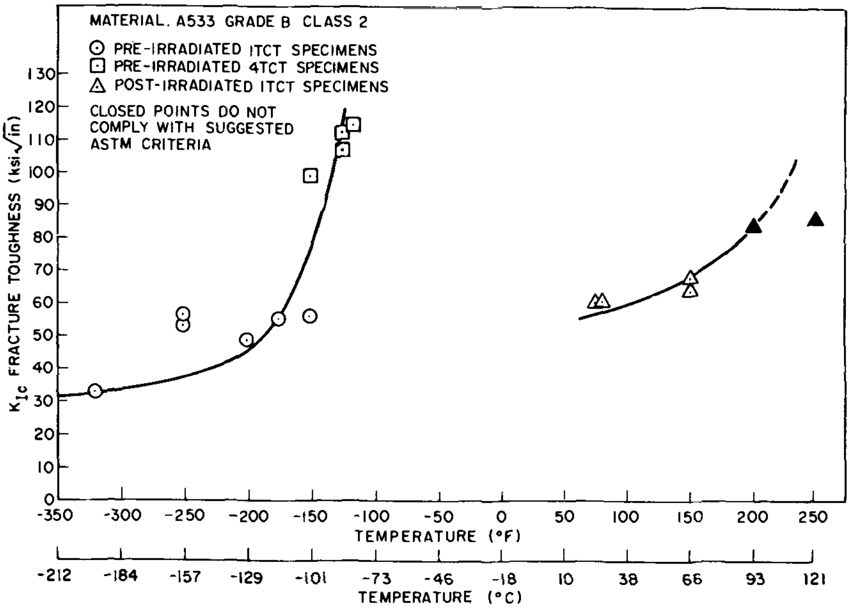

FIG. 4–*Plane strain fracture toughness properties of the 6 3/8-in. A533-B Class 2 test plate before and after irradiation to 3.3 x 10^{19} neutrons/cm^2 >1 Mev.*

By virtue of the ratio limitation, postirradiation K_{Ic} measurement capabilities increase in direct proportion to the radiation-induced increase in yield strength. Accordingly, the study employed a low (<250 F, 121 C) irradiation temperature in the interest of producing a large increase in yield strength and, at the same time, a sharp reduction in C_v shelf energy level. It was envisioned that, with sufficient yield and shelf energy change, K_{Ic} determinations might be carried up to C_v shelf level temperatures.

Consistent with the low temperature and high fluence exposure conditions, the yield strength (75 F, 24 C) was increased by 71.5 percent to 127.3 ksi and the C_v shelf energy level was reduced by 35 percent to 46 ft · lb. Outwardly, such changes would suggest that objectives of the irradiation plan were largely achieved. However, tension specimen tests at elevated temperatures revealed that postirradiation yield strength decreased rapidly with increasing temperature. As a result, the anticipated yield strength advantage for the most part was lost at C_v shelf level temperatures. Moreover, the fracture toughness corresponding to the postirradiation C_v shelf condition appeared to be about the same as that for the unirradiated C_v shelf condition. Specifically, the Rolfe and Novak empirical relationship [*3*] of K_{Ic} to C_v shelf level:

$$\left[\frac{K_{Ic}}{\sigma_{ys}}\right]^2 = \frac{5}{\sigma_{ys}}\left[\mathrm{CVN} - \frac{\sigma_{ys}}{20}\right]$$

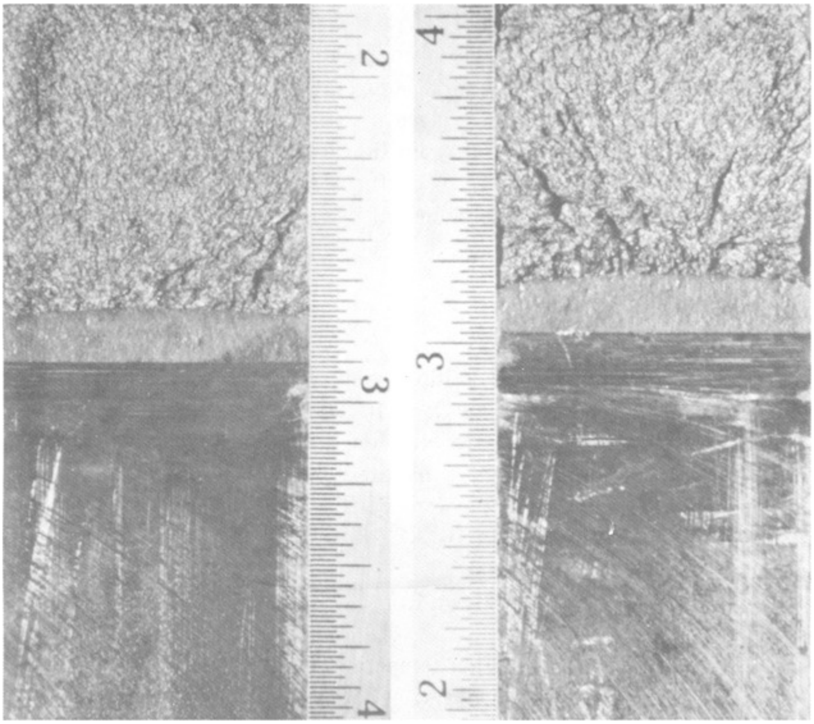

FIG. 5—*Fracture surfaces of 1-in.-thick compact tension specimens irradiated at <250 F and tested at 150 and 250 F. Respective tests resulted in valid and invalid* K_{Ic} *determination for the A533-B Class 2 test plate.*

would suggest a K_{Ic} shelf value for the irradiated material of 155,000 psi $\sqrt{\text{in.}}$ as opposed to 163,000 psi $\sqrt{\text{in.}}$ for the unirradiated condition. According to these calculated values, compact tension specimens at least 5 and 13-in. in thickness, respectively, would be required to measure a valid K_{Ic} on the C_v upper shelf for the irradiated and the unirradiated conditions.

It is interesting to note that Sailors and Corten [9] propose a relationship between K_{Ic} and C_v in the temperature range of the C_v transition. This relationship is given by $K_{Ic} = 15{,}500\,(C_v)\ 1/2$, where K_{Ic} is psi $\sqrt{\text{in.}}$ and C_v is ft · lb. Substituting the limited amount of data from this investigation into the above expression, K_{Ic} values ranging from 49,000 to 73,000 psi $\sqrt{\text{in.}}$ result for C_v values of 10 to 20 ft · lb. These calculated values are noted to compare favorably with the experimental postirradiation determinations (Fig. 4) at temperatures corresponding to C_v 10 to 20 ft · lb (60,000 to 68,000 psi $\sqrt{\text{in.}}$). However, as Corten [9] points out, existing data for irradiated materials are insufficient to establish a relationship between C_v data (transition region) and the fracture toughness parameter, K_{Ic}. As an interim measure, Mager and

Yanichko [10] suggest that for irradiated material, the K_{Ic} curve for unirradiated material should be shifted along the temperature axis by an increment, ΔT, equal to the radiation induced shift in the C_v transition curve. Some support for this suggestion is given by the present study. From Figs. 3 and 4, it is noted that the C_v 30 ft · lb transition temperature was increased 300 F (183 C) by irradiation and the K_{Ic} 65,000 psi $\sqrt{\text{in.}}$ transition temperature was increased by 295 F (164 C). The choice of both index transition temperatures, however, is quite arbitrary.

Conclusions

Charpy-V (C_v), tension, and 1-in.-thick compact tension (CT) specimens from a 6-in.-thick A533 B Class 2 plate were irradiated simultaneously to compare changes in C_v and plane strain fracture toughness (K_{Ic}) behavior by neutron exposure and to explore K_{Ic} to C_v relationships for the irradiated condition. Two separate reactor experiments were performed. Fluences were 3.3 x 10^{19} neutrons/cm^2 >1 MeV and 3.9 x 10^{19} neutrons/cm^2 >1 MeV, respectively, at <250 F (121 C).

Observations and conclusion drawn from the data were as follows:

(1) The C_v 30 ft · lb transition temperature was increased by irradiation to 300 F (149 C) from -30 F (-34 C) [ΔT = 330 F (183 C)]; the C_v shelf energy was decreased from 74 ft · lb to 46 ft · lb. Experimental fluence differences could not be discerned among the data.

(2) The yield strength (0.2 percent offset) at 75 F (24 C) was increased to 127.3 ksi (avg) from 74.2 ksi [Δys = 53.1 ksi]. Experiment fluence differences were apparent from the data.

(3) The postirradiation yield strength decreased markedly with increasing temperature. At 360 F (182 C) corresponding to the postirradiation C_v shelf temperature, the yield strength was 102.7 ksi (avg). By comparison, the preirradiation yield strength at 360 F (182 C) was 66.2 ksi.

(4) The plane strain fracture toughness (K_{Ic}) 65,000 psi $\sqrt{\text{in.}}$ temperature was increased from -160 F (-107 C) to 135 F (57 C) [ΔT = 295 F (164 C)]. One CT test at 150 F (66 C) was valid while a CT test at 250 F(121 C) was invalid. A CT test at 200 F (93 C) satisfied secant offset requirements only.

(5) The CT specimen (1-in. thickness) did not have sufficient thickness to provide ASTM valid K_{Ic} determinations at C_v shelf level temperature for either irradiated or unirradiated conditions. Projections of specimen thickness requirements of irradiated and unirradiated conditions were 5 and 13 in., respectively.

(6) If power reactor surveillance programs restrict test specimen size to a maximum of 1-in. thickness and if the measuring capacity of CT specimens is the function of specimen thickness described by ASTM, an empirical or correlation-projection approach would be required to utilize fracture mechanics specimens in such surveillance programs.

(7) If an index is chosen at or near the center of the brittle-to-ductile transition, the irradiation shift is the same for both C_v and K_{Ic} curves for this particular heat of A533-B Class 2 steel.

References

[1] "Tentative Method of Test for Plane Strain Fracture Toughness of Metallic Materials," ASTM E 399-70T, *Annual Book of ASTM Standards,* Part 31, American Society for Testing and Materials, Philadelphia, 1970, pp. 911-927.

[2] Pellini, W.S., "Advances in Fracture Toughness Characterization Procedures and in Quantitative Interpretations to Fracture-Safe Design for Structure Steels," NRL Report 6713, Naval Research Laboratory; also, published in *Welding Research Council Bulletin,* No. 130, May 1968.

[3] Rolfe, S.T. and Novak, S.R. in *Review of Developments in Plane Strain Fracture Toughness Testing, ASTM STP 463,* American Society for Testing and Materials, Sept. 1970, pp. 124-159.

[4] Hawthorne, J.R., "Trends in Charpy-V Shelf Energy Degradation and Yield Strength Increase of Neutron-Embrittled Pressure Vessel Steels," NRL Report 7011, Naval Research Laboratory; also published in *Nuclear Engineering and Design,* Vol. 11, 1970, pp. 427-446.

[5] Loss, F.J., "Dynamic Tear Test Investigations of the Fracture Toughness of Thick-Section Steel," NRL Report 7056, Naval Research Laboratory, Jan. 1970.

[6] Wessel, E.T., Clark, W.G., Jr., and Pryle, W.H. in *Proceedings of the Second International Conference on Fracture,* Chapman and Hall, London, April 1969, pp. 825-850.

[7] *Plane Strain Crack Toughness Testing of High Strength Metallic Materials, ASTM STP 410,* American Society for Testing and Materials, 1966.

[8] Wessel, E.T., unpublished data.

[9] Sailors, R.H. and Corten, H.T., "Relationship Between Material Fracture Toughness using Fracture Mechanics and Transition Temperature Test," HSST Program Annual Information Meeting, University of Illinois, March 1971, in publication.

[10] Mager, T.R. and Yanichko, S., *Journal of Basic Engineering, Transactions of the American Society of Mechanical Engineers,* Series D, Vol. 93, 1971, pp. 259-264.

R. H. Sailors[1] *and H. T. Corten*[1]

Relationship between Material Fracture Toughness using Fracture Mechanics and Transition Temperature Tests

REFERENCE: Sailors, R.H. and Corten, H.T., "**Relationship between Material Fracture Toughness using Fracture Mechanics and Transition Temperature Tests,**" *Fracture Toughness, Proceedings of the 1971 National Symposium on Fracture Mechanics, Part II, ASTM STP 514,* American Society for Testing and Materials, 1972, pp. 164-191.

ABSTRACT: Although the effect of flaws in stressed bodies can be quantitatively characterized by methods of linear elastic fracture mechanics (LEFM), it is sometimes necessary to assess the fracture susceptibility using only conventional transition temperature tests. In order to gain the advantages and best features of each approach, a correlation between the two methods of fracture assessment is needed. The existing correlations between LEFM results and transition temperature test results are reviewed in light of new data on A533B steel. A complete series of test results obtained by the HSST Program (ORNL) for both LEFM and transition temperature tests in both unirradiated and irradiated conditions permit fracture toughness, K_{Ic} and K_{Id}, to be correlated with charpy V-notch energy, nil-ductility transition temperature, DT transition temperature, and low temperature cleavage stress. By following fundamentals of LEFM, whenever possible, a consistent pattern of fracture behavior is demonstrated for a class of pressure vessel steels similar to A533B.

KEY WORDS: fracture (materials), fracture strength, toughness, transition temperature, impact tests, impact strength, notch sensitivity, brittle fracturing, loading, temperature tests, tear tests, cracks, loads (forces), yield strength, notch strength

Historically, laboratory tests to select materials to avoid brittle fracture have centered around the use of small notched specimens subjected to impact loading. A quantity called transition temperature (TT) is measured. In concept, the transition temperature approach states that below the TT the energy absorbed by a specimen in fracture is small, and fracture may occur at nominal stresses in a structure below the yield strength (frangible), whereas, above the TT the energy absorbed by a specimen in fracture is large, and fracture will not occur until the nominal stress in a structure exceeds the yield strength. While simple in

[1] Research associate and professor, respectively, Department of Theoretical and Applied Mechanics, University of Illinois, Urbana, Ill. 61801.

concept, this approach has been questioned on the basis of fracture experience with high strength steels that exhibit low values of upper shelf energies. In addition, considerable confusion has surrounded the several vaguely related operational definitions of TT.

Premature fracture has been observed to be associated with flaws or cracks accidentally introduced into the structure. Linear elastic fracture mechanics provides a stress analysis of a cracked structure and relates fracture toughness, (K_{Ic}), to nominal stress and flaw size in a quantitative manner [*1*]. Fracture mechanics involves a two-dimensional crack tip stress field characterized by K, however, the contribution of section thickness to crack tip transverse constraint (crack front induced triaxial tensile stresses) was clearly recognized. Further, it was established that minimum toughness was associated with a sharp crack, such as a fatigue crack. Since in most applications numerous load cycles are encountered, the fatigue crack also is potentially typical of the most severe cracks encountered in service. For structural grade steels, it now has been established that the toughness is measurably lowered by rapid loading, such as impact [*2, 3*].

In spite of the quantitative advantages of the fracture mechanics approach, the transition temperature approach often has been favored for material selection and quality control using structural grade steels because of its relative simplicity, low cost and small specimen size. Specifically, Charpy V-notch specimens have been widely used for many years, and the results are particularly well known and useful to the metallurgist for comparing and controlling heat treatments and other production and fabrication processes. Because of this background of experience with Charpy V-notch data, and the small specimen size, it has been used exclusively in the past in nuclear reactor surveillance programs.

These facts clearly indicate the need to establish a relation between toughness, as measured in the Charpy V-notch test, and fracture toughness, as measured in a fracture mechanics test. If such a relationship can be established, then the Charpy V-notch data can be converted to a fracture mechanics characterization and a quantitative evaluation of critical flaw size may be made.

The literature already contains *empirical* correlations between several of the traditional measures of transition temperature and fracture toughness. This paper attempts to use known and generally accepted fracture mechanics fundamentals and existing data to evaluate the relationship between transition temperature type data and fracture mechanics data.

Data for A533, class B, grade 1, plate material including the Charpy V-notch energy values and K_{Ic} values are shown as a function of temperature in Fig. 1 [*4, 5*]. Several general observations are helpful. First, the two measures of toughness in Fig. 1 exhibit somewhat similar trends. This observation forms the basis for attempting empirical correlations between C_v and K_{Ic}. Second, in the low temperature region (below -50 F), plastic deformation preceding fracture is confined to a small region (small compared to notch depth and specimen dimensions) adjacent to the notch tip. Under these conditions, gross plastic

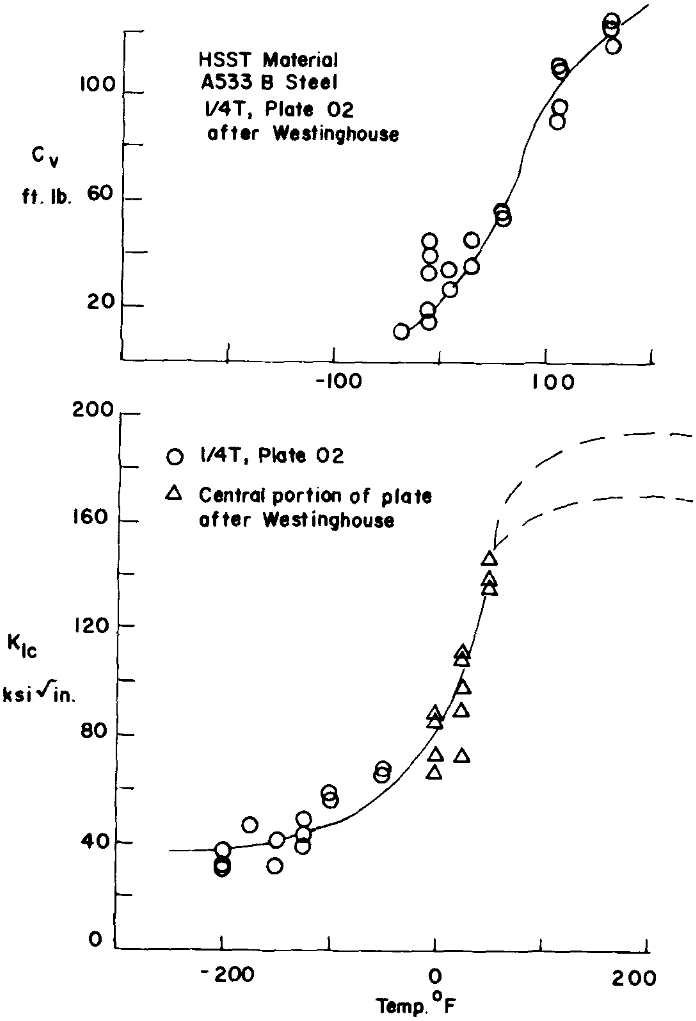

FIG. 1–*Comparison of Charpy energy and* K_{Ic} *as a function of temperature for A533 B steel [4, 5].*

deformation is not measurable, and the fracture surface is predominantly flat. Microscopic examination of flat fracture surfaces in the low temperature region indicates the presence of cleavage facets. Third, in the high temperature region (above 150 F) on the upper shelf, small and moderate size specimens reach limit load conditions and deform in a fully plastic deformation mode prior to fracture. In this region it appears evident that separation is related to the plastic strain and the state of strain at the crack front. For large structures and specimens containing large flaws, the critical separation conditions of plastic strain at the crack front can be developed prior to limit load conditions and possibly when the nominal stress is below the yield strength. For very large structures which may contain correspondingly large flaws, the size of the region of plastic deformation also will be correspondingly large but may be contained by an elastic stress field.

These observations suggest that the relationship between transition temperature type tests, specifically Charpy V-notch energy and K_{Ic}, will most likely be different for two temperature regions, namely a low temperature region including the lower half of the transition temperature range, and a high temperature region above the transition temperature range, that is, on the upper shelf.

Relationship Between C_v and K_{Ic} on the Upper Shelf

While both C_v and TT tests may be useful to measure upper shelf energy, the immediate need is for a relationship between C_v and K_{Ic} on the upper shelf. The empirical relationship developed by Rolfe and Novak [6] is shown in Fig. 2 (solid points). The ordinate, $(K_{Ic}/\sigma_Y)^2$, is a measure of the fracture toughness and also is proportional to the size of the plastic zone in the fracture mechanics specimen. The abscissa, (C_v/σ_Y), is a normalization that caused all of the data in Fig. 2 to fall close to the solid line. The solid line is represented by the relationship,

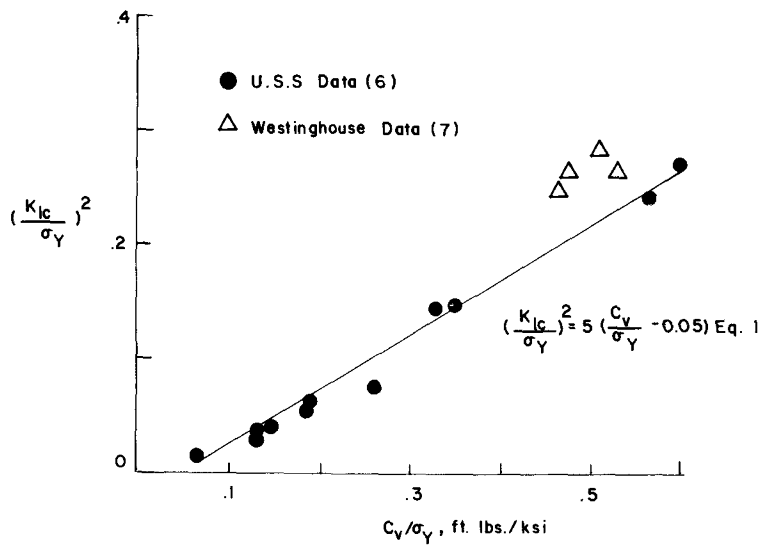

FIG. 2–*Upper shelf correlation between $(K_{Ic}/\sigma_Y)^2$ and (C_v/σ_Y) for a series of steels [6].*

$$\left[\left(\frac{K_{Ic}}{\sigma_Y}\right)^2\right] = 5\left[\frac{C_v}{\sigma_Y} - 0.05\right] \tag{1}$$

where C_v is the energy in ft · lb measured with a standard Charpy specimen at 80 F, (this is on the upper shelf for all of the U.S.S. data) and K_{Ic} is the static value of fracture toughness at 80 F in ksi $\sqrt{\text{in.}}$ The K_{Ic} data were obtained according to the ASTM E-24 recommended practice, except that some of the specimens did not meet the thickness requirements. Rolfe and Novak [*6*] believe that the K_{Ic} data are accurate to within ± 15 percent. The yield strength, σ_Y in ksi, is the standard uniaxial value, again measured at 80 F.

Since the publication of this correlation, Westinghouse has measured K_{Ic} on the upper shelf at elevated temperatures using large specimens made of a rotor forging steel and added four additional data points (triangles) which confirm the solid line in Fig. 2 [*7*]. These data points are considered significant because they represent a different class of steel, the K_{Ic} data satisfied the E-24 recommended practice, and the measurements were made at elevated temperatures.

The relationship, Eq 1, allows an estimation of K_{Ic} on the upper shelf based on the Charpy data for A533 B, HSST plate. The average Charpy energy on the upper shelf is between 100 and 110 ft · lb and the yield strength varies from approximately 60 to 70 ksi. For this range of values of C_v and σ_Y, K_{Ic} is estimated between 170 and 195 ksi $\sqrt{\text{in.}}$ These values of K_{Ic} are approximately 25 percent higher than the measured value of 145 ksi $\sqrt{\text{in.}}$ at 50 F.

In Fig. 3, the relationship, Eq 1, was used to obtain estimates of K_{Ic}, shown as ordinate, in terms of C_v, the abscissa, and the yield strength, σ_Y. For purposes of discussion assume that the Charpy energy upper shelf remained above 50 ft · lb, and the yield strength is 60 ksi or higher. Figure 3 indicates that K_{Ic} will be 120 ksi $\sqrt{\text{in.}}$ or higher. At this point it is important to recognize that fracture toughness data on A533B steel, including plate, weld or HAZ, and data on A508 forgings have not been obtained to substantiate these estimates.

For irradiated steels the Charpy upper shelf is reached at temperatures between room temperature and 400 F. At this time it is not known at what temperature the estimated K_{Ic} values are applicable. Judging from the transition temperature size effect observed in the large drop weight tear test specimens, a temperature increment of 130 F should be added to the NDT temperature to achieve the upper shelf for a 12-in. thick structure. If the 30 ft · lb Charpy "fix" estimates of NDT are used (errors of 75 F have been found [*8*]), the upper shelf estimates of K_{Ic} should be applicable above the 30 ft · lb fix temperature plus an increment of 130 F to 205 F.

This discussion leads to interest in the C_v–K_{Ic} relationship in the transition temperature range for irradiated materials. Specifically, the question arises whether the C_v–K_{Ic} correlations on the upper shelf and in the transition temperature range lead to the same estimate of K_{Ic} at the temperature where the two estimates interface.

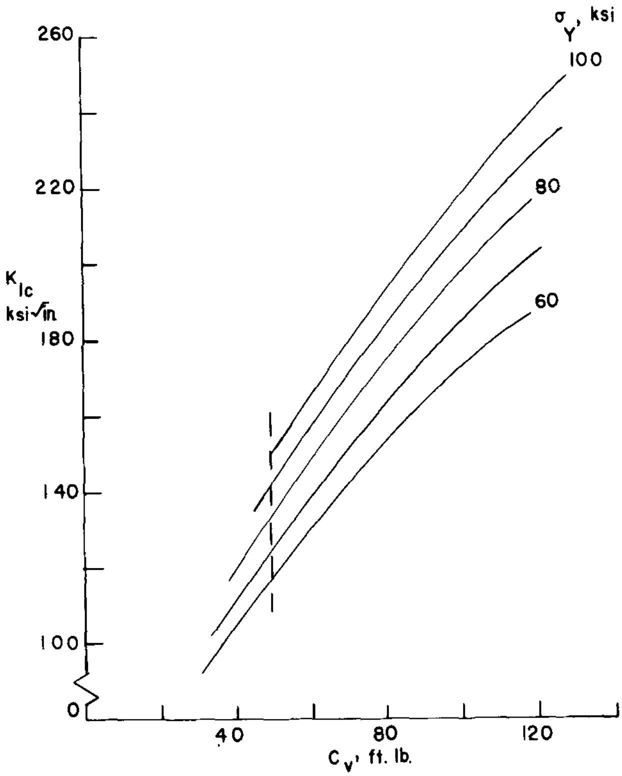

FIG. 3—*Upper shelf relationship between* K_{Ic}, C_V *and* σ_Y *based on Eq 1 [6].*

Relationship Between C_v and K_{Ic} in the Low Temperature and Transition Temperature Range

In the low and transition temperature range fracture mechanics specimens made of A533 B steel have been tested with adequate crack tip transverse constraint (thickness) to produce plane strain conditions up to K_{Ic} = 145 ksi $\sqrt{\text{in}}$. at 50 F (Fig. 1*b*). The increase in toughness with temperature between -100 and 50 F apparently is attributable to a progressive change of the fracture mechanism. As the temperature is increased, the plastic deformation (at fracture) in the vicinity of the crack tip, measured either by the size of the plastic zone or the maximum plastic strain, increased markedly. This phenomenon will be called a "microscopic fracture mechanism transition."

When toughness is measured using small constant size Charpy V-notch specimens, crack tip constraint is relaxed due to through-the-thickness yielding at a relatively low value of toughness $[(K_{Ic}/\sigma_Y)^2 \sim \pi B]$. This thickness transition, when it occurs, causes a rapid increase in toughness that is superimposed upon the microscopic fracture mechanism transition. The C_v

values shown in Fig. 1, involve the superposition of the thickness transition upon the microscopic fracture mechanism transition.

Other differences between the K_{Ic} and C_v specimens involve the influences of a sharp versus a blunt notch and rapid versus slow rates of loading. Each of these features influences the magnitude of the measured toughness and the temperature range in which the transition is observed. In the following, various relationships between K_{Ic} and C_v will be explored. First, the relationship between K_{Ic} (slow loading rate) and C_v energy will be investigated by empirically comparing data for unirradiated and irradiated steels. Next, the dynamic K_{Id} (fast loading rate) will be compared to C_v energy for unirradiated steel. Finally, because the shift in the TT caused by irradiation is commonly used as a measure of irradiation damage, the several features of specimen size, irradiation, notch root radius, etc. that influence the shift in the TT will be investigated in relation to K_{Ic}.

Static Fracture Toughness, K_{Ic} *versus* C_v

Relationship Between C_v *and* K_{Ic}—An empirical relationship between C_v and K_{Ic} in the low and transition temperature range was introduced by Barsom and Rolfe [9] using data from low and medium strength steels. This relationship is given by

$$\frac{K_{Ic}^2}{E} = 2(C_v)^{3/2} \tag{2}$$

where K_{Ic} is the static fracture toughness, in ksi $\sqrt{\text{in.}}$ C_v is impact energy for a standard specimen, in ft · lb, and K_{Ic}^2/E is in psi/in.

The data used to establish Eq 2 exhibited considerable scatter. In the range above C_v = 30 ft · lb, the relationship was strongly influenced by data from rotor forging steels.

In this study, major attention was focused on pressure vessel steels similar to A533 B steel. Other steels were reviewed primarily to assist in establishing trends and in setting limits of applicability on the resulting relationship. Each set of data was examined point by point. This evaluation led to a series of guidelines for evaluating and selecting the data for a correlation of K_{Ic} with C_v.

(1) Charpy V-notch data at one temperature frequently exhibited a rather large scatter. In Charpy testing any error in measuring energy inevitably lead to values that were too high. Therefore, attention was focused upon the lower boundary of the Charpy energy band.

(2) In the low temperature region where the Charpy energy values are low (1 to 10 ft · lb), the inertia of the broken specimen can contribute a significant amount of energy. Therefore, for a correlation on the basis of energy, the low energy values are considered less reliable, and all values less than 5 ft · lb were disregarded.

(3) It was felt that the correlation in the low and transition temperature range should avoid an influence of high Charpy energy, uppershelf values. Therefore, the data were arbitrarily cut off at 50 ft · lb.

(4) Study of the particular data points that deviated most from the correlation line indicated that these points often were for material in which it was known or suspected that the metallurgical structure was different, such as surface material from thick heated plates or weld metal. In regions of metallurgical gradients, such as surface material, it was uncertain whether the small Charpy specimens and the large K_{Ic} specimens represented the same material. These considerations led to a conscious attempt to select only data where metallurgical structure was most uniform (from T/4 to 3T/4) and typical of thick pressure vessel steels.

A correlation diagram between K_{Ic} and C_v was prepared using these guidelines. The results are shown in Figs. 4 and 5. Figure 4 is a log-log diagram and Fig. 5 shows K_{Ic}^2/E versus C_v on a linear scale. The scatter of the data is considerably reduced by using the guidelines stated above. Only a few points remain outside of the dashed-line scatter band drawn in Figs. 4 and 5.

Good fit lines were drawn through the data in the figures. The slope of the line on the log-log diagram, Fig. 4, was very close to 0.5 and has been drawn as such.

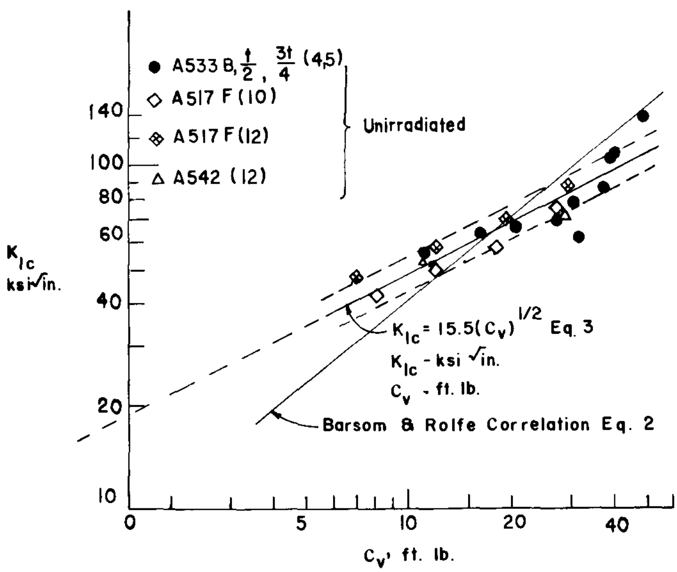

FIG. 4—*Transition temperature correlation between* K_{Ic} *and* C_v *for a series of unirradiated steels.*

From Fig. 4, the empirical relationship is

$$K_{Ic} = 15.5(C_v)^{0.5} \tag{3}$$

where K_{Ic} is static fracture toughness, in ksi $\sqrt{\text{in.}}$ and C_v is impact energy for a standard specimen in ft · lb. This is numerically equivalent to the relationship in Fig. 5 given by

$$\frac{K_{Ic}^2}{E} = 8(C_v) \tag{4}$$

where K_{Ic}^2/E is in psi/in., and $E = 30 \times 10^3$ ksi.

Equations 3 and 4 are considered to provide good empirical representation of the relationship between K_{Ic} and C_v for thick section steels in the range of 5 ft · lb $< C_v <$ 50 ft · lb, in the low and transition temperature range. Equations 3 and 4 have the general form

$$G_{Ic} = \frac{K_{Ic}^2}{E(1-\nu)^2} = C\left(\frac{C_v}{A}\right) \tag{5}$$

which apparently is dimensionally consistent if G_{Ic} is in units (in. · lb/in.^{2}), C_v in (in. · lb) and A in (in.^{2}).

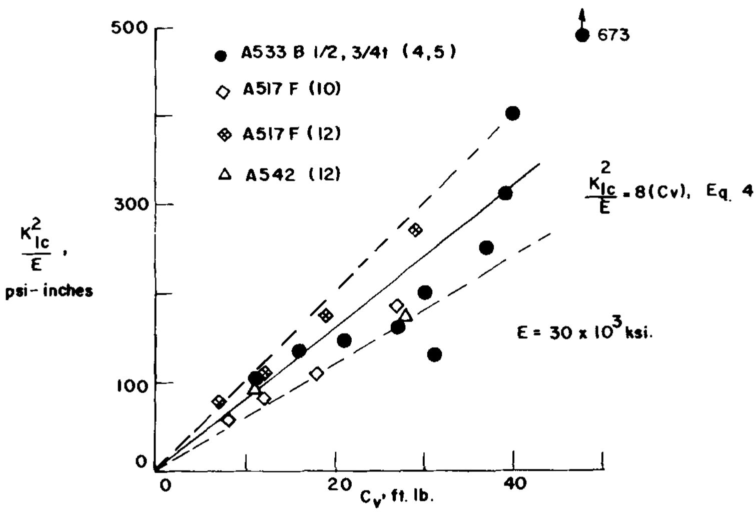

FIG. 5—*Transition temperature correlation between* $(K_{Ic}/E)^2$ *and* C_v *for a series of unirradiated steels.*

Equations 3 and 4 differ from Eq 2 primarily through the exponents. Equation 2 passes close to the centroid of the data in Fig. 4 but underestimates the K_{Ic} value at low values of C_v and overestimates K_{Ic} at higher values of C_v, in the range 5 ft · lb $\leq C_v \leq$ 50 ft · lb.

Comparison of K_{Ic} *Estimated from Charpy Data and the Measured Values for* K_{Ic} *for Unirradiated Steel*—Estimates of K_{Ic} based on Charpy data and Eqs 3 and 4 are compared with measured values of K_{Ic} for an A533 B plate [*4*] including surface, and 1/2T in Fig. 6 and an A517 F plate and weld metal [*10*] in Fig. 7. The estimated values of K_{Ic} from C_v data and Eq 3 or Eq 4 are shown as points and the measured values are represented by cross-hatched bands enclosing the experimental data.

For A533 B plate (1/2T) and A517 F plate, the K_{Ic} values predicted from Eq 3 are within the band of the measured K_{Ic} values. These predictions are considered to be in good agreement with the measured values. Vertical lines representing ± 12 percent about the mean value are shown in Figs. 6 and 7 to represent the scatter band from Fig. 4.

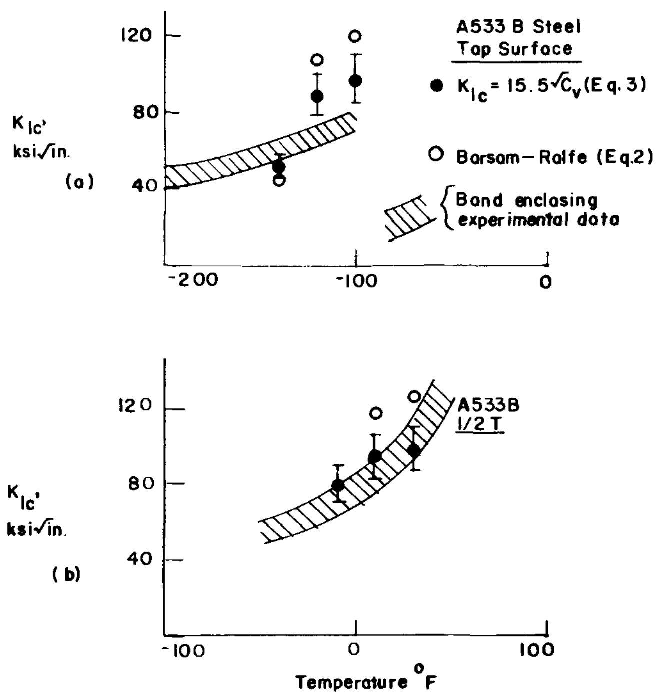

FIG. 6—*Comparison between estimated values (Eqs 2 and 3) and measured values of* K_{Ic} *as a function of temperature for transition temperature behavior.*

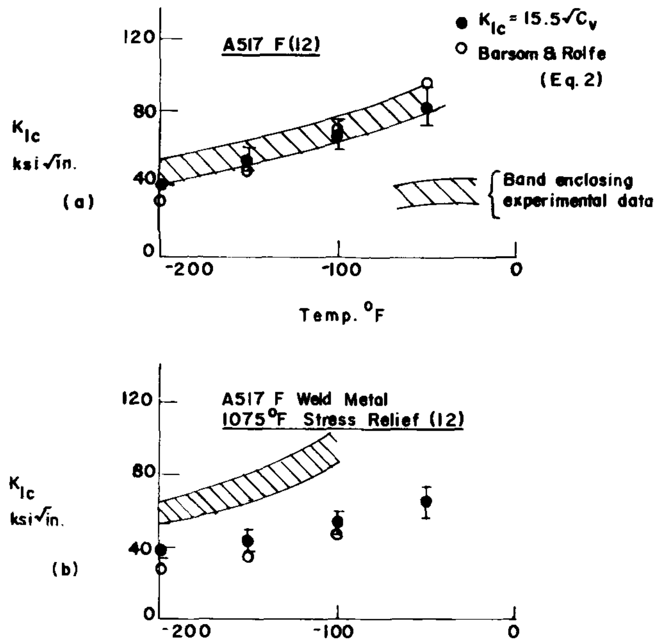

FIG. 7—*Comparison between estimated values (Eqs 2 and 3) and measured values of* K_{Ic} *as a function of temperature for transition temperature behavior.*

The prediction of K_{Ic} from C_v data and Eq 2 are within the band for A517 F steel but appear high for A533 B steel (1/2T).

For the A533 B top surface material (Fig. 6*a*), the estimates of K_{Ic} from Eq 3 appear high and unconservative.

An opposite effect is shown in Fig. 7*b* for A517 F weld metal. Here the estimated K_{Ic} is significantly below the measured values of K_{Ic}, and the estimated K_{Ic} based on Charpy data is overconservative.

Figures 6 and 7 were selected as a representative sampling of data to illustrate instances where the correlation is good, and several where Eq 3 is unconservative or overconservative. These results are intended to warn the would-be user of this correlation (Eq 3) to employ it with caution.

One thing is apparent from Figs. 6 and 7; no single correlation between K_{Ic} and C_v can be devised to accurately fit all available data. It appears that correlations can be devised to fit certain classes of steels, such as metallurgically uniform thick pressure vessel steel plate. Before this correlation can be applied to estimate K_{Ic} from C_v data for other steels, additional data for the particular steels are required to justify its use.

Comparison of K_{Ic} *Estimated from Charpy Data and the Measured Values of* K_{Ic} *for Irradiated Steel*—One of the motivations for this study was the interpretation of C_v data for irradiated material in terms of K_{Ic}. Data in which K_{Ic} and C_v were measured at the same temperature, or where interpolations for either C_v or K_{Ic} could be made are sparse. The data are shown in Fig. 8 on a diagram with K_{Ic} as ordinate and C_v as abscissa. The correlation equations, Eqs 2 and 3, also are shown. Neither equation represents the data well: more important the values of K_{Ic} estimated from Eq 3 (or Eq 2) generally are higher than the measured values of K_{Ic}.

Dynamic Fracture Toughness, K_{Id} *versus* C_v

Barsom and Rolfe [9] also made an empirical correlation between K_{Id} and Charpy type energy for several low and medium strength steels, using data from Charpy specimens that were fatigue cracked prior to testing.

Following this lead, the data used by Barsom and Rolfe were assembled along with selected data for A533 B steel [4, 5]. For the A533 B steel, data for standard Charpy specimens only (ρ = 0.010 in.) were available. These data are shown in Fig. 9 with K_{Id} as ordinate and C_v as abscissa. On this log-log diagram, a straight line was fitted to the data by the method of least squares. The resulting empirical relationship is given by

$$K_{Id} = 15.873\,(C_v)^{0.375} \tag{6}$$

where the coefficients have been evaluated for K_{Id} in units of ksi $\sqrt{\text{in.}}$ and C_v in ft · lb. The 95 percent confidence band on the mean value is also shown.

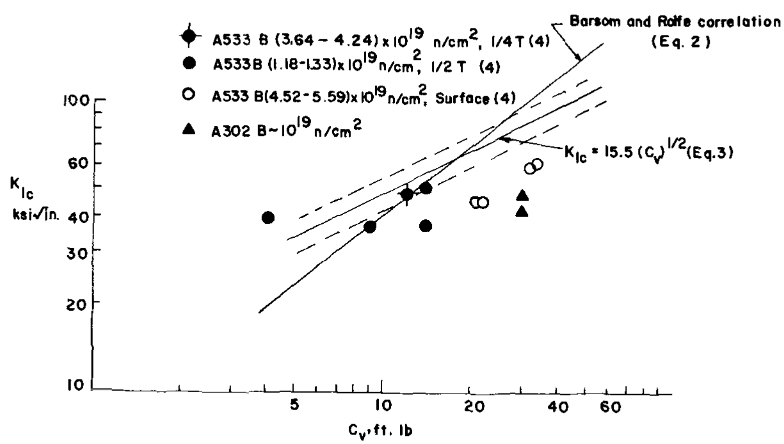

FIG. 8—*Transition temperature correlation between* K_{Ic} *and* C_v *for a series of irradiated steels.*

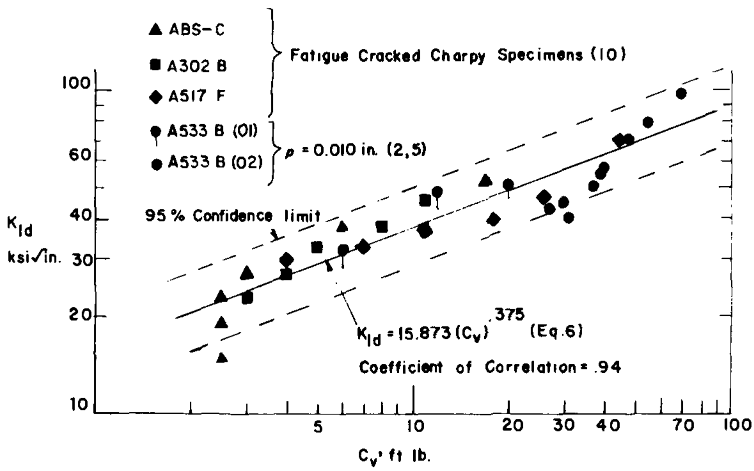

FIG. 9–*Transition temperature correlation between* K_{Id} *(dynamic) and* C_v *for a series of unirradiated steels.*

Comparison of Eq 6 with the data presented by Barsom and Rolfe indicated that the addition of the data for A533 B steel with ρ = 0.010 in. did not noticeably alter the relationship. This observation suggests that the root radius has only a minor influence on the value of Charpy energy.

A comparison of Eqs 3 and 6 indicates that the change in the rate of loading of the fracture toughness specimen had a significant influence on the relationship between K_{Ic} and C_v. Both Eqs 3 and 6 intersect C_v = 1 ft · lb at nearly the same value of K_{Ic} (15.7 ± 0.2). However, the slope of the line in Fig. 9 is 0.375, which is significantly lower than the slope of 0.50 in Fig. 4.

Barsom and Rolfe [9] also obtained K_{Ic} (slow loading) and slow bend Charpy type data. The area under the load deflection curve was used to evaluate the energy to fracture for the slow bend Charpy type specimens (fatigue cracked). The interesting feature of these results [9] was that the relationship between K_{Ic} and slow bend Charpy energy was indistinguishable from the relationship between K_{Id} and dynamic C_v energy (fatigue cracked). Specifically Eq 6 provides a good relationship between fracture toughness and Charpy V-notch energy when both are either static or dynamic.

With these facts in mind, Eq 6 can be rewritten in terms of G_{Id} as

$$G_{Id} = \frac{K_{Id}^2}{E} = \frac{(15.873)^2}{E} (C_v)^{0.75} \tag{7}$$

Because Eqs 6 and 7 provide good correlation for both slow loading (K_{Ic} and slow bend Charpy energy) and fast loading (K_{Id} and C_v), it is considered to be a better, more fundamental correlation than that represented by Eqs 3 and 5. However, Eq 7 lacks the dimensional consistency that was suggested by Eq 5. It now appears that the apparent dimensional consistency of Eq 5 is purely fortuitous and caused by competing or compensating influences.

A major difference between the tests for K_{Ic} and C_v is the toughness measuring point. The toughness measurement point for a K_{Id} test was the onset of rapid crack extension, whereas the total energy to complete separation is used for the Charpy test.

Considering only the influence of the toughness measuring point, observation of instrumented Charpy load-deflection curves [*11, 12*] allows a qualitative partitioning of the total area into energy prior to the onset of crack extension and energy of crack propagation. At low values of energy and temperature, the total energy is made up primarily of energy prior to the onset of rapid crack extension. At higher values of energy and temperature, the energy of crack propagation makes a larger contribution to the total energy of fracture. It appears that development of a standard instrumented Charpy test might provide a means of measuring the energy prior to the onset of rapid crack extension and allow an approximate matching of measuring points in the K_{Id} and C_v tests.

Relationship Between Fracture Toughness and Transition Temperature

In dealing with embrittlement due to irradiation the most common measurement of radiation damage is the shift in transition temperature [*13*]. First we recall the several transition temperatures that frequently are employed.

(1) NDT is an ASTM designation for the transition temperature in a drop weight test employing 5/8, 3/4 or 1-in.-thick standard specimens flawed with a notch in an embrittled weld bead. Below NDT the specimens are completely fractured and above NDT the specimens are incompletely fractured.

(2) $(TT)_{NDT}$ is here adopted to designate the NDT temperature for nonstandard large size drop weight specimens, containing corresponding large cracks in large weld beads.

(3) $(TT)_{DT}$ is used to designate the thickness induced transition temperature in a dynamic tear test for any size specimen. Designation of $(TT)_{DT}$ has not been standardized. In the interests of consistency, the $(TT)_{DT}$ refers to the temperature at which the normalized dynamic tear energy for a given size specimen has increased 10 percent above the normalized DT energy for a much larger specimen. $(TT)_{DT}$ so defined can be evaluated only when data from larger specimens are available for comparison. Experience with this definition makes it clear that a measure of judgment is involved and in many cases it may be necessary to employ a temperature band due to the sparsity and scatter of data.

(4) $(TT)_{50\%}$ refers to the fracture appearance transition temperature (FATT) and corresponds to the temperature at which the fracture appearance was approximately 50 percent fibrous and 50 percent cleavage.

(5) $(TT)_{15\ ft\cdot lb}$ refers specifically to Charpy V-notch data and is the temperature at which the Charpy energy is 15 ft · lb. $(TT)_{30\ ft\cdot lb}$ refers specifically to Charpy V-notch data and corresponds to the temperature at which the Charpy energy is 30 ft · lb.

We first consider the relationship between K_{Id} and $(TT)_x$ for unirradiated material and then consider estimates of K_{Id} for irradiated material in the transition temperature range.

Estimation of K_{Id} *for Unirradiated Materials from* $(TT)_x$ *Measurements*—Our purpose is to relate the transition temperature, $(TT)_x$ to K_{Id}. The dynamic fracture toughness, K_{Id}, is selected for comparison with $(TT)_x$, in order to approximately match the strain rates. The approach employs the following three relationships.

(a) The thickness fracture mode transition commences when: $B \approx 2.5 (K_{Id}/\sigma_{Yd})^2$. Most steels exhibit the thickness transition in a range between $1.0 (K_{Id}/\sigma_{Yd})^2$ and $2.5 (K_{Id}/\sigma_{Yd})^2$. Using the coefficient 2.5 leads to the relationship

$$B^{-1/2} = 0.634 \left(\frac{\sigma_{Yd}}{K_{Id}}\right) \tag{8}$$

(b) Roper, Koschnitzke, and Stout [*14*] observed that when other specimen dimensions were relatively large and constant, the transition temperature, either $(TT)_{NDT}$ or $(TT)_{15\ ft\cdot lb}$, varied linearly with the inverse square root of thickness, $B^{-1/2}$. This relationship may be represented by the equation:

$$(TT)_x = T' - S_1 B^{-1/2} \tag{9}$$

where T' is an intercept on the temperature axis corresponding to $B \rightarrow \infty$ and S_1 is the slope of the line. These constants must be determined from data for each material. Data for $(TT)_{NDT}$ as a function of thickness, B, for two steels are shown in Fig. 10.

(c) Merkle [*15*], observing the hyperbolic variation of (K_{Ic}/σ_Y) with temperature T, suggested that the inverse quantity (σ_Y/K_{Ic}) should give a linear relation with temperature. Employing dynamic values,

$$\left(\frac{\sigma_{Yd}}{K_{Id}}\right) = C - S_2 T \tag{10}$$

where C (intercept at $T = 0$) and S_2 (slope) are constants for each material. This relationship is compared with experimental data in Fig. 11 and found to provide

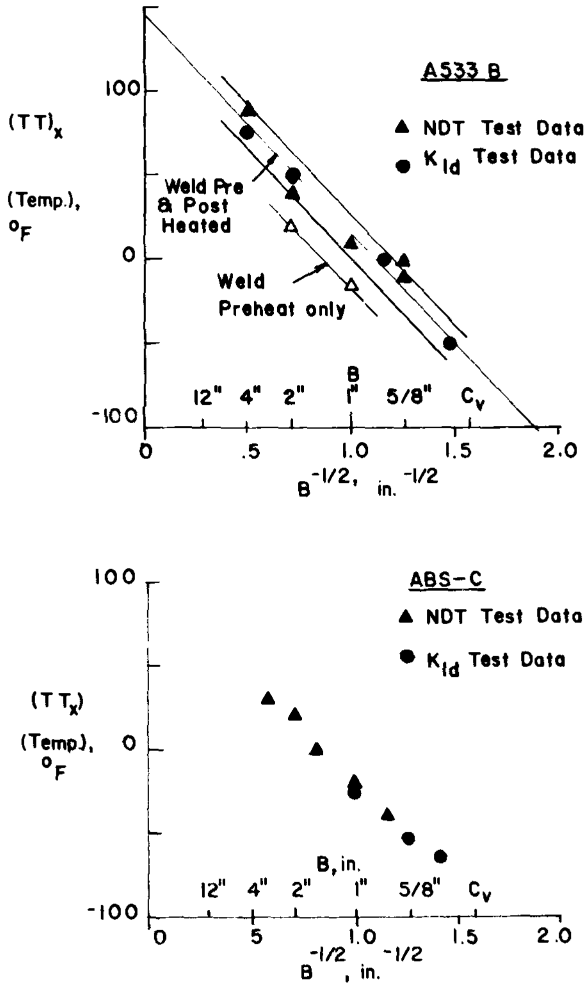

FIG. 10—*Relationship between* $(TT)_{NDT}$ *and thickness* B. *The* $(TT)_X$ *for the* K_{Id} *data are determined by the size requirement:* $B = 2.5\,(K_{Id}/\sigma_Y)^2$.

a good fit to the data over a limited but interesting temperature range (-250 to 0 F or +100 F in one case). Data for both (σ_Y/K_{Ic}) and (σ_{Yd}/K_{Id}) exhibit this linear relationship as a function of temperature.

On the low temperature side, the temperature range of application of Eq 10 is unimportant for the present purpose. However, on the high temperature side, Eq 10 is limited to temperatures T less than $T = C/S_2$. When $T = C/S_2$, the implication from Eq 10 is that (σ_{Yd}/K_{Id}) is zero. Since σ_{Yd} is not zero, then K_{Id} must be very large, that is, $K_{Id} \rightarrow \infty$. Since K_{Id} does not exceed the finite upper shelf value discussed previously, the linear relationship, Eq 10, becomes

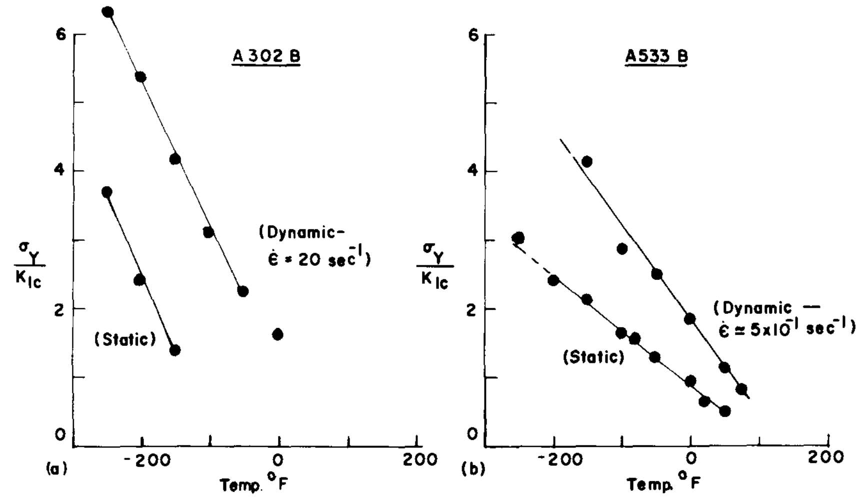

FIG. 11a—*Illustration of linearity between* σ_Y/K_{Ic} *and temperature for A302 B and A533 B.*

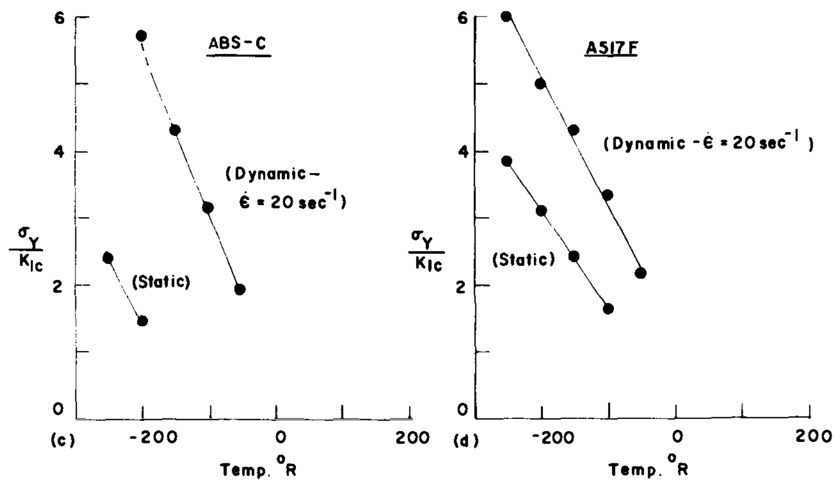

FIG. 11b—*Illustration of linearity between* σ_Y/K_{Ic} *and temperature for ABS-C and A517 F.*
Correction: temperature is in deg F.

invalid as the temperature T approaches (C/S_2). For steels with high upper shelves, it appears that a value of (σ_{Yd}/K_{Id}) between 0.2 and 0.3 may be a reasonable estimate for a lower limit.

Combining the first two observations allows prediction of K_{Id} as a function of temperature from a minimum number of measurements of transition temperature. Equation 8 gives the maximum value of K_{Id}/σ_{Yd} that can be measured with a specimen of thickness, B. For higher values of K_{Id}/σ_{Yd}, the large plastic zone relaxes the transverse constraint and causes the thickness fracture mode transition to occur. In transition temperature terms, the beginning of the thickness fracture mode transition is measured by NDT, $(TT)_{NDT}$, or $(TT)_{DT}$. (Only $(TT)_x$ that detect the thickness fracture mode transition can be combined with Eq 8 for measurement of K_{Id}/σ_{Yd}). This transition temperature is given as a function of B by Eq 9, for a particular steel for which T' and S_1 are material constants. Substituting for $B^{-1/2}$ from Eq 9 into Eq 8 leads to

$$\frac{\sigma_{Yd}}{K_{Id}} = \frac{T' - (TT)_x}{0.634\,S_1} \tag{11}$$

where $(TT)_x$ represents NDT, or $(TT)_{NDT}$ in large specimen drop weight tests, or $(TT)_{DT}$ in dynamic tear tests.

Since each determination of transition temperature $(TT)_x$ provides an estimate of (σ_{Yd}/K_{Id}) at that temperature (Eq 11), the variation of (σ_{Yd}/K_{Id}) with temperature can be obtained by determining $(TT)_x$ for a series of different size specimens.

To illustrate the results obtained with Eq 11, consider the $(TT)_{NDT}$ measurements obtained by Loechel [16] for 1, 2, and 4-in -thick specimens of A533 B steel tested in a drop weight test. For these three thicknesses, the $(TT)_{NDT}$ are listed below along with the value of K_{Id}/σ_{Yd} calculated from Eq 11.

B, in.	1	2	4
$(TT)_{NDT}$, deg F	10	40	90
K_{Id}/σ_{Yd}, in.$^{1/2}$	0.61	0.784	1.646
σ_{Yd}, ksi	94	90	85
G_{Id} $\frac{\text{in}\cdot\text{lb}}{\text{in.}^2}$	109	166	654

The constants T' and S_1 in Eq 9 were evaluated from the data in Fig. 10 as: $T' = 145$ F and $S_1 = 130$ F in.$^{1/2}$. These values of T' and S_1 are average best fit values determined from the three data points in the table above plus NDT results for 5/8 in.-thick specimens. The values of σ_{Yd} shown above were estimated from a yield strength time-temperature relationship [17]. Using the values of K_{Id}/σ_{Yd} and σ_{Yd} listed, the values of G_{Id} were calculated. Measured values of K_{Id} [2] were converted to G_{Id} values ($G_{Id}E = K_{Id}^2$) and are shown as a function of temperature in Fig. 12. The experimental data are shown as circles

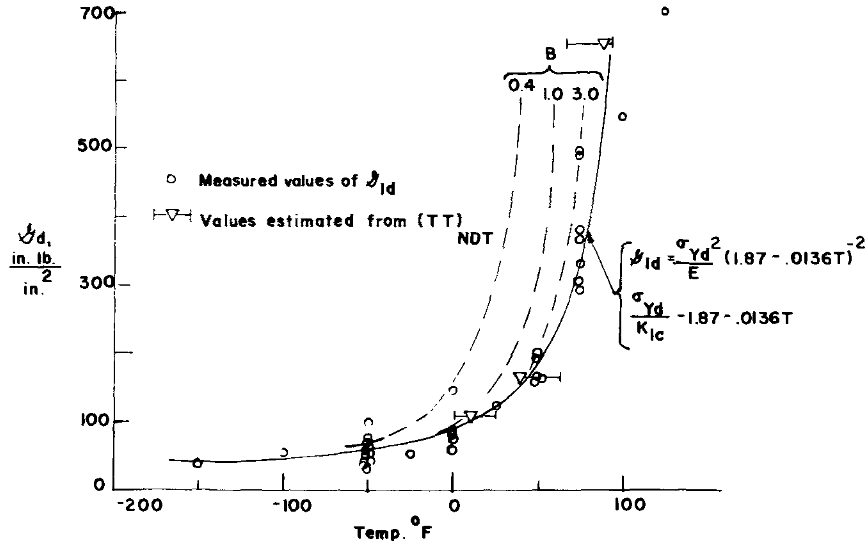

FIG. 12–*Dynamic fracture toughness, G_{Id}, and estimates of G_d as a function of temperature and specimen thickness.*

and the solid curve in Fig. 11 is Eq 10 fitted to the data ($C = 1.87, S_2 = 0.0136$) based on the straight line in Fig. 10*a*.

The values of G_{Id} estimated from $(TT)_{NDT}$ measurements in the table above are compared with the measured values of G_{Id} in Fig. 12. The triangular points, representing these estimates of G_{Id}, are augmented with horizontal lines representing the range of temperatures (25 F) employed in Fig. 10. The agreement of the values of G_{Id} estimated from $(TT)_{NDT}$ data is considered excellent.

Looking next at the results of the dynamic tear test, in principle a similar estimate of K_{Id} or G_{Id} can be made. For use in Eqs 9 and 11, the $(TT)_{DT}$ must correspond to the thickness fracture mode transition. The data in Fig. 13 indicate a consistent pattern of behavior. The temperature range of rapid increase of DT energy decreases as the specimen thickness (size) decreases. One major difficulty is encountered: the determination of the appropriate transition temperature $(TT)_{DT}$. When one attempts to select the temperature where the smaller specimens deviate from the larger specimens, it is clear that the precision of this estimate is not good. Two factors contribute to this problem. First, the data in Fig. 13 have been "normalized" to cause all of the upper shelf energies to coincide at 1.0. It is clear that this method of normalization is simple and convenient but lacks rational justification. On the other hand, other simple methods of normalization raise similar questions of rational justification. The second factor that contributes to the difficulty of selecting the appropriate value of $(TT)_{DT}$, is the sparsity of data for large specimens in the lower temperature range.

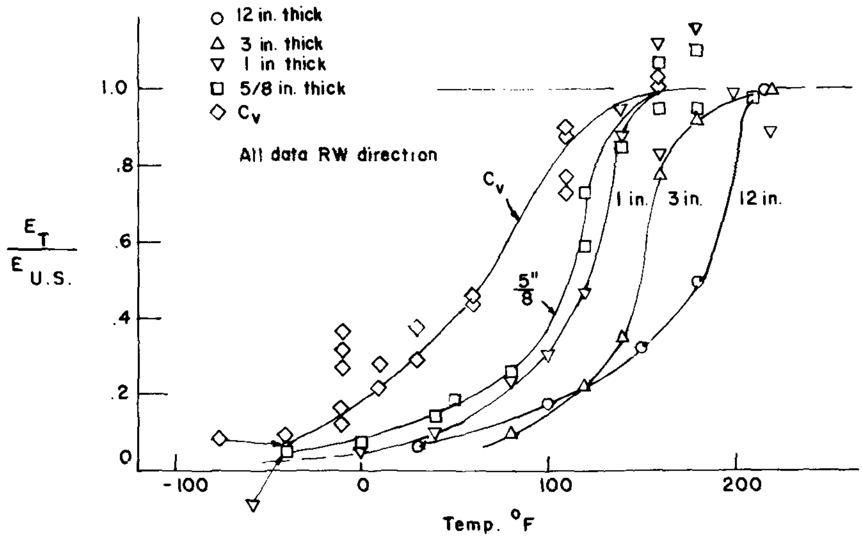

FIG. 13–*Dynamic tear energy normalized to the upper shelf values as a function of temperature.*

We have made estimates of $(TT)_{DT}$ from the data in Fig. 13. These values of $(TT)_{DT}$ are shown as a function of thickness, B, in Fig. 14. In general, the estimates of $(TT)_{DT}$ involved temperature ranges 50 F wide. The temperature band from Fig. 10*a* is also shown in Fig. 14 and it may be observed that the pattern is consistent. Thus the dynamic tear specimens appear to fit the general

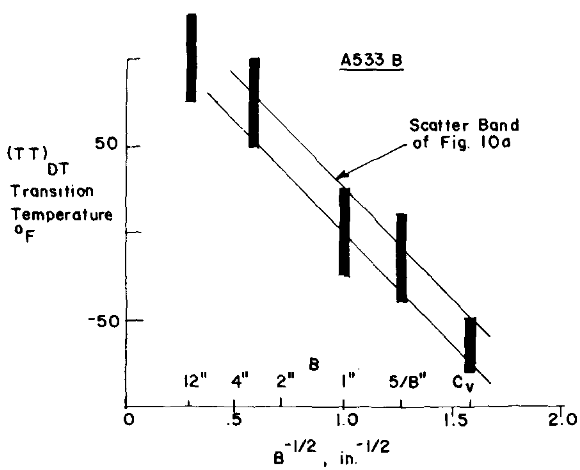

FIG. 14–*Transition temperature, $(TT)_{DT}$, as a function of specimen thickness.*

behavior pattern, however these data are not well suited for the determination of a thickness fracture mode transition, $(TT)_{DT}$. Also shown in Fig. 14 is the transition temperature, $(TT)_{DT}$, estimated from the Charpy data shown in Fig. 13. This estimate of $(TT)_{DT}$ lies on the same "band" as the DT data as well as the $(TT)_{NDT}$ data band from Fig. 10. Thus, measurements of $(TT)_{DT}$ provide the same basic results as the measurements of NDT and $(TT)_{NDT}$. When these results are represented by Eq 9 and combined with Eq 8, the values of K_{Id}/σ_{Yd} estimated from the $(TT)_{DT}$ are the same as shown for the NDT and $(TT)_{NDT}$ shown in Fig. 12. For A533 B steel the transition temperature type data in Figs. 10, 13, and 14 present a pattern which is consistent with the G_{Id} data shown in Fig. 12. The consistent patterns and relationships illustrated above between $(TT)_x$ and K_{Id} each have required data for large specimens for comparison with the data for small specimens.

For one steel, A533 B, a complete behavior pattern has been demonstrated. For several other steels, some portions of a similar behavior pattern have been observed. For steels similar to A533 B steel (in terms of strength and high upper shelf toughness) we can only assume a behavior pattern in terms of specimen size similar to that demonstrated for A533 B steel.

For unirradiated materials the variation of $(TT)_x$ as a function of thickness (Fig. 10) is both expected from considerations of fracture mechanics and observed with all available data. Uncertainty is associated with the slope of the line in Fig. 10. Roper, Koschnitzke, and Stout [14] summarized data for a number of structural grade steels employing $(TT)_{50\%}$ with a variety of slow and dynamic tests. The slopes of the lines appear to depend both upon the material and the test. For an ABS-C steel, different tests produced a measurable variation in slopes. Further, the slopes appear to be somewhat different for an ABS-C steel in the annealed condition, as compared with a normalized condition, as compared with a spray quenched condition. This variation of slope of $(TT)_x$ as a function of $B^{-1/2}$ is unfortunate because it implies that extensive testing of large specimens of each material is needed and that at this time we must adopt a conservative interpretation of small specimen data.

For the purpose of measuring irradiation damage, the use of the shift in $(TT)_x$ of C_v specimens depends upon the pattern of behavior developed for unirradiated material. Figure 15 is a schematic diagram of $(TT)_x$ as ordinate and $B^{-1/2}$ as abscissa. The lowest band including the data from Fig. 10, represents a starting point. The quantity $B^{-1/2}$ corresponding to the Charpy specimen thickness is marked in the diagram. Two other bands for irradiated material have been drawn parallel to the band for unirradiated material. For a fluence of 1.18-1.33 x 10^{19} neutrons/cm^2 at 550 F, a $\Delta T \approx 100$ F shift is indicated. Similarly for a fluence of 3.64-4.24 x 10^{19} neutrons/cm^2 at 550 F, a $\Delta T \approx 150$ F shift is shown. In practice, as in drawing this diagram, it is assumed that the two cross-hatched bands in Fig. 15 shift parallel to the band for unirradiated data. If we view irradiation as changing the material, it is clear that evidence does not exist that the cross-hatched bands in Fig. 15 shift parallel to the unirradiated

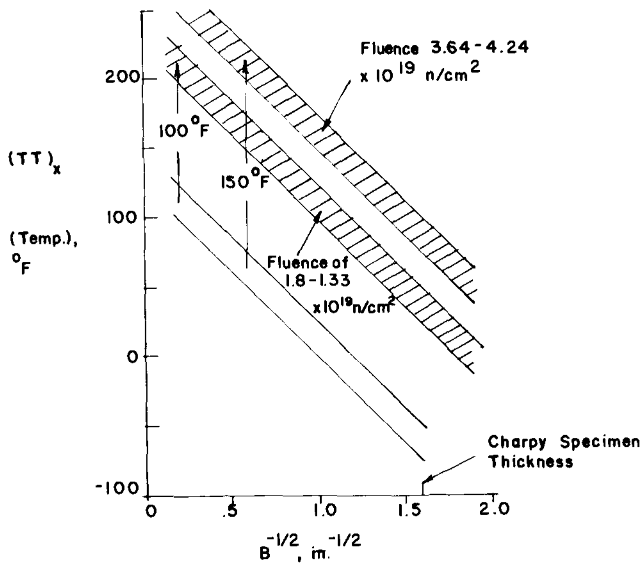

FIG. 15—*Estimated effect of irradiation on the transition temperature,* $(\mathrm{TT})_x$, *as a function of specimen thickness for two fluences.*

band. This uncertainty regarding the shift in $(\mathrm{TT})_x$ for thick irradiated members again requires a conservative approach to the interpretation of small specimen data.

Estimation of K_{Id} *for Irradiated Material in the Transition Temperature Region*—Two methods of estimating K_{Id} from C_v data have been presented. A method was presented that depends upon an empirical correlation of K_{Id} and C_v data (Eq 6). A second method was presented based upon an empirical correlation between K_{Id} and a $(\mathrm{TT})_x$ that measures the beginning of the thickness fracture mode transition (Eqs 8, 9, 10, and 11). A third method proposed by Malkin and Tetelman [*18*] is also used and compared with the results of the first two methods.

The first series of estimates of K_{Id} are based on C_v data for irradiated material and Eq 6. The estimated values of K_{Id} are shown as a function of temperature for two fluence levels, approximately 1.25×10^{19} neutrons/cm^2 in Fig. 16 and approximately 4×10^{19} neutrons/cm^2 in Fig. 17. In Fig. 16 the estimated values of K_{Id} cover a temperature range from 0 to 150 F. The estimated values of K_{Id} extend from 50 to 200 F in Fig. 17.

The second method of estimating K_{Id} is based on measuring the thickness fracture mode transition using small specimens which have been treated to the fluence of interest. Measurements of $(\mathrm{TT})_x$ as a function of $B^{-1/2}$ are shown in Fig. 15 for unirradiated material as well as estimates of $(\mathrm{TT})_x$ for the two fluence levels of interest.

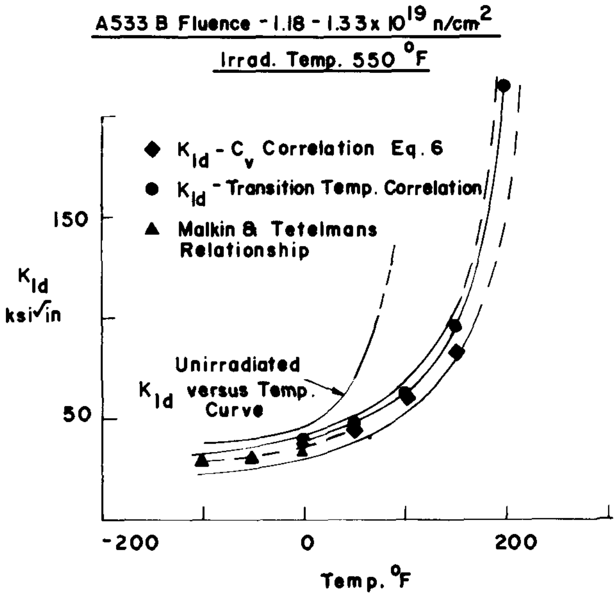

FIG. 16—*Estimated* K_{Id} – *temperature curve obtained by three methods.*

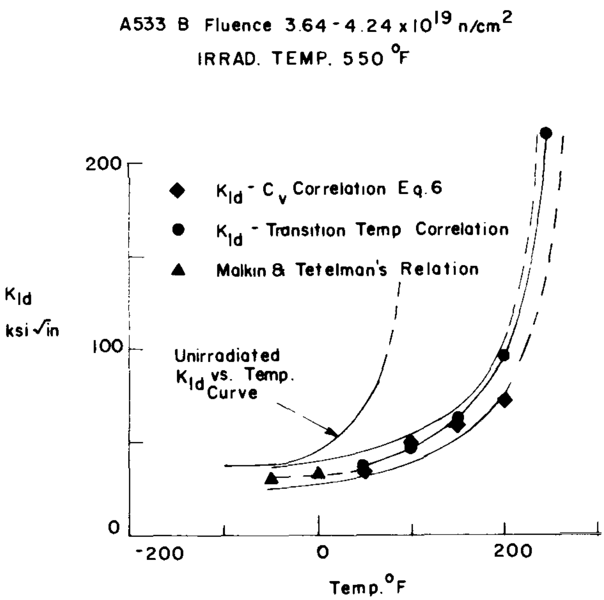

FIG. 17—*Estimated* K_{Id} – *temperature curve obtained by three methods.*

At the two fluence levels in Fig. 15 the only available $(\mathrm{TT})_x$ data were for C_v specimens. The cross-hatched bands in Fig. 15 were obtained by shifting the band for the unirradiated data along the temperature axis by the temperature increment, ΔT, indicated by the Charpy data.

In adopting this approach, the values of the constants, T' and S_1 in Eq 11 for the irradiated material are automatically evaluated. The value S_1 (slope) is identical for both unirradiated and irradiated material. The intercept T' is

$$T'_{\mathrm{irrad}} = T'_{\mathrm{unirrad}} + \Delta T_{C_v}$$

The value of $(\sigma_{Yd}/K_{\mathrm{Id}})$ may be calculated at any desired temperature, $(\mathrm{TT})_x$, corresponding to a specimen of minimum thickness, B, that would be required to make the measurement of $(K_{\mathrm{Id}}/\sigma_{Yd})$. For the calculation, the value of σ_{Yd} was estimated from a yield strength time-temperature relation [*17*].

In Fig. 16, for a fluence of approximately 1×10^{19} neutrons/cm^2, K_{Id} is shown as the solid line as a function of temperature from 0 to 200 F. Similarly in Fig. 17, corresponding to a fluence of approximately 4×10^{19} neutrons/cm^2, the estimate of K_{Id} is shown as a solid line as a function of temperature from 50 to 250 F. The temperature ranges covered by these estimates of K_{Id} correspond approximately to the toughness values that could be measured by a specimen of thickness somewhat smaller than the Charpy specimen at the low temperatures, to the toughness values that could be measured by a 12-in. thick specimen at the high temperature end (see Fig. 15).

The third method of estimating K_{Id}, the Malkin-Tetelman method, was used to estimate K_{Id} as a function of temperature based on a low temperature value of σ_f^* that could be calculated from a measurement of K_{Id} at low temperature using a small specimen. The value of σ_f^* was taken as 320 ksi and σ_{Yd} was estimated from a yield strength time-temperature relation [*17*]. The values of K_{Id} so estimated are shown in Figs. 16 and 17 as dotted lines for comparison with the other estimates of K_{Id}. Because the values of σ_f^*, calculated from measured values of K_{Id}, begin to increase in the temperature interval from 0 to 50 F, it is anticipated that K_{Id} estimated from a constant low temperature value of σ_f^*, will deviate from the other estimates of K_{Id} in this same temperature interval. In fact, this is observed in Figs. 16 and 17 in this same temperature interval.

The feature brought out by Figs. 16 and 17 is the consistency exhibited by the three methods of estimating K_{Id} in appropriate temperature ranges. Dynamic K_{Id} data are nonexistent for irradiated materials, thus the estimated values cannot be considered as established. What is established is the internal consistency among the several methods of estimating K_{Id} for irradiated material within the limitations that have been stated. These results contribute to establishing a consistent pattern of representing fracture behavior using the several empirical methods that have been discussed.

In the transition temperature range, the fracture toughness, both K_{Ic} and K_{Id}, of A533 B plate have been measured and exhibit a consistent pattern of behavior as a funtion of specimen size and temperature. Other plates of the same nominal material and hopefully forging of similar composition can be expected to exhibit a similar pattern of behavior. Small specimens can be used, on a comparative basis, to insure maintenance of equivalent high quality of material. Small specimens can also be used on a comparison basis to measure changes in the A533 B steel caused by radiation exposure. In the low and transition temperature range, measurements of K_{Ic} for unirradiated and irradiated material suggest that the influence of irradiation is to shift the K_{Ic} curve to higher temperatures by an increment $\Delta T_{K_{Ic}}$ [5]. Similarily, C_v measurements of $(TT)_{30\ ft \cdot lb}$ from the same unirradiated and irradiated material indicate a shift in the C_v curve to higher temperatures by an increment ΔT_{C_v} that is approximately equal to $\Delta T_{K_{Ic}}$. Simply stated, the K_{Id} versus T curve for irradiated material can be estimated by shifting the K_{Id} versus T curve for unirradiated material along the temperature axis by a temperature shift, ΔT, equal to the temperature shift measured by Charpy data [19].

Summary

The toughness of the material in pressure vessels and other structures is needed in terms, such as fracture toughness, that can be related quantitatively to the applied stress and the allowable flaw size. Charpy V-notch specimens have been and continue to be widely used for surveillance and material quality control because of the small specimen size and the convenience and low cost of the Charpy test data. The question that must be resolved is whether the necessary quantitative information concerning toughness can be directly or indirectly extracted from the Charpy data. A review and evaluation of the relationships between Charpy data, either C_v energy or a transition temperature, and the fracture toughness, K_{Ic}, is made in this paper.

On the upper shelf, the Rolfe-Novak empirical relationship between K_{Ic} and C_v was reviewed. The recent addition of valid K_{Ic} data for a forging steel in the upper shelf temperature range by Westinghouse adds confidence that this empirical relationship may have wide applicability. Because of the high average toughness of A533 B steel, no valid K_{Ic} or K_{Id} data are available for this material in the upper shelf temperature range.

Several items of work are needed to clarify the situation in the upper shelf temperature range. First, more attention should be given to recent advances in the theoretical treatment of elastic-plastic and strain hardening behavior around crack tips. The *J*-integral introduced by Rice [20] appears to be a prime candidate for a fracture criterion in the tough behavior upper shelf temperature range. The second item consists of the optimization of the small specimen for use in this range. With a small specimen it is not contemplated that plane strain

behavior in terms of ASTM size requirements can be achieved. However, a study is required to optimize the net section depth (crack run) with respect to thickness, the notch depth and the root radius, and produce an optimum small specimen for correlation with K_{Ic} and the potential fracture criterion, J_c, in the upper shelf high temperature range.

In the transition temperature range, three independent correlations between Charpy data and fracture toughness were reviewed. The first correlation is between C_v and K_{Ic}. The Barsom-Rolfe relationship was modified to better fit the available data for C_v energy and K_{Ic} in the range of C_v from 5 to 50 ft · lb. This relationship is Eq 3 or 4. It is demonstrated that this relationship produces reasonably accurate estimates of K_{Ic} from C_v data for material near the center of thick plates. However, for surface material from thick plates the estimate of K_{Ic} is unconservative and for weld material (A517 F), the estimate of K_{Ic} is over-conservative. For irradiated plate material the estimate of K_{Ic} from C_v data is unconservative. This relationship cannot be recommended for general use.

Eliminating the strain rate difference between the fracture toughness test and the Charpy test by comparing K_{Id} (dynamic) with C_v lead to a modified correlation equation, Eq 6. This equation provided a better fit to all of the available data than did Eq 3. While this better correlation seems reasonable, the amount of K_{Id} data is limited: (that is, K_{Id} data are not available for irradiated material). Thus it is uncertain whether or not this correlation (Eq 6) provides a relationship that has general applicability.

The third relationship between fracture toughness and Charpy data is based on the concept that Charpy and larger size drop weight and dynamic tear type specimens exhibit a thickness fracture mode transition which begins at a temperature, $(TT)_{DT}$, where the size requirements for the K_{Ic} test are just met in the K_{Ic} specimen. Actually these size requirements are applied to K_{Id} data in order to better match the strain rate of the fracture toughness test with the impact tests. While exhibiting some scatter, this relationship appears consistent for all of the available data. The most complete set of data for large DT, large drop weight, and large K_{Ic} specimens is available for A533 B steel. All of these data, including the Charpy data, appear to fit a consistent pattern of fracture behavior. In addition, certain portions of the consistent behavior pattern are found for other steels where data are available.

This third relationship between K_{Id} and $(TT)_x$ takes on particular significance in terms of fracture toughness of irradiated materials. Toughness degradation due to irradiation has been most extensively studied in terms of the shift along the temperature axis of the transition temperature, ΔT. The implications of the relationship between K_{Id} and $(TT)_x$ is that the shift in transition temperature, ΔT, can provide a needed link between K_{Id} for unirradiated material and irradiated material in the transition temperature range. Specifically this correlation suggests that the toughness, K_{Id}, of the irradiated material can be obtained from the toughness, (K_{Id}/σ_{Yd}) of the unirradiated material by shifting the (K_{Id}/σ_{Yd}) (unirradiated) curve along the temperature axis by an increment, ΔT, determined from unirradiated and irradiated Charpy $(TT)_x$ measurements. In this process the changes in the dynamic yield strength, σ_{Yd}, due to irradiation presumably should be included.

Shifting the (K_{Id}/σ_{Yd}) curve with temperature is equivalent to shifting the K_{Id} and σ_{Yd} curves by the same temperature increment, ΔT. If the actual irradiated yield stress is greater than the value indicated by the shifted σ_{Yd} curve and used in subsequent calculations, then the predicted value of K_{Id} will be less conservative than if the K_{Id} curve were simply shifted by the temperature increment ΔT.

Conclusions

1. Based on the current state of the art, the toughness, K_{Id}, of unirradiated and irradiated steel should be estimated in a conservative manner using C_v data.

2. In the temperature range of the upper shelf the Rolfe-Novak relationship (Eq 1) appears to give a reasonable and conservative estimate of K_{Ic} based on C_v energy data for unirradiated data.

3. In the low and transition temperature range, K_{Id} should be estimated using Eq 6 based on C_v energy data and compared with an estimate based on Eq 11 using the drop weight NDT data.

4. For irradiated steel, in the transition temperature range, an estimate of K_{Id} should be obtained by shifting the K_{Id} curve for unirradiated steel along the temperature axis by an increment ΔT measured in Charpy tests for unirradiated and irradiated specimens.

5. These recommendations should be considered tentative because they are based on empirical correlations for a limited number of steels. A sound theoretical analysis of the elastic-plastic behavior and a fracture criterion is required to put these empirical relationships on a sounder basis for general use.

References

[*1*] Irwin, G.R., Krafft, J.M., Paris, P.C., and Wells, A.A., "Basic Aspects of Crack Growth and Fracture," Section 7 in *Technology of Steel Pressure Vessels for Water-Cooled Nuclear Reactors,* G.D. Whitman, G.C. Robinson, Jr., and A.W. Savolainen, Eds., *ORNL-NSIC-21*, Oak Ridge National Laboratory, Dec. 1967; see also, *NRL Report 6598*, U.S. Naval Research Laboratory, 21 Nov. 1967.

[*2*] Shabbits, W.O., "Dynamic Fracture Toughness Properties of Heavy Section A533 Grade B Class 1 Steel Plate," Westinghouse Nuclear Energy Systems, WCAP-7623, HSST Technical Report 13, Dec. 1970.

[*3*] Shoemaker, A.K. and Rolfe, S.T., "The Static and Dynamic Low-Temperature Crack-Toughness Performance of Seven Structural Steels," AD 846 126L, 29 Nov. 1968 (available from Defense Documentation Center).

[*4*] Shabbits, W.O., Pryle, W.H., and Wessel, E.T., "Heavy Section Fracture Toughness Properties of A533 Grade B Class 1 Steel Plate and Submerged Arc Weldment," Westinghouse Atomic Power Divisions, WCAP 7414, HSST Technical Report 6, Dec. 1969.

[*5*] Mager, T.R. and Thomas, F.O., "Evaluation by Linear Elastic Fracture Mechanics of Radiation Damage to Pressure Vessel Steels," Westinghouse Atomic Power Divisions, WCAP-7328 HSST Technical Report 5, Nov. 1969.

[6] Rolfe, S.T. and Novak, S.R. in *Review of Developments in Plane Strain Fracture Toughness Testing,* W.F. Brown, Jr., Ed., *ASTM STP 463,* American Society for Testing and Materials, 1970.

[7] T.R. Mager, private communication, 1970.

[8] Loss, F.J., Hawthorne, J.R., and Serpan, C.Z., Jr., *Journal of Basic Engineering, Transactions of the American Society of Mechanical Engineers,* Series D, Vol. 93, No. 2, June 1971, pp. 247-258.

[9] Barsom, J.M. and Rolfe, S.T. in *Impact Testing of Metals, ASTM STP 466,* American Society for Testing and Materials, 1970.

[10] Gentilicore, V.J., Pense, A.W., Stout, R.D., *Welding Journal,* Aug. 1970 (paper presented at the AWS 51st Annual Meeting, Cleveland, Ohio, 8-12 June 1970).

[11] Berggren, R.G., "Studies of Impact and Slow-Bend Charpy-Type Specimens," HSST Program Semi Annual Progress Report for Period ending 28 Feb. 1970, ORNL-4590, pp. 20-30.

[12] *Impact Testing of Metals, ASTM STP 466,* American Society for Testing and Materials, 1970.

[13] Steele, L.E., *Atomic Energy Review,* Vol. VII, No. 2, International Atomic Energy Agency, Vienna, 1969.

[14] Roper, C.R., Koschnitzke, K.A., and Stout, R.D., *Welding Journal,* Research Supplement, June 1967, pp. 254s-258s.

[15] Merkle, J.G., *Journal of Basic Engineering, Transactions of the American Society of Mechanical Engineers,* Series D, Vol. 93, No. 2, June 1971, pp. 265-273.

[16] Loechel, L.W., "The Effects of Section Size on the Transition Temperature in Steel," Martin-Marietta Corp., Denver, Colo., HSST-TR-2, 1969.

[17] Bennett, P.E. and Sinclair, G.M., "Parameter Representation of Low Temperature Yield Behavior of Body-Centered Cubic Transition Metals," ASME paper 65-Met-11, 1965.

[18] Malkin, J. and Tetelman, A.S., "Relation Between K_{Ic} and Microscopic Strength for Low Alloy Steels," U.S. Army Office, Durham, Technical Report 1, DAH-04-68-C-0008, Aug. 1969.

[19] Mager, T.R. and Yanichko, S.E., *Journal of Basic Engineering, Transactions of the American Society of Mechanical Engineers,* Series D, Vol. 93, No. 2, June 1971, pp. 259-264.

[20] Rice, J.R., *Journal of Applied Mechanics, Transactions of the American Society of Mechanical Engineers,* June 1968, pp. 379-386.